Study on the Development of Ultra-miniaturized Motion Analysis System and Its Medical Applications

超小型運動解析システムの開発とその医療応用に関する研究

2011 年 2 月

Zhuohua LIN

林 焯華

Study on the Development of Ultra-miniaturized Motion Analysis System and Its Medical Applications

超小型運動解析システムの開発とその医療応用に関する研究

2011 年 2 月

早稲田大学大学院 先進理工学研究科
生命理工学専攻 バイオ・ロボティクス研究

Zhuohua LIN
林 焯華

To my dear wife, Weixian

ACKNOWLEDGMENTS

"If I have seen farther than others, it is because

I was standing on the shoulders of giants."

Isaac Newton, 1676

The completion of a PhD project is hardly possible without support of other people. During the past three years, I had a pleasure to study in a foreign country and university, surrounded by many enthusiastic foreign colleagues and friends. This has allowed me to learn more about science, research, and people. Here, I would like to express my gratitude to all of you who were involved in my study and life, and who made me feeling home in Japan.

First of all, I would like to gratefully thank my supervisor Prof. Atsuo Takanishi for his confidence in my ability to complete the PhD courses. His trust on me and supervising me was very inspiring and encouraging. His bright guidance and warm leadership foster a vibrant and positive atmosphere for research that made my experience in his laboratory outstanding.

My special appreciation goes to Dr. Massimiliano Zecca for his guidance, patience, and friendship during my studies and living in Japan. He encouraged me to grow not only as an engineer but also as an instructor and an independent thinker.

During the period under which this research was completed, the advice and guidance from Dr. Hiroyuki Ishii, Dr. Salvatore Sessa and Dr. Kazuko Itoh did much to help me limit the scopes of the work and keep in the right research direction when I felt little or no progress was being made. I would like to sincerely thank them for their on-going support. I would also like to express my gratitude to Dr. Kenji Hashimoto, Dr. Kotaro Fukui and Dr. Hideki Kondo for their kind supports in the completion of my graduation procedure.

Thanks gratefully secretaries Mrs Hisako Ohta and Miss Terumi Itou for helping me solve a lot of problems on regular university affairs and living in Japan, which made me be capable of concentrating on my research. Thanks also the other members of Takanishi laboratory, especially the students who have contributed to this research.

I would like to express my deepest gratitude to Prof. Shuji Hashimoto, Prof. Mitsuo Umezu, Prof. Masakatsu G. Fujie and Prof. Hiroshi Iseki who gave me a lot of advices on how to complete my thesis and the corrections of my dissertation.

This is a doctorate in mechanical engineering. However, it involved the study of several topics that were normally associated with electrical engineering. I am not an electrical engineer, but through many hours, the patience and teaching skills of Dr. Salvatore Sessa and Mr. Luca Bartolomeo brought me as close as I will ever be.

It is my sincere pleasure to acknowledge the Department of Advanced Medical Initiatives at Kyushu University, especially Prof. Makoto Hashizume, Prof. Morimasa Tomikawa, Mr. Munenori Uemura and other colleagues who supporting me with valuable discussions of laparoscopic training and experiment organization.

I would like to thank gratefully Prof. Hiroshi Iseki and Dr. Takashi Suzuki at Tokyo Women's Medical University, for the medical knowledge support in neurosurgery and the organization of experiments in neurosurgical training.

It is very difficult to find fearless volunteers that allow you to measure and assess their skills. Most of the measurements in this research had been performed in Kyushu University, Tokyo Women's Medical University and Waseda University. Therefore, I would like to thank all the surgeons, medical students, and engineering students for participating in my studies.

This research has been partially supported by the Advancement of University Education Project of Chinese government Grant # [2007] – 3020, and a Grant by STMicroelectronics, which also provided the core sensors and the microcontroller. This work is also supported in part by Global COE Program "Global Robot Academia", MEXT, Japan; and the P2BL projects # [P2BL0807] and # [P2BL0904] of Waseda University. I would also like to express my gratitude to Okino Industries LTD, Japan ROBOTECH LTD, SolidWorks Corp, Dyden Corp, for their supports to the research.

Finally, and most importantly, I would like to thank my dear wife. Her support, encouragement, quiet patience and unwavering love were undeniably the bedrock upon which the past years of my life have been built.

ABSTRACT

Since the emphasis on medical safety and the complexity of modern surgical technologies and equipments continuously increase, it is essential to develop innovative and safe training and evaluation methods for surgical operative skills. Training devices, such as box trainers and virtual reality simulators, have already been developed to learn fundamental operative skills outside the operation room. However, the science of objective evaluation of operative performance is still in its infancy. Although there is growing amount of researches to assess medical operative competence objectively using motion analysis, they provide only the kinematics information of instruments or trainee' hands for evaluating the performance in a single training device. To date, there is no general methodology capable of integrating human body and instrument motion analysis to achieve objective skill evaluation in various training devices. Moreover, most current skill evaluation methods are limited to the applications in surgery, but can neither be extended to other medical scopes nor clinical practice.

In this thesis, the road towards the realization of common skill evaluation system for multiple medical applications is presented. After a deep review of the state of the art, a general methodology based on the development of ultra-miniaturized motion tracking system is proposed. The approach is to analyze the kinematic data describing the movements of trainee's upper body and the utilized medical instruments. The inertial-sensor-based ultra-miniaturized wearable motion tracking systems are used to measure and analyze these movements. A data processing model of motion information is defined to evaluate trainee's performance and provide quantitative feedback of significant motion features.

The validity of the resulting skill evaluation system is verified in laparoscopy, neurosurgery and in the clinical practice of mastication analysis. The evaluation for surgery is

based on the assumption that expert surgeons have better operative skills than novices. With a set of motion used to complete the training tasks, it allows us to evaluate the skill competence by comparing the motion features between expert surgeons and novices. The performance evaluation for mastication is analyzed while trainee chewing different kinds of food with different hardness and chewing gum with different sides of molars, in order to evaluate the jaw motion ability and mastication patterns for assisting clinical diagnosing and treatment.

The results are extremely promising, and show that the skill dexterity and competence could be effectively assessed and classified by using the developed skill evaluation system.

TABLE OF CONTENTS

LIST OF ABBREVIATIONS

ABS	acrylonitrile butadiene styrene
CDF	cumulative distribution function
CF	chewing frequency
CT	chewing time
DA	discriminant analysis
DTW	dynamic time warping
EKF	extended Kalman filter
ET	execution time
HMM	hidden markov models
IMU	inertial measurement unit
JMA	jaw measurement analysis
MEMS	micro-electro-mechanical system
MOA	mouth opening angle
PCA	principal components analysis
PCB	printed circuit board
PSD	power spectral density
RMS	root mean square
SEU	system electronics unit
UWB	ultra wide band
VR	virtual reality
WB	Waseda bioinstrumentation

LIST OF FIGURES

LIST OF TABLES

Chapter 1

Introduction

1.1 Background

1.1.1 Modern Technologies for Surgical Operation and Clinical Diagnosing

In recent years, there has been an ever increasing amount of research and development of technologies and methods to improve the quality and the performance of surgical operation and clinical practice [1-4]. Technological advance plays an increasingly important role in modern medical systems.

In the fields of minimally invasive procedures, laparoscopic surgery is currently the standard for an increasing number of abdominal and pelvic operations [5, 6]. Unlike open surgery, which requires a long incision, laparoscopic surgery is performed using special long and slender instruments which are inserted into the patient's body through short incisions. The straight-line body of laparoscopic instrument normally offers 5 mm in diameter and more than 330 mm in length [7]. Made with high quality stainless steel and durable modern materials, these instruments are designed to accommodate various surgical procedures. Some additions to the instruments are the rotating and non-rotating slide lock graspers, which offer an ergonomic and precise ratcheting mechanism. Visual feedback of the operating area is obtained by a laparoscope, which provides a 2D image on a monitor (Figure 1.1). For most patients, this leads to significantly less postoperative pain, a shorter hospital stay, faster recovery and, in some cases, a better overall outcome [8].

(a) Overview of laparoscopic surgery.

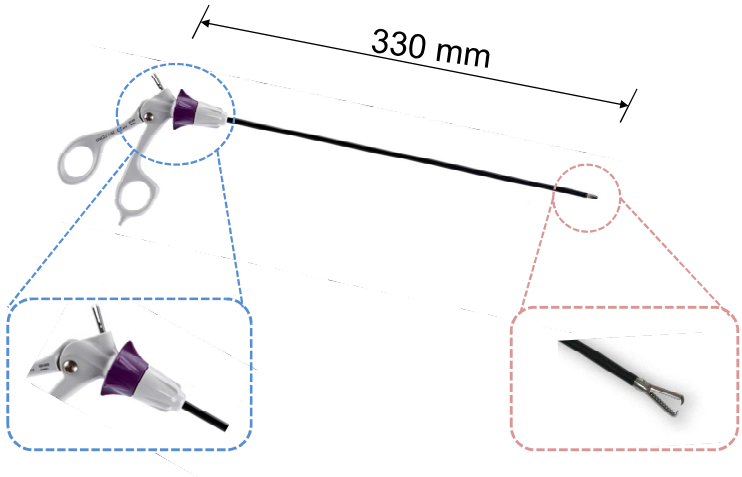

(b) Example of laparoscopic instrument.

Figure 1.1: Overview of laparoscopic surgery (up) and instrument example (down).

Surgical capabilities are also greatly widened by the introduction of the innovative instruments of microsurgery, that is, the use of magnifying systems and very precise tools to operate at the microscopic level (Figure 1.2) [9]. Awake craniotomy, for instance, is one kind of the brain surgery, which employs microscope for magnifying and locating the operation area, and helping the doctors dislodge and remove the brain tumors [10]. Using such methods, doctors could also reattach vessels and nerves of severed limbs, operate on the inner ear, remove tumors of the spinal cord, and other such operations once considered impossible.

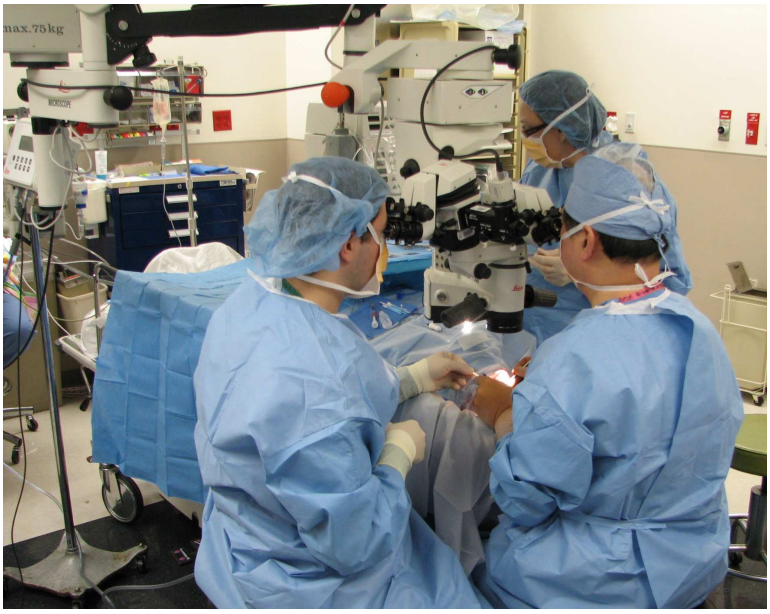

(a) Overview of laparoscopic surgery.

(b) Example of microscope.

Figure 1.2: Overview of microsurgery (up) and example of microscope (down).

In the fields of endoscopy, through the development of long, flexible tubes called endoscopes, doctors are able both to see and to operate on deep-lying regions of the body with minimal trauma to the patient. Colonoscopy (Figure 1.3), for example, is an endoscopic examination of the colon with a colonoscope - a fiber optic camera on a flexible tube- passed

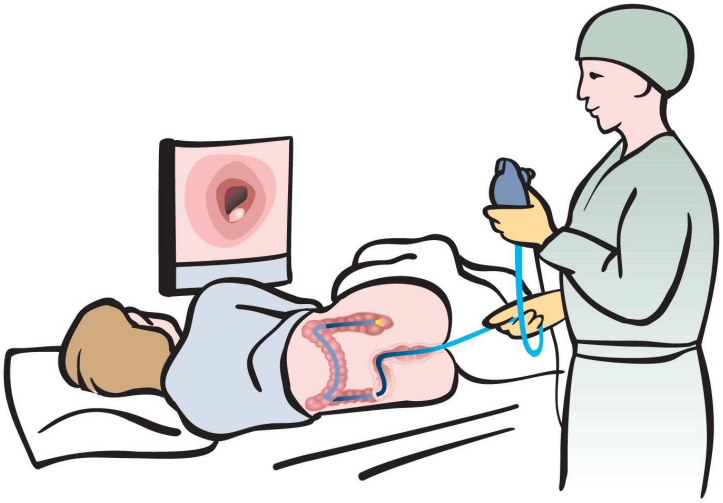

(a) Overview of colonoscopy.

(b) Example of colonoscope.

Figure 1.3: Overview of colonoscopy (up) and example of colonoscope (down).

into the anus and advanced through the entire colon [11]. The procedure generally takes between 20 minutes and one hour, depending on the doctor's operative competence.

Many advanced technologies have also been developed for assisting the clinical practice. For example, the analysis of mastication has long been used as a measure for clinical diagnosis and treatment of prosthodontics, orthodontics, and oral surgery. The use and development of devices for quantitatively measuring and analyzing jaw movement has recently become more common and popular in the clinic. The jaw motion tracking devices for evaluating masticatory performance could improve the diagnosing procedures and realize better dental treatments (Figure 1.4) [12, 13].

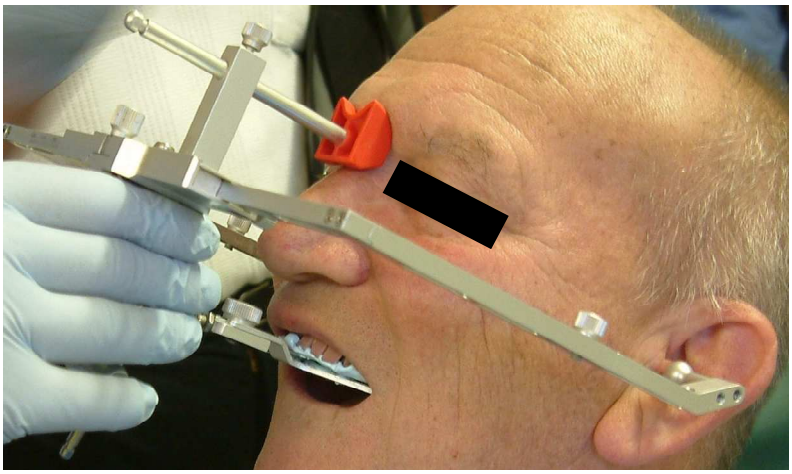

Figure 1.4: Instruments for jaw position tracking.

The introduction of these technologies in various medical applications improves the existing medical procedures and provides innovative approaches to solve critical medical problems. The advantages of these innovative technologies, however, are accompanied by special demands on the doctors, who need to possess certain operative skills that are more difficult and complicated than in conventional devices.

For example, laparoscopic surgery imposes limitations to doctors in visual and haptic perceptions. The use of 2D monitor reduces the depth perception of the operative field and causes special commands for doctors on eye-hand coordination ability; the use of slender instruments reduces haptic feedback; the motions of instruments are limited due to the trocar-induced invariant points. In microsurgery, the extremely small operation area and high requirements of precise hand movements have created great challenges to the doctors. The procedure is executed through the microscope binocular view, which also requires higher eye-hand coordination ability to the doctors. In endoscopy, the doctors need to handle the special long endoscope, which has similar limitations with laparoscopic surgery in the respects of reducing depth perception. Moreover, it is very difficult for the doctors to redirect the endoscope at some critical positions of the colon, such as the corners, which may cause pains to patients. In the case of jaw movement tracking, the instruments usually use special mechanisms put on the head in order to capture jaw position and movements. These mechanisms are relatively bulky and might make the patients feel not natural during the routine tests [14]. In addition, the doctors are required to have technical skills for calibrating and operating these instruments.

All of these limitations and skill requirements in different medical applications take the doctors a relatively long learning curve to master these modern technologies fully. The doctor could put a patient at risk if he/she did not strengthen the operative skills of these technologies. Therefore, to guarantee the safe use of these technologies, proper trainings of the operative skills are of paramount importance. [15-17].

1.1.2 Training for Operating Modern Medical Technologies

Traditionally, trainees learn basic psychomotor skills while performing operations under the supervision of an expert doctor [18]. However, this method is time consuming, requires significant human resources, and does not provide a standardized means of assessing operative skills. At the same time, financial pressures on hospitals have increased due to increasing costs of malpractice insurance, surgical equipments, personnel salaries, and the cost of training young doctors. Therefore, various new facilities to train the medical operative skills, such as box trainers and virtual reality (VR) simulators, have been developed outside of the operating room.

Box trainer is a box that is used to mimic the surrounding and a part of a patient's body (e.g., abdomen). The content of the box can vary between different synthetic inanimate models (e.g., simple physical objects such as pegs), synthetically produced organs, and animal parts. Box trainers provide an environment with natural force feedback, which is obtained due to the use of conventional instruments and equipments (Figure 1.5).

VR simulators can be defined as a collection of technologies, which allow an interaction with a computer-simulated environment (Figure 1.6) [19, 20]. VR simulators are used to simulate real or imagined environment that can be experienced in various ways (e.g., visually). Some of current VR simulators are equipped with mimicked force feedback. Force feedback in VR simulators, however, is costly and not very similar to the feedback obtained when using the conventional instruments during operation.

Studies have shown that training on those kinds of box trainers and VR simulators can improve the doctors' operative skills [21]. From the clinical point of view, it is important that a doctor develops a high degree of operative skills. Without development of those basic psychomotor skills, the doctors could put a patient at risk [22, 23]. Therefore, objective evaluation methods to credential doctors as technically competent and ready to operate on a

patient are needed. Skill evaluation methods in these current training facilities, however, are still far from being objective or even missing in some regular trainings. Moreover, they do not provide general and common assessments for qualifying skill competences of doctors in different medical scenarios.

Figure 1.5: Laparoscopic training with box trainer.

Figure 1.6: VR simulator for laparoscopic training.

1.1.3 Evaluation of Medical Operative Skills

The skill level of a doctor is determined by several factors, including cognitive capabilities, decision-making, and operative dexterity [24]. The first two can be taught in classroom-style settings and are to a large degree evaluated by using traditional paper or oral examination methods. However, methods to differentiate and standardize operative skill levels for the purposes of teaching and assessing skill have proven elusive [25].

Operative skill evaluation methods basically can be divided into two categories: subjective and objective. In most of the current training facilities, such as box trainers used in routine training courses, evaluation of surgical operative skills heavily relies on subjective measures and scoring by an expert, which may be a variably biased opinion using vague criteria (Figure 1.7). The methodology for assessing surgical skill now is strongly motivated to change from subjective scoring to a more objective, quantitative analysis [26].

The VR simulators, which are now commercially available, have been comprehensively validated as a surgical data analysis tool. These simulators, which are embedded with objective skill evaluation methods, provide low-level scoring results by using the execution time and instrument trajectory information recorded during the training to assess operative skills (Figure 1.8). In addition, the embedded skill evaluation methods of VR simulators are just for those specific training devices, which cannot be used for other training devices and medical applications. Moreover, no matter how exhaustive or excellent the VR simulator might be, they can still only serve as a good complementary solution to training on real-world scenarios [27].

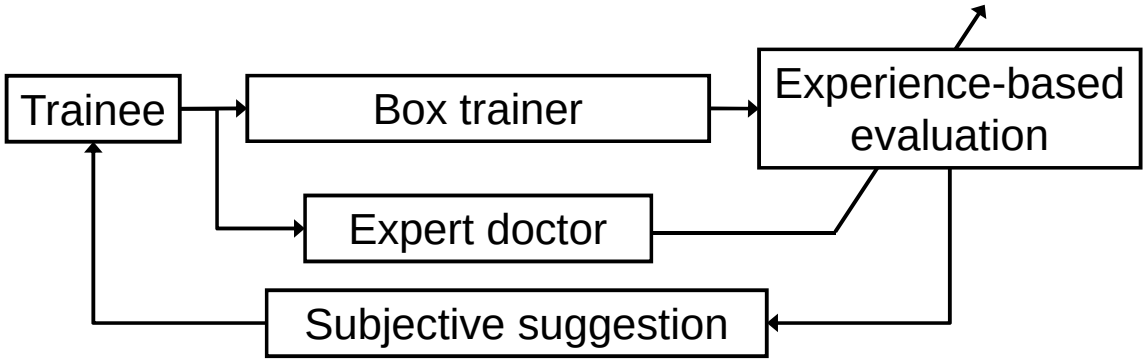

Figure 1.7: Conventional skill evaluation model of box trainer.

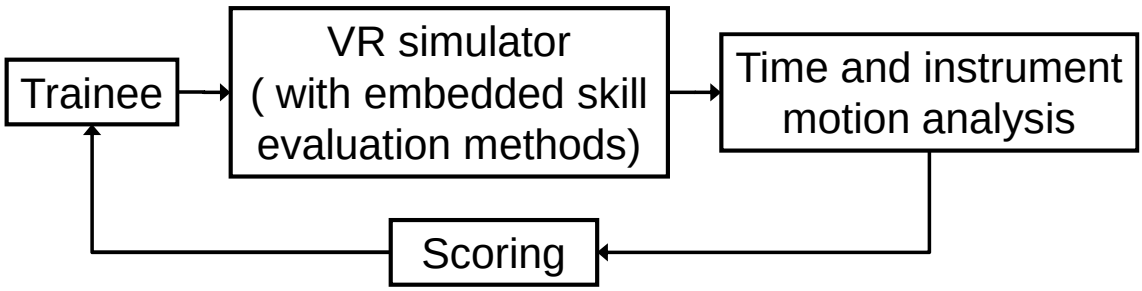

Figure 1.8: Conventional skill evaluation model of VR simulator.

1.1.4 Motion Analysis for Operative Skill Evaluation

In the literature, it has been demonstrated that fundamental operative skills for manipulating the new medical technologies can be objectively assessed by analyzing the motions of the trainees [15]. This follows the school of thought that psychomotor skill is learned and that the movements made by the trainees will eventually become more efficient. Computational analysis of operation movements acquired using a data collection system thus offers the potential to assess skill more objectively and cost effectively.

In order to use motion analysis as the assessment tool, a motion tracking system is needed to record and analyze these movements. Presently, there are a number of commercially available devices for tracking movements in medical applications. In general, one may consider the tracking system as an independent component from the training devices. These tracking systems are specific for different environments: Box trainers, VR simulators, or real operation rooms. In VR simulators such tracking systems are inherently present for measuring the instrument motion. Tracking systems that can measure both instrument and human motion during real medical operation or for various training devices are still in their infancy.

Though specific examples of various types of tracking systems are discussed in the following survey, no attempt is made to comprehensively cover the multitude of tracking systems currently available on the market or being researched. Rather, the purpose is to discuss the general limitations of the various motion tracking technologies while being applied for the evaluation of medical operative skills during regular trainings, real operation and clinical practice, and to establish the technological environment under which the new ultra-miniaturized inertial-based wearable tracking system is proposed for skill evaluation in this thesis.

1.1.5 Survey of Related Research on Motion Tracking Technologies

Motion tracking systems are intended as an interface between humans and computers. In terms of hardware, three components required in such systems can be distinguished: a source that generates a signal, a sensor that receives the signal, and a data acquisition system, which processes the signal and communicates with the computer. Depending on the technology, either the source or the sensor is attached to the object, while the other serves as a reference point and is located at a fixed point in the environment. Many of the currently used tracking systems are active; the sensor, which measures the actual movement, is attached to the target to be tracked. Passive tracking systems localize the markers or transmitters that have been placed on objects to be tracked in the field. The sole task of the tracking system is to measure the position (x, y, and z coordinates) or the orientation (yaw, pitch, and roll) of the objects with respect to a fixed reference frame.

Current technologies for human motion tracking are primarily based on mechanical tracker, optical sensing, acoustic tracker, electromagnetic tracker, inertial sensing, and hybrid tracking.

A) Mechanical tracker

Mechanical tracking systems are perhaps the oldest motion tracking technology. These systems are fairly accurate and have low latency. Performer wears a human-shaped set of straight metal pieces (like a very basic skeleton) that is hooked onto the performer's body; as the performer moves, this exoskeleton is forced to move as well and sensors in each joint feel the rotations. These angle measuring devices provide joint angle data to kinematic algorithms which are used to determine end effecter position as well as body posture.

Itoh et al. developed the Waseda bioinstrumentation system WB-1 which can measure the arm motion (Figure 1.9) [28]. The frame with 12-DOFs per arm, which consisted of 6-DOFs from the back origin to the shoulder and 6-DOFs from the shoulder to the wrist, was developed in order to follow the movements of the rotation center. This system had a serial link mechanism with a potentiometer at each joint.

Burns et al. developed an upper-limb powered exoskeleton which was an external structural mechanism with joints and links corresponding to those of the human body (Figure 1.10) [29]. Worn by the human, the exoskeleton transmitted torques from proximally located

actuators through rigid exoskeleton links to the human joints. It can be used for human motion tracking, tele-operation, rehabilitation medicine and virtual reality simulation.

The Zebris® Medical GmbH developed a jaw measurement analysis (JMA) system recorded all the 3D movements of the lower jaw without contact, using the principle based on measuring the travel time of ultrasound impulses (Figure 1.11) [30]. This system consisted of a face bow with integrated receiver sensors and a lower jaw sensor for measuring near the joint, which was optimally balanced. The reference plane, e.g. the axial-orbital plane, was entered using a probe tip. The system enabled a hinge axis to be determined i.e. in a central condyle position or as a kinematic axis from the protrusion and opening movements.

Figure 1.9: Waseda Bioinstrumentation system WB-1.

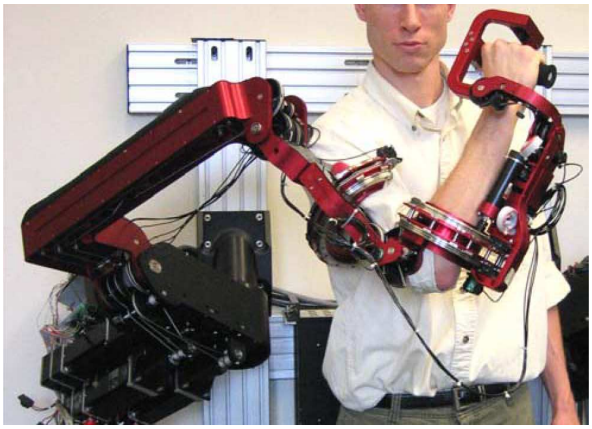

Figure 1.10: Exoskeleton composed of three joint configurations.

Figure 1.11: Zebris JMA system.

Due to variations in anthropometric measurements, mechanical tracking systems must be recalibrated for each user. This recalibration can be complicated and require an extensive period of time. The most significant drawback of these systems is user encumbrance. Users must bear the relative heavy weight of the exoskeleton as well as the annoyance of having a cumbersome framework attached to their body. The exoskeleton may make it difficult to interact with physical objects in a natural manner. For instance, in the surgical operation, it may be difficult for a surgeon to interact with other members due to the bulky mechanism of the mechanical motion tracking system. All of these problems make the mechanical tracking systems difficult to be applied for the medical applications.

B) Optical sensing

Optical sensing encompasses a large and varying collection of technologies. More researches are underway in this area than any other motion tracking technology. The cost and the performance of different optical sensing technologies vary widely. The commonality between them is the dependence upon the sensing of some types of light. It may be generated by a source under the control of the tracking system or it may be passive. Detectors may range from ordinary video cameras to lateral-effect diodes.

Most widely used optical motion tracking systems are camera-based systems which determine position by using multiple cameras to track predetermined points on moving objects within a working volume. Performer wears the markers that are followed by several cameras and the information is triangulated between them. The markers themselves may be either passive (retroreflective) or active (light-emitting diodes). The performer feels free to move due to no cables connecting body to the equipment, and more performers are possible in

the same configured environment. A great deal of research effort is currently being expended on systems which are able to track natural objects in real-time without adding markers.

The Vicon Company developed camera-based motion tracking system using light sources placed very near each camera to generate light (Figure 1.12) [31]. This system used cameras to rapidly acquire three-dimensional coordinate positions from reflective markers placed on the subjects. Images were processed within the optical sensing cameras where markers were identified and the coordinates were calculated before being transferred to the computers. After the completion of the movements, the system could provide 3D coordinate and kinematic data. During the post-processing of the motion capture data, an operator of the system must assist with marker identification.

The Optotrak system manufactured by Northern Digital, Inc. utilized three linear CCDs in a single instrument (Figure 1.13) [32]. This provided both excellent spatial accuracy (claimed to be better than 0.1 mm) as well as high sampling rates up to 4600 Hz. Markers were IR LEDs which were pulsed sequentially so that as the number of markers increased, the sampling rate decreased. The Optotrak had a measurement volume about 7.0 x 4.2 x 3.0 m and can track up to 512 markers, thus allowing very detailed motions to be captured. Its disadvantages included subject encumbrance by the trailing cables that strobe the markers and provided power, and only one side of the body can be studied with a single instrument.

Figure 1.12: Vicon motion capture system.

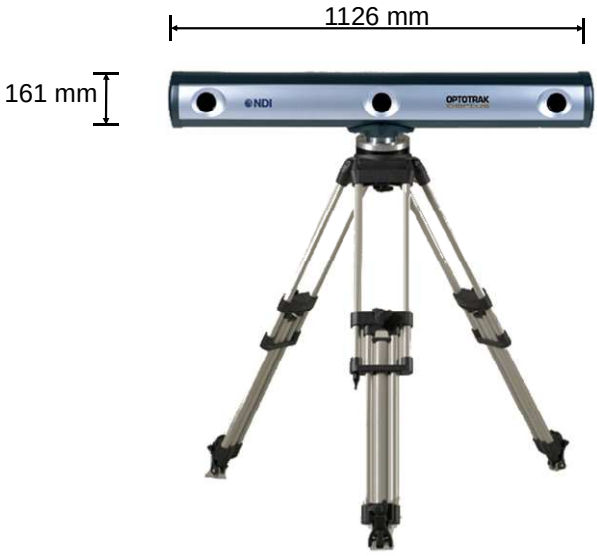

Figure 1.13: Optotrak motion tracking system.

Figure 1.14: Organic Motion STAGE markerless motion capture system.

Organic Motion, Inc. developed the world's first commercially available markerless motion capture system named STAGE (Figure 1.14) [33]. It introduced several unprecedented features for real-time 3D human tracking. This breakthrough technology unlocked human motions and freed the subject – allowing every person to be sized and tracked instantly without wearing any kind of physical markers. STAGE had a scan space up to 4 x 4 x 2.5 m in a configured room, positional accuracy up to 1.0 mm and rotational accuracy up to 1 deg. These high performances allowed it to radically redefine the motion capture techniques for the applications in animation and entertainment industries.

In general, most of the marker-based optical sensing technologies for motion tracking suffer from occlusion problems whenever a required light path is blocked. Interference from other light sources may also be a problem. Lighting conditions must be controlled in order for the camera to consistently see objects in the environment. Depending upon the type of light in use, there may be severe range limitations. Therefore, these systems in fact can be used only in the calibrated room, but not outdoor. The marker used for motion tracking should be always be seen by several cameras, which cannot be satisfied at all times, for example if we consider the movement measurements of the appending surgeons inside real operation room, which might be interfered by the surrounding assistants. Even the markerless motion capture systems require the objects always be in sight. Moreover, these systems normally can track the positions of the object, but if we want to calculate the orientations of the object, at least 3 markers are needed, which might be a problem for measuring some small object's orientations, such as some small surgical instruments or even surgeon's fingers. For many of these systems which are relatively high accuracy or without the data sorting problems, the costs are quite high.

C) Electromagnetic tracker

Electromagnetic tracking devices function by measuring the strength of the magnetic fields generated by sending current through three small wire coils, oriented perpendicular to one another. These three coils are embedded in a small unit that is attached to whatever the system needs to track. The current has the effect of making each wire into an electromagnet while the current is flowing through it. By sequentially activating each of the wires, and measuring the magnetic fields generated on each of three other perpendicular wire coils, it is possible to determine the position and orientation of the sending unit. These systems are relatively cost-effective solutions for motion tracking. They can provide reasonable accuracy with no serious obstruction or shadowing problems.

One of the most well-known producers of electromagnetic sensor technology was Polhemus Liberty 240/8 [34]. This system provided extremely low latency (less than 4 ms) and had the ability to track multiple objects concurrently in 240 Hz update rate with a measurement rang of 1.8 m. Liberty included a system electronics unit (SEU), one sensor and one source. It also allowed us to expand the system by adding three additional sensors and

with the factory installation of an additional circuit board, four more for a total of eight sensors (Figure 1.15). The source contained electromagnetic coils enclosed in a molded plastic shell that emit magnetic fields. The source was the system's reference frame for sensor measurements.

Northern Digital Inc. developed the Aurora electromagnetic measurement system with 6 DOF measurements which can be achieved with a single miniaturized sensor (Figure 1.16) [35]. Aurora had a maximum update rate at 40 Hz and measurement volume about 500 x 500 x 500 mm. The sensor coil and lead wires were surrounded by a protective material which facilitates integration. These sensors were designed for tool integration where a small diameter was the dominant requirement (e.g. needles, multi-lumen catheters, and miniaturized medical instruments).

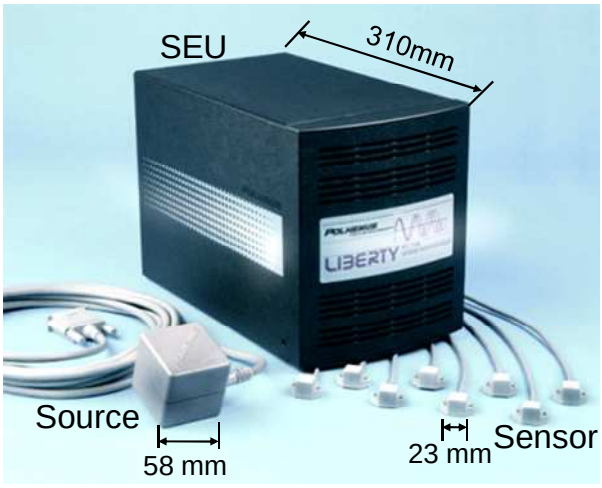

Figure 1.15: Plohemus liberty electromagnetic tracking system.

(a)System control unit.　　(b) Sensor coil.

Figure 1.16: Aurora electromagnetic measuring system.

The susceptibility of magnetic tracking systems to interference makes them unsuitable for robust synthetic reality applications. The presence of any magnetic materials or power sources within or near the working volume can severely degrade performance. Perhaps even more critical limitation is the limited measurement volume of these devices. This limitation makes it nearly impossible to track more than one user in wide working area and restricts the size of the measurement volume to that of a small room. The measurement volume problem limits this kind of motion capture system for the applications of surgical training and operation, where the working areas normally are relative broad.

D) Acoustic tracker

Acoustic or ultrasonic trackers are an inexpensive alternative to magnetic trackers. They provide modest accuracies and update rates. Acoustic tracking devices use ultrasonic sound waves for measuring the position and orientation of the target object. There are two ways of doing this: so-called time-of-flight tracking and phase-coherence tracking. Time-of-flight tracking works by measuring the amount of time that it takes for sound emitted by transmitters on the target to reach sensors located at fixed positions in the environment. The transmitters emit sounds at known times, and only one is active at a time. By measuring when the sounds arrive at the various sensors, the system can determine the length of time it took for the sound to travel from the target to the sensors, and thereby calculate the distance from the target to each of the sensors. Phase coherence tracking works by measuring the difference in phase between sound waves emitted by a transmitter on the target and those emitted by a transmitter at some reference point.

The Hexamite Company developed an indoor ultrasonic positioning system HX17 (Figure 1.17) [36]. It utilized modulated signal exchange to extract precision position timing. Three basic components were used to form a HX17 network, i.e. ultrasonic receiver hx17rx, ultrasonic tags hx17tx and a network reader hx17nr. The HX17nr synchronized the network and collected tag IDs plus time of flight of the ultrasonic signal. This data was transmitted to a readout device like the PC through a USB port. Using multiple networks an object can be positioned coverage up to 2100 m^2 per network at 9mm absolute accuracy

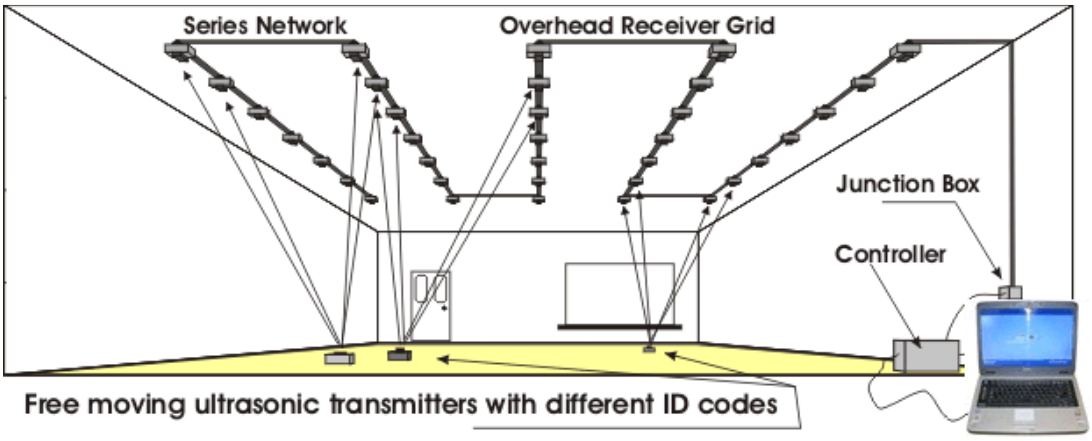

Figure 1.17: HX17 ultrasonic positioning system.

These systems typically suffer from a low update rate, brought about by the low speed of sound in air. The speed of sound in air is also affected by such environmental factors as temperature, barometric pressure, and humidity. Since they work by periodic updates of position, rather than by measuring absolute position at each time step, phase-coherence tracking devices are subject to error accumulation over time. Moreover, the transmitters used in these systems are relatively big and heavy, which might be not sufficient enough for human motion tracking.

E) Inertial sensing

Inertial sensing technology is a relative newcomer to the motion tracking area. It is based on miniature inertial sensors, biomechanical models and sensor fusion algorithms. The motion data of the inertial sensors is often transmitted wired or wirelessly to a computer, where the motion is recorded or viewed. A naive approach to inertial orientation tracking would simply involve a single integration of angular rate data to determine orientation. However, this solution, which is found using only one type of sensor, would be prone to drift over time due to the buildup of small bias and drift errors. In order to avoid drift, inertial tracking systems make use of other complementary sensors to continuously correct the orientation estimate. Commonly, these sensors include an inclinometer or accelerometers to sense the vertical gravity and a set of magnetometers to sense the direction of the local magnetic field. In order to track all orientations, there must be a separate accelerometer, rate sensor and magnetometer

for each of the three coordinate axes of a rigid-body. Benefits of using inertial systems include: high performance, wearablility, portability, and large measurement volume.

Zecca et al. developed a bioinstrumentation system WB-2R which can measure the movements of whole body by using twelve inertial measurement units (IMUs) for upper body and eight IMUs for lower body (Figure 1.18) [37]. The communication between all the IMUs and PC was by using Bluetooth devices. Therefore, it can realize a portable and wearable motion tracking system used for different kinds of applications, such as human-robot interaction, surgical skill evolution, and so on.

Xsens Company developed a motion capture system named MVN BIOMECH (Figure 1.19) [38]. It was based on state-of-the-art micro-electro-mechanical systems (MEMS) of inertial sensors, biomechanical models and sensor fusion algorithms. MVN BIOMECH was ambulatory, can be used indoors and outdoors regardless of lighting conditions. It consisted of 17 MTx inertial sensors attached to the body by a lycra suit (also available in straps), which can provides 6 DOF tracking of the whole body.

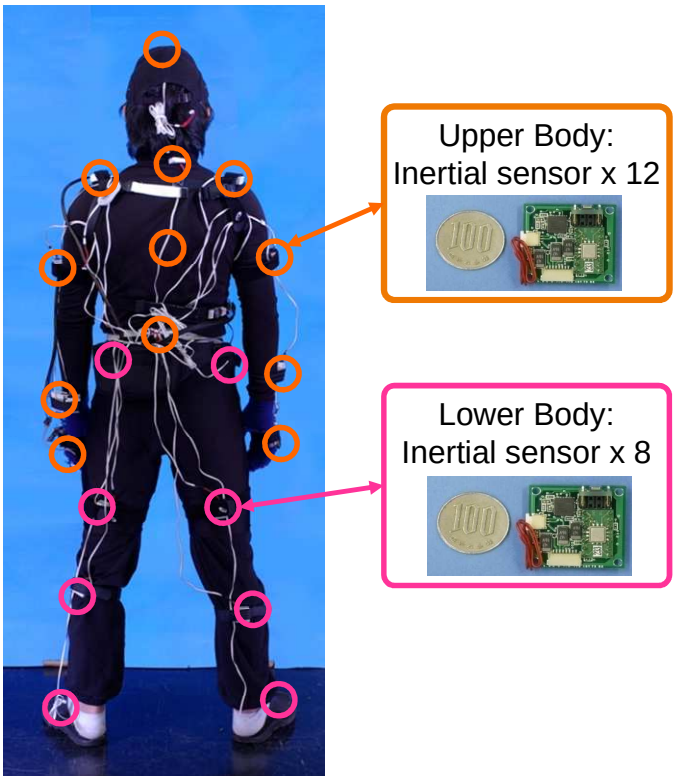

Figure 1.18: Waseda Bioinstrumentation system WB-2R.

Figure 1.19: MVN BIOMECH system of Xsens Company.

The main limitation of the inertial sensing technology in the current state is that the sizes of the inertial trackers are not compact enough for measuring some small object's motion. The wearable performance limits the application scopes of these systems. For example, the sizes and weights of most current inertial sensing systems are still too big to be attached to some microsurgery instruments, which are normally with the size from 50 to 150 mm, and weight from 20 to 50 g [39].

F) Hybrid tracking

Each type of tracking technology has its own set of strengths and weaknesses. Many systems use one type of technology for sensing orientation changes and another for sensing position. Some merely use two separate technologies and choose whatever estimate seems to be the most accurate at a particular time instant. The best systems take data from multiple sensor types and use filtering algorithms to combine them and arrive at some type of optimal estimate.

Kinect is a controller-free gaming and entertainment experience interface developed by Microsoft Corporation for the Xbox 360 video game platform (Figure 1.20) [40]. Based around a webcam-style add-on peripheral for the Xbox 360 console, Kinect enables users to

control and interact with the Xbox 360 without the need to touch a game controller, through a natural user interface using gestures and spoken commands. The Kinect consists of a RGB camera, two depth sensors and multi-array microphone, which provide full-body 3D motion capture, facial recognition and voice recognition capabilities. The depth sensor consists of an infrared laser projector combined with a monochrome CMOS sensor, which captures video data in 3D under any ambient light conditions. However, the Kinect has a practical ranging limit of 0.7 to 6 m distance, and performs overall position and gesture estimate of human motion with detail and high accuracy information.

Corrales et al. introduced a human tracking system based on the integration of the measurements from an inertial motion capture system and an ultra wide band (UWB) location system [41]. On the one hand, the rotational measurements from the inertial system were used to track precisely all limbs of the body of the human. On the other hand, the translational measurements from both systems were combined in order to obtain a precise global localization of the human in the environment.

Ogris et al. demonstrated how ultrasonic hand tracking can be used to improve the performance of a wearable, accelerometer and gyroscope based activity recognition system [42]. He introduced several methods of fusing the ultrasound and motion sensor information.

Although the hybrid tracking systems can combine the advantage of various different tracking technologies, more hardware or facilities generally are needed in order to acquire more motion information, which will result in more expense and more complicated system configuration.

Figure 1.20: Kinect from Microsoft Corporation.

1.1.6 Summary of Motion Technologies for Medical Skill Evaluation

A brief survey of tracking technologies which are currently being researched or commercially marketed was discussed above. Through these investigations, it is clear that all of the tracking devices have their own advantages and disadvantages, and have good performance capabilities for some environments and tasks, and fail on others.

In order to develop a objective operative skill evaluation system which can be adaptive to various medical applications based on motion analysis, several key aspects of the tracking technologies are considered to be significant important in this thesis: accuracy; price; measurement volume; wearability; portability; implementable environment. A comparison among all the tracking technologies at these aspects is listed in Table 1.1.

Table 1.1: A comparison among all the tracking technologies.

	Accuracy	Price	Measurement Volume	Wearability	Portability	Environment
Mechanical tracking	Low	Low	High	Low	High	BT, VR, CP
Optical tracking	High	High	Medium	Medium	Low	BT, OR, CP
Electromagnetic tracking	High	Medium	Low	Medium	Medium	BT
Acoustic tracking	Low	Low	Medium	Low	Low	BT
Inertial tracking	Medium	Low	High	High	High	BT, VR, OR, CP
Hybrid tracking	High	High	Medium	Low	Low	BT, CP

Here, BT means box trainer; VR means virtual reality; CP means clinical practice; OR means operation room.

Box trainer approaches (Non-VR approaches) for operative skill evaluation have focused on instrument movements and trainee's hand motion tracking, and have derived various metrics of varying skill levels. Most of these researches are using mechanical, electromagnetic or optical sensing technologies for tracking the tips of instruments or trainee's hands motion, and provide only the trajectory and average moving speed information for the skill evaluation. However, the trainee's body motion analysis which is also considered as an important feature for the skill evaluation is still missing, due to the poor wearability of these tracking technologies which are not suitable enough for putting on human body. The

skill evaluation based on both the instrument and human body motion analysis has been still elusive.

The VR approaches provide only the training instrument's motion information for the skill evaluation by using the electromagnetic sensing technologies. These evaluation methods are limited to those specific simulators, and moreover, they cannot analyze the trainee's body motion for more insight information of the skill levels.

Considering all the characteristics of tracking technologies listed in Table 1.1, the inertial tracking technology is chosen in this thesis for realizing the comprehensive operative skill evaluation system capable of analyzing instrument and human body motion. Inertial tracking technology satisfies most of the required aspects and performance to develop a common skill evaluation system for various medical trainings and applications. It allows us to measure the trainee's body motion data and instrument movements with high wearability and portability performance.

1.2 Problem Statement

Among all the current training devices, there is one common need, which is the objective skill evaluation system. Objective skill assessment which is more reliable than the subjective method could provide insight of doctors' operative skill competence and verify whether the doctors have qualified abilities for the real operation on the patients. Moreover, objective skill evaluation could provide quantitative feedback to doctors to improve their skills more efficiently. Objective evaluation of operative skills is a very important factor in developing an effective training curriculum, as it also motivates trainees to actively engage with the regular training tasks.

However, the skill evaluation systems on most of the current training facilities have several limitations, which can be basically summarized into three aspects:

1) In the cases of box trainers, evaluation of operative skills heavily relies on subjective measures and scoring by an expert doctor, which may be a variably biased opinion using vague criteria. In the cases of VR simulators, they provide only low-level skill scoring by using the execution time and instrument's motion information for completing the training tasks, without quantitative body motion information feedback to the trainees.

2) The current skill evaluation methods in VR simulators, which are embedded with those specific training devices, could not be extended to be used for other medical training systems, such as box trainers. This will result in increasing the financial burden for hospitals to purchase different kinds of skill evaluation systems, in order to evaluate doctors' skills in different medical fields. An independent and common skill evaluation system combining body and instrument motion analysis is still missing.
3) Most of the current skill evaluation methods can only be used for evaluating surgical skills during regular trainings, but could not be further implemented in clinical practice or other medical scopes.

1.3 Goal of this Thesis

1.3.1 Aims

The routine operative training involves a multidimensional series of tasks requiring the doctors to satisfy the psychomotor skill requirements in handling the operation instruments. It has been demonstrated that motion analysis is a valuable objective skill assessment method for the fundamental training.

Therefore, the goal of this thesis is to develop an ultra-miniaturized motion analysis system for medical operative skill evaluation in various medical applications, which is covering three aims:

1) to develop an ultra-miniaturized human motion tracking system suitable for analyzing the motion of medical instruments and trainee's upper body during both the box trainer trainings and VR trainings.
2) to develop a common skill evaluation system based on the human motion analysis, which is independent from the training devices and can be adaptive for various medical training scenarios.
3) to verify the proposed skill evaluation system can be implemented in multiple medical applications for evaluating the surgical operative skills and assisting clinical practice.

1.3.2 Innovation

This research demonstrates a general methodology for objectively evaluating the medical operative skills based on motion analysis.

The resulting system, which is separated from the training devices, constructs a motion tracking system capable of accurately determining human body gestures and instrument movements for classifying the skill levels of the trainees with different operative experience.

The motion-based skill evaluation system, which benefits from its ultra-miniaturized design and high performance, can be used not only for regular surgical operative skill trainings, but can be also further implemented for clinical practice and other medical scenarios.

1.3.3 Contribution of this Research

This research develops two versions of ultra-miniaturized inertial-based motion analysis system for skill evaluation that overcome the limitations of medical skill training and evaluation systems currently in use.

The developed motion analysis systems are capable of providing wide area tracking of instrument and trainee's motions during various training tasks. Therefore, the proposed methodology for skill evaluation can provide objective and quantitative motion information to the trainees for improving the training efficiency.

Three different medical applications of laparoscopic surgery, neurosurgery and mastication analysis are assessed in this thesis, which verifies that the proposed skill evaluation system can be implemented in various medical fields.

1.4 Methodology

The proposed methodology block diagram is showed in Figure 1.21. The subject block in the diagram indicates the doctors whose operative skill needed to be trained and evaluated, or the patients whose motion performance needed to be assessed for clinical practice. This methodology can combine the objective skill evaluation from motion analysis with subjective evaluation from expert doctors, in order to integrate the advantages of both methods. The blocks with blue color are the primary novel items and contributions of this thesis.

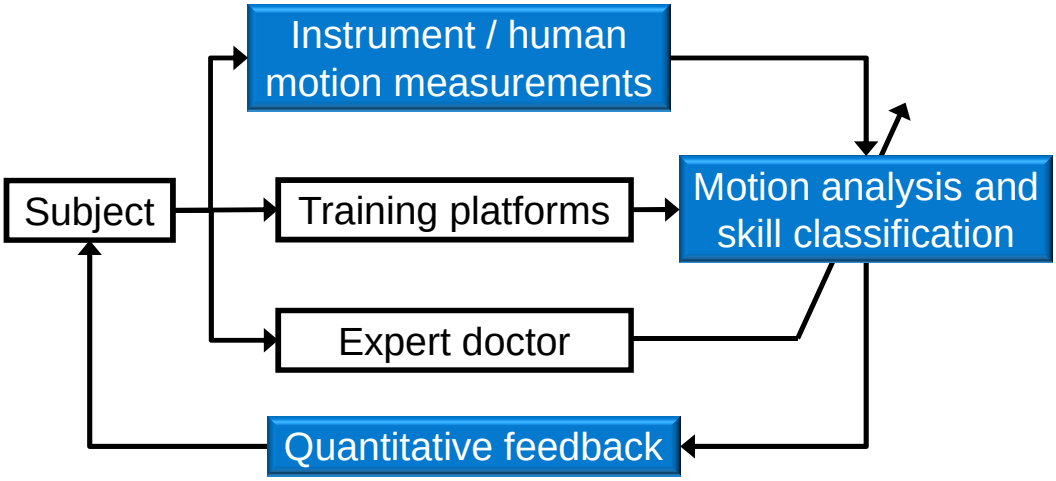

Figure 1.21: Proposed skill evaluation methodology.

Block of instrument/human motion measurements: The developed motion tracking systems are used for the instrument and human motion measurements. They can record the motion data of the subjects or the manipulated instruments during various skill training tasks, and provide this information as the basis for skill evaluation.

Block of training platforms: They can be the box trainers and VR simulators in different medical applications, or certain clinical diagnosing practice, such as mastication.

Block of motion analysis and skill classification: It extracts the significant motion features and classifies the skill levels of the subjects based on the statistical pattern recognition model.

Block of quantitative feedback: It provides the motion information of the significant features to the subjects, and presents which motion still has poor performance and needed to be improved.

1.5 Thesis Outline

This thesis contains three primary parts: Part I introduces the robust ultra-miniaturized wearable motion capture systems developed in this thesis, and evaluates the system performance; Part II deals with the evaluation of surgical operative skills based on analysis of subject's upper body motion in the fields of laparoscopic trainings and neurosurgery trainings; and Part III introduces the extended application of the proposed skill evaluation system for clinical practice of masticatory performance evaluation in order to assist clinical diagnosing

and treatment of dental diseases. Figure 1.22 shows the research flow in this thesis and the relation between each chapter. The remainder of the thesis is laid out as follows:

I. To develop robust ultra-miniaturized inertial-based motion tracking systems for evaluating the operative skill and motion performance during surgical training and clinical practice.
   - Chapter 2 introduces the development of two versions of motion tracking system: WB-3 and WB-4. WB-3 system and WB-4 system are based on the use of wired inertial measurement units and wireless inertial measurement units, respectively.
   - Chapter 3 studies the rigid body orientation estimate by using quaternion-based extended Kalman filter (EKF) algorithm, and introduces the biomechanical analysis of human upper limb with different joint movements.

II. To evaluate the surgical operative skills during regular trainings by using the proposed skill evaluation methodology.
   - Chapter 4 describes the use of WB-3 system to evaluate the expert surgeons and novice students' surgical operative skills during regular laparoscopic training tasks based on the kinematics information analysis of upper body.
   - Chapter 5 presents the application of the proposed skill evaluation system in neurosurgery. A simple pick and place test is evaluated with a group of non-medical novices and one professional neurosurgeon. The skill evaluation is based on the analysis of the instrument motion acquired by WB-3 system.

III. To apply the proposed skill evaluation system for mastication analysis which is significant important to the clinical diagnosing and practice.
   - Chapter 6 describes the use of the proposed skill evaluation system to evaluate the mastication performance. The experiments are elaborated by free chewing of three types of food with different shapes and hardness, and chewing gum by different sides of molars. The WB IMUs are attached to the subject's mandible in order to track the jaw motion.

Finally, Chapter 7 concludes the evaluation results and considerations in this thesis, and discusses about the future work which are proposed as a perspective to continue the research direction.

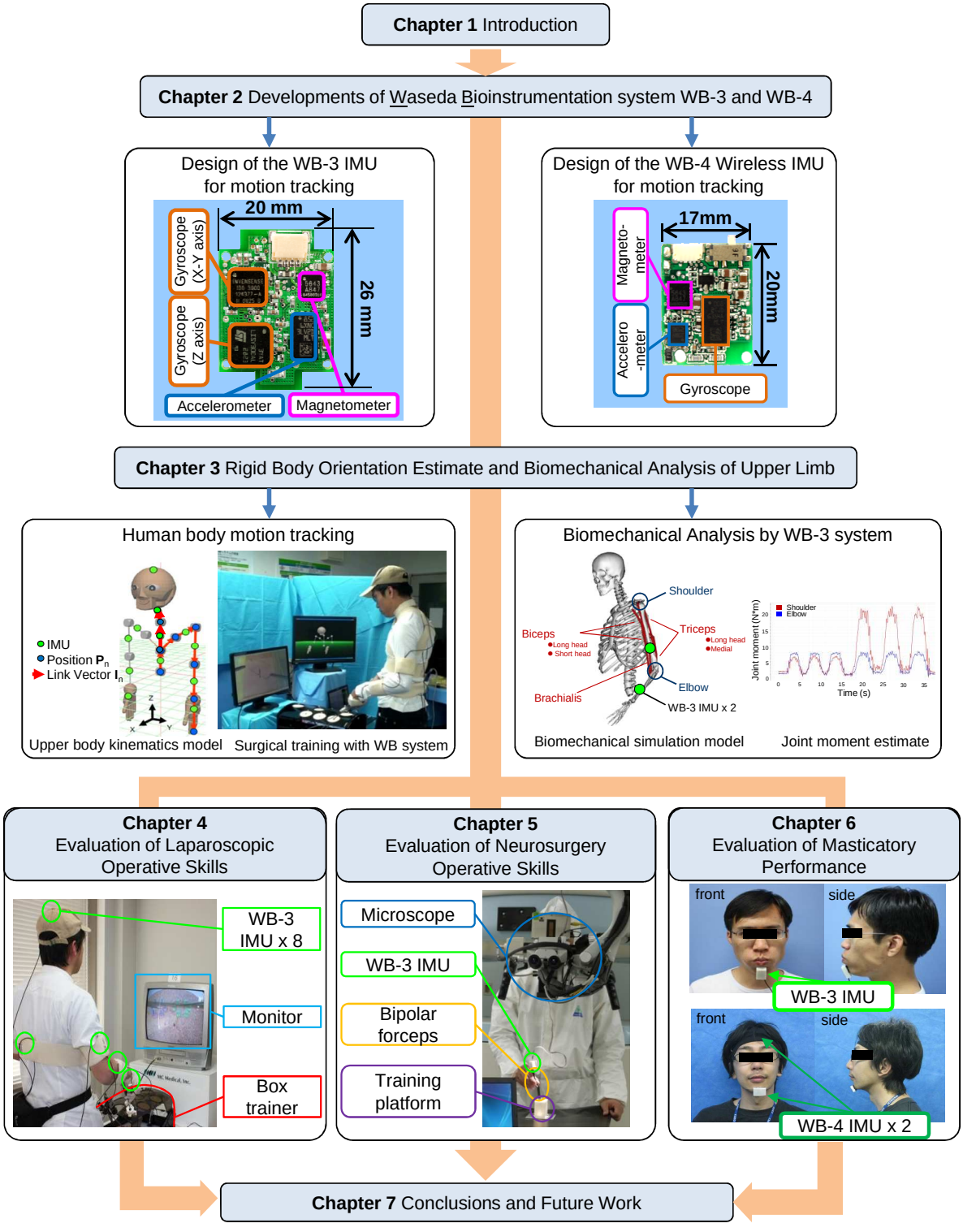

Figure 1.22: Flow chart of thesis chapters.

Chapter 2

Developments of Waseda Bioinstrumentation System WB-3 and WB-4

2.1 Introduction

2.1.1 Background

In the last years the interest on motion tracking systems is increased in many application fields. Medical applications, for example, paid a growing attention to human motion tracking systems to obtain more efficient rehabilitation therapies [43, 44], and to build monitoring networks for patients and elder people in the hospitals and in their own homes [45-47]. In game industry, the market trend is towards active game platforms, where a smart wearable motion capture suite could expand the capability of this kind of games and open total virtual reality scenarios at the edge of the augmented reality. Moreover, distributed sensors architectures for motion capture would be hosted on different structure of robots, like manipulators and rovers. Industrial manipulators, small smart arms and, in general, exoskeleton parts with these sensors and cognition capability could help people to avoid any physical risk in object manipulation and environment interaction.

Although several motion tracking technologies have been developed in the past years, such as optical [48], mechanical [49], magnetic, and acoustic [50] described in chapter 1, these methods do not cover all the application fields discussed above. For example, optical motion tracking systems are preferred in the computer-animation community, in the film industry and medical contexts [51, 52], because they offer a reliable and accurate way to record the motions of complex systems; however, these approaches are expensive and poor in portability. In fact, these systems use 3D markers, such as light-emitting diodes or passive reflectors, placed on the body. They compute the exact locations of the markers from the images recorded by the surrounding cameras using triangulation methods; therefore, they can be used only in a structured environment.

A very promising frontier on the wearable and reliable motion tracking system is based on inertial sensors which can be virtually used everywhere. Inertial sensor based tracking is appealing due to a lack of dependence on an artificially generated source. It thus does not suffer from range limitations and interference problems of sourced technologies. All delay or latency is due to data processing and transmission. The availability of low-cost, small-size micro-electro-mechanical systems (MEMS) inertial sensors has made it possible to build wrist-watch-sized, self-contained inertial/magnetic sensor modules for human motion tracking [53, 54].

2.1.2 Inertial Sensors

A) Accelerometer

An accelerometer measures proper acceleration, which is the acceleration it experiences relative to freefall and is the acceleration felt by people and objects. Such accelerations are popularly measured in terms of G-force. An accelerometer at rest relative to the Earth's surface will indicate approximately 1G downwards, because any point on the Earth's surface is accelerating downwards relative to the local inertial frame.

An accelerometer behaves as a damped mass on a spring. A single axis accelerometer consisting of a mass, suspended by a spring in the housing is showed in Figure 2.1. When the accelerometer experiences an acceleration *a*, the mass is displaced to the point that the spring is able to accelerate the mass at the same rate as the casing. The displacement is then measured to give the acceleration. The mass is allowed to move in one direction which is the

sensitive direction of the accelerometer. Springs (within their linear region) are governed by a physical principle known as Hooke's law. Hooke's law states that a spring will exhibit a restoring force which is proportional to the amount it has been expanded or compressed. Specifically, $F = kx$, where k is the constant of proportionality between displacement x and force F. The other important physical principle is that of Newton's second law of motion which states that a force operating on a mass which is accelerated will exhibit a force with a magnitude $F = ma$. This force causes the mass to either compress or expand the spring under the constraint that $F = ma = kx$. Hence if we observe a displacement of x, we know the mass has undergone an acceleration of $a = kx/m$. In this way, the problem of measuring acceleration has been turned into one of measuring the displacement of a mass connected to a spring.

In order to measure multiple axes of acceleration, this system needs to be duplicated along each of the required axes. A 3D accelerometer, based on only one mass with three translational degrees of freedom was constructed by Lötters et al. [55]. Lötters used a capacitive distance measurement in three directions to measure the displacement of a cubic mass, suspended in its housing by rubber springs (Figure 2.2). The measured displacement can be related to the difference between acceleration and gravity in the same way as in the case of a single axis accelerometer. The 3D displacement of the mass with respect to the housing is measured capacitively, enabling the sensor to be used as a 3D accelerometer

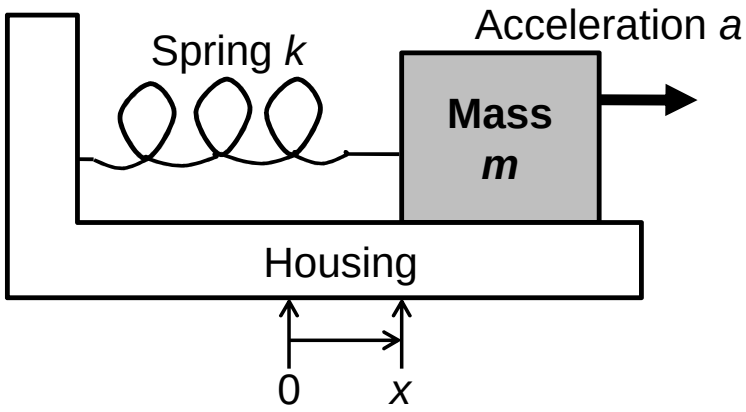

Figure 2.1: A single axis accelerometer experiencing acceleration on the base to the right resulting in an expanded spring.

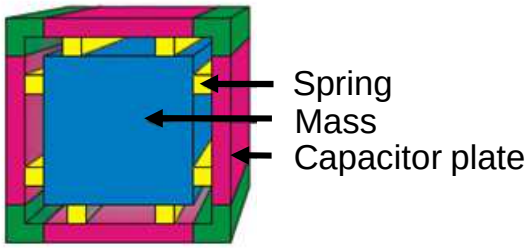

Figure 2.2: Schematic representation of the accelerometer designed by Lötters.

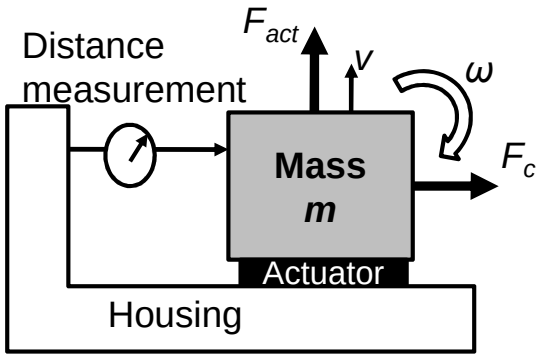

Figure 2.3: 2D view of a typical single axis vibratory gyroscope design.

B) Micromechanical vibratory gyroscope

The micromechanical vibratory gyroscopes are small, inexpensive and have low power requirement, making them more ideal for human movement analysis than other gyroscopes, such as solid-state gyroscopes, laser ring gyroscopes, and fiber optic gyroscopes which cannot be miniaturized. A 2D view of a typical vibratory gyroscope design is drawn in Figure 2.3. It consists of a mass that is actuated in the direction given by F_{act}, often using a piezoelectric element. The displacement of the mass m is measured in the direction perpendicular to the actuation direction. When the gyroscope is rotated, the mass will not only vibrate in the actuation direction, but will also undergo an additional displacement in the direction perpendicular to both the momentary mass speed v and the angular velocity vector ω. Thus this additional displacement, also known as the Coriolis effect, is used as a measure of angular velocity, given by $F_c = -2m(\omega \times v)$. Like the 3D accelerometer setup, a 3D gyroscope can be assembled using three single axis gyroscopes.

2.1.3 Magnetometer

Magnetometers can sense the direction of the local magnetic field. Thus, use of data from these complementary sensors can be used to eliminate the drift by continuous correction of the orientation obtained using gyroscope data.

MEMS magnetic sensors or magnetometers can use several different methods to sense the local magnetic field. Hall effect sensors consist of a conducting material, usually a semiconductor, through which a current is passed. In these sensors, changes in anisotropic magnetoresistance occur when a magnetic field is applied perpendicular to the current flow. Two magnetoresistive sensing elements or contacts may be placed on opposite corners of the device. Sensing contacts are also placed on the remaining corners of the device, opposite each other and perpendicular to the current flow. Changes in the magnetic field perpendicular to the plane of the contacts are detected as a change in the potential difference between the two sensing contacts.

2.1.4 Inertial Measurement Unit

The inertial sensor based motion tracking system basically consists of a set of inertial measurement units (IMU), which are attached to the human segment for tracking human gesture. The IMU normally is composed of a three axial accelerometer, a three axial gyroscope and a three axis magnetometer, approximately mounted in one unit. In theory, a calibrated IMU measures 3D angular velocity, 3D acceleration and 3D local earth magnetic value with respect to the sensor housing. Given an initial position and orientation, ideally these signals would contain sufficient information to derive the IMU kinematics completely.

There are currently some commercial products of IMUs available on the market for human motion tracking. Xsens Company developed the MTx IMU with size at 53 x 38 x 21 mm and weight at 30 g for human motion capture (Figure 2.4) [38]. This module was integrated a 3D magnetometers, with an embedded processor capable of calculating the orientation by Kalman filter, as well as outputting calibrated 3D linear acceleration, rate of turn (gyro) and (earth) magnetic field data.

InterSene Inc. developed the InertiaCube3 with size at 39 x 26 x 15 mm and weight at 17 g (Figure 2.5) [56], which provided 3-DOF orientation tracking for mobile applications, and

autonomous head and body tracking applications. InertiaCube3 integrated nine discrete sensing elements with Kalman filtering algorithms for the data fusion.

MicroStrain. Inc developed the 3DM-GX3 with size at 44 x 25 x 11 mm and weight at 11.5 g (Figure 2.6) [57], which had similar functions with MTx and InertiaCube3. This module was aimed at the applications of animation, navigation, and machine tools of manufacturing.

Figure 2.4: MTx of Xsens Company.

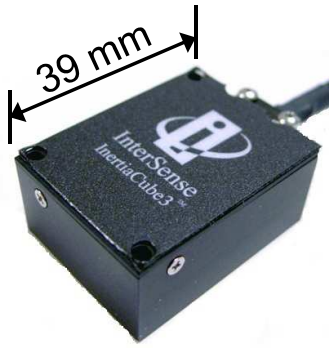

Figure 2.5: InertiaCube3 of InterSense Inc.

Figure 2.6: 3DM-GX3 of MicroStrain Inc.

2.1.5 Problems Statement

The above introduced commercial IMUs with high performance, however, are accompanied by some limitations, especially for the medical applications. The size and weight of those commercial IMUs are still relative too big to be attached on some small objects for motion tracking, such as the bipolar forceps (header size 94 x 10 x 10 mm and weight 34 g) used in neurosurgery [39]. While using these IMUs for tracking the orientation of small instruments, they might affect surgeon's performance due to the poor system wearability.

2.1.6 Objective

This research, therefore, is to develop ultra-miniaturized inertial-sensor-based motion tracking system for surgical motion analysis and operative skill evaluation.

- The light weight and compact size make the system possible to realize a better wearable and portable motion tracking system, which extends the prospect of the system applications to more various medical scenarios.
- The ultra-miniaturized motion tracking system is the key component of the proposed skill evaluation methodology discussed in Chapter 1. The resulting skill evaluation system based on this ultra-miniaturized motion tracking system is independent from the skill training devices so that it could be adaptive to different medical applications, which achieves the goals of this thesis.

Therefore, two different versions of motion tracking system: wired and wireless, have been developed in this thesis, respectively named as WB-3 system and WB-4 system. The detail information of each motion tracking system will be discussed in the following sections.

2.2 Design of WB-3 System

2.2.1 System Specification

To determine the minimum system requirements for motion tracking performance, it is necessary to analyze the speed and frequency of human motion. Since the hand and arm motions represent the quickest motions of the body, it can be assumed that a system capable

of tracking the hands and arms will be able to track the rest of the body [58]. Especially in surgical trainings and operations, the operative skills are strongly related to the movements of surgeons' upper limbs.

Normal arm movements are accomplished with wrist tangential velocities of up to 3 m/s and motion bandwidth less than 5 Hz [18, 59]. Based on these values, a sampling rate on the order of 10 Hz would satisfy the requirements of the Nyquist sampling theorem [60]. In applications using sensors which are susceptible to noise, a general rule of thumb calls for 20 times oversampling. Thus, if 5 Hz is taken as the normal bandwidth of hand motions, human motion tracking requires a sampling rate of 100 Hz. For the wrist or elbow, a change of approximately 2 deg can be perceptible by human. The case of shoulder rotation is about 0.8 deg [61]. Therefore, the motion tracking system should be capable of achieving orientation resolution less than 0.8 deg and accuracy within 2 deg in the dynamic conditions (wrist and elbow rotations), which will not be in conflict with the kinaesthetic nervous system of the users.

In order to realize a more wearable and portable motion capture system for skill evaluation in medical applications, the size and weight of the hardware system specification are significant required in this research. The size and weight of the developed system should be miniaturized 50% less than most products currently in the market. At the meantime, the system price should be comparable with the commercial products. The WB-3 IMU performance requirements have been summarized in Table 2.1.

Table 2.1: System requirements of WB-3 IMU.

Parameter	Value
Size [mm]	<30 x 30 x 10
Weight [g]	<10
Power consumption [mW]	<200
Sampling rate [Hz]	>100
Resolution [deg]	<0.8
Accuracy [deg]	<2
Cost [USD]	<2000

2.2.2 Materials and Methods

A) System overview

The WB-3 system primarily consists of twelve WB-3 IMUs which are used to measure and analyze human's upper body movements (Figure 2.7). The human segments to which the IMUs attached are: left hand; left forearm; left upper arm; left shoulder; right hand; right forearm; right upper arm; right shoulder; head; neck; back and trunk. Therefore, each IMU could be used for tracking the orientation of each human segment on the upper body. The communication between all the IMUs and PC is performed using CAN BUS interface at 1 Mb/s.

B) WB-3 Inertial Measurement Unit

A picture of the WB-3 IMU which is very compact and lightweight (size 26 x 20 x 8 mm and weight 2.9 g), is showed in Figure 2.8. This IMU was designed by using the Altium Designer software from Altium Company [62]. The layer configuration of printed circuit board (PCB) is shown in Figure 2.9. It contains 6 layers for signal, power and GND routing, which results in the current compact size.

The WB-3 IMU is primarily composed of a microcontroller STM32F103CBT6 and the following sensors: 3-axis accelerometer LIS3LV02DL; 2-axis gyroscope IDG300; 1-axis gyroscope LISY300AL; and 3-axis magnetometer HMC5843. The sensor characteristics of WB-3 IMU have been summarized in Table 2.2.

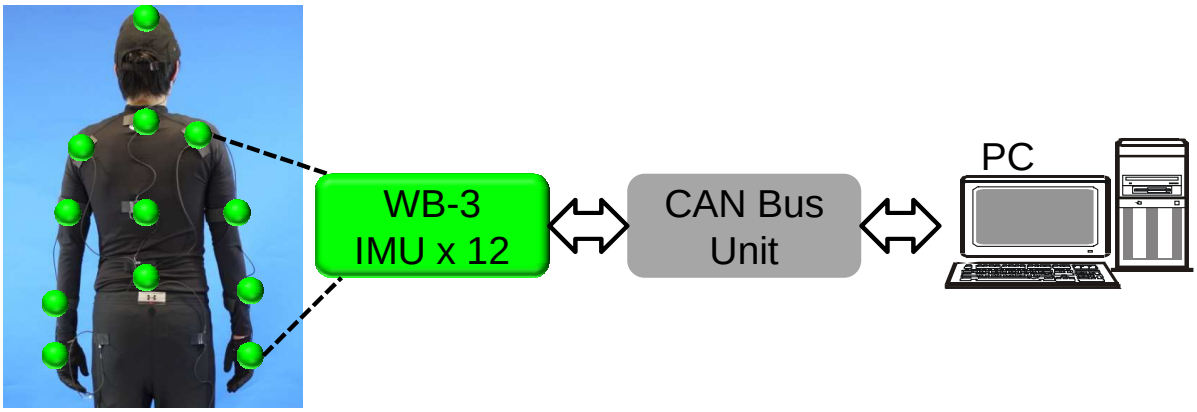

Figure 2.7: WB-3 system overview.

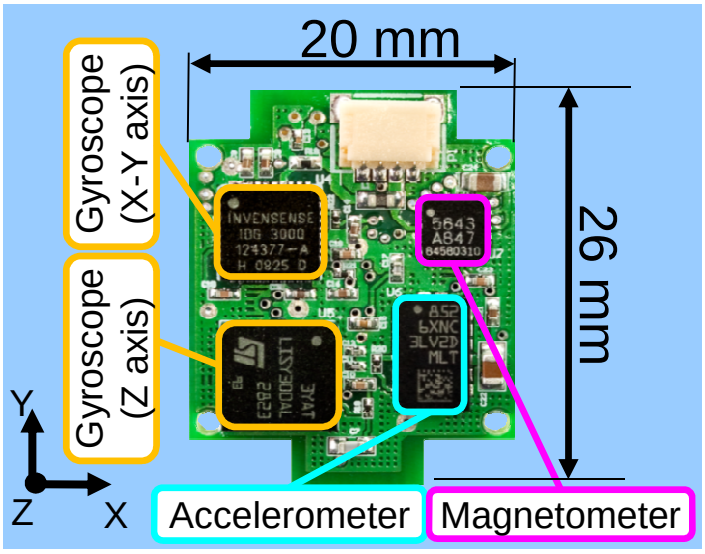

Figure 2.8: WB-3 IMU.

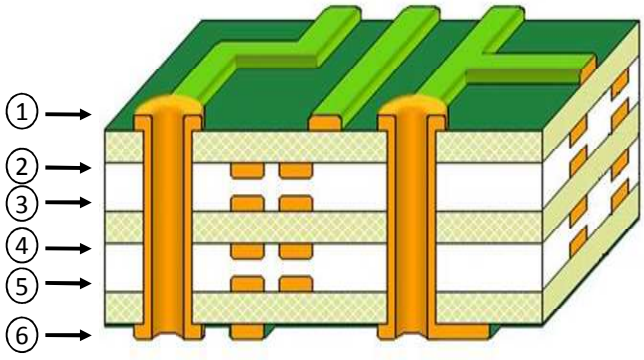

(1) Top signal layer; (2) GND layer; (3) Mid-signal layer1;

(4) Mid-signal layer2; (5) Power layer; (6) Bottom signal layer.

Figure 2.9: Layer configuration of WB-3 PCB.

Table 2.2: Main characteristics of the sensors in WB-3 IMU.

	LIS3LV02DL	IDG300	LISY300AL	HMC5843
Category	accelerometer	gyro	gyro	magnetometer
Axis	3-axis	2-axis	1-axis	3-axis
Range	±2 G	±500 deg/s	±300 deg/s	±4 Gauss
Resolution	12 bit	12 bit	12 bit	12 bit
Bandwidth	40 Hz	140 Hz	88 Hz	40 Hz
Linearity	±2%	<1%	±0.8%	±0.1%
Noise level	<1 bit	<2 bit	<2 bit	<2 bit

1) Gyroscope

In order to measure 3-axes angular velocity, a 2-axis gyro IDG300 (InvenSense Inc.) and a 1-axis gyro LISY300AL (STMicroelectronics Inc.) were employed. The LISY300AL is a miniaturized 7.0 x 7.0 x 1.9 mm z-axis gyro sensor. Its full-scale is ±300 deg/s with a Bandwidth of 88 Hz and a sensitivity of 3.3 mV/deg/s. The IDG300 size is 6.0 x 6.0 x 1.5 mm, the measurement range is ±500 deg/s and the sensitivity is 2.0 mV/deg/s. The mixed configuration of two gyroscopes allows our IMU to obtain all the 3 axis of angular velocity in one planar layer. The output of both gyroscopes is analog signal which is filtered by a first order low-pass analog filter at frequency 40 Hz.

2) Accelerometer

The LIS3LV02DL (STMicroelectronics, Inc.) is a 3-axis accelerometer, whose small size (4.4 x 7.5 x 1 mm) and high performance characteristics are fully compatible with the requirements of the human motion analysis. The resolution with a full-scale ±2 G and Bandwidth of 40 Hz is about 1mG, with noise level of about 0.005 m/sec^2, less than one bit. The accelerometer transmits the data to microcontroller by using I^2C communication.

3) Magnetometer

The 3-axis magnetometer HMC5843 whose size is 4.0 x 4.0 x 1.5 mm is used to measure the local earth magnetic field. Its full scale is ±4 Gauss with a noise level less than two bits. The communication between the magnetometer and microcontroller is also using I^2C.

4) Microcontroller

WB-3 IMU contains a STMicroelectronics 32-bit microcontroller STM32 Cortex for embedded signal elaboration and data transmission. The complete STM32F103x performance line family includes devices in different package types, and the STM32F103CBT6 with the package LQFP48 (7 x 7 x 1.4 mm) is chosen for this design. The STM32F103x performance line family incorporates the high performance ARM® Cortex™-M3 32-bit RISC core operating up to 72 MHz, high-speed embedded memories (Flash memory 128 Kbytes), and an extensive range of enhanced I/Os and peripherals connected to two APB buses. All devices offer three 12-bit ADCs, four general purpose 16-bit timers plus one PWM timer, as well as standard and advanced communication interfaces: two I2Cs, three SPIs, five USARTs, an

USB and an SDIO. The STM32F103x performance line family operates from 2.0 to 3.6 V power supply.

The configuration block diagram of the WB-3 IMU is showed in Figure 2.10. The communication of WB-3 IMU with the PC is performed using the CAN BUS interface at 1 Mb/s. The firmware of the microcontroller can be updated by using the JTAG interface. One user LED is also employed on the IMU for operating mode notation. The power supply "V_{cc}" used for WB-3 IMU ranges from 2.8 to 3.3 V. The final housing appearance of WB-3 IMU is showed in Figure 2.11, with size at 27 x 23 x 11 mm and weight at 6 g.

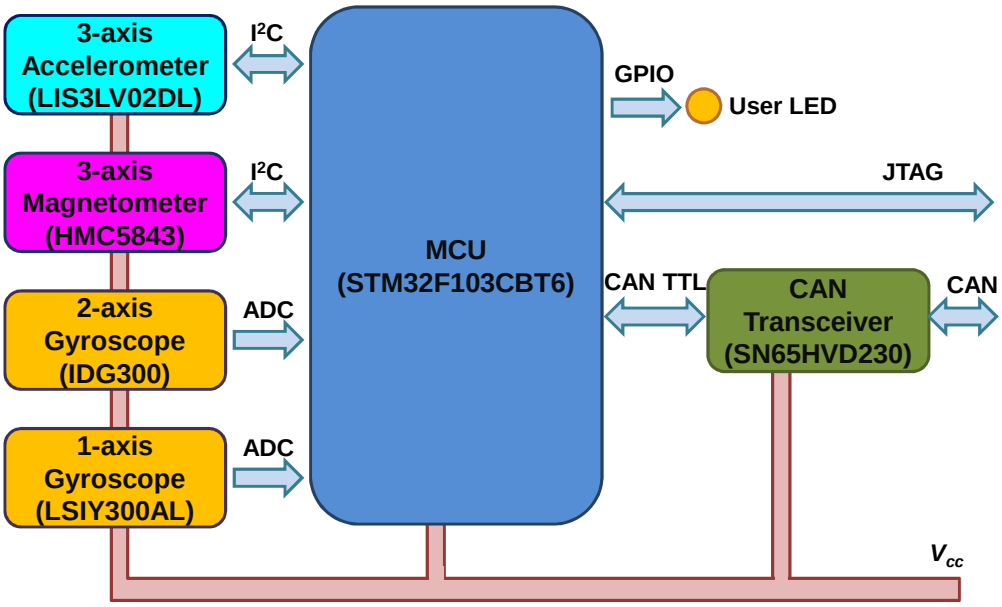

Figure 2.10: WB-3 IMU block diagram.

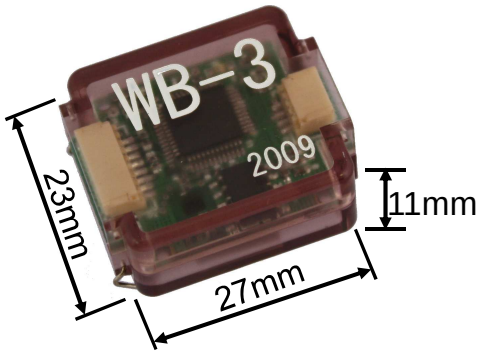

Figure 2.11: WB-3 IMU with housing.

C) Calibration system

In order to better calibrate the sensors of WB-3 IMU, a calibration system named WBCal-1 has been developed (Figure 2.12) in this thesis. The WBCal-1 is made by two different parts, a base and a frame both made in aluminum for reducing the magnetic distortions. The base (85 x 130 x 30 mm) is maintained horizontal with a mechanism of adjustable screws and a bubble indicator. The frame (60 x 100 x 140 mm) where the IMU is located for the evaluation can rotate around a shaft, on which an incremental encoder (8192 pulses) is mounted. The characteristics of the absolute encoder used for the calibration system are summarized in Table 2.3

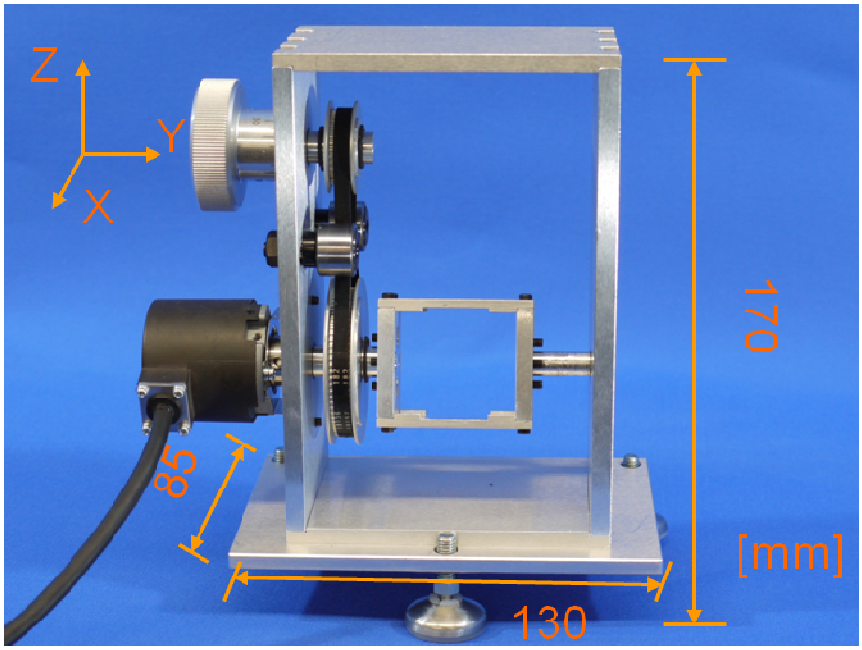

Figure 2.12: Calibration system WBCal-1.

Table 2.3: Encoder characteristics.

Feature	Value
Maker	Nemicon
Model	NAR-H13M-AD-05-8-050
Size	φ39×44 mm
Resolution	213 pulses/revolution
Power supply	DC 5 V
Power consumption	120 mA
Baud rate	1 Mbps

D) WB-3 IMU firmware

In order to realize real-time human motion tracking and analysis, the firmware of WB-3 IMU have been well constructed and optimized. The working flow of the program inside the WB-3 microcontroller is showed in Figure 2.13. The firmware starts from the initializations of microcontroller and sensors, to set up the hardware functions and prepare for the data acquisition. The sensor calibration function is to load the gain parameters of all the sensors from the flash memory, and to initialize the biases of the gyroscopes when the IMU is in the static condition. The gain parameters of all the sensors are calibrated by the WBCal-1 system in advance. After the completion of the first three function steps, the IMU will be kept in the waiting state until it receives the start signal of acquiring sensor data from the user PC. The IMU will then keep on running the loop steps of sensor data acquisition, data filtering, extended Kalman filter (EKF) calculation (The EKF will be introduced in detail at Chapter 3) and data transmission to PC, until it receives the stop running signal from the user. The moving average algorithm with a window size of 5 is used for the data filtering and smoothing [63].

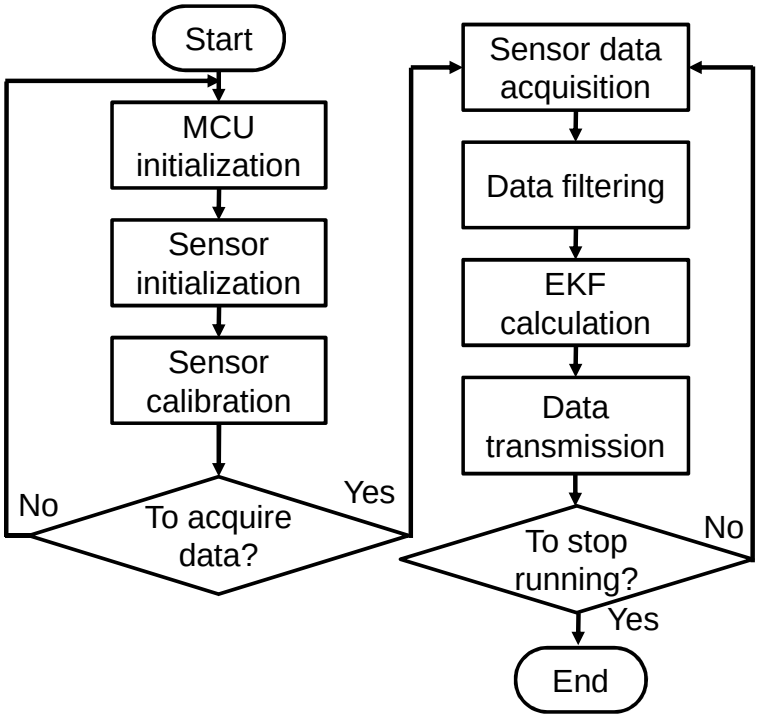

Figure 2.13: Working flow of WB-3 IMU firmware.

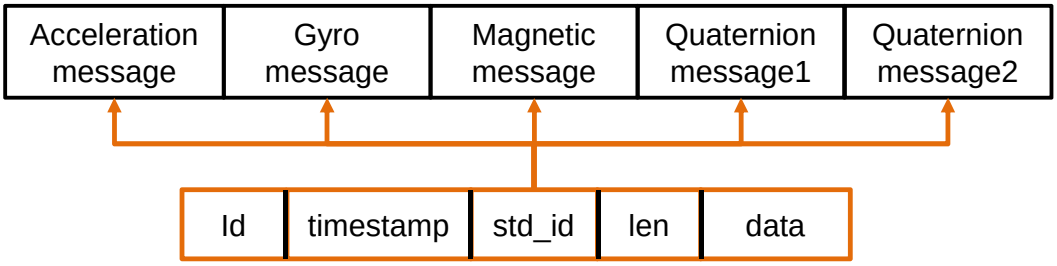

Figure 2.14: Communication protocol between WB-3 IMU and PC.

The data transmitted to PC are the calibrated acceleration, magnetic and angular velocity value; the quaternion representing the orientation from the EKF is also sent to the user PC. Therefore, five standard CAN messages totally are used for the communication protocol between PC and WB-3, which includes 1 message for accelerometer data, 1 message for gyroscope data, 1 message for magnetometer data and 2 messages for the quaternion data (Figure 2.14). Each message is using 8 bytes for data length. The "id" of the message contains the information of the IMU and sensor identity number. The hardware timestamps of the CAN message could be used for checking the communication error, calibrating the system sampling frequency and synchronizing the sensor data.

E) Communication between multiple WB-3 IMUs

The communication method between multiple WB-3 IMUs and the PC is showed in Figure 2.15. All the WB-3 IMUs are connected by using CAN Bus interface with PC. One of the IMUs as the "Master IMU" is used for sending the interrupt signal to other "Slave IMUs" for the data synchronization. It is important to notice that it is possible to replace the "CAN Bus Unit" with a CAN-Bluetooth converter to further realize the wireless communication with the PC.

The state flows of the master IMU and slave IMUs are showed in Figure 2.16 and Figure 2.17, respectively. The master IMU primarily contains 5 states during the operation. The master IMU keeps staying in the waiting state until it receives the start command from the user PC. It then changes to the synchronization signal transmission state for sending the interrupt signal to slave IMUs. The state loop of synchronization signal transmission, sensor data acquisition, data elaboration and data transmission will be kept on shifting until the master IMU receives the stop command from the PC, and then returns to the waiting state.

The state flow of the slave IMU will not be started until it receives the synchronization signal from the master IMU at each system time step.

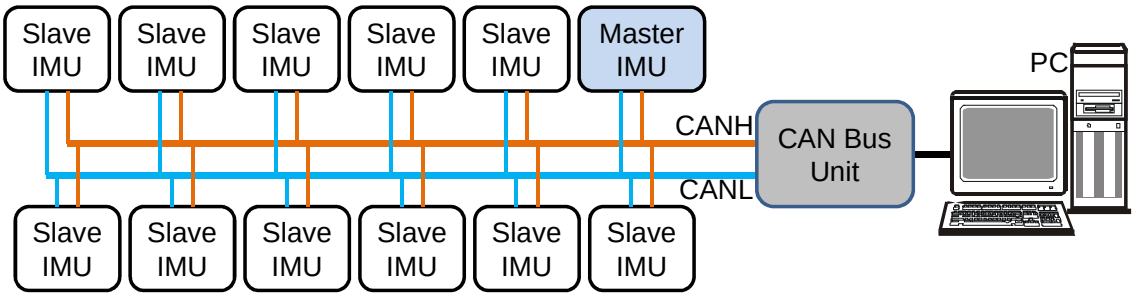

Figure 2.15: System configuration of multiple WB-3 IMUs.

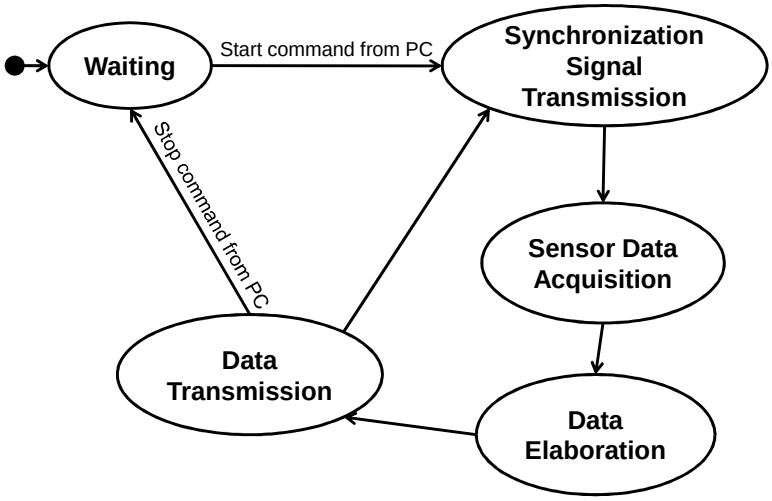

Figure 2.16: State flow of the master IMU.

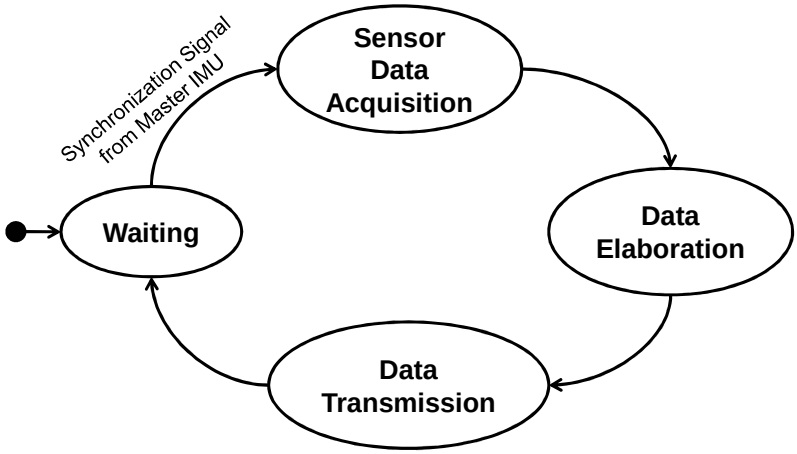

Figure 2.17: State flow of the slave IMUs.

2.2.3 Experimental Evaluation

A) Experiment objective

The inertial and magnetic sensors should be calibrated before the sensor fusion algorithm in order to achieve better orientation estimate results. Therefore, the experiment is aimed at calibrating the sensors of WB-3 IMU by using the calibration system WBCal-1, and evaluating the calibration performances of the sensors compared with the previous version of WB-2 IMU to verify the sensor improvements [37]. Good performance of each sensor guarantees the better performance of IMU.

B) Experiment setup and protocol

The calibration trial consisted in a complete forward rotation (360 deg) and a complete backward rotation (-360 deg) around each axes of the WB-3 IMU. Using respectively the sensor data of gyroscope, accelerometer and magnetometer, the rotated angle of the IMU during the trial could be reconstructed and compared with the encoder angle. The evaluation is focused on the analysis of z axis data, which has normally worse performance than x, y axis due to the manufacture difficulty in vertical plane of 3-axis sensors.

The calibration is performed by the WB-3 IMU compared with the previous system version named WB-2 IMU, in order to evaluate the performance improvements of the new sensors in WB-3 IMU and verify the effect of the calibration system. The Figure 2.18 shows a layout comparison between WB-3 IMU and WB-2 IMU. The size and weight of WB-2 IMU are 30 x 30 x 13 mm and 5.8 g, respectively. Therefore, the WB-3 IMU has reduced 50% at weight and 43% at size from WB-2 IMU.

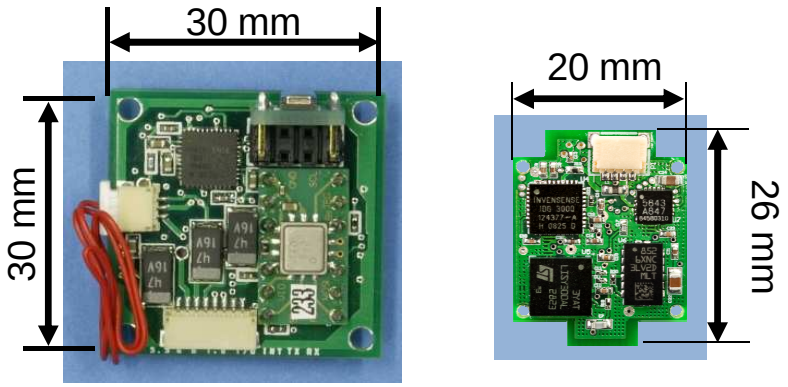

Figure 2.18: WB-2 IMU (left) and WB-3 IMU (right).

2.2.4 Experimental Results

A) Evaluation of accelerometer

Figure 2.19 shows the angle reconstruction using only the accelerometer data of WB-2 IMU, with the hypothesis of quasi-static movements. The total range of error for the WB-2 IMU is 30 deg. During the dynamic periods of 3 s to 6 s and 8 s to 11 s, the accelerometer has poor performance up to 22 deg of error.

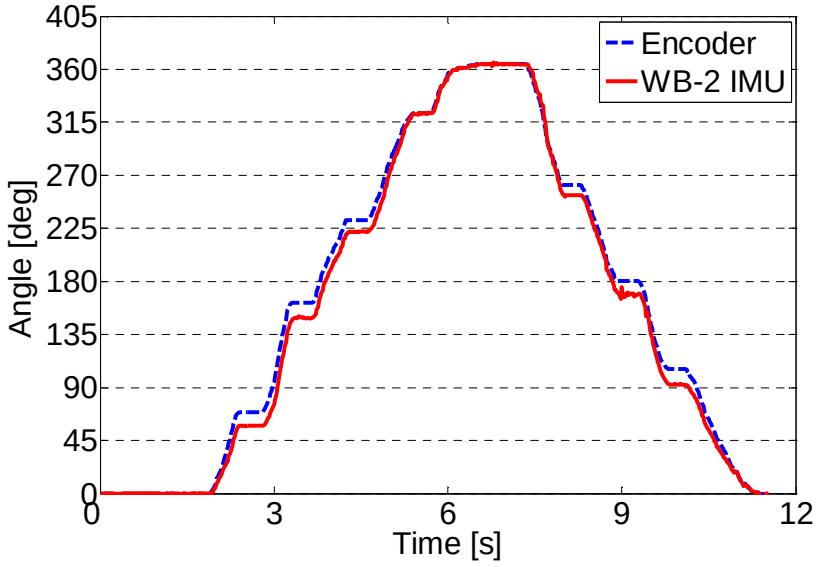

(a) Angle calculated from accelerometer data compared with Encoder

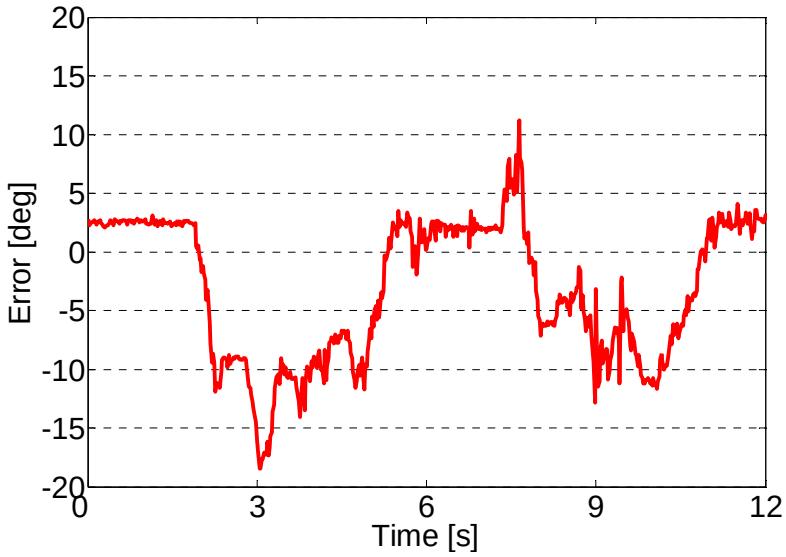

(b) Error on the angle calculated from accelerometer data

Figure 2.19: Accelerometer performance of WB-2 IMU.

Figure 2.20 shows the angle reconstruction using only the accelerometer data of WB-3 IMU. For the accelerometer of WB-3 IMU, the total range of the error is just 10 deg, which is one third of the error of WB-2 IMU. It is also clear that the dynamic performance (less than 10 deg) of the new accelerometer in WB-3 IMU is much better than the one in WB-2 IMU.

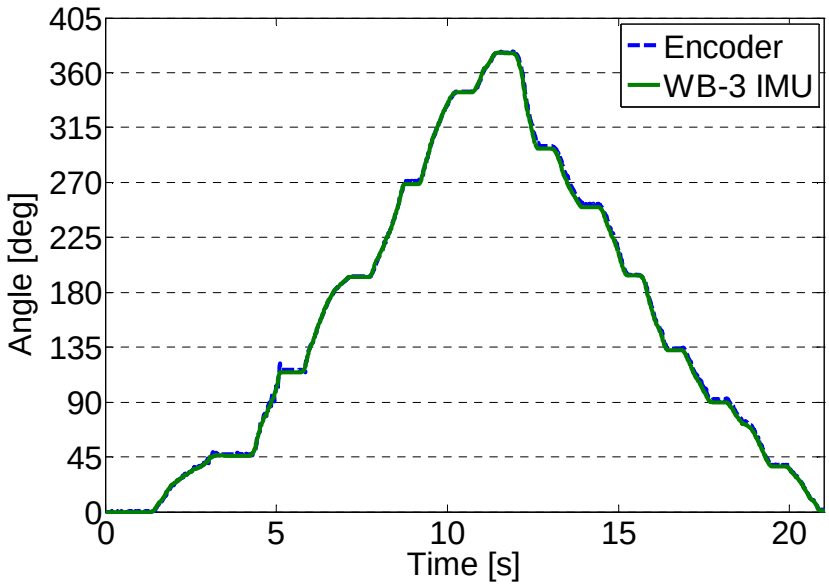

(a) Angle calculated from accelerometer data compared with Encoder

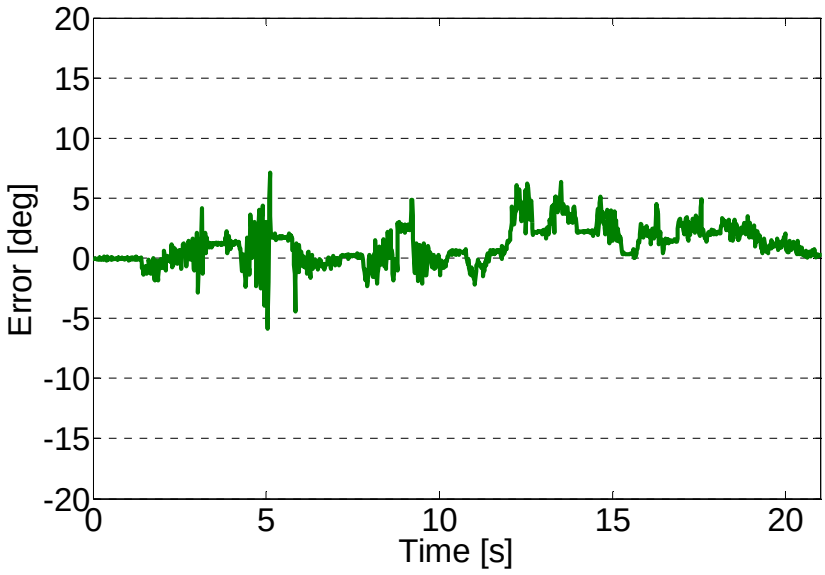

(b) Error on the angle calculated from accelerometer data

Figure 2.20: Accelerometer performance of WB-3 IMU.

B) Evaluation of magnetometer

Figure 2.21 shows the angle reconstruction using only the magnetometer data of WB-2 IMU. In this case, the total range of error for the WB-2 IMU is 75 deg. Similar with the results of accelerometer, the magnetometer of WB-2 IMU has poor performance (up to 70 deg error) during the dynamic condition. Moreover, there is a leap of about 65 deg at the moment of 8 s, which means that the magnetometer has great latency and unstable data output performance.

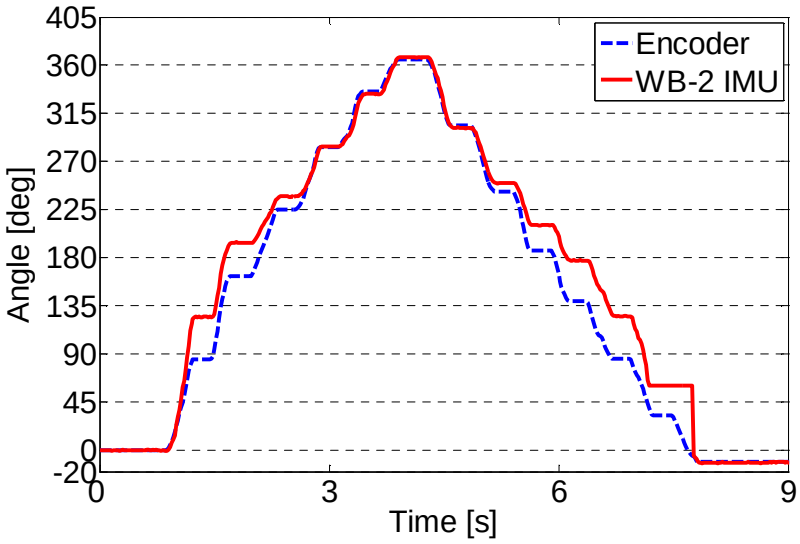

(a) Angle calculated from magnetometer data compared with Encoder

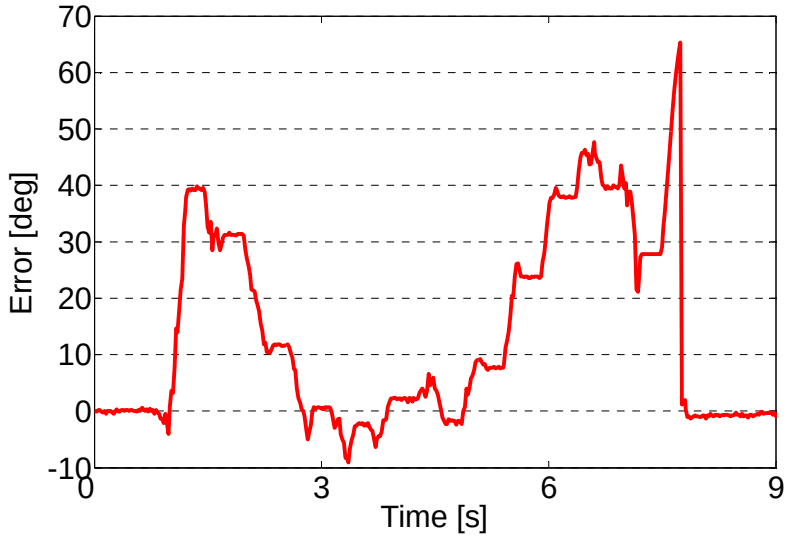

(b) Error on the angle calculated from magnetometer data

Figure 2.21: Magnetometer performance of WB-2 IMU.

Figure 2.22 shows the angle reconstruction using only the magnetometer data of WB-3 IMU. The total range error for the magnetometer of WB-3 IMU is less than 60 deg, which are 15 deg less than the one in WB-2 IMU. The dynamic performance with about 60 deg error is also better WB-2 IMU. At the moment of the 3 s, there is a leap of error about 19 deg, which is due to the problem of the encoder data. The magnetic data at that point is still significantly smooth.

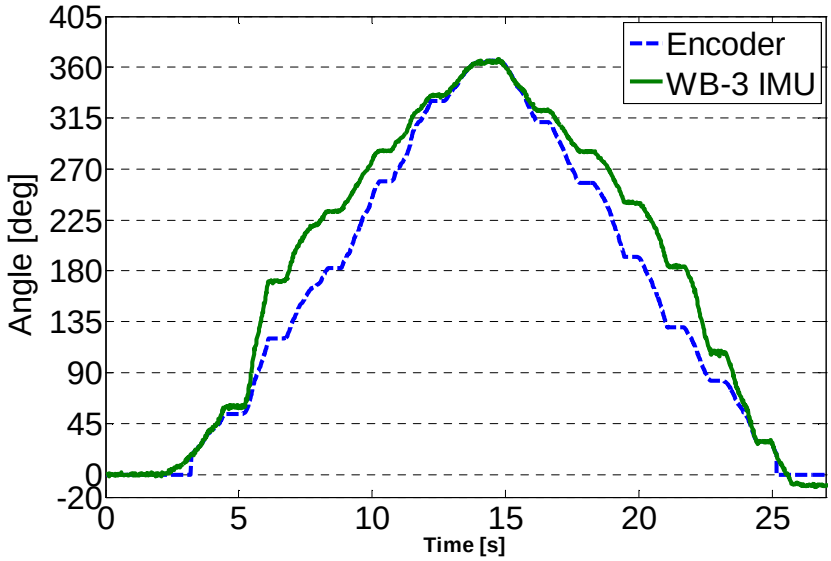

(a) Angle calculated from magnetometer data compared with Encoder

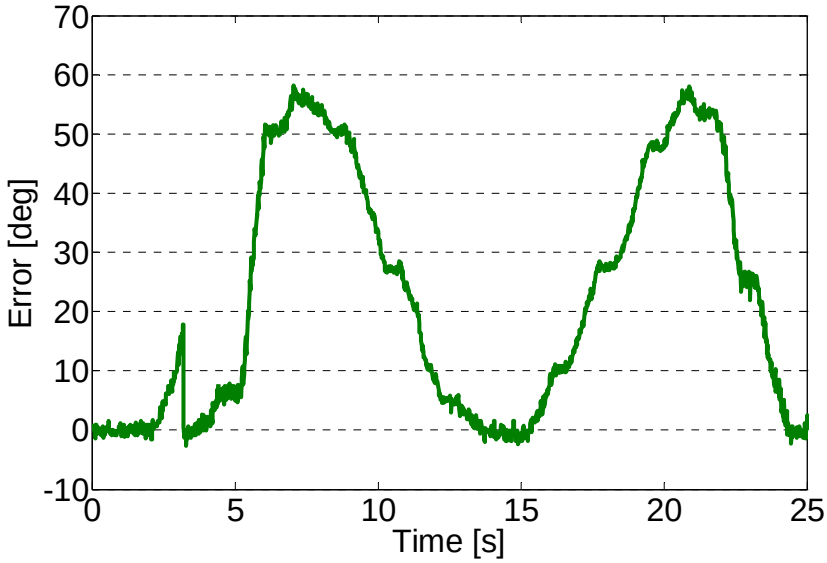

(b) Error on the angle calculated from magnetometer data

Figure 2.22: Magnetometer performance of WB-3 IMU.

C) Evaluation of gyroscope

Figure 2.23 shows the angle reconstruction using only the gyroscope data of WB-2 IMU. The algorithm for obtaining the angle from the angular speed is Euler integration without any mechanism of error reset. In this case, the integration error of WB-2 is 135 deg after 5 s period, which means that this gyroscope has strong angular speed noise and drift problem.

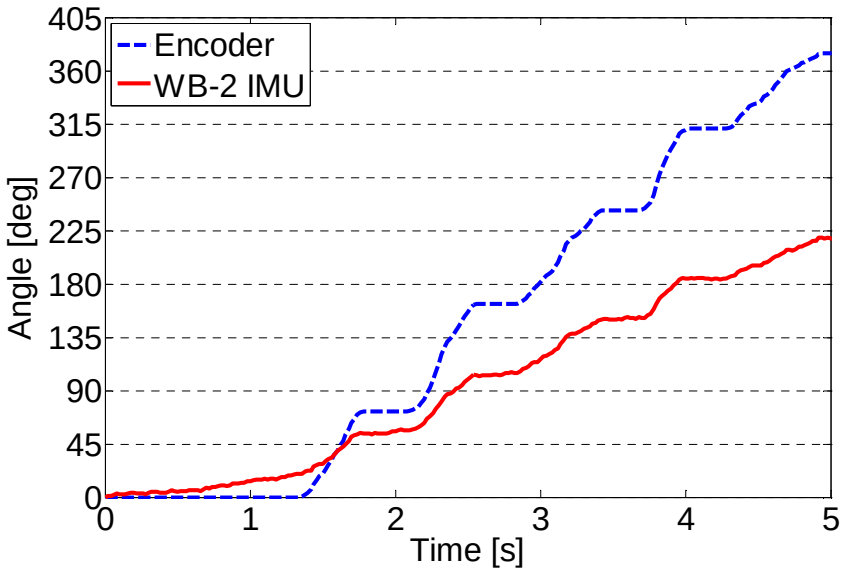

(a) Angle calculated from gyroscope data compared with Encoder

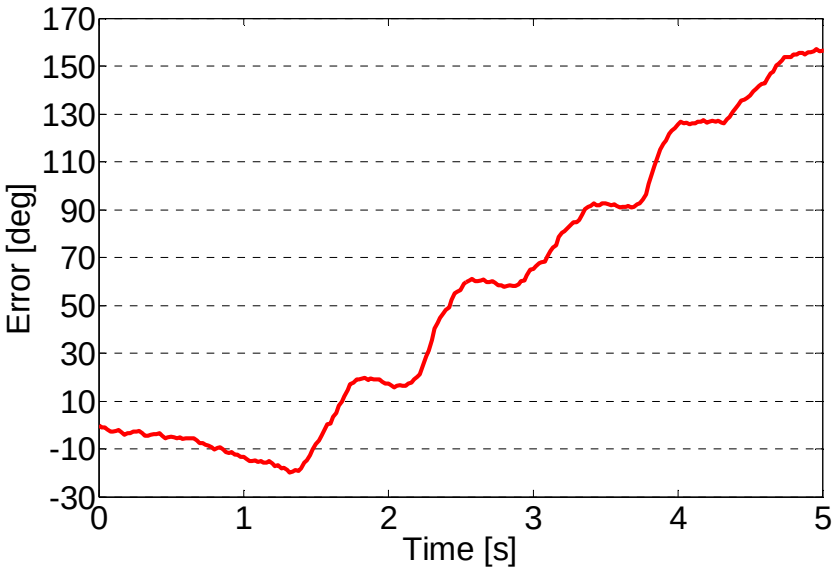

(b) Error on the angle calculated from gyroscope data

Figure 2.23: Gyroscope performance of WB-2 IMU.

For WB-3 IMU, the gyroscope performance is showed in Figure 2.24. The integration error is about 90 deg after 10 s period, which is much better than the performance of the gyroscope in WB-2 IMU. The gyroscope of WB-3 IMU could achieve better bias estimation and reduce the drift problem.

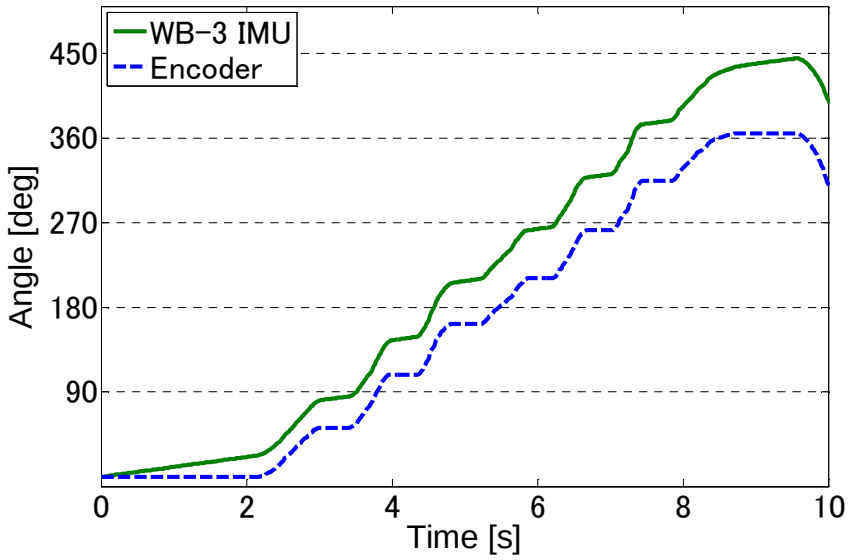

(a) Angle calculated from gyroscope data compared with Encoder

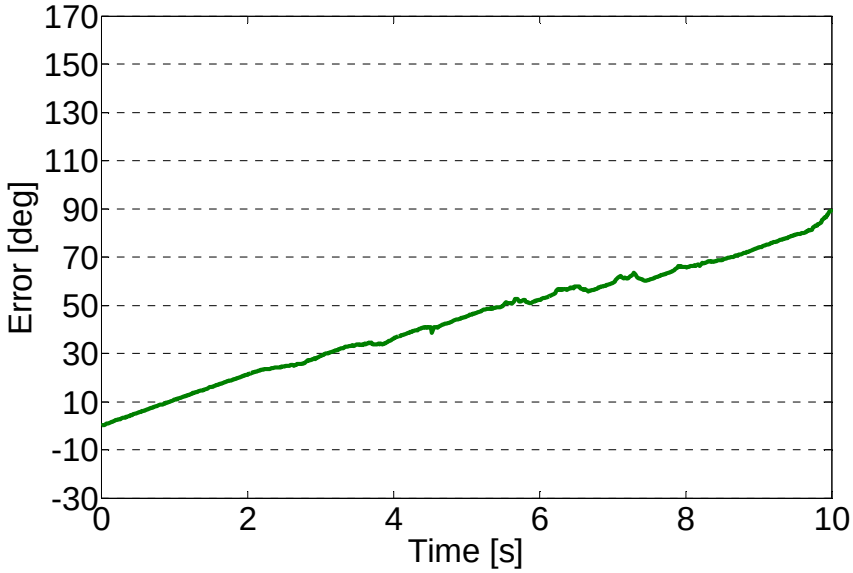

(b) Error on the angle calculated from gyroscope data

Figure 2.24: Gyroscope performance of WB-3 IMU.

2.2.5 Overall System Performance of WB-3

The sampling frequency of WB-3 IMU could be up to 200 Hz by using the firmware configuration discussed above, which is fully compatible with the requirements of real-time motion tracking for trainee's movements in various medical procedures. It is also important to notice that WB-3 IMU could achieve better sampling rate performance by moving the execution of sensor fusion algorithm from microcontroller to PC. In this way, the WB-3 IMU will only transmit raw sensor data to PC, which could attain up to 500 Hz sampling rate performance.

Benefiting from the ultra-miniaturized design and robust firmware implementation, the WB-3 IMU has high performance in different features, which satisfy the requirements of the system specification. A comparison of these features between WB-3 IMU and other commercial products has also been listed in Table 2.4 to verify the system advance of WB-3. The values of commercial products are normalized to the values of WB-3 IMU for an easier visual comparison.

It is clear that WB-3 IMU has much less size and weight than commercial products. This allows WB-3 system to be more wearable and adaptive for measuring the movements of some small medical instruments. In other features, WB-3 IMU has also great improvements and better performance than those commercial products, such as less power consumption; faster system sampling rate, and less cost.

Table 2.4: Comparison between WB-3 IMU and commercial products.

	WB-3 IMU	InertiaCube3	MTx	3DM-GX3
Size [mm]	27 x 23 x 11	26 x 39 x 15	38 x 53 x 21	44 x 25 x 11
(Normalized value)	(1)	(2.2)	(6.2)	(1.8)
Weight [g]	6	17	30	11.5
(Normalized value)	(1)	(2.8)	(5)	(1.9)
Power consumption [mW]	150	240	360	400
(Normalized value)	(1)	(1.6)	(2.4)	(2.7)
Resolution [deg]	0.03	0.03	0.05	<0.1
Accuracy [deg]	<2	<2	<2	<2
Sampling rate [Hz]	200	180	120	237
(Normalized value)	(1)	(0.9)	(0.6)	(1.2)
Cost [USD]	1500	3000	4000	3600
(Normalized value)	(1)	(2)	(2.7)	(2.4)

2.3 Design of WB-4 System

2.3.1 System Specification

The general requirements of WB-4 system are similar to WB-3 system, such as the system price, sampling rate, angular resolution and accuracy for tracking human motion. The main different feature between them is the wireless communication. The wireless system could provide better wearability for human without any cable constraint. WB-4 system should integrate the motion sensors with the wireless communication module and battery into one unit, in order to realize the wireless motion tracking system. At the mean time, it should also have reasonable size and weight for tracking small object's motion in medical applications, which is similar to WB-3 system. Therefore, the size and weight of WB-4 system become the significantly difficult and important parts in the design.

Since the time for each regular surgical training task is normally less than 1 hour, the WB-4 system should be capable of keeping running at least 1 hour. The wireless communication distance required at more than 5 meters guarantees less disturbance from the PC operator to the trainees. The WB-4 system performance requirements have been summarized in Table 2.5.

Table 2.5: System requirements of WB-4 wireless IMU.

Parameter	Value
Size [mm]	<40 x 30 x 20
Weight [g]	<10
Power consumption [mW]	<300
Sampling rate [Hz]	>100
Resolution [deg]	<0.8
Accuracy [deg]	<2
Continuous working time [hour]	>1
Wireless communication distance [m]	>5
Cost [USD]	<2500

2.3.2 Materials and Methods

A) WB-4 wireless IMU

The WB-4 system configuration is similar with WB-3 system, which primarily consists of a set of WB-4 wireless IMUs. The WB-4 wireless IMU contains a mother board for motion

sensing, a Bluetooth module for wireless communication and a Li-Polymer battery for power supply. A picture of this IMU is showed in (Figure 2.25). The WB-4 IMU is very compact and lightweight (size 37 x 23 x 12 mm and weight 7 g) – at present the smallest, lightest wireless IMU in the world.

This IMU uses two-layer configuration for the connection between the mother board and Bluetooth module (Figure 2.26). A pair of board to board connectors is used for the layer positioning and signal transmission. The mother board is primarily composed of a 32-bit microcontroller STM32F103CBT6, a DC regulator ST1S12 and the following sensors: 3-axis digital accelerometer LIS331DLH; 3-axis analog gyroscope LYPR540AH; and 3-axis digital magnetometer HMC5843 (Figure 2.27). The sensor characteristics of WB-4 IMU have been summarized in Table 2.6.

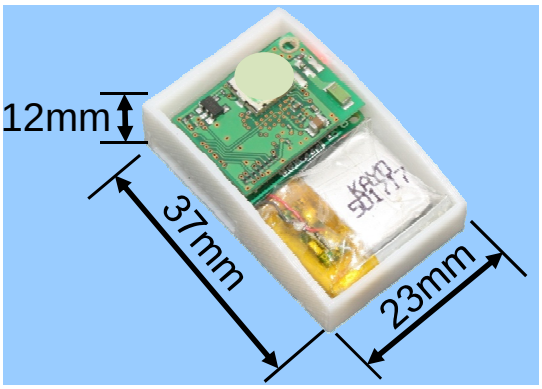

Figure 2.25: WB-4 wireless IMU.

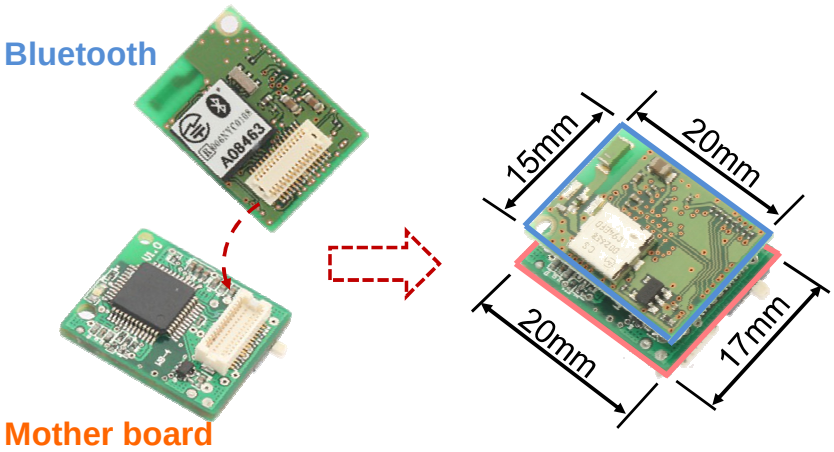

Figure 2.26: Two-layer configuration for WB-4 mother board and Bluetooth module.

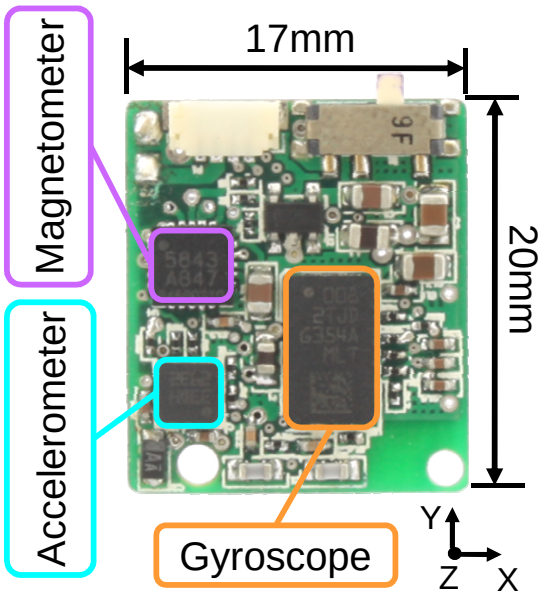

Figure 2.27: Sensor side of the WB-4 mother board.

Table 2.6: Main characteristics of the sensors in WB-4 wireless IMU.

	LIS331DLH	LYPR540AH	HMC5843
Category	Accelerometer	Gyroscope	Magnetometer
Axis	3-axis	3-axis	3-axis
Size	3 x 3 x 1 mm	4.4 x 7.5 x 1.1 mm	4 x 4 x 1.3 mm
Range	±2/±4/±8 G	±400/±1600 deg/s	±4 Gauss
Resolution	1 mG/digit@±2 G 2 mG/digit@±4 G 3.9 mG/digit@±8 G	3.2 mV/dps@±400 deg/s 0.8 mV/dps@±1600 deg/s	12 bit
Bandwidth	25 Hz@±2 G 50 Hz@±4 G 500 Hz@±8 G	140 Hz	50 Hz
Current consumption	0.25 mA	10.8 mA	0.9 mA

1) Gyroscope

In order to measure 3-axis angular velocity, a tri-axial analog gyroscope LYPR540AH (STMicroelectronics Inc.) has been employed. The LYPR540AH is a miniaturized 4.4 x 7.5 x 1.1 mm 3-axis gyroscope sensor. Its full-scale is ±1600 deg/s with a Bandwidth of 140Hz and

a sensitivity of 0.8 mV/deg/s. It has the possibility to be amplified internally with a gain of 4 achieving a full scale of ±400 deg/s with a sensitivity of 3.2 mV/deg. The output of the gyroscope is analog signal which is filtered by a first order low-pass analog filter at frequency 40 Hz.

2) Accelerometer

The LIS331DLH (STMicroelectronics Inc.) is a 3-axis accelerometer, whose small size (3 x 3 x 1 mm) and high performance characteristics are fully compatible with the requirements of the human motion analysis. The dynamic range, selectable, is from ±2 G to ±8 G in full scale: in this way slow movements can be detected with higher definition (sensitivity is 1 mG/digit at ±2 G), together with faster movements and good definition (sensitivity is 3.9 mG/digit at ±8 G). The device has very low power consumption: 250 uA in normal mode, 10 uA in low power mode, and finally it is equipped with double digital output, I^2C and SPI, to be easily interfaced with the 32-bit microcontroller in WB-4 IMU.

3) Magnetometer

The 3-axis digital compass HMC5843 whose size is 4.0 x 4.0 x 1.5mm is used to measure the magnetic field in 3 axes by converting the incident magnetic field in voltage per each axis, x, y and z. Its full scale is ±4 Gauss with a noise level less than two bits. The communication between the magnetometer and microcontroller is using I^2C. This magnetometer is also implemented in WB-3 IMU.

4) Microcontroller

WB-4 IMU contains a STMicroelectronics 32-bit microcontroller of STM32 Cortex series for sensor data acquisition, signal elaboration and data transmission to PC. The STM32F103CBT6 with the package LQFP48 (7x7x1.4 mm) is chosen for the WB-4 IMU design. It is also implemented in WB-3 IMU. The STM32F103CBT6 incorporates the high performance ARM® Cortex™-M3 32-bit RISC core operating up to 72 MHz, and high-speed embedded memories (Flash memory 128 Kbytes). It also offers 12-bit ADCs, as well as standard and advanced communication interfaces I^2Cs. The operating power ranges from 2.0 to 3.6 V.

5) DC regulator

To give flexibility in using different kinds of external batteries, a DC regulator ST1S12 (STMicroelectronics Inc.) is selected for WB-4 IMU. The maximum current rate of this regulator is 700 mA with an input voltage up to 6.5 V, giving wide margin for our applications. The total dimension, including the pins, is 2.8 x 2.9 mm. Additionally, the regulator is protected against high temperature with an internal thermal shutdown with an arming temperature of 130° C: due to the small size of the board, this component is acting also as temperature protection for the entire system; because if it stops the operation, all the sensors and microcontroller are not powered on.

6) Bluetooth module

The Bluetooth module used in WB-4 IMU is the Zeal-C01 from the Musenka Company [64]. The compact size (20 x 15 x 4.7 mm), light weight (1 g) and high performance of this module satisfy efficiently the system requirements of WB-4 for motion tracking. The Zeal-C01 uses UART interface for the communication with microcontroller, which make it much convenient for users to program the wireless data transmission. This module has 3 modes for data transmission: low speed mode; standard speed mode; and high speed mode; which can be customized for different applications. The power consumption is about 36 mA at the standard speed mode. The required power of this module is 3.3 V which is compatible with the microcontroller and other components of WB-4 IMU.

7) Battery

One Li-Polymer battery KPL501717 from Kayo Inc. is embedded in the WB-4 IMU [65]. The capacity of this battery is 80 mAh with the size 17 x 17 x 5 mm. The total system power consumption of WB-4 IMU is 80 mA, this battery, therefore, can support the WB-4 IMU continuously working for one hour. The KPL501717 can be recharged fully within 30 min.

B) WB-4 IMU configuration

The configuration block diagram of the WB-4 IMU is showed in Figure 2.28. The communication of WB-4 IMU with the PC is performed using the Bluetooth communication up to 921.6 Kb/s. The firmware of the microcontroller can be updated by using the JTAG

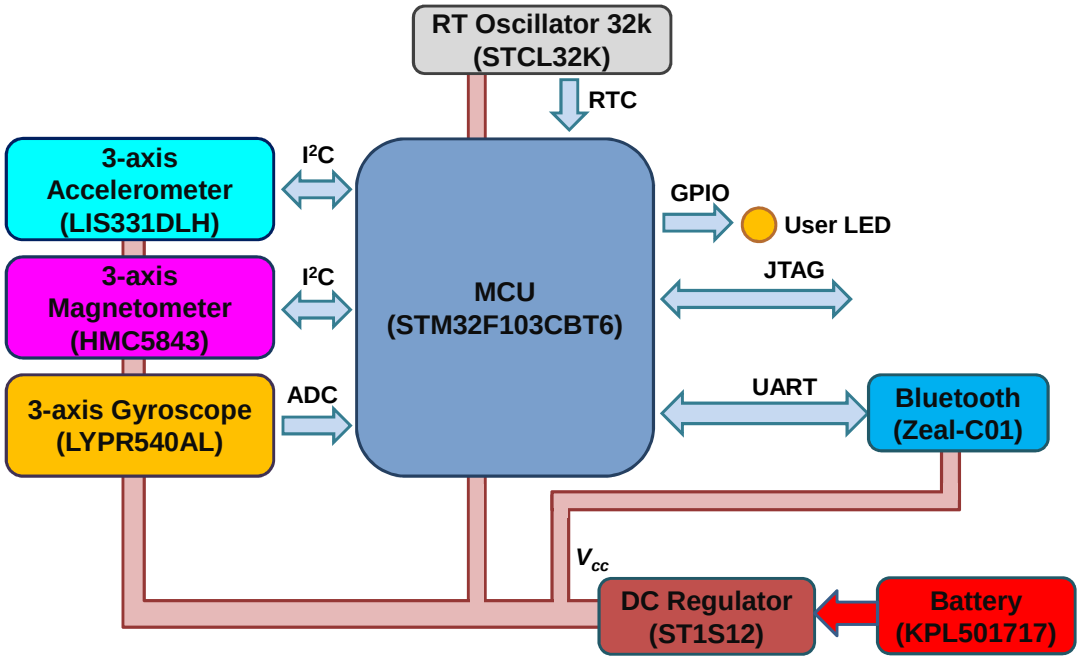

Figure 2.28: Configuration block diagram of WB-4 IMU.

interface. One user LED is also employed on the IMU for operating mode notation. The "*Vcc*" after the DC regulator for WB-4 IMU is 3.3 V. It is important to notice that the UART interface could be replaced by the CAN Bus or USB interface to realize different kinds of communication protocols.

C) WB-4 IMU firmware

In order to realize the jaw motion tracking and analysis, the firmware of WB-4 IMU have been well constructed and optimized, which is similar to the WB-3 IMU. The working flow of the program inside the microcontroller of WB-4 is showed in Figure 2.29. The firmware starts from the initializations of microcontroller, Bluetooth module and the sensors, to set up the hardware functions and prepare for the data acquisition and transmission. The sensor calibration is to load the gain parameters of all the sensors from the flash memory, and to initialize the biases of the gyroscope when the IMU is in the static condition. After the completion of the first four functional steps, the IMU will be kept in the waiting state until it receives the start signal of acquiring sensor data from the user PC. The IMU will then keep on running the loop functional steps of sensor data acquisition, data filtering, EKF calculation and data transmission to PC, until it receives the stop running signal from the user. The

moving average algorithm with a window size of 5 is used for the data filtering and smoothing [63].

The data transmitted to PC are the calibrated acceleration, angular velocity and magnetic value; the quaternion representing the orientation calculated from the EKF is also sent to the user PC for estimating the jaw attitude. Therefore, the data package contains totally 40 bytes data. The communication protocol between PC and WB-4 is showed in Table 2.7. The “Header” and “End” are the flags for indicating the start and stop of the data package. The “Package Counter” is used for denoting the package number and evaluating the data errors of wireless transmission.

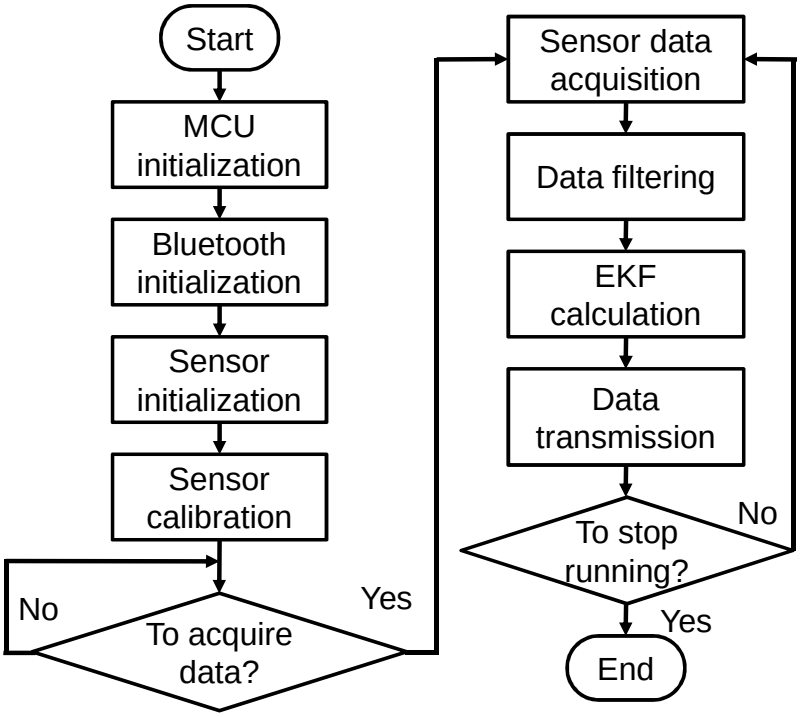

Figure 2.29: Working flow of WB-4 IMU firmware.

Table 2.7: Communication protocol between WB-4 and PC.

Header	Acceleration	Angular velocity	Magnetic	Quaternion	Package Counter	End
2 bytes	6 bytes	6 bytes	6 bytes	16 bytes	2 bytes	2 bytes

2.3.3 Overall System Performance of WB-4

The system sampling frequency of WB-4 IMU could be up to 200 Hz by using the firmware configuration discussed above, which is fully compatible with the requirements of human motion measurement. It is also important to notice that, similar with WB-3 IMU, the sampling rate could be improved by moving the execution of sensor fusion algorithm from microcontroller to PC. In this way, the WB-4 IMU will only transmit raw sensor data to PC, which could attain up to 500 Hz sampling rate performance.

Benefiting from the ultra-miniaturized design and robust firmware implementation, the WB-4 wireless IMU has high performance in different features, which satisfy the requirements of the system specification.

A performance comparison between WB-4 and WB-3 IMU is listed in Table 2.8. Due to the wireless design with the Bluetooth module and battery, the values of WB-4 IMU are bigger than WB-3 IMU in the features of size, weight, power consumption, and cost; but they still satisfy the system design requirements. Moreover, the WB-4 IMU without cable connection for data acquisition can realize a more wearable and portable abilities for the motion tracking.

Table 2.8: Comparison between WB-4 and WB-3 IMU.

	WB-4 IMU	WB-3 IMU
Size [mm]	37 x 23 x 12	27 x 23 x 11
Weight [g]	7	6
Power consumption [mW]	240	150
Resolution [deg]	0.05	0.03
Accuracy [deg]	<2	<2
Communication method	wireless	wired
Communication distance [m]	10	Limited to cable length
Continuous working hour	1	unlimited
Sampling rate [Hz]	200	200
Cost [USD]	2000	1500

2.4 Discussion

WB-3 IMU and the mother board of WB-4 wireless IMU were developed by using 6 layer configuration of PCB design in order to realize the ultra-miniaturized size of system requirement, which was the most critical and difficult part of the system design. In theory, it is feasible to reduce the size of electronic board by increasing the layer number of PCB design. More layers allows us to place the components in more compact size on the top and bottom layers, and route the signal lines in other middle layers. However, it is also necessary to keep enough spaces for placing via through all the layers. Therefore, it is extremely difficult to optimize the layout of component positions and via positions, which limits the layer number of PCB design. In the cases of WB-3 IMU and the mother board of WB-4 wireless IMU, the maximum layer number can just achieve up to 6 due to space limitations of placing components and via on the top and bottom layers. Moreover, more layer configuration will increase the manufacture expense of the system, which might affect the cost requirement of system specification. Therefore, the current designs of WB-3 and WB-4 system have been optimized between the PCB sizes and manufacture expense.

The size and performance of WB-3 and WB-4 system could be improved by using novel MEMS-based multiple axis inertial sensors. The WB-3 IMU was composed of a 1-axis gyroscope, a 2-axis gyroscope, a 3-axis accelerometer and a 3-axis magnetometer, and WB-4 wireless IMU contained a 3-axis gyroscope, a 3-axis accelerometer and a 3-axis magnetometer. These sensors could be replaced by the novel advanced MEMS sensors, such as 6 axis accelerometer and magnetometer in one single IC, 6 axis gyroscope and accelerometer in one single IC, which help miniaturize the system design. Moreover, these novel inertial sensors normally have multiple measurement ranges. This widens the system applications for evaluating different human motions and performance.

The sensor calibration system WBCal-1 can effectively calibrate and improve the performance of each sensor of WB-3 IMU. The experimental results showed that each sensor of WB-3 had better performance than the sensors of WB-2 system. With the same calibration method for these two systems, the system errors of WB-3 were efficiently reduced more than WB-2. This calibration system was still in its first prototype, which could be improved by adding motor control for rotating the sensors and measuring angular speed to calibrate the gains of gyroscopes.

With the implementation of Bluetooth technology, WB-4 IMU provided the wireless communication for data transmission, which could avoid the constraints caused by cable connection and achieve a more wearable and portable performance. The communication distance of current Bluetooth model was up to 10 m under the open circumstances. In a closed room, the communication distance would be decreased. This can be improved and enhanced by using the novel Bluetooth modules with higher performance, such as Zeal-S01 from Musenka Company. Accompanied with high performance, these Bluetooth modules also have higher power consumption, which will reduce the continuously working time of WB-4 system.

The current Li-Polymer battery with the capacity of 80 mAh could support the WB-4 IMU continuously working for one hour. This feature could be improved by using higher capacity of battery to increase the working time of WB-4 IMU, but which will also result in bigger size of the system.

The ultra-miniaturized motion tracking system is the key component of the proposed skill evaluation system discussed in Chapter 1. It could use either the WB-3 system (wired version) or WB-4 system (wireless version) for motion analysis and skill assessment, depending on the requirements of different medical applications.

2.5 Conclusion of this Chapter

The developments of the Waseda Bioinstrumentation system WB-3 and WB-4 were presented in this chapter. Both these systems satisfied the performance requirements of human motion tracking and their applications for medical skill evaluation.

- The resulting size of WB-3 IMU was 27 x 23 x 11 mm, whose total volume was less than the system requirement of 30 x 30 x 10 mm. Only the height was 1 mm higher than the system specification, and the length and width completely satisfied the requirements.
- The weight of WB-3 was 6 g, which fully satisfied the requirement of 10 g.
- WB-3 IMU was achieved with the power consumption of 150 mW, sampling rate of 200 Hz, resolution of 0.03 deg, average accuracy of 2 deg, and cost of 1500 USD. All these features satisfied the system specifications of power consumption (<200 mW), sampling rate (>100 Hz), resolution (<0.8 deg), accuracy (<2 deg) and cost (<2000 USD).
- The data synchronization problem of multiple WB-3 IMUs was solved by using master and slave IMU configuration of CAN BUS communication.

- The sensor calibration problem of WB-3 IMU was solved by the development of the calibration system WBCal-1. The experimental results showed that the sensors of WB-3 IMU had better performance than the previous system WB-2 after calibration.
- The resulting size and weight of wireless WB-4 IMU were respectively 37 x 23 x 12 mm and 7 g, which satisfied the system specification of 40 x 30 x 20 mm in all the dimensions and weight of less than 10 g.
- The 10 m wireless communication distance of WB-4 IMU satisfied the system specification of more than 5 m.
- The WB-4 IMU achieved other performance of power consumption of 150 mW (<200 mW), sampling rate of 200 Hz (>100 Hz), resolution of 0.03 deg (<0.8 deg), average accuracy of 2 deg (<=2 deg), and cost of 1500 USD (<2000 USD).

WB-3 and WB-4 systems overcome the wearability limitation of most current inertial-sensor-based motion tracking systems for surgical operative skill evaluation, and extend the prospects of the system applications to more various medical scenarios benefiting from the better wearable and portable performance.

In order to achieve the goals of skill evaluation, the software system should be capable of effectively calculating the human and instrument motions. Next chapter will discuss the algorithms for sensor fusion, human motion tracking and biomechanical analysis of how the software system integrating with these high performance hardware systems.

Chapter 3

Rigid Body Orientation Estimate and Biomechanical Analysis of Upper Limb

3.1 Introduction

3.1.1 Representation of Rigid Body Orientation

The human body can be modeled as a set of links or limb segments arranged in a tree-like structure. Individual limb segments can be treated as rigid bodies. The rigid body is an idealization of a body with volume and mass which has a shape that cannot be changed. That is, such bodies are solid and completely inelastic. Specifying the posture of this model involves descriptions of the orientation and position of the individual segments [66, 67]. Specification of the nature of the relationships between the links in the structure will determine whether the positions and orientations of the segments are described individually or are specified relative to one another. The formalisms chosen will have a bearing upon the ability to represent all orientations, computational efficiently, storage requirements, and transmission bandwidth requirements when operating within networked synthetic environment architecture. In human body tracking applications, the type and quality of sensor input being used to drive the animation of the human model should also be considered.

Body tracking using inertial and magnetic sensors is a relatively new technology. Many studies of human motion tracking using these inertial sensors have been performed [37, 68-71]. A naive approach to inertial orientation tracking might involve integration of angular rate data to determine orientation. However, this solution would be prone to drift over time due to the buildup of bias and drift errors. In order to avoid drift, inertial tracking systems make use of additional complementary sensors. Commonly, these sensors include triads of accelerometers and magnetometers for respectively referencing the gravity and magnetic field vectors. Measuring the gravity vector in the sensor coordinate frame using accelerometers allows estimation of orientation relative to the horizontal plane. However, in the event that the sensor module is rotated about the vertical axis, the projection of the gravity vector on each of the principal axes of the accelerometer triad will not change. Therefore, magnetometers are used to measure the local magnetic field vector in sensor coordinates, and allow the determination of orientation relative to the vertical rotation.

The data from these incorporated sensors is normally fused by different filtering algorithms in order to estimate the segment orientation, such as Kalman filter, particle filter and complementary filtering algorithm [72-76]. Among these algorithms, the Kalman filter is the most common one due to its high accuracy of orientation estimate and computational efficiency for real time applications. Generally, there are two kinds of methods for orientation representation used in Kalman filter: Euler -based and quaternion-based. The quaternion-based method is relatively more dominant than Euler-based method for two reasons. First, the quaternion representation does not suffer from the singularity problem associated with the Euler angle representation. Second, it avoids trigonometric functions in the filter algorithm, making it more efficient and easier to implement in real time by microcontrollers [68, 77-79].

3.1.2 Biomechanical Analysis

Biomechanical analysis of motion such as reaching, pushing/pulling, grasping/throwing, lifting up/putting down, has been studied for different areas including motor control and learning, sports science, neurophysiology, surgical procedure simulation, human factors, and so on. The ultimate aim of biomechanical analysis is to know what the muscles are doing: the timing of their contractions, the amount of force generated (or moment of force about a joint),

and the power of the contraction. These quantities can be derived from the kinematics information using the laws of physics, specifically the Newton-Euler equations [80].

The critical item in biomechanical analysis is the inverse dynamics problem. Inverse dynamics, the procedure in which motion data is used to estimate torques (i.e., moments of muscle force) produced at the joints, is a primary tool for analysis of human movements (Figure 3.1). It is a simple and effective technique which can be used to infer which and how muscles are used in a motor task. A variety of data are needed to make the necessary calculations, including a record of the limb movements, and often a record of ground reaction forces and the anthropometric parameters specifying the inertial properties of each limb. The records of limb movements and ground reaction forces could be acquired by various motion capture system with the ground force plate in some configured rooms. The most critical issue in biomechanical analysis is the anthropometric parameters which are different among human and difficult to be measured. Therefore, to be broadly applicable, a biomechanical model of the musculoskeletal system must be accessible to users, and provides accurate representations of muscles and joints, and captures important interactions between joints.

In this context, computer models of the musculoskeletal system, for example, have been used to characterize limb impedance, analyze muscle coordination [81], and design neuro prosthetic devices [82]. Models that define the geometry and force-generating properties of individual muscles allow researchers to study inter-muscular coordination and to examine the contributions of specific muscles to movements, joint replacements and tendon transfers [83].

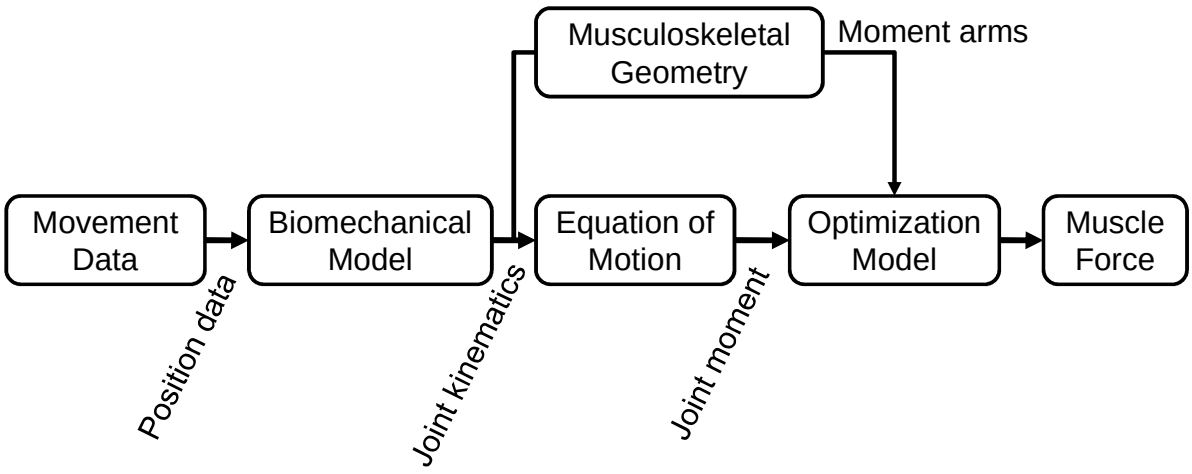

Figure 3.1: Flow chart of inverse dynamics procedure.

Recent advances in musculoskeletal modeling techniques and computational methods make it possible for development of new approaches to solve the problems of biomechanical analysis. The methods of dynamic simulations of movements allow us to study neuromuscular coordination, analyze athletic performance, and estimate internal loading of the musculoskeletal system. Simulations can also be used to identify the sources of pathological movements and establish a scientific basis for treatment planning [84].

3.1.3 Objective

A) Orientation estimate

This study is aimed at employing the quaternion-based extended Kalman filter (EKF) for sensor data fusion and orientation estimate of WB IMUs, which should achieve the system performance requirements described in Chapter 2 (accuracy: < 2 deg).

In particular, an innovative technique of R-Adaptive algorithm is proposed in this study to integrate with EKF. Evaluating the measurement covariance matrix in EKF, the R-Adaptive algorithm could overcome the problems on the correction of pitch and roll angles when there is a strong hypothesis of negligible linear accelerations in respect to the gravity.

The proposed sensor fusion algorithm is implemented in WB-3 IMU for performance validation. A comparison between WB-3 IMU and commercial IMU InertiaCube3 in regard to the Vicon motion capture system is elaborated to verify the algorithm performance. The techniques used in the experiments for data synchronization among these three different measurement systems are also discussed.

Twelve WB-3 IMUs are attached to the segments of human upper body for representing the human gesture. The upper body kinematics model then is developed based on the segment orientation acquired from each WB-3 IMU.

B) Biomechanical analysis of upper limbs

This study is aimed at investigating the upper limb's biomechanical parameters, such as joint moments and muscle tendon forces derived from different inter-segmental movements, by using the WB-3 motion tracking system with a biomechanical simulation model developed at [84].

The kinematics information of each joint is acquired from the experimental data by using WB-3 system, and then as the input to the simulation model for estimating the joint moments and muscle tendon forces.

The biomechanical analysis with WB-3 system could be a basis for us to look more insight into the doctor's operation skills while executing different medical procedures, and allows us to understand how the biological status going.

3.2 Methods and Materials

3.2.1 Sensor Fusion Algorithm

A) EKF for orientation estimation

The idea behind the sensor fusion is that, using several kinds of sensors, the characteristics of one type of sensor overcome the limitations of other sensors. In this way, the Kalman filter is useful for combining data from several different noisy measurements. In fact, gyroscopes measure orientation by integrating angular rates, and the accelerometer and magnetometer provide noisy and disturbed but drift-free measurements of orientation. The Kalman filter weights the three sources of information appropriately with knowledge about the signal characteristics based on their models, to make the best use of all sensor data [85].

In general, the EKF algorithm addresses the problem of trying to estimate the state of a discrete-time process described by the equations below [86]:

$$x_{k+1} = A_k x_k + B_k u_k + w_k \tag{3.1}$$

$$z_k = H_k x_k + v_k \tag{3.2}$$

Where, $\boldsymbol{x}$ is the state vector; $\boldsymbol{u}$ is the input vector; $\boldsymbol{A}$, $\boldsymbol{B}$, $\boldsymbol{H}$, are respectively state, input, and output matrix; $\boldsymbol{w}$, $\boldsymbol{v}$ are state and measurement noise. The state and measurement noise are Gaussian and white noise sources with covariance matrix $\boldsymbol{Q}$ and $\boldsymbol{R}$, respectively.

At each time step, the algorithm propagates both the state estimation and the error covariance matrix. The latter provides an indication of the uncertainty associated with the current state estimation. These are evaluated in the prediction equations.

The Kalman gain is derived from minimizing the a posteriori error covariance, and it could be considered as a measurement of the level of confidence to give to the predict state.

B) Quaternion-based EKF

In the IMUs, the main problem is that the orientation is computed by the integration of the gyro signals including any superimposed sensor drift and noise. The orientation drift errors, resulting from gyro output errors, can be bounded by additional sensors (in this case the 3-axis accelerometer and 3 axis magnetometer), whose information allows correcting the orientation drift. In this way the earth's gravitational and magnetic field vectors are resolved by the aiding system in the body frame, with their known representation in the absolute reference frame [86]. In the present work, a classic state augmentation technique is applied in the process model, and the state vector is composed by orientation and gyro bias. Quaternion is used to represent space orientation to improve computational efficiency and avoid singularities. After EKF running, the computed quaternion could be translated into roll, pitch and yaw angles, through transformation equations [68].

The continuous-time, non linear system equations are:

$$\dot{x} = f(x, \omega) + w \tag{3.3}$$

$$y = h(x) + v \tag{3.4}$$

where $\boldsymbol{x} = [\boldsymbol{q}\ \boldsymbol{b}_{\omega}]^T$ represents the state of the system composed by the quaternion $\boldsymbol{q} = [q_w\ q_x\ q_y\ q_z]$ and the rate gyro bias $\boldsymbol{b}_{\omega} = [b_{\omega x}\ b_{\omega y}\ b_{\omega z}]$; $\boldsymbol{\omega}$ is the angular velocity vector $[\omega_x\ \omega_y\ \omega_z]^T$; $\boldsymbol{y} = [\boldsymbol{a}\ \boldsymbol{m}]^T$ is the measurement vector composed by the acceleration measurements and magnetic measurements $[a_x\ a_y\ a_z\ m_x\ m_y\ m_z]^T$; $\boldsymbol{w}$, $\boldsymbol{v}$ are the state and measurement noise, respectively.

In a strap-down inertial navigation system, the rigid body angular motion is described by the differential equation [68]:

$$\dot{q} = \frac{1}{2}\begin{bmatrix} 0 & -\omega^T \\ \omega & [\omega\times] \end{bmatrix} q \tag{3.5}$$

Where

$$[\omega\times] = \begin{bmatrix} 0 & -\omega_z & \omega_y \\ \omega_z & 0 & -\omega_x \\ -\omega_y & \omega_x & 0 \end{bmatrix} \tag{3.6}$$

with the assumption that $|\boldsymbol{q}| = 1$.

Using the sensor model described in [68], in quasi static condition, the acceleration acting on the body is negligible compared to the gravity acceleration as described by:

$$\begin{cases} \omega = G_g \omega_r + b_\omega + v_g \\ a = G_a\left[C_n^b(q)(g)\right] + v_a \\ m = G_m[C_n^b(q)(H)] + v_m \end{cases} \tag{3.7}$$

where $\boldsymbol{G_g}$, $\boldsymbol{G_a}$, $\boldsymbol{G_m}$ are respectively gyroscope, accelerometer and magnetometer gain, supposed constant; $\boldsymbol{v_g}$, $\boldsymbol{v_a}$, $\boldsymbol{v_m}$ are respectively gyroscope, accelerometer, magnetometer noise; $\boldsymbol{\omega_r}$ is the gyroscope raw data $[\omega_{rx}\ \omega_{ry}\ \omega_{rz}]^T$; $\boldsymbol{C_n}^b(q)$ is the direction cosine matrix in terms of orientation quaternion, which represents the coordinate transformation from the inertial coordinate systems "*n*" to the sensor body frame "*b*":

$$C_n^b(q) = \begin{bmatrix} q_w^2 - q_x^2 - q_y^2 + q_z^2 & 2(q_w q_x + q_y q_z) & 2(q_w q_y - q_x q_z) \\ 2(q_w q_x - q_y q_z) & -q_w^2 + q_x^2 - q_y^2 + q_z^2 & 2(q_x q_y + q_w q_z) \\ 2(q_w q_y + q_x q_z) & 2(q_x q_y - q_w q_z) & -q_w^2 - q_x^2 + q_y^2 + q_z^2 \end{bmatrix} \tag{3.8}$$

The $\boldsymbol{g} = [0\ 0\ -G]^T$ is the gravity vector; $\boldsymbol{H} = [H_x\ 0\ H_z]^T$ is the local magnetic field in the inertial frame.

The non-linear functions, $f(\boldsymbol{x}, \boldsymbol{\omega})$, and $h(\boldsymbol{x})$ in (3.3) and (3.4) can be further explained as:

$$f(x,\omega) = \begin{bmatrix} \frac{1}{2}\begin{bmatrix} -q_x & -q_y & -q_z \\ q_w & -q_z & q_y \\ q_z & q_w & -q_x \\ -q_y & q_x & q_w \end{bmatrix}\begin{bmatrix} \omega_{rx} - b_{\omega x} \\ \omega_{ry} - b_{\omega y} \\ \omega_{rz} - b_{\omega z} \end{bmatrix} \\ b_{\omega}^{T} \end{bmatrix} \tag{3.9}$$

$$h(x) = \begin{bmatrix} C_n^b(q)\,g \\ C_n^b(q)\,H \end{bmatrix} \tag{3.10}$$

Because of its non-linearity, the system is linearized by calculating the Jacobian of f and h functions, therefore the EKF is implemented.

The estimation step of the EKF uses the angular velocity to make a prediction of the state. Furthermore, the acceleration and magnetic data are used to correct roll, pitch and yaw angles in the "Roll-Pitch Update" and "Yaw Update" blocks as showed in the Figure 3.2. The correction of yaw angle can be performed using the magnetometer. Magnetic interference is a major concern when using magnetometers in environments containing changing or distorted magnetic fields. No compensation for external magnetic effects is performed in the work described in this thesis. The problems and limitations of the magnetic correction in the EKF are now under further investigation from the author and several researchers in [87-90].

C) R-Adaptive algorithm

The main limitation of EKF algorithm in most current researches is related to the "quasi-static condition", in which the linear accelerations are negligible compared to the gravity acceleration. In the case of human motion tracking (i.e. during walking or running), often this condition is not verified.

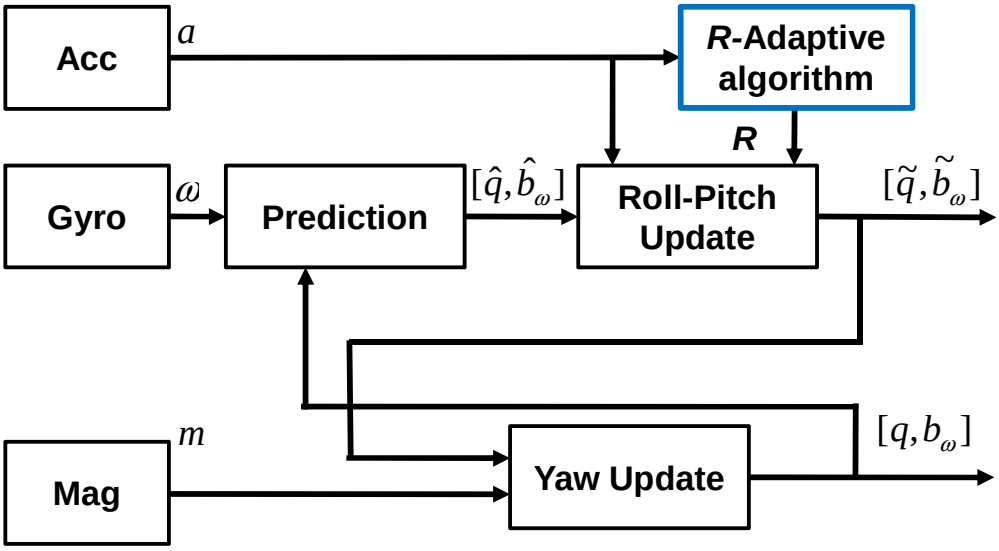

Figure 3.2: Block diagram of EKF with R-Adaptive algorithm.

To overcome the problems related to the correction of the attitude using the data from the accelerometer, several techniques have been previously used [91]. Some techniques check the angular rate and the module of acceleration to determine quasi-static conditions. If a quasi-static condition is detected, the "Roll-Pitch Update" phase of the EKF is performed, otherwise it is just skipped. These techniques solve quite efficiently the drawback of the EKF, however the threshold that discriminates between the dynamic and static conditions must be chosen opportunely. Furthermore, it is difficult to set the coefficients of the measurement covariance matrix ***R***. Not only the measurement noises, but also the errors due to the centripetal accelerations of rotations and linear accelerations should be considered for a correct evaluation. To overcome these problems, the R-Adaptive algorithm has been proposed and implemented in the EKF to adaptively estimate the coefficients of acceleration measurement covariance matrix ***R*** (Figure 3.2).

R is assumed to be in this form:

$$R = \begin{bmatrix} \sigma_x^2 & 0 & 0 \\ 0 & \sigma_y^2 & 0 \\ 0 & 0 & \sigma_z^2 \end{bmatrix} \tag{3.11}$$

Where, σ_x, σ_y, and σ_z are the standard deviations of the measurements respectively for the x, y and z axis of the acceleration sensor.

Considering the sensor axis with the same noise characteristics ($\sigma_x = \sigma_y = \sigma_z = \sigma$), it is possible to model the standard deviation as:

$$\sigma = \sigma_o + \sigma_d \tag{3.12}$$

Where, σ_0 is the standard deviation in static condition, due to the accelerometer noise; σ_d is the standard deviation due to acceleration of different movements, that deviates from static conditions. σ can be estimated at each step by a temporal window with the following formula:

$$\sigma_k^2 = \frac{1}{N+1}\sum_{k-N}^{k}(|a_k| - |a_{k-1}|)^2 \tag{3.13}$$

Where, N is the number of samples of the temporal window; σ_k^2 is the estimated variance at step k; and $|a_k|$ is the module of the acceleration measured by the accelerometer at the step k.

3.2.2 Segment Orientation Representation of Human Upper Body

In order to represent the orientation of a rigid body, it is conventional to choose a coordinate system attached to an appropriate inertial frame, and then express all vectors in component form relative to this coordinate. A commonly used coordinate system is the inertial “flat Earth” system with an arbitrarily selected origin on the surface of the Earth with coordinate axes x, y, and z directed in the local north, east and up directions, respectively. To specify orientation, it is also necessary, for each rigid body, to specify a “body fixed” coordinate system or frame which is attached to the rigid body. The superscript or subscript “*n*” is most often used to designate inertial coordinates, while “*b*” is typically used to signify sensor body coordinates. The description of the orientation of a rigid body expresses the relationship between these two coordinate systems (Figure 3.3).

The quaternion-based EKF has been designed to track human segment orientations relative to the inertial Earth-fixed reference coordinate.

The WB-3 system is consisted a human upper body model which attached by 12 WB-3 IMUs on the human segments as showed in Figure 3.4. This model can be used to accurately track upper body gestures in real time. Attachment of the WB-3 IMU to each of the major limb segments of a human makes it possible to independently determine the orientation of each segment relative to the inertial Earth-fixed reference frame. The human model is constructed from multiple independently oriented limb segments that are constrained by their attachment to each other. Relative orientation between limb segments can be easily determined by the inertial orientation of those limb segments.

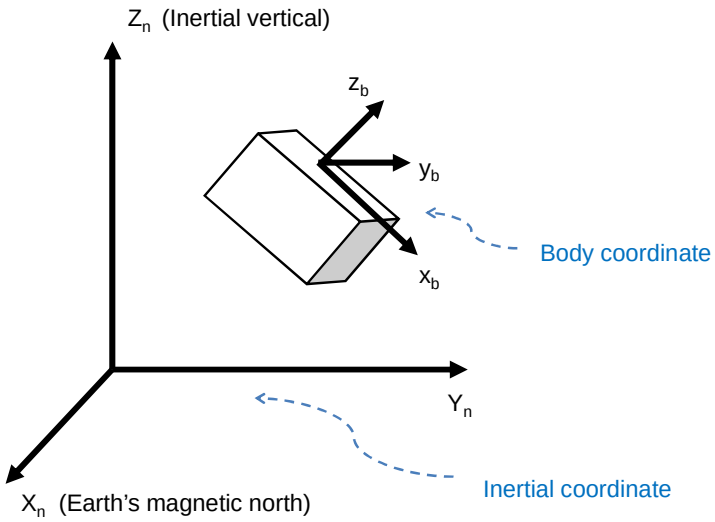

Figure 3.3: Description of inertial coordinate and body coordinate.

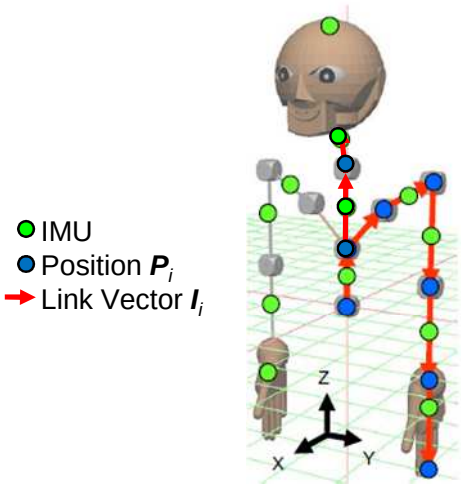

Figure 3.4: Upper body kinematics model (initial gesture).

WB IMU can estimate the orientation of the sensor module itself. The relation between the sensor frame and the frame of body segment on which the sensor is mounted has to be known. This is so-called offset/initial gesture for the human model calibration procedure. In the calibration procedure, sensor data is recorded while the body segment is kept on some pre-defined positions, such as the initial gesture showed in Figure 3.4. The quality of this calibration procedure determines the quality of the practical motion assessment. Here the offset gesture is denoted as E^{i}_{offset} for each link. The motion is then calculated by the rotation matrix from the quaternion of EKF by the following formula:

$$R_i = \begin{bmatrix} 1-2q_y^2-2q_z^2 & 2q_xq_y-2q_zq_w & 2q_xq_z+2q_yq_w \\ 2q_xq_y+2q_zq_w & 1-2q_x^2-2q_y^2 & 2q_yq_z-2q_xq_w \\ 2q_xq_z-2q_yq_w & 2q_yq_z+2q_xq_w & 1-2q_x^2-2q_y^2 \end{bmatrix} \tag{3.14}$$

Where, i means the link segment number. Therefore, the orientation of each segment in the inertial coordinate at each system time step is calculated by the following formula:

$$E^{i} = R_i E^{i}_{offset} \tag{3.15}$$

The position $\boldsymbol{P}_i$ is then calculated by the following formula:

$$P_i = P_{i-1} + E^{i-1} l_{i-1} \tag{3.16}$$

Where, the $\boldsymbol{l}_i$ is the length vector of each link segment.

3.2.3 Biomechanical Simulation Model

The simulation model is a musculoskeletal upper limb modeled as a three-dimensional 4 degrees of freedom (DOF) system, linked to the shoulder which has been considered as reference frame (Figure 3.5). The shoulder joint and elbow joint have 3 DOF and 1 DOF, respectively. The model simulates the muscle–tendon lengths and moment arms for each of the muscles over a wide range of postures.

For the musculoskeletal geometry, muscles are modeled as line segments with 'via points' that allows muscles to wrap around bones and joints. These muscles include the major flexor and extensors surrounding the elbow and shoulder joints, which includes the biceps short head (BICshort), biceps long head (BIClong), brachialis (BRA), triceps long head (TRIlong), and triceps medial (TRImed). Muscle origins and insertions are initially represented in the different segment coordinate systems and transformed into a common system for the purposes of calculating musculo-tendon length. The force generated by each muscle is multiplied by the respective moment arm and summed across muscles to yield the muscle torque. All these procedures are implemented by the simulation software OpenSim [84]. Given a pattern of muscle activations, the model estimates muscle forces and joint moments.

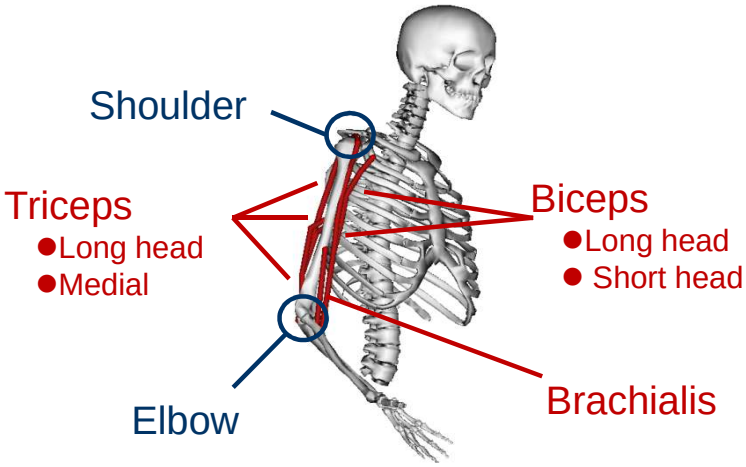

Figure 3.5: Biomechanical simulation model of upper limb.

3.2.4 Biomechanical Analysis Sequence with WB-3 system

Following the conceptual inverse dynamics model described above, the biomechanical analysis sequence with WB-3 IMUs and simulation model is showed in Figure 3.6, to simulate and estimate the human planar arm movements, joint moments and muscle tendon forces. The sequence starts from the movement data acquisition and analysis to achieve the joint kinematics information from WB-3 system. The multi-joint dynamics function block includes the equations of motion to evaluate the joint moment values. The biomechanical model with the musculoskeletal geometry information and optimization model in OpenSim environment is used to generate the tendon force information of each muscle.

In the biomechanical model, the upper limb is represented as a multi-segment rigid body system. For simplification, each segment of upper limb is modeled as a rigid body with a corresponding length, mass and moment of inertia. The hand position, with respect to the reference frame of shoulder joint, is expressed in terms of the joint angles and segment geometry parameters.

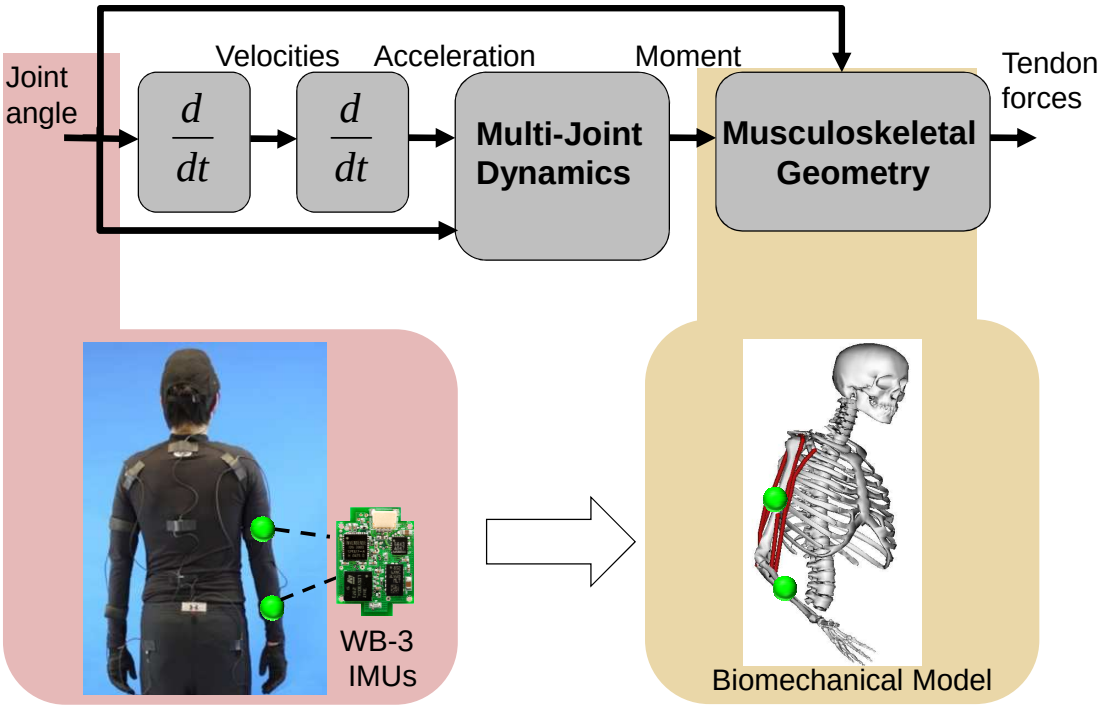

Figure 3.6: Inverse dynamics analysis with WB-3 system.

3.3 Experimental Evaluation

3.3.1 Experiment #1 for Orientation Estimate

A) Experiment objective

This experiment is aimed at evaluating the performance of the proposed R-Adaptive algorithm with EKF used in WB IMU for orientation estimate, which should satisfy the system specification described in Chapter 2.

The experiments are elaborated by using the WB-3 IMU compared with the commercial IMU (InertiaCube3 by InterSense Inc.) in regard to the Vicon motion capture system, to verify whether the WB system is capable of tracking object's orientation with less than 2 deg accuracy.

The data processing model for the performance comparison among these three systems is showed in Figure 3.7. The Vicon system which has the highest accuracy among these three systems is used as the reference system.

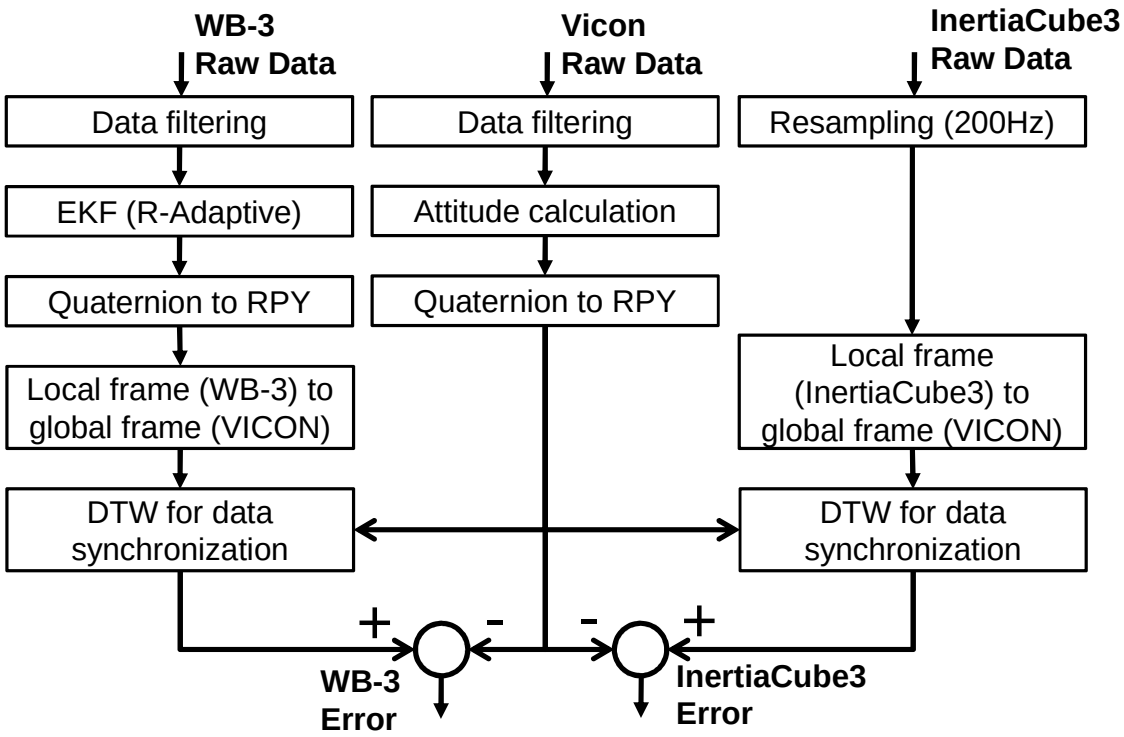

Figure 3.7: Data processing model for performance comparison among WB-3, InertiaCube3 and Vicon systems.

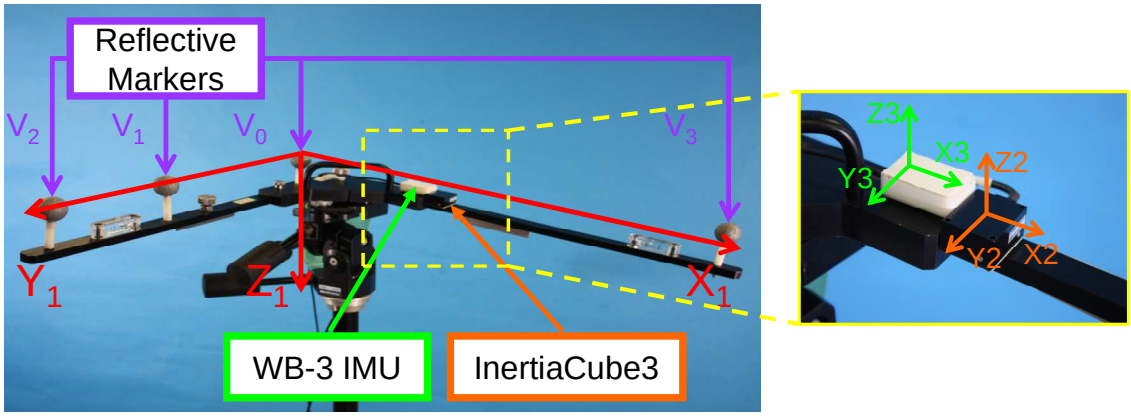

Figure 3.8: Experimental setup of L-frame with reflective markers, InertiaCube3 and WB-3.

B) Experiment setup and protocol

To construct the data set for the analysis, the WB-3 IMU and InertiaCube3 were linked with a metallic L-frame using adhesive (Figure 3.8). The metallic L-frame had four reflective markers for determining its exact attitude in the global Vicon reference system.

In order to evaluate the performance of R-Adaptive algorithm with EKF, the experiments were focused on analyzing the rotation movements about x and y axis, which are related to the "Roll-Pitch Update" of EKF affected by acceleration data. Two trials were elaborated, and all the data were logged for off-line analysis.

1) For the first trial, the systems were rotated about x-axis of the L-frame at different speeds for more than 10 rotation repetitions;
2) For the second trial, the systems were rotated about y-axis of the L-frame at different speeds for more than 10 rotation repetitions.

3.3.2 Experiment #2 for Biomechanical Analysis of Upper Limb

A) Experiment objective

The objective of this experiment is to compare the generated joint moments and muscle forces caused by different movements and gestures of upper limb to complete planar motion tasks. It allows us to understand which gesture or what kind of motion is better and easier for executing the task with less biological energy consumption.

Therefore, the human subject in this experiment is conducted to perform a lifting task by using different joint motion of right upper limb. Kinematic data collected by WB-3 system is used as the input to the biomechanical analysis for the estimate of joint moments and muscle tendon forces.

B) Experiment setup and protocol

Two WB-3 IMUs used in the experiment were attached to the human subject's forearm and upper arm, respectively (Figure 3.9). The subject was instructed to sit on a chair and perform lifting tasks of load with 1000 g. The task included two steps:

1) Elbow rotation: Lifting up the load from the vertical attitude to the level attitude of forearm, using only the rotations of elbow joint, while upper arm keeping vertical attitude. Three repetitions are required.
2) Shoulder rotation: Lifting up the load from the vertical attitude to the level attitude of whole limb, using only the rotations of shoulder joint. Three repetitions are required.

Therefore, six rotations (3 elbow rotations and 3 shoulder rotations) for lifting up the load were executed.

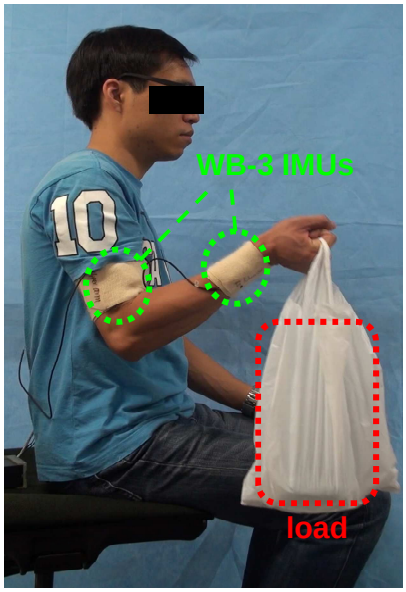

Figure 3.9: Experimental setup of biomechanical analysis.

3.4 Experimental Results

3.4.1 Results of Experiment #1

A) Data synchronization

The WB-3 IMU and Vicon system had a sampling frequency of 200 Hz which is enough for the majority of applications in human body movement analysis. The commercial IMU InertiaCube3 sampled internally the sensors at 180 Hz, but the attitude angle update frequency actually given by this IMU was quite variable (Figure 3.10). The main update rate of InertiaCube3 was 40 Hz (every 25 ms) with about 77% samples. The other update rates were widely distributed at 25 Hz (40 ms), 18 Hz (55 ms), 11.8 Hz (85 ms), 8.7 Hz (115 ms) and 7 Hz (140 ms), with totally about 23% samples. In the case of WB-3 IMU, its sampling rate was very stable, 100% of the samples were transmitted with a sampling time of 5 ms (200 Hz). This guarantees the system calculation accuracy with constant time step and shows the advance of WB-3 IMU in sampling rate performance.

For an effective comparison with these three systems, the data of InertiaCube3 has been over-sampled in post-elaboration at the frequency of 200 Hz.

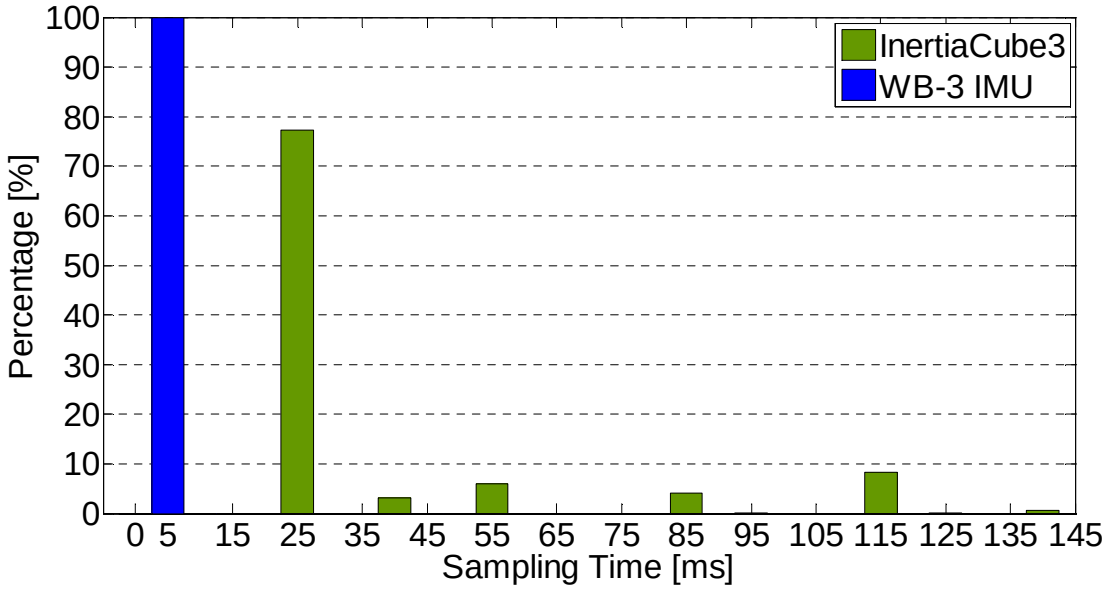

Figure 3.10: Histogram of the sampling time of WB-3 IMU and InertiaCube3.

An important phase for the performance comparison of WB-3 IMU with other systems is the data synchronization problem. The Euclidean distance is an efficient distance measurement that can be used to determine similarity between time series (in our case the orientation measurements).

The Euclidian distance between two time series is simply the sum of the squared distances from each point nth in one time series to the nth point in the other. The main disadvantage of using Euclidean distance for time series data is that its results are very unintuitive. If two time series are identical, but one is shifted slightly along the time axis due to a no-perfect synchronization or variation of the sampling time, then Euclidean distance may consider them to be very different from each other.

To overcome this limitation and give intuitive distance measurements between time series, the dynamic time warping (DTW) algorithm was implemented in this study [92]; DTW scales the time dimension reducing the problems of both global and local shifts in the time. One part of the results of DTW on the data obtained from WB-3 IMU synchronized with Vicon system is showed in Figure 3.11. It is clear that the DTW could match these two time series data well. Therefore, all the data from WB-3 IMU and InertiaCube3 have been synchronized to the data of Vicon system by DTW algorithm for performance comparison.

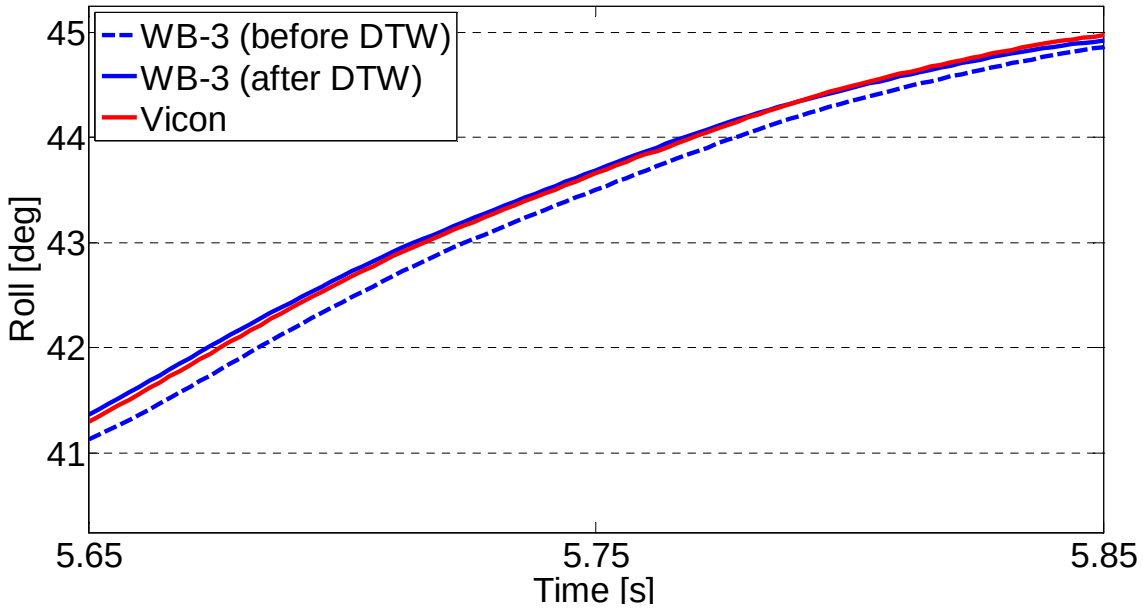

Figure 3.11: DTW elaboration of WB-3 IMU data to Vicon data.

B) Results of first trial

The resulting root mean square (RMS) errors of orientation estimate by WB-3 IMU and InertiaCube3 in the first trial are presented in Table 3.1. InertiaCube3 had the RMS errors of 6.57 deg for the roll movements; 2.94 deg for the pitch movements and 4.52 deg for the yaw movements. Conversely, WB-3 IMU had the RMS errors of 2.22 deg for roll angle, 0.63 deg for the pitch angle and 1.80 deg for the yaw angle, which were much lower than the results of InertiaCube3. It is clear that WB-3 had much better dynamic performance in this trail. Although the error of roll angle of WB-3 IMU was (0.22 deg) bigger than 2 deg, the average performance (1.55 deg) of these three angles was still within the system specification of less than 2 deg.

Table 3.1: WB-3 IMU performance evaluation during rotations about x axis.

	RMS Roll Error [deg]	RMS Pitch Error [deg]	RMS Yaw Error [deg]
WB-3 IMU	2.22	0.63	1.80
InertiaCube3	6.57	2.94	4.52

More detail information about all the results of this trial is showed in Figure 3.12 and Figure 3.13.

Figure 3.12 shows the roll, pitch and yaw angles of three systems during the whole rotation procedure. It is clear that WB-3 IMU could follow the trajectory of Vicon system better than InertiaCube 3. In the case of roll angle, the InertiaCube3 had some critical errors at the peaks of the signal, which were the turning moments of the rotation movements. At these turning points, there were strong changes of angular speeds which will result in big variance of centripetal acceleration. This will affect the performance of “Roll-Pitch Update” in EKF. For WB-3 IMU, it could adapt to this condition better with the dynamic acceleration covariance estimate. Similar results were happened in the angles of pitch and yaw. WB-3 IMU had more close performance to Vicon system in this trial.

Figure 3.13 shows the correspondent errors of WB-3 and InertiaCube3 compared to the Vicon system. The results give evidence of better dynamic performance of WB-3 IMU, in particular for the roll movements as indicated in Table 3.1. In the case of pitch and yaw, WB-3 IMU also had smaller angle error ranges than InertiaCube3.

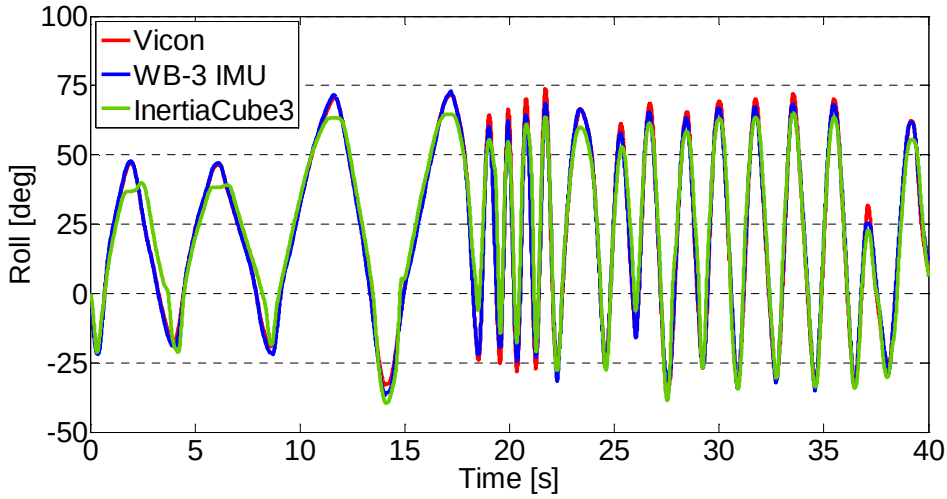

(a) Roll angle.

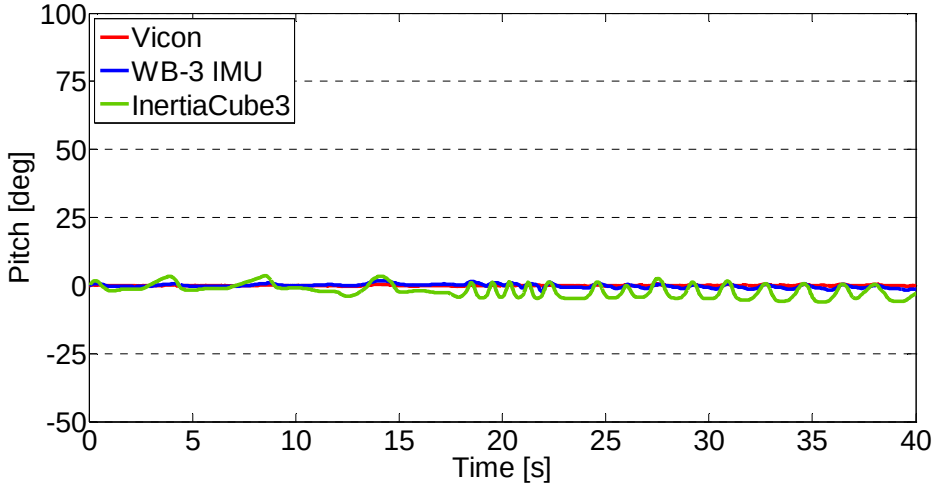

(b) Pitch angle.

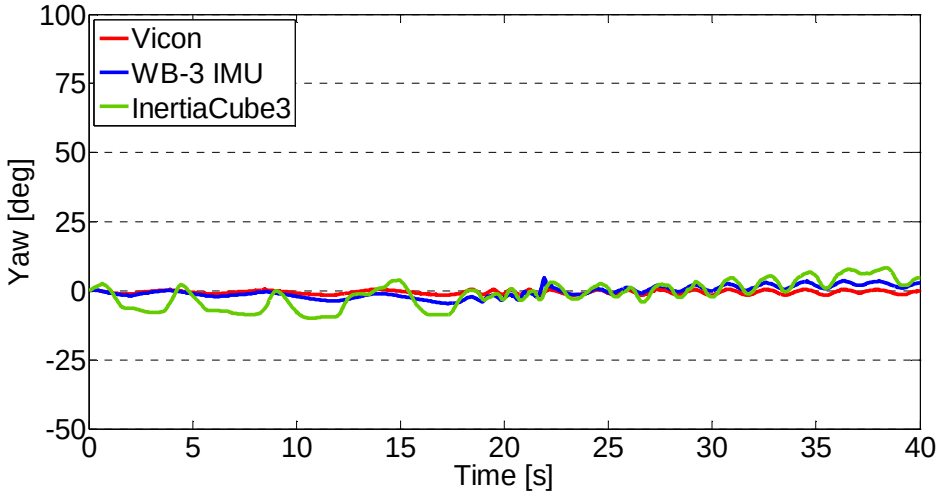

(c) Yaw angle.

Figure 3.12: Comparison of WB-3 and InertiaCube3 with Vicon during rotations about x axis.

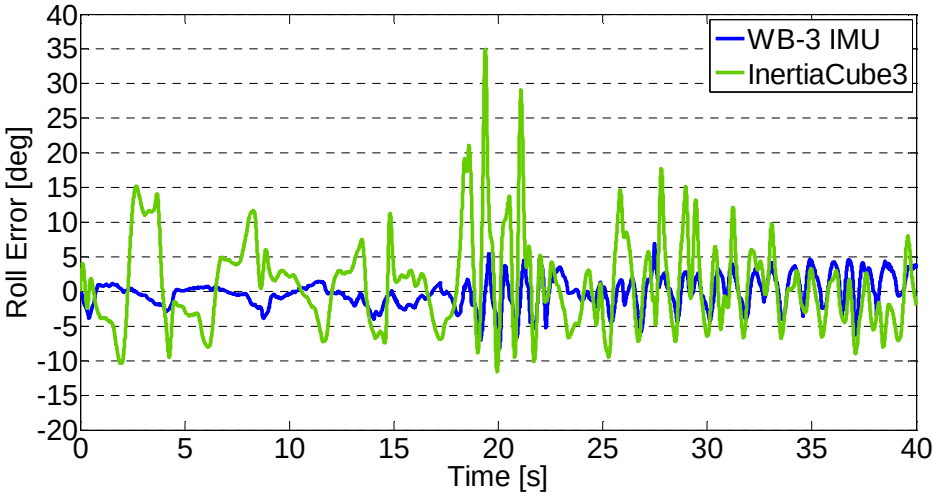

(a) Roll angle error.

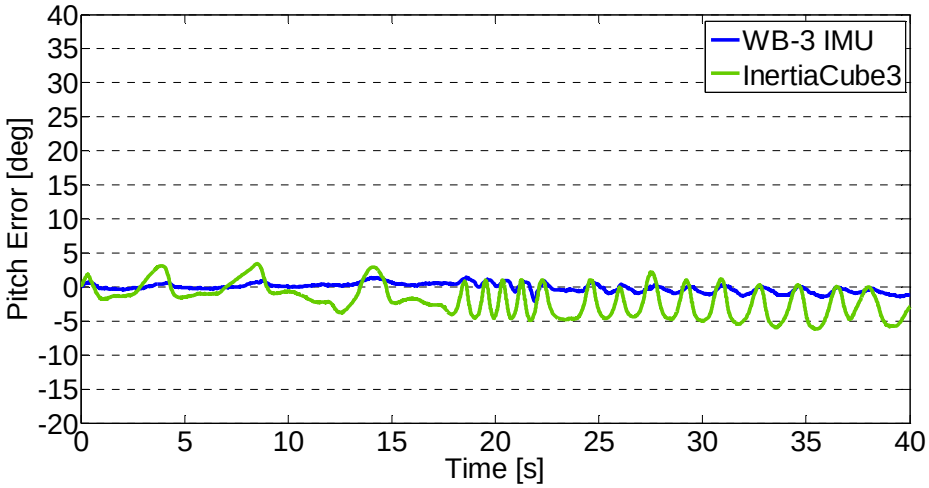

(b) Pitch angle error.

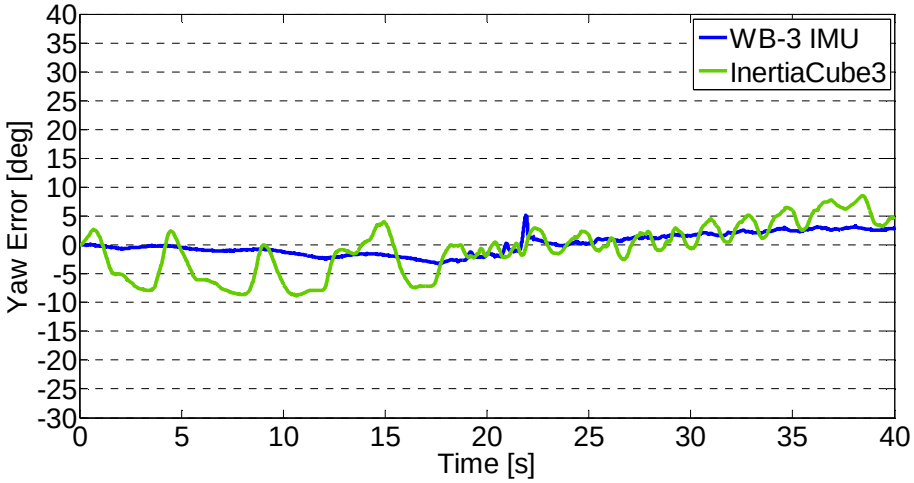

(c) Yaw angle error.

Figure 3.13: Angle errors of WB-3 and InertiaCube3 during rotations about x axis.

C) Results of second trial

The resulting RMS errors of second trial are presented in Table 3.2. The InertiaCube3 had better performance than WB-3 IMU in both roll and pitch angles in this trial. It had the RMS errors of 1.06 deg for the roll movements, 1.53 deg for the pitch movements and 1.40 deg for the yaw movements. Conversely, WB-3 had the RMS errors of 1.88 deg for roll angle, 2.69 deg for the pitch angle and 1.32 deg for the yaw angle. Although the error of pitch angle of WB-3 IMU was (0.69 deg) bigger than 2 deg, the average performance (1.96 deg) of these three angles was still within the system specification of less than 2 deg.

Table 3.2: WB-3 IMU performance evaluation during rotations about y axis.

	RMS Roll Error [deg]	RMS Pitch Error [deg]	RMS Yaw Error [deg]
WB-3 IMU	1.88	2.69	1.32
InertiaCube3	1.06	1.53	1.40

Figure 3.14 shows that InertiaCube3 could follow the trajectory of Vicon system better than WB-3 IMU in this trial. In the case of pitch angle, WB-3 IMU had bigger peak values than Vicon and InertiaCube3 systems. In the other hand, it performed much smoothly in the roll and yaw angles.

Figure 3.15 shows the error comparison of WB-3 IMU and InertiaCube3 in regarding to Vicon system. Both systems showed angle error spikes during the rotations. In the cases of roll and pitch angles, InertiaCube3 had smaller values of error range than WB-3 IMU, contrarily, it performed worse in the yaw angle with some peak errors.

Although WB-3 IMU had worse performance of roll and pitch angles than InertiaCube3 in this trial, it still had reasonable dynamic performance as in the first trial, which satisfied the system requirements.

It is also important to notice that, the attitude reconstruction algorithm of InertiaCube3 did not work if the pitch angle was around 90 deg because of singularity problems due to the Euler angle representations. The WB-3 algorithm was not affected by this problem because of the quaternion angle representation of EKF.

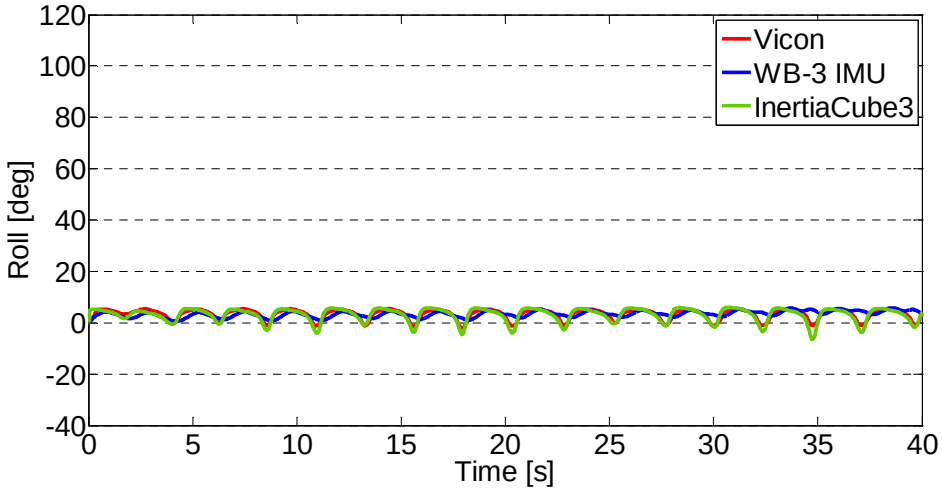

(a) Roll angle.

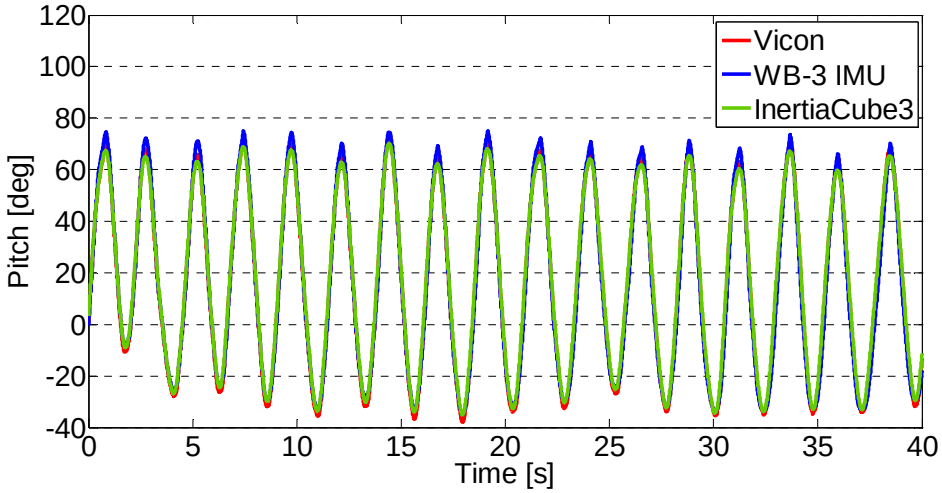

(b) Pitch angle.

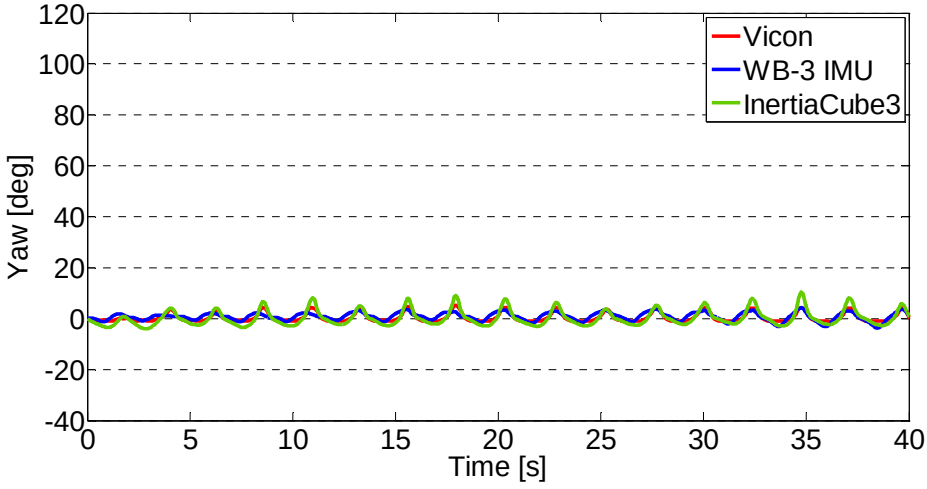

(c) Yaw angle.

Figure 3.14: Comparison of WB-3 and InertiaCube3 with Vicon during rotations about y axis.

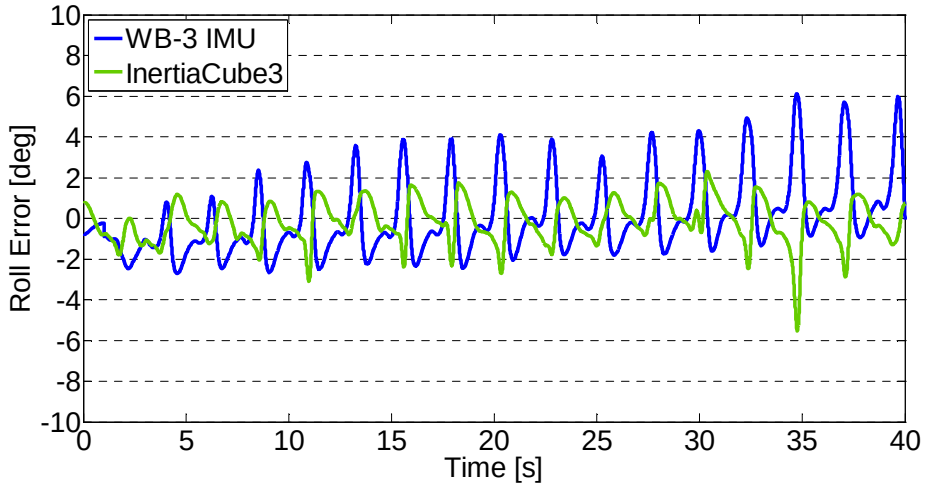

(a) Roll angle error.

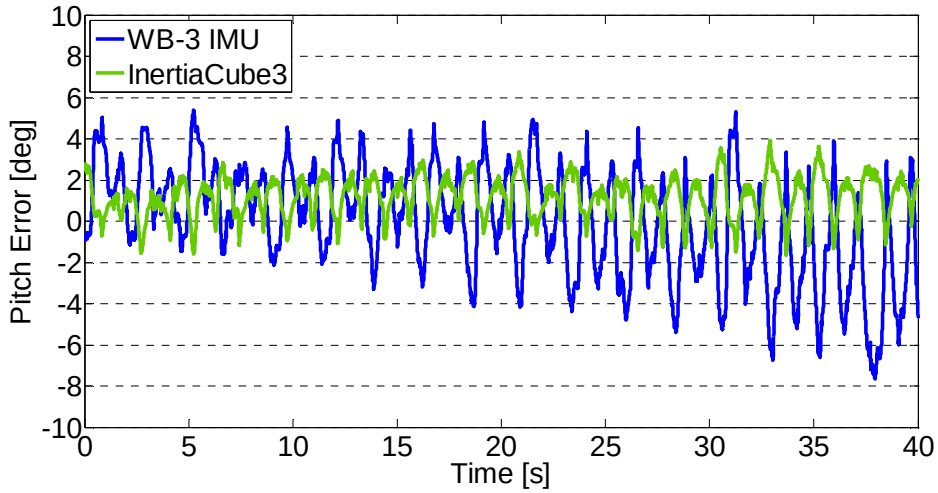

(b) Pitch angle error.

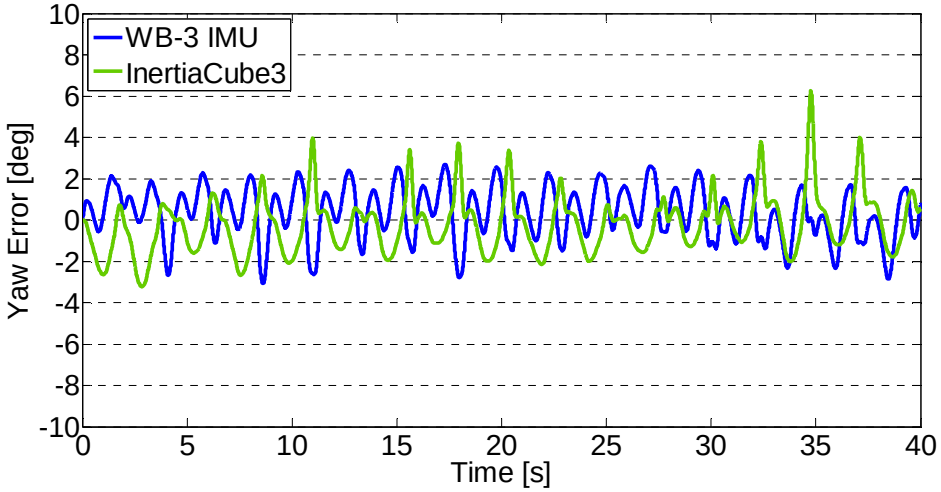

(c) Yaw angle error.

Figure 3.15: Angle errors of WB-3 and InertiaCube3 during rotations about y axis.

D) Demonstration of WB-3 IMU motion tracking

Figure 3.16 shows a real time demonstration of WB-3 IMU orientation estimate based on the described sensor fusion algorithm. The 3D visualization of the WB-3 IMU was showed in the user PC by using the OpenGL. The sampling rate of WB-3 IMU was 200 Hz. On the right side of each subfigure, the WB-3 IMU was being rotated by the operator. On the left side, it was visualizing the 3D orientation of WB-3 IMU in inertial frame. It is clear that WB-3 system is capable of measuring the majority of human motion in real time scenario.

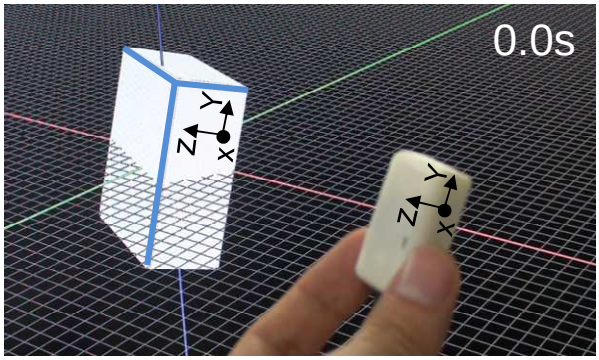

(a) initial position.

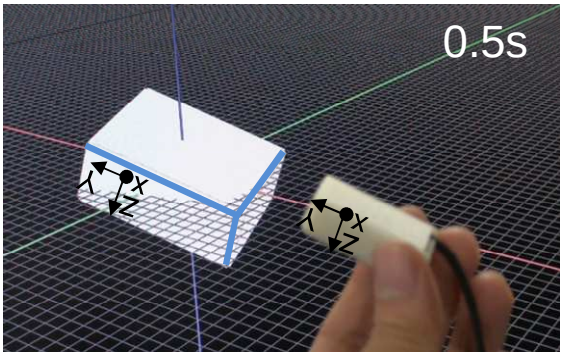

(b) rotating about 90 deg.

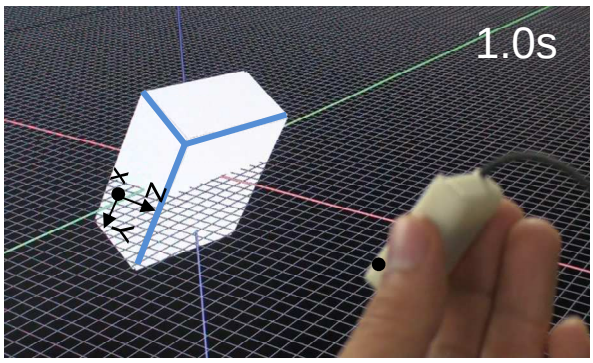

(c) rotating about 180 deg.

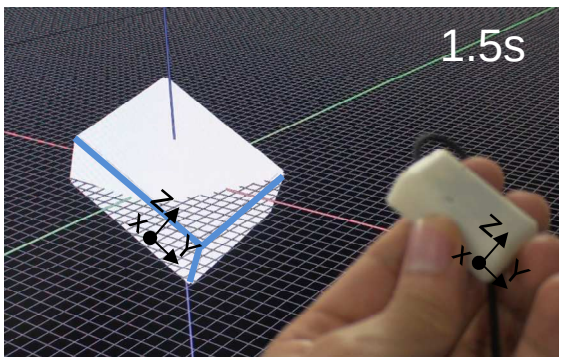

(d) rotating about 270 deg.

Figure 3.16: Real time motion tracking of WB-3 IMU during the rotations about x axis.

E). Demonstration of upper body motion tracking

The Figure 3.17and Figure 3.18 are the WB-3 motion tracking demonstrations of upper limb movements and a behavior of drinking water, respectively.

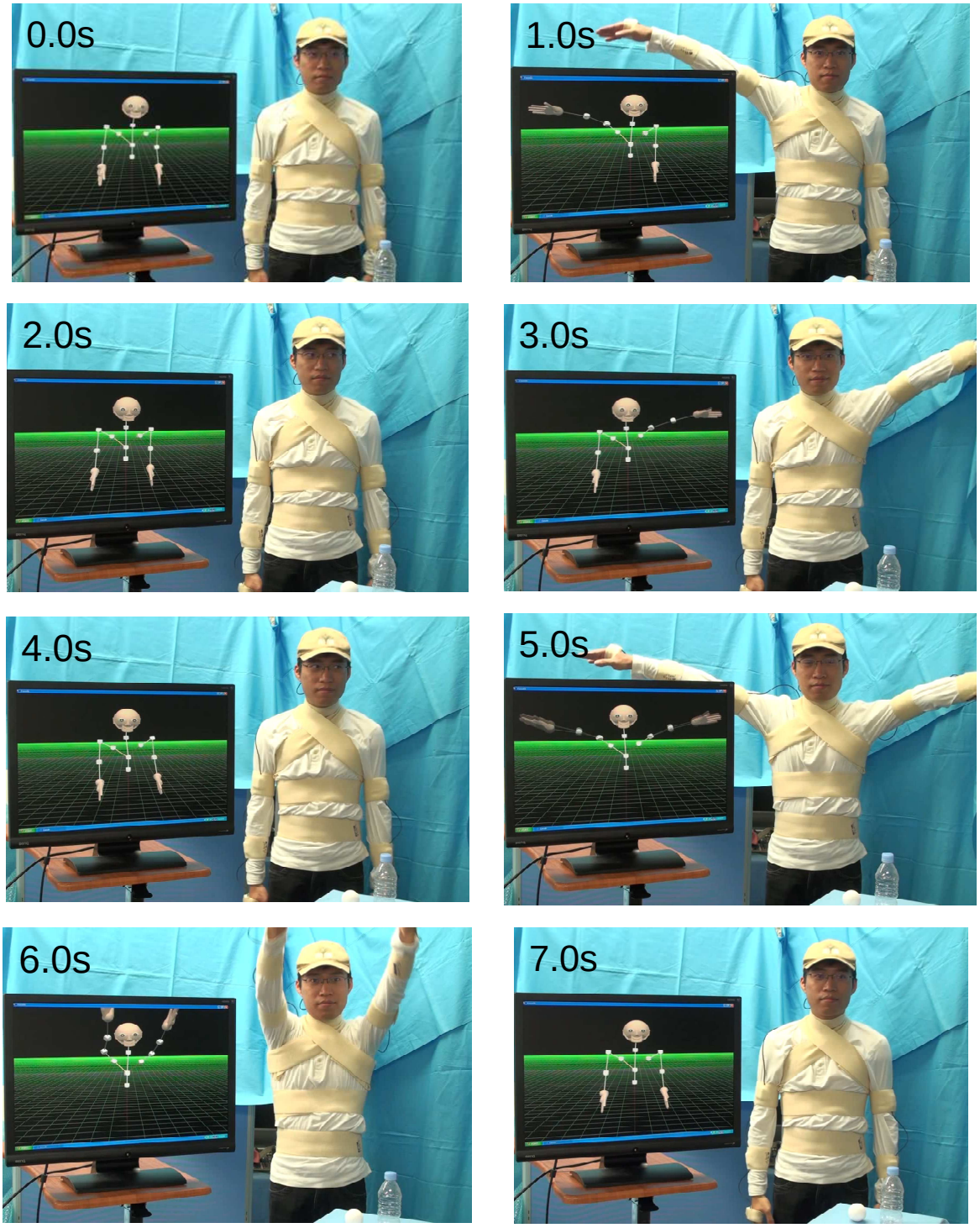

Figure 3.17: WB-3 motion tracking demonstration for upper limb movements.

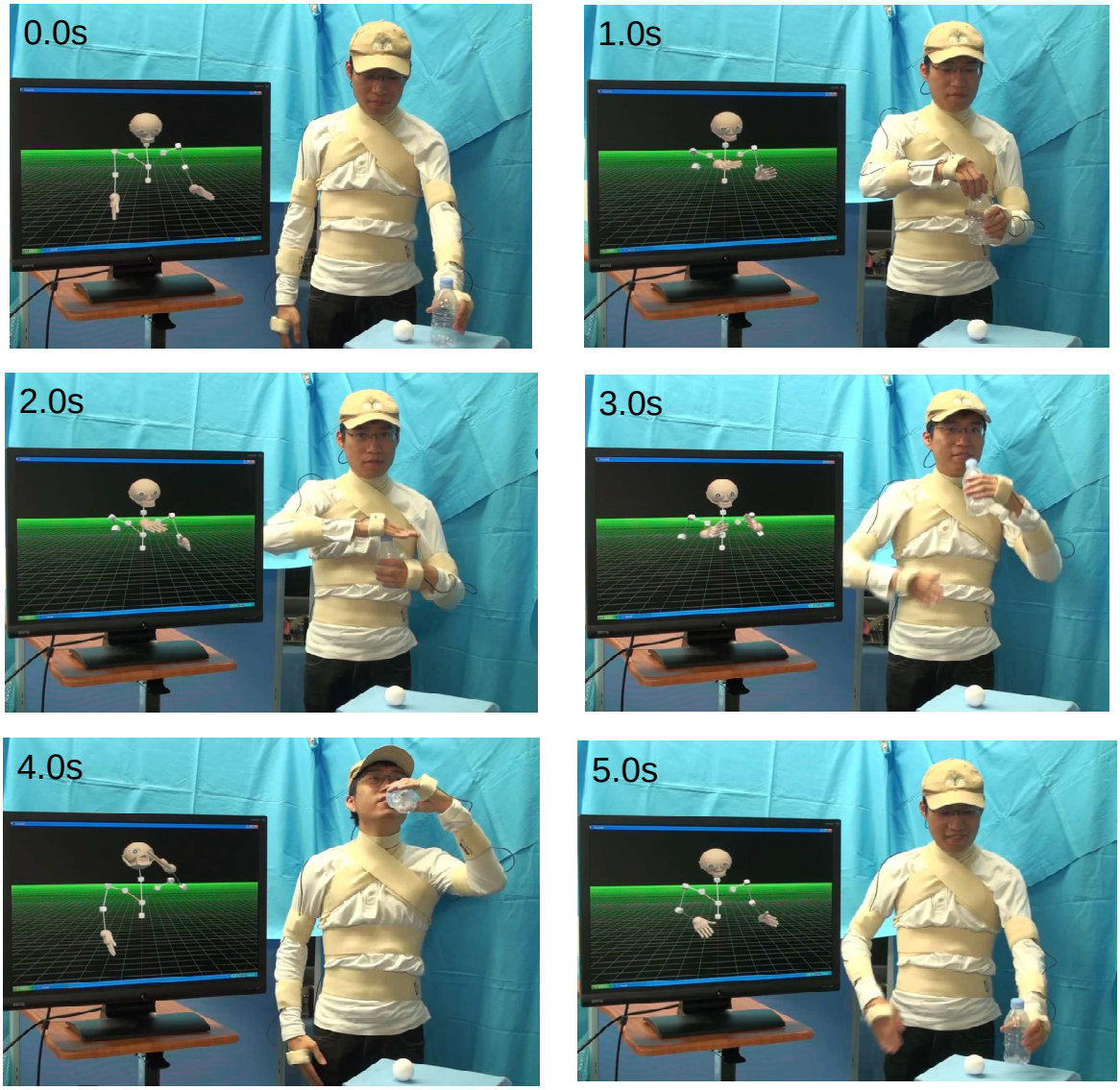

Figure 3.18: WB-3 motion tracking demonstration for drinking water movements.

3.4.2 Discussion of Experiment #1

The experiment evaluated the performance of the sensor fusion algorithm for orientation estimate of WB system compared with a 3D optical tracking system Vicon and inertial system InertiaCube3. The RMS difference between WB-3 system and Vicon system was less than 2 deg in average, which verifies the advance of R-Adaptive algorithm with EKF in WB system. The experimental results showed that the dynamic accuracy of WB-3 IMU was better than the commercial IMU InertiaCube3 in the first trial for x axis rotations, however, the opposite results happened in the second trial for y axis rotations. In fact, the results were heavily relied on the signal synchronization problem. If the WB-3 IMU and InertiaCube3 could match the signals of Vicon system well, the RMS errors estimate would be much close to the real conditions. As we can see in the results of first trial, the InertiaCube3 could not follow the trajectory of Vicon system well, which might be due to the problem of the DTW accuracy. A more detail and optimized comparison between WB-3 system and other motion tracking technologies should be evaluated with better solutions for signal synchronization, such as by hardware interrupt signal. Some possible differences in the results will be also related to the Vicon system, which had the variation in the 3D position measurements of markers.

The performance of WB-3 IMU was evaluated without prior sensor calibration in this experiment, which means that the bias and gain of each sensor were acquired from the default values of datasheets. Therefore, WB-3 IMU could even achieve better accuracy performance after calibrating the all the sensors by WBCal-1 system. The experimental result of sampling rate showed that, WB-3 IMU had much more stable performance than the InertiaCube3 IMU. This significant feature allowed WB-3 IMU suitable for analyzing widely the motion with different frequencies. This experiment was elaborated in a structured environment of Vicon system, where the force plate might affect the performance of yaw angle by the magnetic interference [93].

3.4.3 Summary of Experiment #1

The WB-3 IMU angular accuracy performance was evaluated by the comparison with a commercial IMU InertiaCube3 in regard to Vicon reference system. The experimental results verified that the performances of WB-3 IMU were comparable with the commercial product and satisfied the system requirements discussed in Chapter 2. Moreover, the implementation

of the R-Adaptive algorithm with EKF allowed the WB-3 IMU to achieve better performance than the InertiaCube3 in the first trial and achieved more stable dynamic accuracies in both trials.

3.4.4 Results of Experiment #2

A) Motion representation

The kinematic data collected from subjects by WB-3 system was inputted to the simulation model, the joint moment and individual muscle forces were simulated. Figure 3.19 and Figure 3.20 show the motion representation of the first step (only elbow rotations) and the second step (only shoulder rotations) of lifting task in the OpenSim software, respectively. It is clear that the WB-3 system could track and analyze the human motion effectively, and the motion data could be used for the biomechanical analysis with the simulation model.

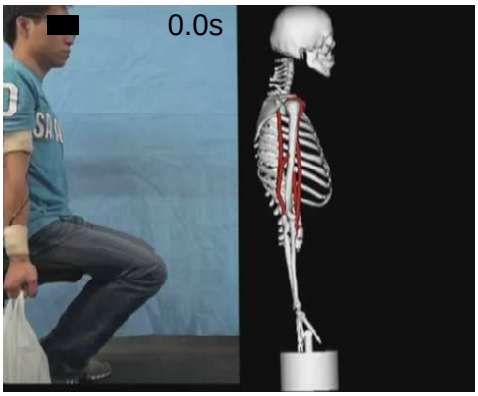

(a) initial posion.

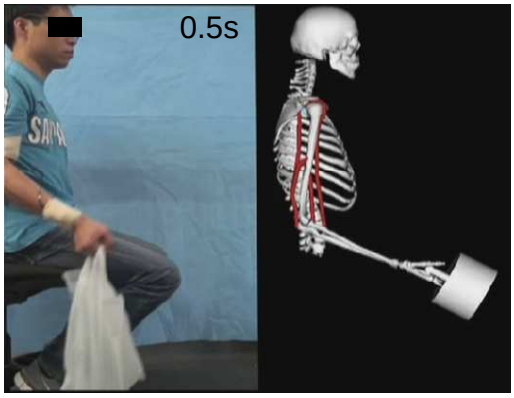

(b) lifting up progress.

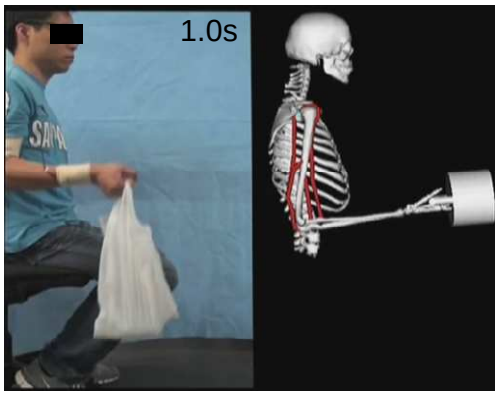

(c) end posion.

Figure 3.19: Motion representation of only elbow rotations in the lifting up task by using WB-3 system.

(a) initial posion. (b) lifting up progress.

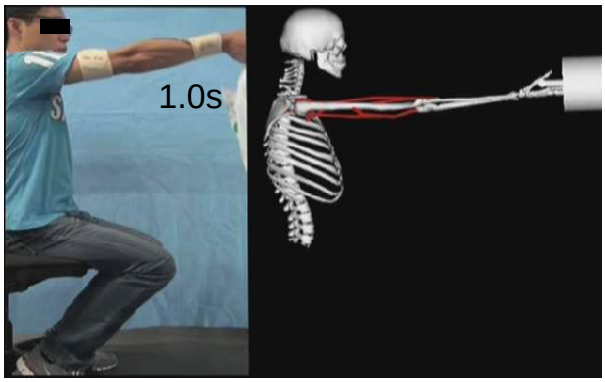

(c) end posion.

Figure 3.20: Motion representation of only shoulder rotations in the lifting up task by using WB-3 system.

B) Estimate of joint moment and tendon force

Figure 3.21 graphically shows the simulation results of the joint moments at shoulder and elbow. At the first step, the joint moment values used at shoulder and elbow were similar while only using elbow rotation to lift up the load. However, the shoulder moments significantly increased at the second step of the task while using only the shoulder rotation. The joint moment values of shoulder become almost 3 times bigger than the ones at the first step, which means that lifting up the load by using only shoulder rotation was more difficult and energy consumed than using the elbow joint. It is compatible with the physical theory, as the moment arm in the second step was much longer. Therefore, the joint moment could be estimated by using the kinematics data from the WB-3 motion tracking system.

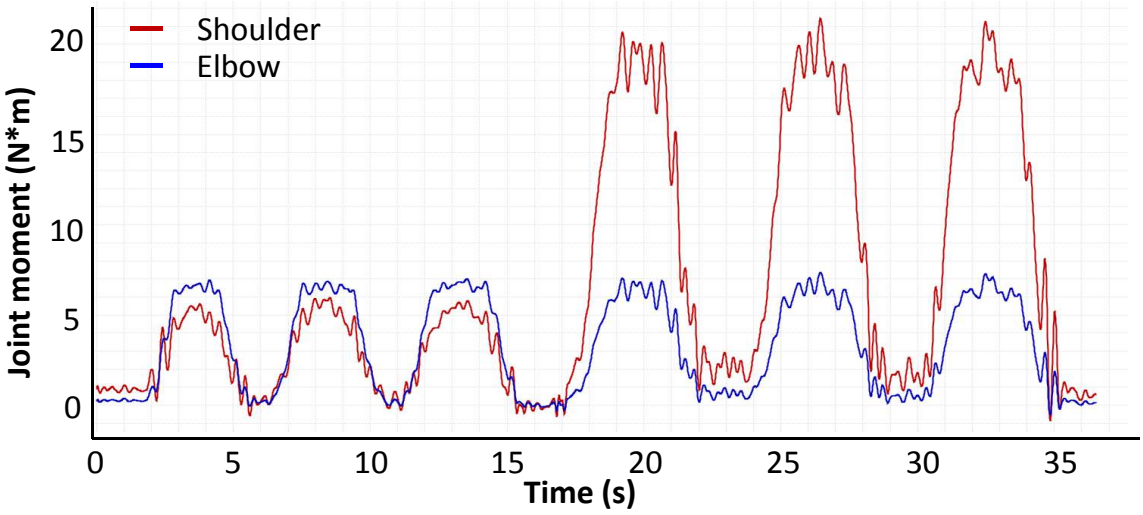

Figure 3.21: Joint moments of shoulder and elbow.

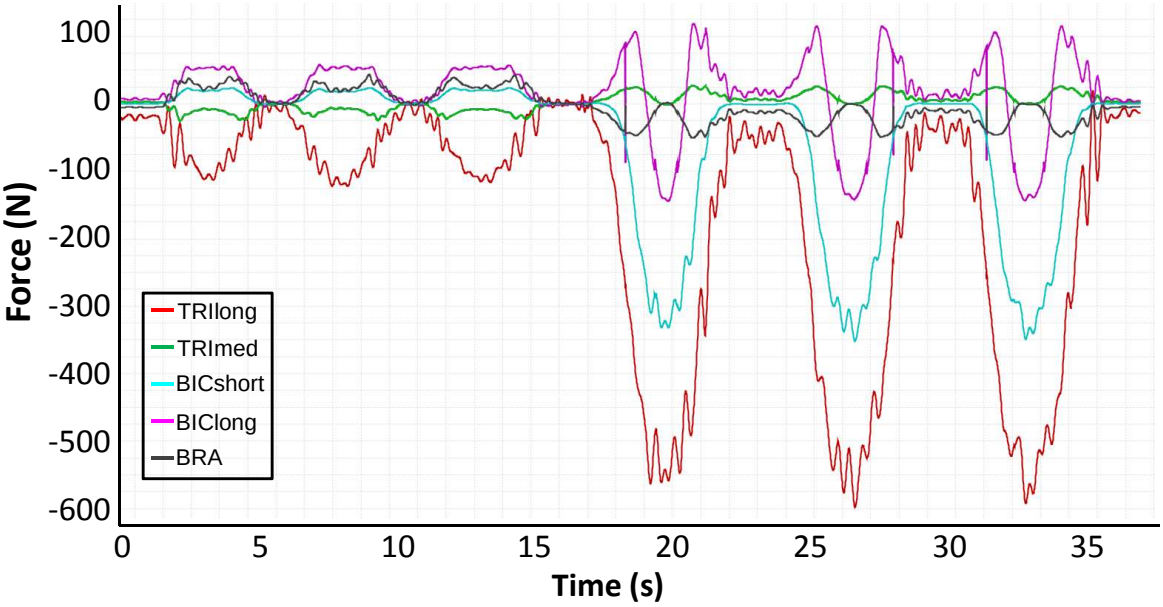

Figure 3.22: Muscle tendon forces of upper limb.

Based on the results of joint moment calculation, we can further estimate the individual muscle forces by using the musculoskeletal geometry information in the biomechanical simulation model. Figure 3.22 graphically shows the simulations muscles forces for lifting up task. As observed from the plot, the subject's TRIlong muscle generally was activated in a relatively high value in both steps. At the first step, the elbow rotations primarily used the TRIlong, BIClong and BRA to lift up the load, as these muscles were wrapped with the

forearm and upper arm. At the second step, the TRIlong, BICshort and BIClong become the most activated muscles in order to lift up the load with bigger joint moments. These results were compatible with the joint moment results.

3.4.5 Discussion of Experiment #2

The biomechanical analysis was performed by a lifting up task of 1 kg load to evaluate the joint moments and muscle tendon forces of upper limb. Two WB-3 IMUs were used to measure the arm movements during the experiments and integrated with the simulation software for the joint moment and muscle tendon force estimate.

The described biomechanical simulation model represented an adult male of average size with muscle parameters from OpenSim software. Subject-specific models using an individual's muscle parameters and muscle paths would be useful for designing subject-specific surgical plans. This could be achieved by revising the musculoskeletal geometry in the simulation model, including the arm DOF, length and number of muscles, incision point of each muscle, and so on. The simulation model could be further scaled to fit different individual subjects more accurately.

The results showed the shoulder used significant bigger joint moments to lift up the load while using only shoulder rotation, which was due to the bigger moment arm in this condition. Moreover, the tendon forces were apparently increased during the shoulder rotations. The most activated muscles were the TRIlong, BICshort and BIClong for lifting up the load. All these results were just the estimate of the real conditions, which allowed us to understand how the biological status going. More complementary information is needed in order to improve the data accuracy and reliability, such as EMG signal, detail human geometry data.

3.4.6 Summary of Experiment #2

This experiment evaluated the biomechanical analysis by using WB-3 system with the simulation software. The results verified that the joint moments and muscle tendon forces of different inter-segmental movements could be effectively estimated by using the kinematic information acquired by WB-3 system, which satisfied the objective of this study.

3.5 Discussion

Kinematics and biomechanical analysis are the significant aspects for operative skill evaluation. As the proposed methodology in Chapter 1 was based on the human and instrument motion analysis, it is essential to evaluate the WB system performance for achieving reliable and robust skill evaluation system.

In this chapter, the performance of data fusion algorithm for orientation estimate was evaluated in WB-3 IMU, which could also be extended to WB-4 IMU. The results showed that the accuracy performance of WB-3 IMU satisfied the system specification, and could be further improved by prior sensor calibration. A demonstration of human upper body motion tracking was also presented to verify the system ability for human motion analysis.

Biomechanical models of the musculoskeletal system are frequently used to study neuromuscular control and simulate surgical procedures, which could provide us more insight information for the surgical operative skill evaluation. The WB-3 system with the simulation software was proved to be an effective tool for biomechanical analysis. The experiential evaluation was performed by one single lifting up task to estimate the joint moments and tendon forces of upper limb, which could be further verified by more experiments with different human motions.

3.6 Conclusion of this Chapter

This chapter presented the sensor fusion algorithm for WB-3 IMU orientation estimate, and discussed the biomechanical analysis by using kinematics data of WB-3 system.

The WB-3 IMU angular accuracy performance was evaluated by the comparison with a commercial IMU InertiaCube3 in regard to Vicon reference system. The experimental results verified that the performances of WB-3 IMU were comparable with the commercial product and satisfied the system specification requirement (less than 2 deg) discussed in Chapter 2.

The joint moments and individual muscle forces of multi-joint movements were investigated by using WB-3 system at a lifting up task. By using the kinematics data from WB-3 system, the biomechanical simulation model in OpenSim software can estimates the individual muscle forces based on the biomechanical approaches, which could allow us to

further analyze the activation patterns of key muscles of the upper limb during various surgical trainings and medical procedures for realizing a better operative skill evaluation system.

With the high performance of motion tracking and analysis of WB system, it allows us to evaluate the medical operative skills based on the proposed methodology described in Chapter 1. The resulting skill evaluation system is implemented for practical surgical applications discussed in detail from next chapter.

Chapter 4

Evaluation of Laparoscopic Operative Skills

4.1 Introduction

4.1.1 Background

Laparoscopic surgery, one type of the minimally invasive surgery (MIS), has become the dominant technology in modern surgery due to its great advantages in less postoperative pain, shorter hospital stays and an earlier return to normal life for patients. While this new technique has many advantages for patients, it often requires surgeons to undergo long and difficult trainings. Mainly, laparoscopic surgery imposes limitations to surgeons in visual and haptic perceptions, and creates challenges unique to this type of surgery:

- reduced depth perception of the operative field caused by the use of 2D monitors;
- poor eye-hand coordination as a result of location of the monitor;
- variable amplification;
- mirrored movement and disorientation;
- motion limitations due to trocar-induced invariant points;
- reduced haptic feedback from the use of long and slender surgical instruments.

As a result, with the shift from open surgery to laparoscopic surgery, new problems have arisen related to the training of surgeons [5, 94].

In this context, various training methods and metrics have been developed for training laparoscopic surgical skills, which can be roughly divided into two categories: (a) box trainer including physical objects or latex organ packs with natural haptic feedback, such as Endowork Pro II [95]; (b) virtual reality (VR) simulator including graphical representation of virtual objects, and some of them simulating forces and torques as the result of interaction between virtual objects and surgical tools by using force feedback device, such as Procedicus MIST-VR [96].

Studies have showed that trainings on these kinds of box trainers and VR simulators improve psychomotor skills of laparoscopic surgery [21]. Skill evaluation methods in these facilities, however, are still far from being objective for the routine laparoscopic training [97]. Therefore, there is a critical need for the development of consistent and reliable methods to evaluate operative skills of routine training before the surgeons enter the real operation theater.

In most of the current training facilities, such as box trainers utilized in routine training courses, evaluation of surgical operative skills heavily relies on subjective measures and scoring by an expert, which may be a variably biased opinion using vague criteria. The methodology for assessing surgical skill now is strongly motivated to change from subjective scoring to a more objective, quantitative analysis [26]. The VR simulators, which are now commercially available, have been comprehensively validated as a surgical data analysis tool [98]. These simulators provide low-level analysis of the instrument's trajectory, and execution time recorded during training to assess surgical skills. However, no matter how exhaustive or excellent the VR simulator might be, they can still only serve as a good complementary solution to training on real-world scenarios [27].

The routine laparoscopic training involves a multidimensional series of tasks requiring the surgeons to satisfy the psychomotor skill requirements in handling the special long and slender laparoscopic instruments. It has been demonstrated that motion analysis is a valuable objective skill assessment method for the fundamental laparoscopic training [15]. Non-VR approaches for surgical skill evaluation have focused on motion tracking and have derived various metrics of varying skill levels.

In the fields of basic analysis and modeling, Moorthy et al. [18, 99, 100] introduced a skill evaluation system called Imperial College Surgical Assessment Device (ICSAD) for assessing the dexterity of surgical competence (Figure 4.1). The ICSAD used electromagnetic markers placed on the dorsal side of each hand and the Isotrak II system (Polhemus Inc.) to track the

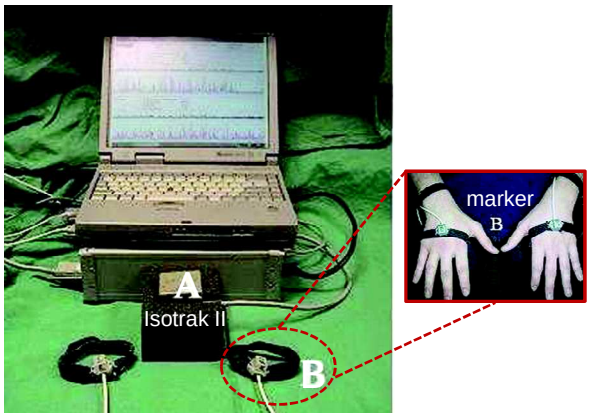

Figure 4.1: Imperial college surgical assessment device (ICSAD).

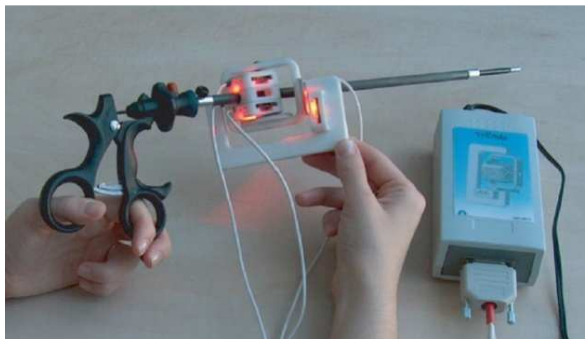

Figure 4.2: TrEndo system for tracking laparoscopic instruments.

trainee's hand movements in open surgical simulated tasks. This system analyzed the task execution time, the number, speed, and distance traveled of hand movements at 20 Hz, to discriminate the performance of different trainees. However, it had a limited measurement range of 1.5 m which might not be sufficient for the real operation of wide working space. Moreover, the motion analysis of other parts of trainee's upper limbs, which is also considered to be an important feature for skill evaluation, was still lacked in this system.

Chmarra et al. [101, 102] developed a four degrees of freedom, low-cost device called TrEndo for tracking laparoscopic instruments (Figure 4.2). This device consisted of a gimbal mechanism with three optical computer mouse sensors, to guide and measure the instrument movements. This system can classify the trainees as experts, intermediates, and novices according to their basic laparoscopic skillS. However, the movement analysis of trainee's upper limbs was still missing in this study. Moreover, this system can only be used in the routine training course to evaluate the surgical skillS, but cannot be further performed and evaluated in real operation and other medical fields.

Figure 4.3: WB-2R system for laparoscopic skill evaluation.

In the high-level modeling fields, Rosen et al. [103-106] demonstrated to use hidden markov models (HMM) to objectively assess surgical skillS based on integration of haptic information in tool/tissue interactions and motion data of laparoscopic instruments. The results showed that HMMs incorporating haptic and motion information provided an objective tool for representing the significant different competence level between expert surgeons and novices. However, their approach expected the expert surgeons to provide movement specifications for building the topology of HMM, which might not be easily applied to a new training task. Similar studies were also done by Hager et al. [27, 107]. They also made use of HMM for statistical modeling the motion data acquired from the da Vinci surgical system to evaluate surgical skill. The results showed that the model can efficiently classify the expert surgeons and novices, and can identify the skill levels. However, this method can only be used for evaluating the surgical skills of manipulating the robotics-assisted surgical system.

In our previous work, the Waseda Bioinstrumentation system WB-2R (Figure 4.3), which can objectively measure the movements of the head, the arms, and the body, was proposed to be used for evaluating laparoscopic skill improvements after the trainee finished a two days' routine laparoscopic training course [108]. The previous results showed that motion analysis of trainee's upper limbs can efficiently identify the performance improvements after the training course. However, the previous system was still not wearable enough for no constrain to trainee's movements, and the skill classification method between expert surgeons and novices was missing.

4.1.2 Objective

This study is aimed at defining a skill evaluation system to objectively evaluate and classify surgical performance and skill expertise, and to be used practically and efficiently in routine laparoscopic training courses.

In particular, this surgical operative skill evaluation system for laparoscopy should satisfy the following requirements:

- Capability of measuring trainee's upper body movements during regular laparoscopic trainings.
- Extraction of the significant motion features between the expert surgeons and novices.
- Classifying the trainees with different laparoscopic experience into expert group or novice group.
- More than 90% correct rate of the classification results.
- Feedback of quantitative motion information to trainees to show up how they performed while comparing with the experts.

4.2 Materials and Methods

According to the general methodology introduced in Chapter 1, the block diagram of the corresponding methodology for realizing the objective operative skill evaluation system of laparoscopic surgery is showed in Figure 4.4.

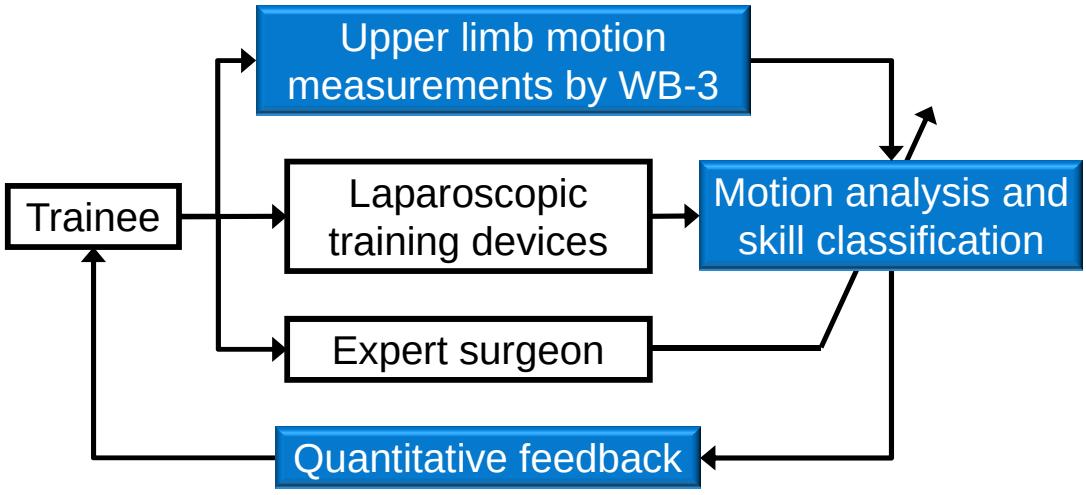

Figure 4.4: Methodology for laparoscopic operative skill evaluation.

The approach is to define a processing model which analyzes the kinematic data describing the movements of trainee's upper limbs. The WB-3 system is used to measure and analyze these movements. The processing model is trained by using the trainees' significant motion features acquired from WB-3 system and further validated to classify the expertise level of each trainee into expert group or novice group. The feedback of quantitative motion information to trainees shows which motion parameter has poor performance and should be improved.

4.2.1 Experimental Evaluation

A) Experimental setup

The experimental setup is showed in Figure 4.5. Eight WB-3 IMUs were put on the trainee's upper body and distributed as below:

- Head: 1 IMU;
- Back: 1 IMU;
- Upper arm: 2 IMUs, one for left and right upper arms, respectively;
- Forearm: 2 IMUs, one for left and right forearms, respectively;
- Hand: 2 IMUs, one for left and right hands, respectively.

This resulted in measuring the movements of the arms, the head and body. The total weight of this system setup was 500 g which was 50 % less than WB-2R system (1000 g), and trainees felt no constraint to their movements with this setup.

The box trainer used in the experiments was Endowork-pro II (MC Medical Inc., Japan) [95]. A camera mounted in the box trainer grabbed a remote image of the operating area which was showed in a monitor. The two laparoscopic instruments were the KAR #26173 (Figure 4.6) by Karl Storz Company [109].

Five expert surgeons and 11 novice medical students (totally 16 subjects) at Kyushu University, Japan, kindly participated in the experiments after providing informed consent. The expert surgeons had experience of more than 100 laparoscopic surgical operations. None of the medical students had any previous trainings of laparoscopic surgery or any experience assisting with laparoscopic operation.

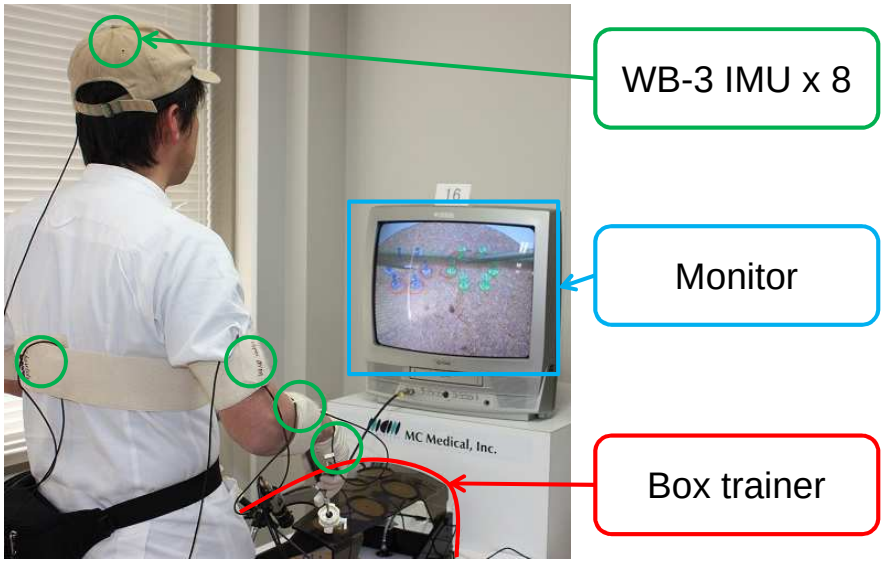

Figure 4.5: Regular laparoscopic training with WB-3 system.

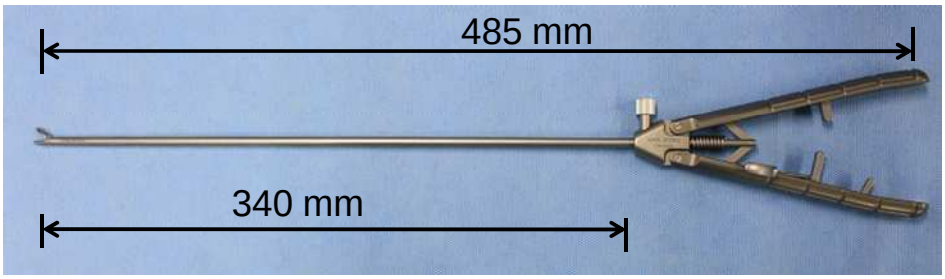

Figure 4.6: Laparoscopic instrument.

Two regular training tasks were selected for this study: peg-board training and pipe-cleaner training (see in Figure 4.7 and Figure 4.8, respectively). The peg-board training was regularly used to train eye-hand coordination in the training courses of laparoscopic training center in Kyushu University, and therefore, the expert surgeons were very familiar with this task. The pipe-cleaner training was also regularly used to train the eye-hand coordination at Leiden University Medical Centre in Netherlands [110], and all of the expert surgeons participating in this experiment had no any experience with this training.

In order to provide the same conditions of experiment setup for all the subjects, the positions of the training platforms inside the box trainer, the instruments used, and the incision points for the camera and instruments were identical for everyone. The start and end positions of both laparoscopic instruments, marked as ‘L’ and ‘R’ in Figure 4.7 and Figure 4.8, were predefined for the tasks and were the same for each subject.

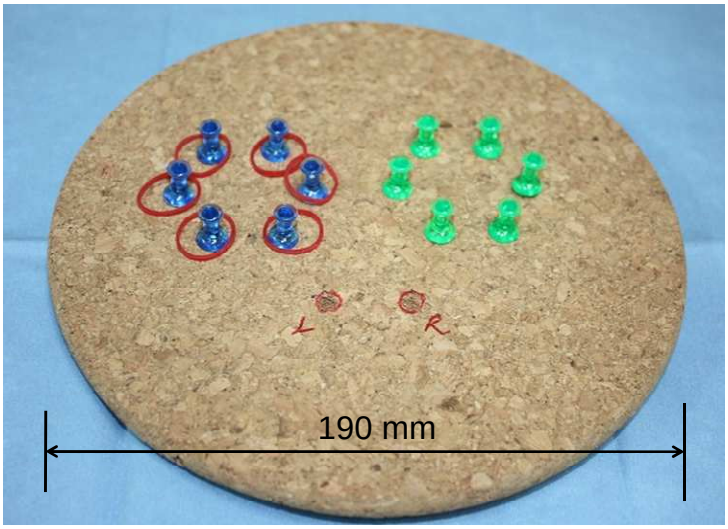

Figure 4.7: Peg-board training platform.

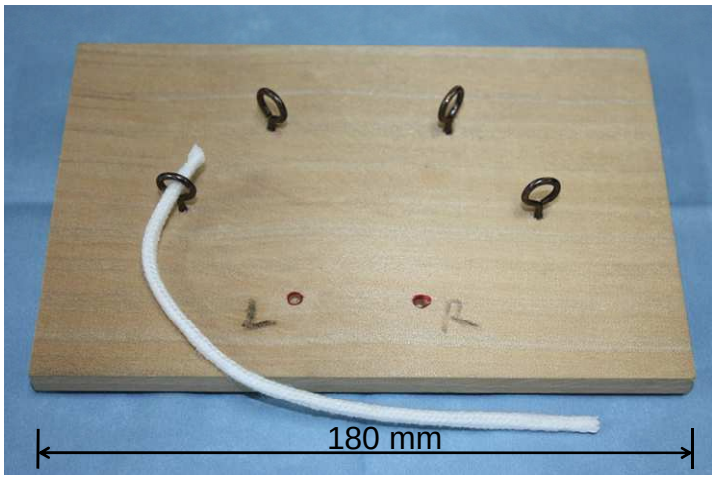

Figure 4.8: Pipe-cleaner training platform.

B) Experimental protocol

The operative sequences of peg-board training and pipe-cleaner training are showed in Figure 4.9 and Figure 4.10, respectively. All the procedures in Figure 4.9 and Figure 4.10 were defined as 1 trial for the peg-board training and the pipe-cleaner training, respectively. Each subject executed the trial totally 3 repetitions for each training task in this study. There was no requirement of execution time limitation to complete a trial. All the tests were performed in the box trainer with WB-3 system put on the subjects. Each subject completed a short questionnaire about his/her experience of laparoscopic surgery and a prior practice trial for each task before the experiments started.

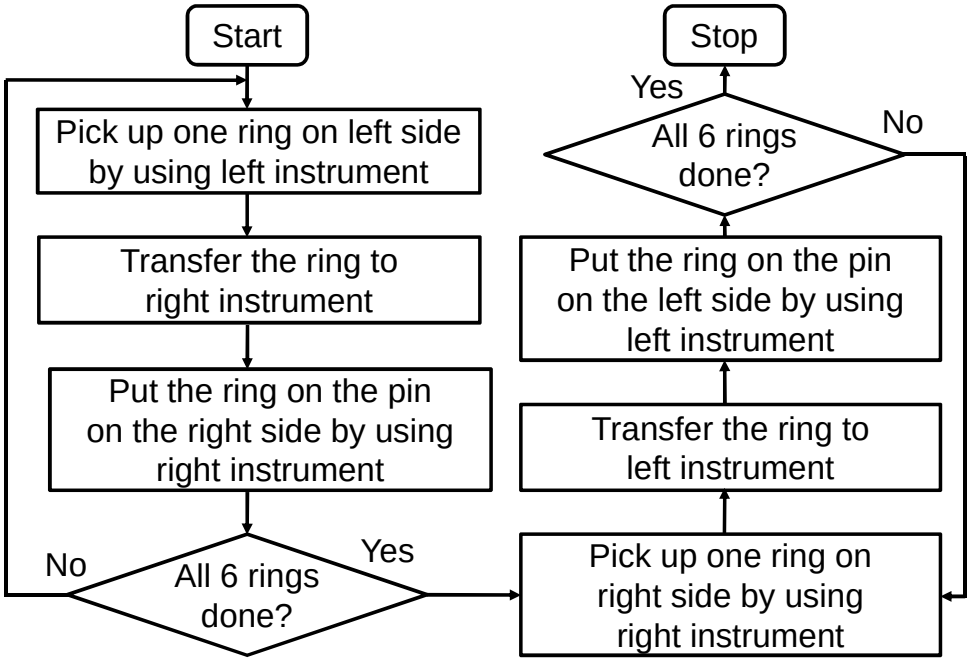

Figure 4.9: Operative sequence of peg-board training.

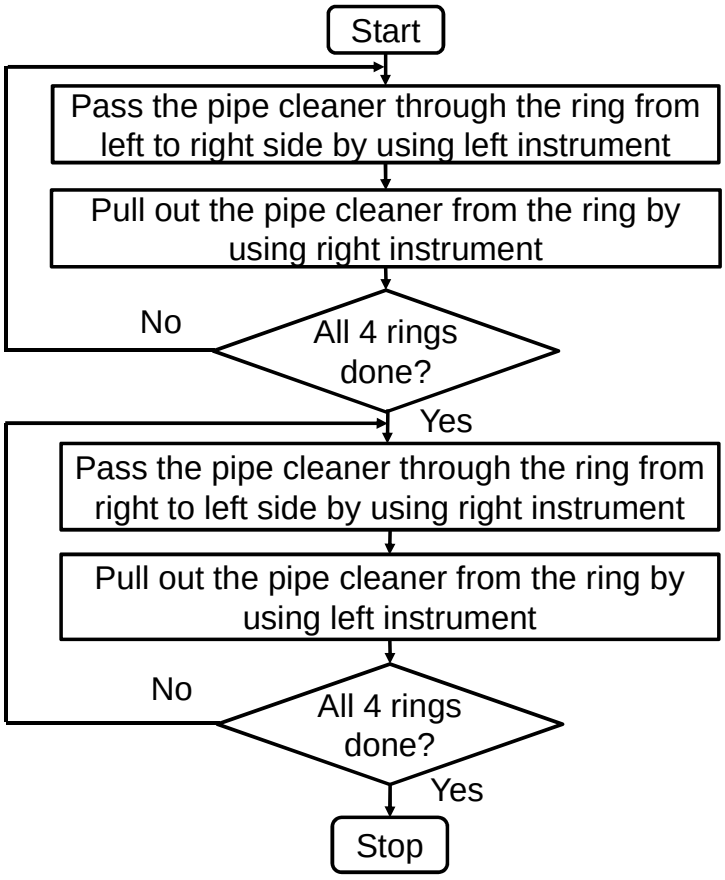

Figure 4.10: Operative sequence of pipe-cleaner training.

4.2.2 Data Processing Model

Data were acquired on a PC and saved for storage and offline analysis. All the data were saved as CSV (comma separated value) files, and they were loaded in Matlab™ (The MathWorks, Inc.) for further processing and analysis [111].

Since the movements of the head and back were not significant in these two training tasks, the evaluation is only focused on the movement analysis of subject's upper limbs based on the data from 6 corresponding IMUs.

As pre-processing, all the acceleration, angular speed and magnetic raw data are filtered and smoothed by using a moving average algorithm with a window size of 5 [63]. As each IMU has 9 axis output, the data set of each experiment trial consists of 54 dimensions of raw data (9 axis x 6 IMUs) with the data length of L_k, and it is denoted as $\boldsymbol{X}_k$, after pre-processing, where k is the repetition number.

Data is then further processed by the model showed in Figure 4.11. The data processing model mainly contains four components: feature extraction, feature normalization, principal components analysis (PCA) and discriminant analysis (DA). These analyses are done using the statistics toolbox of Matlab. The data set of $\boldsymbol{X}_k$, as the input of this processing model will be used to classify the surgical skill expertise of each subject into expert group or novice group for both training tasks. Each functional block will be described in detail in the following sections.

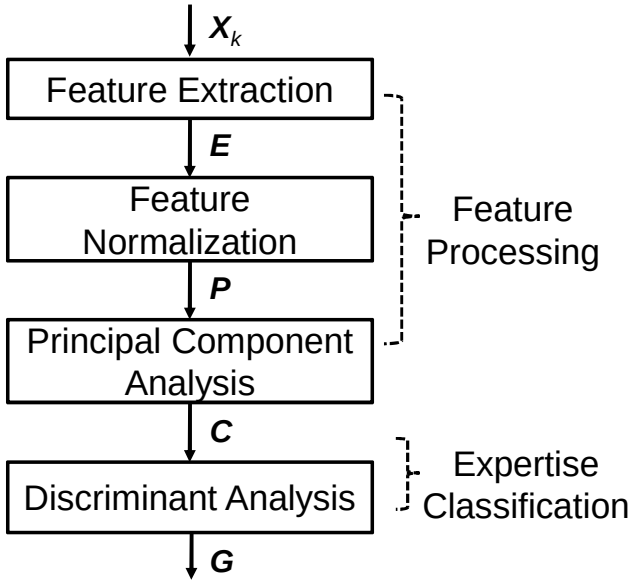

Figure 4.11: Functional block diagram of data processing model.

A) Feature extraction

Feature extraction takes advantage of the pre-processing data set $\boldsymbol{X}_k$, to calculate and analyze some significant motion feature parameters based on the implementation of human model described in Chapter 3. The orientations of subject's upper limbs are estimated by using quaternion-based extended Kalman filter described also in Chapter 3.

Different feature parameters are evaluated, such as the joint angle, joint angular speed $|\omega|$, cumulative distribution function (*CDF*) of $|\omega|$ and joint rotating frequency of $|\omega|$. The mean power spectrum density (*PSD*) of $|\omega|$ in each joint is also analyzed to estimate how much energy that joint uses for the rotations during the trainings. All these parameters are averaged by the 3 repetitions for each subject in each training task, and the variance of each parameter is also considered for the performance discrimination between experts and novices.

In order to extract the significant feature parameters which can distinguish the skill expertise, a t-test is used for comparing the parameters between experts and novices. When significant difference ($p<0.05$) between these two groups is found, the parameter is considered to be statistically significant for the skill evaluation.

The fast Fourier transformation (*fft*) of $|\omega|$ in each joint, which is used for estimating the *PSD*, is calculated with fft_{size} = 8192 samples and frequency resolution f_{res} = 0.0112 Hz. The *PSD* is estimated in using the following formula:

$$PSD = (fft * conj(fft)) / fft_{size} \tag{4.1}$$

The mean *PSD* is evaluated in the frequency range 0.1 - 3 Hz to take into account only the voluntary movements [59]. The *CDF* of $|\omega|$ is calculated for 90% cumulative distribution.

Seven significant feature parameters between experts and novices are found in the peg-board training, which are listed as below:

- left shoulder mean angular speed (*LSMAS*);
- right shoulder mean angular speed (*RSMAS*);
- left shoulder angular speed *CDF* (*LSASC*);
- right shoulder angular speed *CDF* (*RSASC*);
- left shoulder angular speed frequency (*LSASF*);
- right shoulder angular speed frequency (*RSASF*);

- right shoulder used rate (*RSUR*).

The shoulder used rate is proposed and defined in this thesis using the following formula. If the shoulder used rate is high, it indicates that the subject uses more frequently the rotations of shoulder; otherwise he/she uses more rotations of the elbow and wrist during the trainings.

$$UR_{shoulder} = PSD_{|\omega|\_shoulder} / (PSD_{|\omega|\_elbow} + PSD_{|\omega|\_wrist}) \quad (4.2)$$

Where, $PSD_{|\omega|\_shoulder}$, $PSD_{|\omega|\_elbow}$ and $PSD_{|\omega|\_wrist}$ are the mean *PSD* of $|\omega|$ in shoulder, elbow and wrist, respectively.

In the case of pipe-cleaner training, five significant feature parameters are found, which are listed as below:

- right shoulder angle standard deviation (*RSASD*);
- right shoulder angle range (*RSAR*);
- left shoulder angular speed frequency (*LSASF*);
- right shoulder angular speed frequency (*RSASF*);
- right shoulder used rate (*RSUR*).

Among these 5 parameters, the last three are also found in peg-board training. They have similar results in these two training tasks.

All of the significant parameters found in the tasks are related to the shoulder joint, which indicates that the shoulder movements are significantly important to the operative performance. These significant parameters as the output of feature extraction function are denoted as $\boldsymbol{E}$ with N = 16 of the subject number in data length. It contains 7 dimensions representing the significant parameters in peg-board training and 5 dimensions representing the significant parameters in pipe-cleaner training, respectively. The detailed results of these feature parameters compared between experts and novices in each training task, are present in the “Experimental Results” section of this chapter.

B) Feature normalization

Since the units of the feature parameters are different, the ranges of values that they take are significantly different. These differences in dynamic range often hurt the performance of a

classifier or a recognition system. Therefore, the mean and variance of each parameter are used for the normalization by applying a simple transformation:

$$P_{i,j} = \frac{1}{\delta_j^2}(E_{i,j} - \mu_j) \tag{4.3}$$

Where,

$$\mu_j = \frac{1}{N}\sum_{i=1}^{N} E_{i,j} \tag{4.4}$$

$$\delta_j^2 = \frac{1}{N}\sum_{i=1}^{N}(E_{i,j} - \mu_j)^2 \tag{4.5}$$

Where, ***P*** is the normalized significant feature parameters, N is the total number of subjects, u_j is the mean and δ_j is the standard deviation of each parameter.

C) Principal component analysis

The normalized data with many significant parameters might be measuring the same driving principle governing the behaviors during the trainings. In order to verify the real useful inherent information and reduce the dimension of the normalized data, the well-known PCA is employed [112].

Given a set of input features (in our case the normalized significant feature parameters ***P***), PCA extracts a set of "principal components". Each principal component is a linear combination of the input features:

$$PC_i = \sum_{i=1}^{n} \omega_i F_i \tag{4.6}$$

Where, ω_i serves as weight, F_i is the input features. The principal components are ordered according to the amount of variance they explain. The first component accounts for as much of the variance in the data as possible, and each succeeding component accounts for as much

of remaining variance as possible. Then the cumulative variance explained (CVE) forms a criterion for selecting the number of principal components to be used in the DA described in the following section. Figure 4.12 and Figure 4.13 respectively show the variance results of PCA in the peg-board training and the pipe-cleaner training. It is clear that the first two principal components of both training tasks account for more than 95% of the variance. These two principal components, denoted as ***C***, therefore, are employed for the DA leave-one-out cross validation.

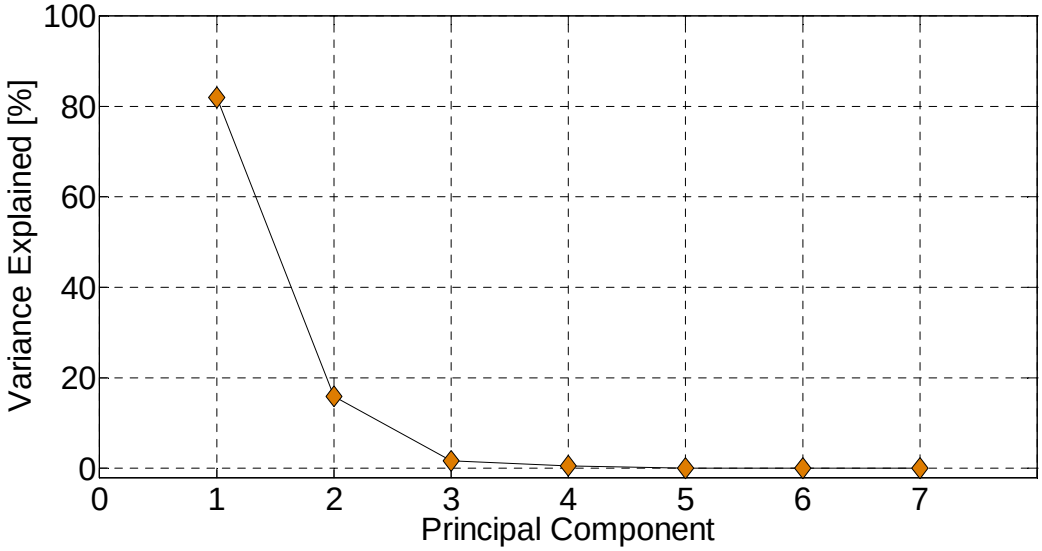

Figure 4.12: Variance explained of all principal components in peg-board training.

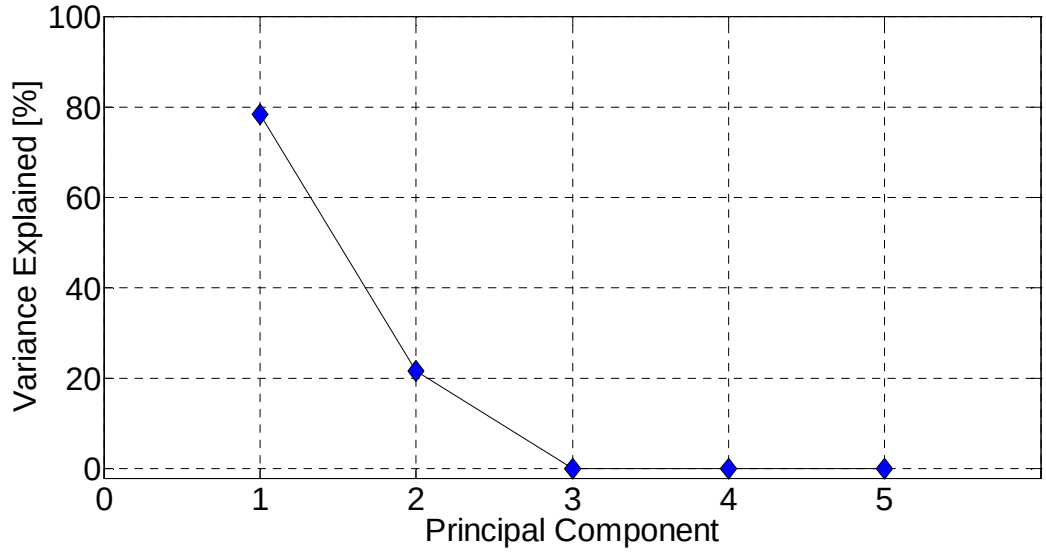

Figure 4.13: Variance explained of all principal components in pipe-cleaner training.

The weight for each parameter in the first two principal component calculations is respectively listed in Table 4.1 and Table 4.2 for peg-board training and pipe-cleaner training. It is clear that the weights for *LSASF* and *RSASF* are much bigger than other parameters, which indicates that these two feature parameters are more important for the performance discrimination.

Table 4.1: Weights used in principal component calculation of peg-board training.

	LSMAS	*RSMAS*	*LSASC*	*RSASC*	*LSASF*	*RSASF*	*RSUR*
C_1	-0.063	-0.053	-0.025	-0.020	-0.800	-0.592	0.015
C_2	-0.014	-9.2e-4	-0.003	- 7.2e-4	-0.594	0.805	0.003

Table 4.2: Weights used in principal component calculation of pipe-cleaner training.

	RSASD	*RSAR*	*LSASF*	*RSASF*	*RSUR*
C_1	0.006	0.002	-0.592	-0.806	0.007
C_2	0.019	0.005	-0.806	-0.591	-7e-4

D) Discriminant analysis

Discriminant analysis [113] is used to decide whether a subject is an expert or novice, according to his/her basic psychomotor skill expertise. DA needs a training set, consisting of the first two principal components of each subject. DA uses the training data to learn the distribution of components and classify the subjects into expert or novice group, denoted as ***G***. When the WB-3 system data of a new subject is provided and completed the feature processing sequence, DA estimates the most likely group to which the subject belongs by comparing the principal components of the new subject to the previously trained distribution. The results of DA are present in detail in the “Experimental Results” section.

E) Leave-one-out cross validation

Performance of the classification methods is examined using a leave-one-out cross validation. In each leave-one-out validation case, one subject is selected as the test case, and the remaining subjects are used as training set [27]. This is repeated so that each subject is used once as a test case, which results in 16 leave-one-out validation cases in this study. The results of the entire leave-one-out cross validation are presented in the next section.

4.3 Experimental Results

4.3.1 Significant Feature Parameters in Peg-board Training

A) Shoulder mean angular speed

The first two significant parameters are the mean angular speeds of left and right shoulders, showed in Figure 4.14 and Figure 4.15, respectively.

The expert group had significantly ($p<0.01$) higher angular speeds of the left and right shoulders than the novice group, which was corresponded with the fact that experts performed in higher efficiency and competence to complete this training task. The novice subject #11 had good performance in the case of right shoulder mean angular speed, which was bigger than the average value of expert group.

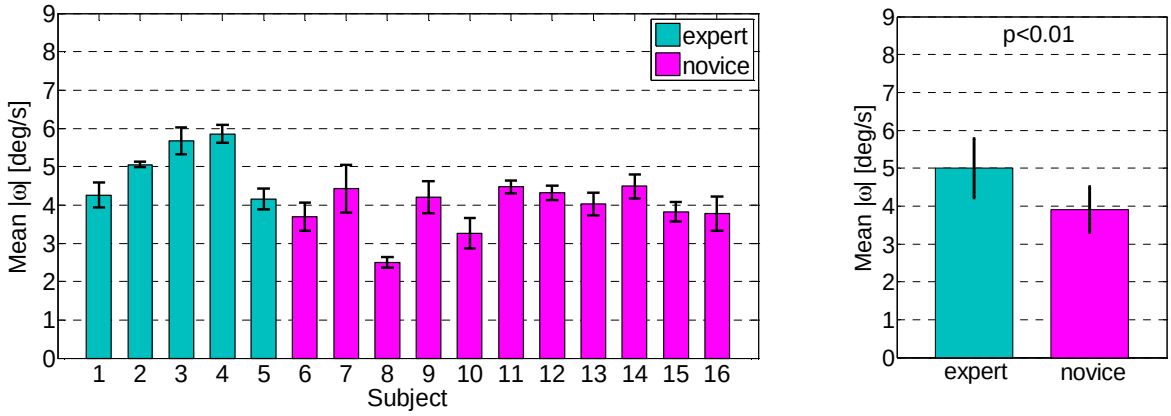

(a) among all the subjects.　　(b) between two groups.

Figure 4.14: Mean angular speed of left shoulder.

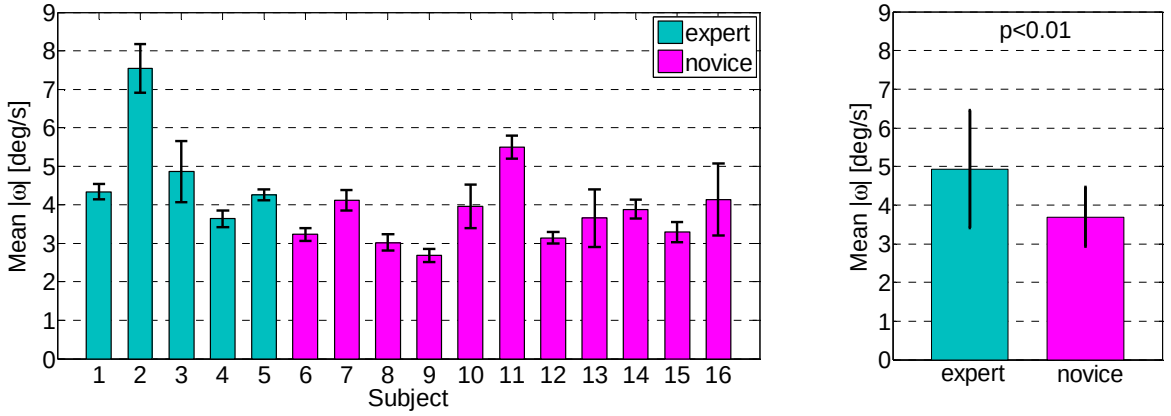

(a) among all the subjects.　　(b) between two groups.

Figure 4.15: Mean angular speed of right shoulder.

B) Cumulated distribution of shoulder angular speed

The 90% cumulated distributions of left and right shoulder angular speeds are showed in Figure 4.16 and Figure 4.17, respectively.

They show significant difference ($p<0.05$) between expert group and novice group. Similar to the results in shoulder mean angular speed, most of the experts had higher values in cumulated angular speeds. These results also indicate that the expert surgeons were completing the task more efficiently through the whole procedure. The novice subject #11 also had good performance in the case of right shoulder with 12 deg/s cumulated angular speed, which was bigger than the average value of expert group.

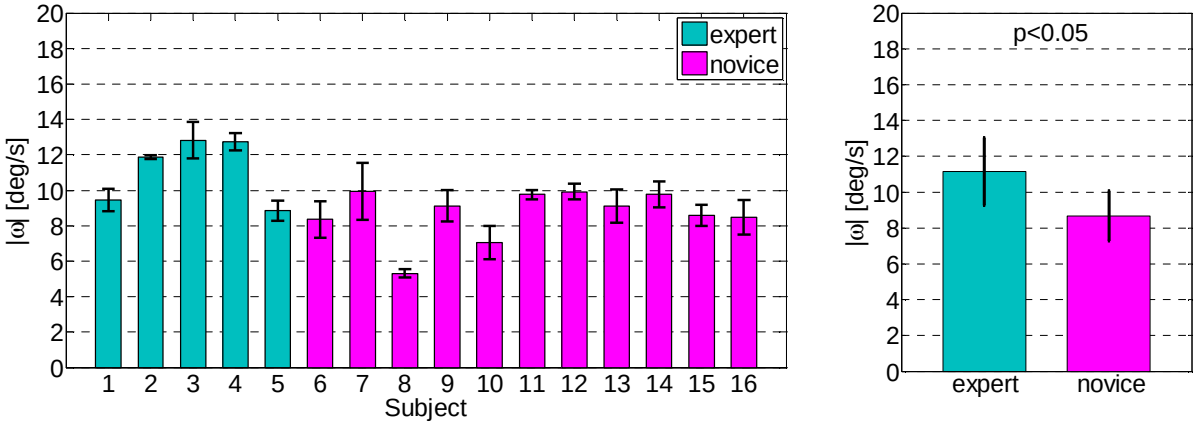

(a) among all the subjects. (b) between two groups.

Figure 4.16: 90% cumulated angular speed distribution of left shoulder.

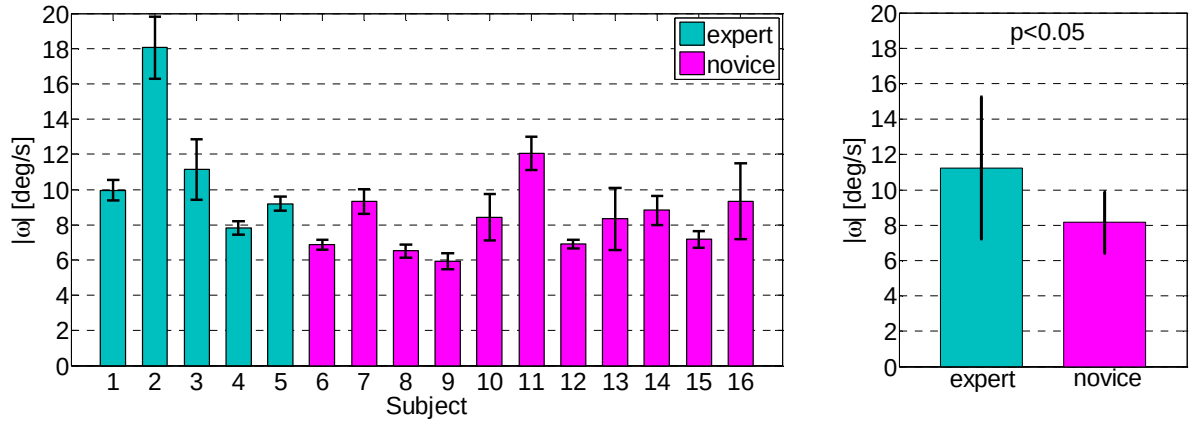

(a) among all the subjects. (b) between two groups.

Figure 4.17: 90% cumulated angular speed distribution of right shoulder.

C) Shoulder angular speed peak frequency

The left and right shoulder angular speed peak frequencies are respectively showed in Figure 4.18 and Figure 4.19, which clearly show that the main movements of most expert surgeons during the trainings were significantly ($p<0.01$) faster than novices on both shoulders. It is related to better skill competence and movement efficiency of expert surgeons.

In the case of left shoulder, only novice subject #11 had the performance close to expert group, which was corresponded to the results of shoulder average and cumulated angular speeds. In the case of right shoulder, both novice subject #8 and #11 had similar performance to expert group.

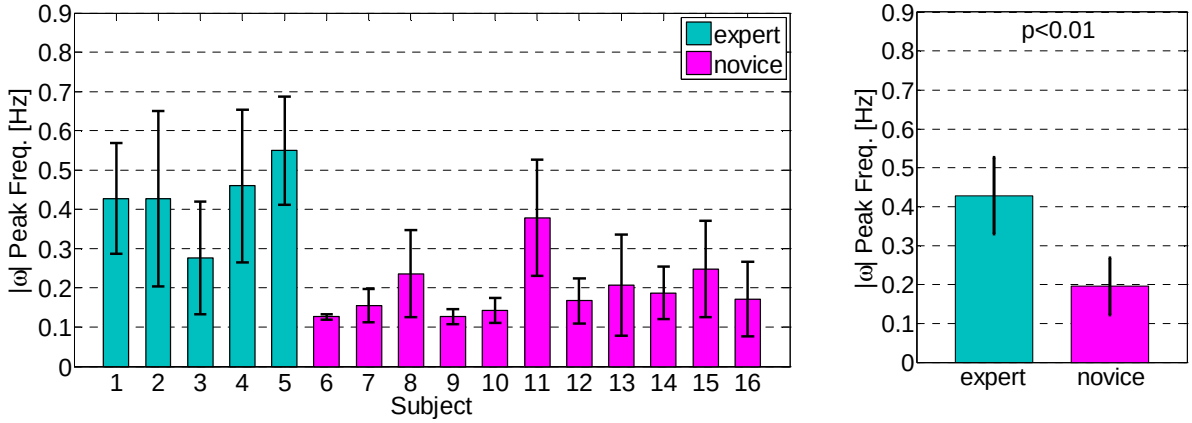

(a) among all the subjects.　　(b) between two groups.

Figure 4.18: Angular speed peak frequency of left shoulder.

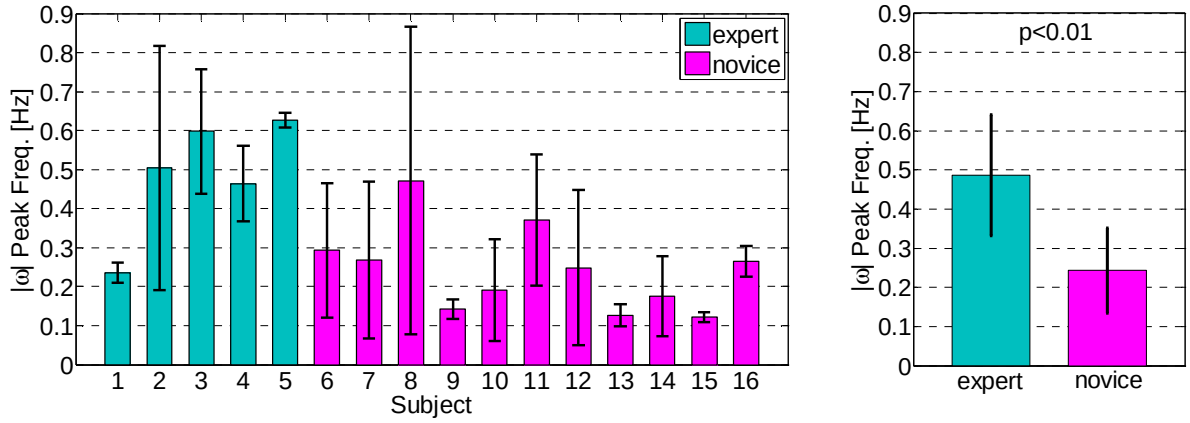

(a) among all the subjects.　　(b) between two groups.

Figure 4.19: Angular speed peak frequency of right shoulder.

D) Shoulder used rate

The shoulder used rate of right side is found to be a significant feature between expert group and novice group (Figure 4.20). However, there is no significant difference between the experts and novices on the left shoulder of this feature.

Figure 4.20 shows that all the expert surgeons had less right shoulder used rate. This might indicate that the rotations of elbow and wrist were more important than the rotations of shoulder for this training task. Only the novice subject #12 had similar performance to the expert surgeons.

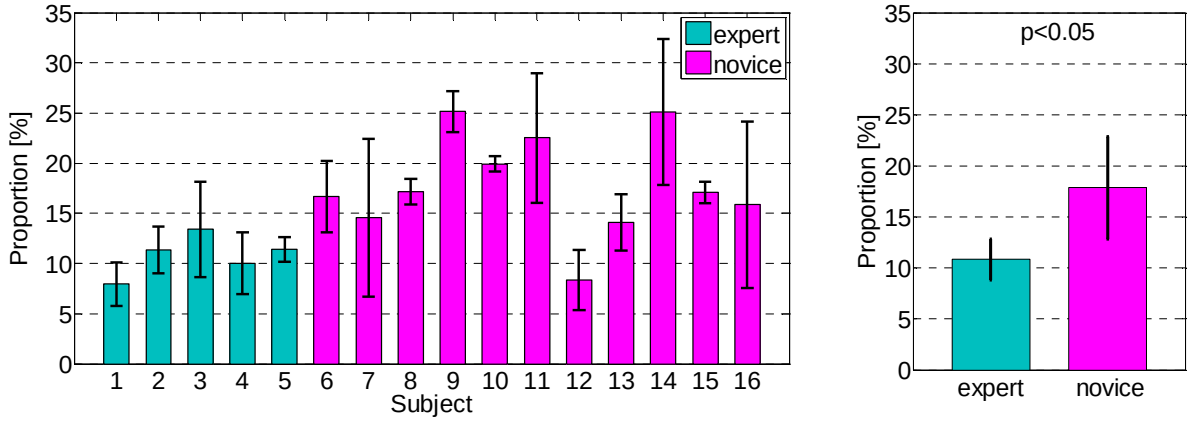

(a) among all the subjects. (b) between two groups.

Figure 4.20: Right shoulder used rate in peg-board training.

4.3.2 Significant Feature Parameters in Pipe-cleaner Training

A) Shoulder angle standard deviation

The angle standard deviation of left shoulder is found to be a significant feature (Figure 4.21). It shows that the expert surgeons had significantly ($p<0.05$) smaller left shoulder angle standard deviation than the novices, which indicates that they had more stable movements on the left shoulder during the trainings. Both novice subject #8 and #11 had similar performance to expert group.

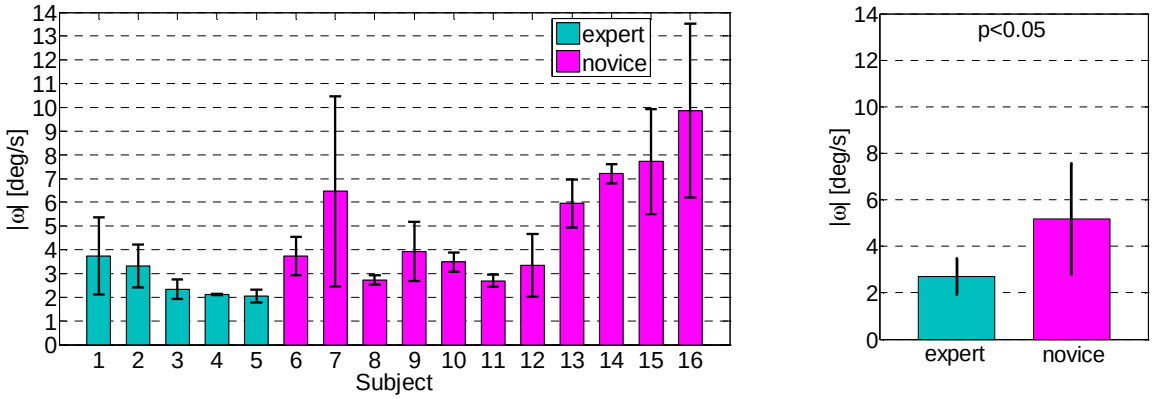

(a) among all the subjects.　　(b) between two groups.

Figure 4.21: Left shoulder angle standard deviation.

B) Shoulder angle range

Figure 4.22 shows that all of the surgeons had significantly ($p<0.05$) smaller rotating ranges of left shoulder angle than novices, which also indicates that the expert surgeons had more stable movements on the left shoulders.

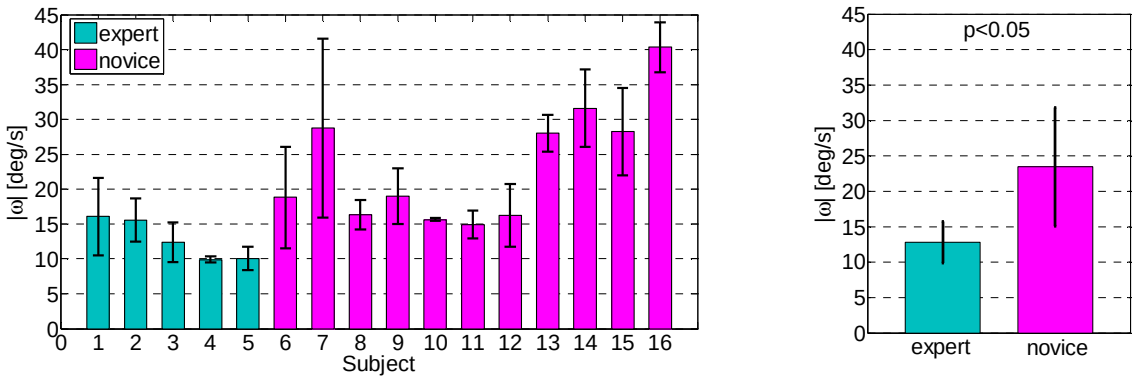

(a) among all the subjects.　　(b) between two groups.

Figure 4.22: Left shoulder angle range.

C) Shoulder angular speed peak frequency

The left and right shoulder angular speed peak frequencies (Figure 4.23 and Figure 4.24, respectively) clearly show that the main movements of all expert surgeons during the trainings were significantly ($p<0.01$) faster than novices, which was similar to the results in peg-board training.

In the case of left shoulder, only novice subject #8 had the performance close to expert group. In the case of right shoulder, both novice subject #14 and #16 had similar performance to experts.

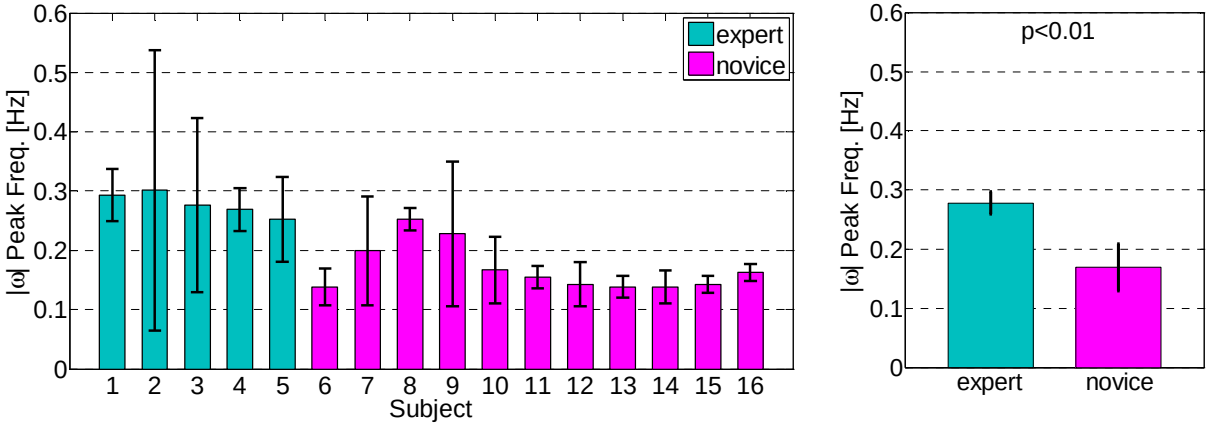

(a) among all the subjects. (b) between two groups.

Figure 4.23: Angular speed peak frequency of left shoulder.

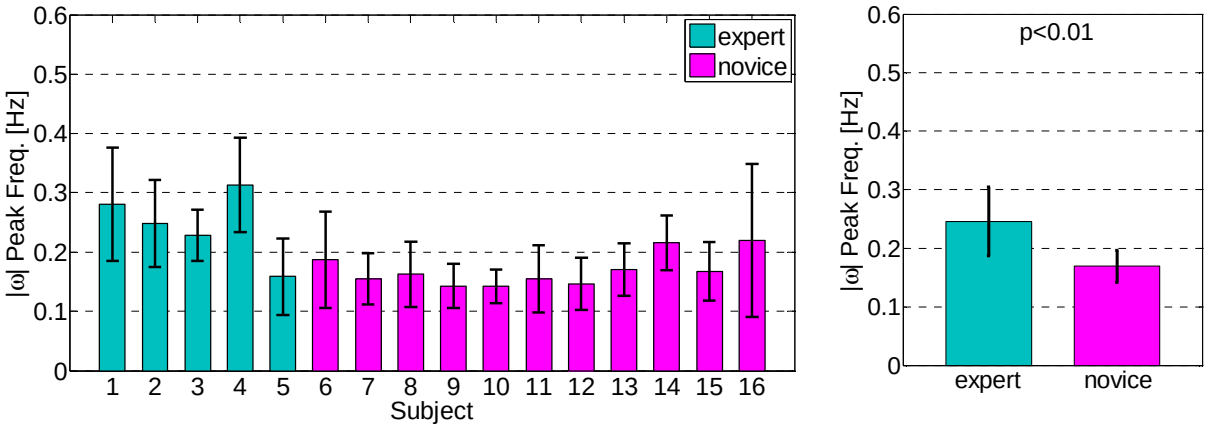

(a) among all the subjects. (b) between two groups.

Figure 4.24: Angular speed peak frequency of right shoulder.

D) Shoulder used rate

Only the right shoulder used rate is found to be a significant feature (Figure 4.25), but not found in the case of left side.

Similar to the results in peg-board training, it shows that most expert surgeons had less right shoulder used rates than novices, which might indicate that the rotations of elbow and wrist were more important than the rotations of shoulder for this training task. Only the novice #13 had similar performance to expert group.

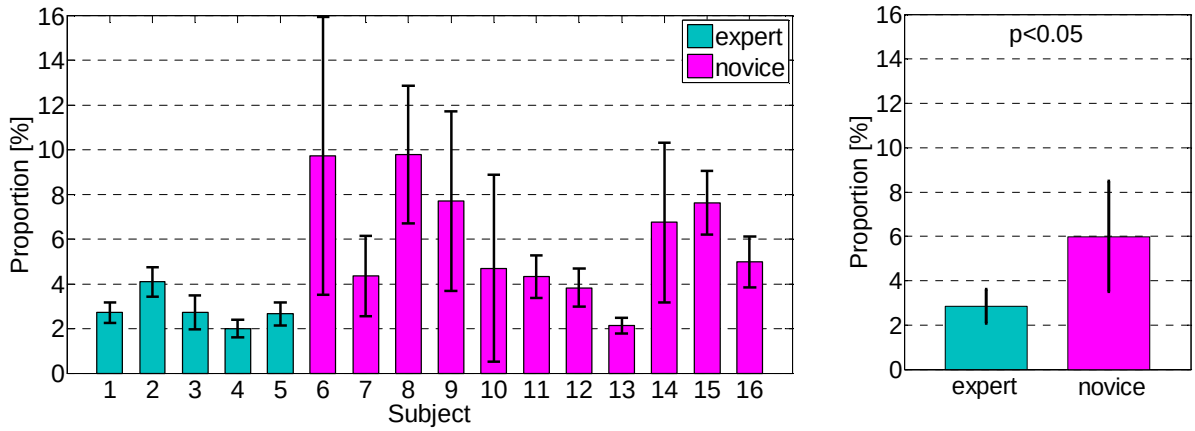

(a) among all the subjects.　　(b) between two groups.

Figure 4.25: Right shoulder used rate in pipe-cleaner training.

4.3.3 Discriminant Analysis in Leave-one-out Cross Validation

The results of the DA performed in the leave-one-out cross validation are showed in Table 4.3. This method can correctly classify 15 subjects (totally 93.75%) based on their laparoscopic skill expertise in both training tasks.

In the case of peg-board training, it achieves 100% correct rate to classify the expert surgeons, which is compatible with the fact that the experts were proficient in completing this task, as it was the regular training item in Kyushu University. In the case of pipe-cleaner training, only 80% correct rate is achieved. One expert is classified unsuccessfully. This might be due to the factor that this expert could not adapt himself well to this novel training item. However, there are still 80% of experts performed in similar ways under this novel task. For the novices, both training tasks achieve more than 90% correct rate of classification, in the case of pipe-cleaner, even 100%. This verifies that the data processing model has high performance for expertise classification.

Table 4.3: Classification results by discriminant analysis.

Task	Subject	Quantity	Successful Case	Failed Case	Correct Rate
Peg-board	expert	5	5	0	100%
	novice	11	10	1	90.9%
	total	16	15	1	93.75%
Pipe-cleaner	expert	5	4	1	80%
	novice	11	11	0	100%
	total	16	15	1	93.75%

The failed classification cases in the peg-board training and the pipe-cleaner training are showed in Figure 4.26 and Figure 4.27, respectively. In Figure 4.26, the performance of novice subject #11 with failed classification is close to experts' performance. There is also the novice subject #8 whose performance is very close to the separation line between experts and novices, which can be considered as the intermediate expertise level. In Figure 4.27, the performance of expert subject #5 is far from the separation line and is classified into novice group, which indicates that this expert surgeon could not adapt himself to this new type of training well. Other four expert subjects have still good performance in this new training. They performed the tasks by using similar movements which distinguish the performance from novices.

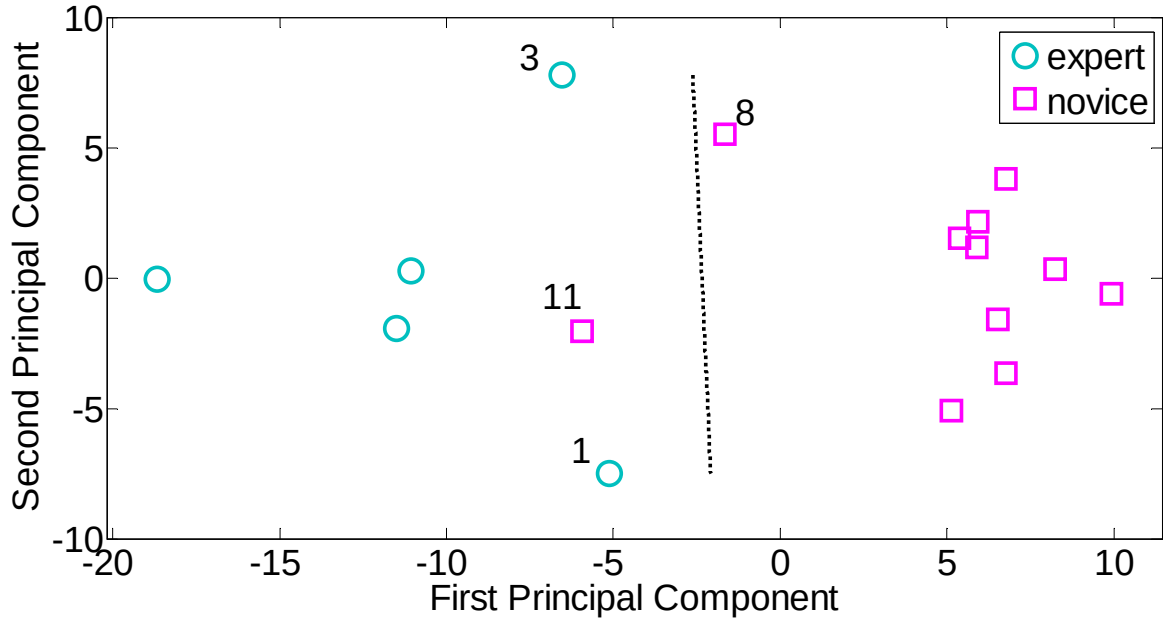

Figure 4.26: Failed classified case in peg-board training.

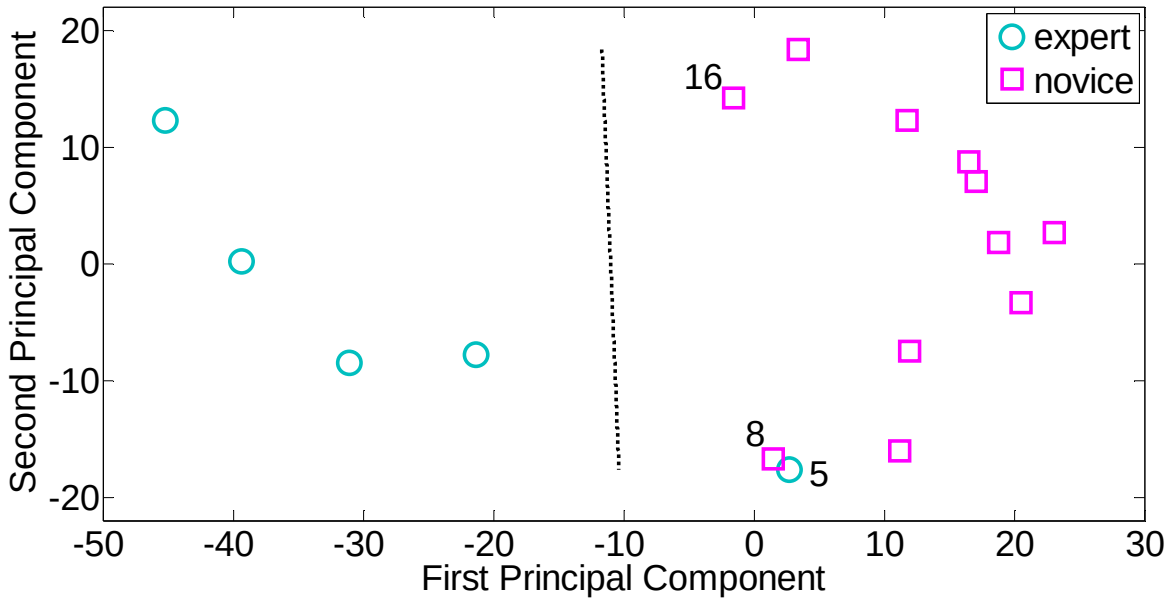

Figure 4.27: Failed classified case in pipe-cleaner training.

4.4 Discussion

From the clinical point of view, it is necessary to find appropriate parameters that can measure the quality of movements for objectively evaluating surgeons' operative skills. It is also necessary to determine how these parameters should be combined. Using the correct motion parameters and their combination will be possible to provide information about the levels of the operative skills. This chapter introduced the WB-3 system for measuring the subjects' upper limb movements and objectively classifying the subjects as experts or novices according to their movements during regular laparoscopic trainings. The data processing model used the statistical techniques t-test, PCA and LDA to evaluate the skill competence. Various feature parameters calculated for the training tasks were integrated without the need for any user-defined weighting factors. The classification was based on a set of training samples where the subjects were with known laparoscopic skill levels. The classification results in both training tasks showed that the proposed methodology had good discriminant validity.

The experimental results showed that, in the peg-board training, the rotation speeds of expert surgeons' shoulders were faster, and the main movement frequencies of surgeons' shoulders were also bigger than novices. This might be an indication of a higher proficiency in executing the tasks. Moreover, expert surgeons used more energy for the rotations of wrist and elbow, but not shoulder, which might indicate that the rotations of elbow and wrist were more important than the rotations of shoulder for this training task. The novices should use less rotations of shoulder in order to achieve better operative performance and save biologic energy. Similar results of some parameters were also found in pipe-cleaner training, such as the shoulder main movement frequency and the right shoulder used rate. All of the significant parameters found in these two tasks were related to the shoulder joint, which indicates that the movements of shoulder are significantly important to the operative skill performance and expertise. Novice should master and control his/her shoulder movements better in order to improve the skills more efficiently. For the evaluation system, therefore, 2 WB-3 IMUs for tracking the shoulder movements might be sufficient enough to realize more simplified evaluation system.

The results were limited to the subject number of 16, which could be improved and further evaluated with more training subjects. Moreover, there were wide differences between the

skill levels of the subjects participated in the experiments. This is necessary for building the database of training samples in the classification procedure. In the other hand, it is also important for the evaluation system to have the capability to classify the subjects with intermediate levels. This would be conducted by some young surgeons with the experience of laparoscopic surgery between 1 and 100 real operations.

Two basic training tasks for eye-hand coordination were selected in this study, other training tasks, such as fundamental laparoscopic tasks (FLS) proposed by American Gastrointestinal and Endoscopic Surgeons (SAGES) [114], would be further considered for evaluating the performance of the proposed skill evaluation system.

4.5 Conclusion of this Chapter

This chapter presented the WB-3 system as a tool to evaluate the operative skill expertise of expert surgeons and novice students during regular laparoscopic trainings.

The WB-3 system was capable of measuring and analyzing the movements of subject's upper limbs during regular laparoscopic trainings, and extracting the significant motion features between expert surgeons and novices. The classification results of 93.75% correct rates satisfy the objectives of this study. Moreover, the significant motion features, as the quantitative feedback to the trainees, could provide insight information about which motion he/she should improve. This study represents a significantly important step and basis towards the realization of operative skill evaluation in the real operation theater.

In order to verify the proposed skill evaluation system could be adaptive to different surgical trainings, it is necessary to assess the resulting system in more practical applications. Therefore, the proposed evaluation system is further implemented in neurosurgery described in next chapter, with the focus on instrument motion analysis for skill evaluation.

Chapter 5

Evaluation of Neurosurgery Operative Skills

5.1 Introduction

5.1.1 Background

In recent years, more and more technologies have entered the operating theater of neurosurgery [1]. By using cameras or microscopes and miniaturized tools, surgeons are allowed to operate in smaller and smaller spaces, thus obtain better results and higher performance [115]. While these new technologies have many advantages and benefits for patients, they often require surgeons to undergo long and difficult trainings [116].

These trainings have been needed particularly in which neurosurgery has been deeply influenced by the new technologies. Fine techniques targeted to obtain treatments minimally invasive and traumatic are required. Intra-operative false movements can be devastating, leaving patients paralyzed, comatose or dead. The precision of the surgical movements and gesture is related both to the experience of the surgeons and accuracy of the available technological instruments. In this frame, medical training is particularly important.

Traditional techniques for trainings in neurosurgery use animals, phantoms, cadavers and real patients. The main limitation of these approaches is that live tissue has different properties from dead tissue and that animal is also different from the human, and trainings on

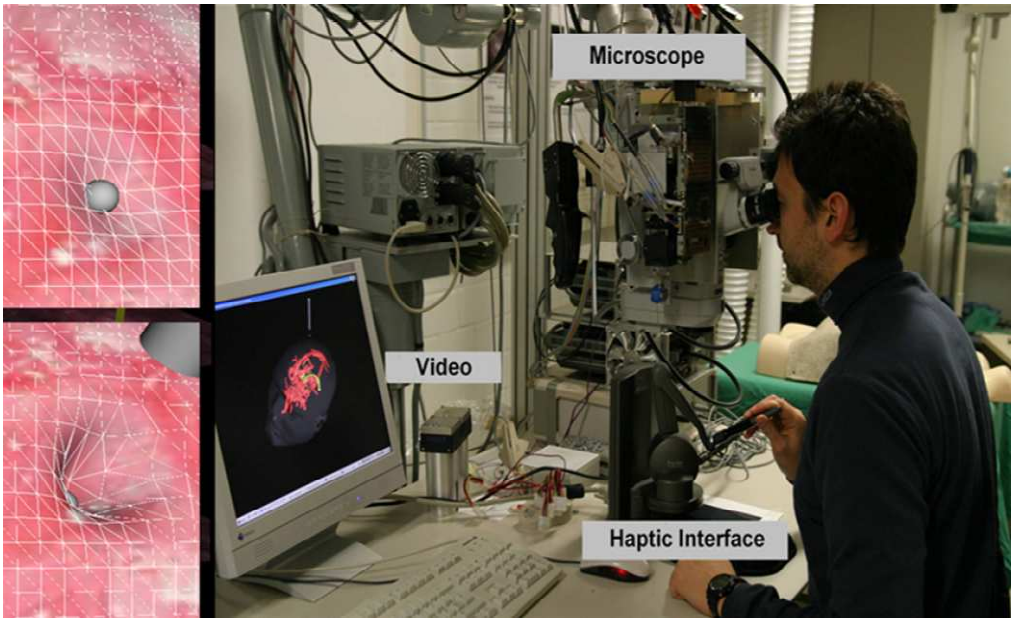

Figure 5.1: VR simulator for neurosurgical training.

the real patients are significantly dangerous. In other words, they lead the realism of the surgical trained procedures [117]. Nowadays, this classical training is improved by the use of well-illustrated books and excellent training movies recorded directly in the operation room but the main trainings for surgeons are still performed on the real patients [16, 118]. Recently, Mauro et al. presented a virtual reality training system (Figure 5.1) for neurosurgical interventions based on a real surgical microscope and on a haptic interface for a better visual and ergonomic realism [119, 120]. The simulation takes advantage of an accurate tissue modeling, a force feedback device and the rendering of the virtual scene directly to the oculars of the operating microscope.

One of the paramount issues in these trainings is the objective evaluation of surgical skills. Historically, this kind of evaluation has been subjectively performed by senior surgical expert in both regular trainings and operating environments. In other fields, such as laparoscopic surgery for example, several metrics [15, 23, 121, 122], and segmentation procedures [22, 123, 124] have already been proposed and employed to characterize different phases of surgical movements in laparoscopic surgery, with interesting results. The extremely small movements and operation target area involved in neurosurgery, however, have prevented until now the developments of similar skill evaluation methodologies and systems. Although there

are some training metric, such as the traditional trainings and VR trainings, the general operative skill evaluation system is still missing.

Analysis of the movements of neurosurgical instruments is a valuable method for objective skill evaluation. Surgeons with different experience and skill dexterity of neurosurgery normally perform different motion of the instruments during the operation. Intra-operative false movements of these instruments can be leaving patients paralyzed, comatose or dead. Therefore, tracking devices are needed for neurosurgical operative skill evaluation in order to analyze these movements. Currently, tracking methods used in neurosurgery are either optical or electromagnetic. Optical technologies are high priced, high-resolution systems. The markers are placed on surgical tools for the real time tracking (Figure 5.2). However, these markers are relatively heavy and bulky with the specific mechanism for mounting, and they need to be always in sight with the cameras, which is not always possible [125]. The sensing coils of electromagnetic tracking devices are very compact, but whose measurement volumes are relatively small, thus limiting their use in wide operation area [35].

One possibility for the realization of compact measurement systems is offered by MEMS technology, which is becoming widely popular in inertial sensors for measuring angular speed, acceleration, and inclination, offering multiple-axis response with high resolution and low power consumption in a single package. However, the previous researches such as WB-2 IMU or commercial systems (Xsens MTx, InterSense InertiaCube3, and so on) are still too big and heavy for the application of operative skill evaluation in neurosurgery [126].

Figure 5.2: Markers of optical tracking technologies on the surgical tool.

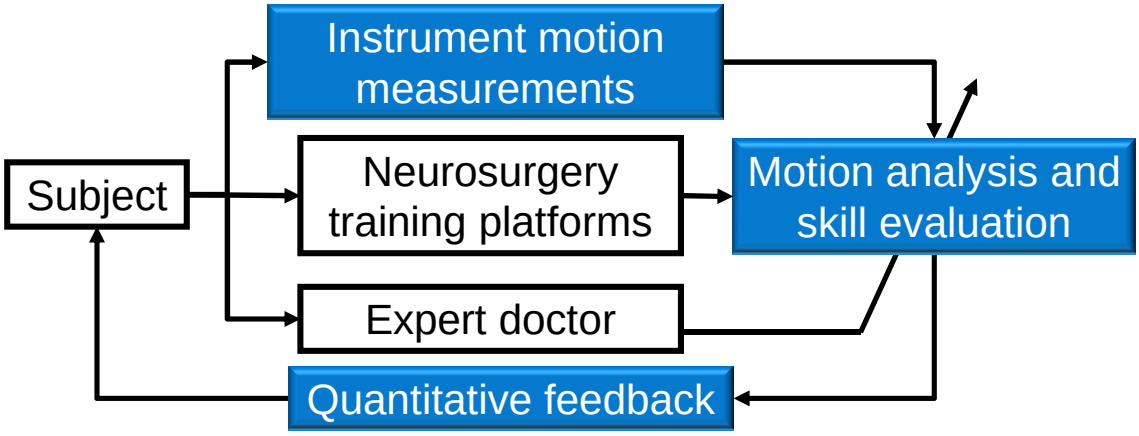

Figure 5.3: Proposed methodology for neurosurgical operative skill evaluation.

5.1.2 Objective

The aim of this study, therefore, is to develop skill evaluation system to objectively assess subject's operative skills based on the motion analysis of neurosurgical instruments.

In particular, this skill evaluation system for neurosurgery should satisfy the following requirements:

- Capability of measuring the movements of neurosurgical instruments during regular neurosurgical trainings.
- Extraction of the significant motion features between the expert surgeons and novices.
- Illustrations of the overall movement performance compared between expert surgeons and novices.
- Feedback of quantitative motion information to trainees to show up how they performed while comparing with the experts.

5.2 Materials and Methods

According to the general methodology introduced in Chapter 1, the block diagram of the corresponding methodology for realizing the objective operative skill evaluation system in neurosurgery is showed in Figure 5.3

The approach is to utilize the ultra-miniaturized WB-3 IMU to measure neurosurgical instrument's motion for analyzing subject's hand movements, and define a set of parameters that allow us to characterize these movements during various surgical procedures, in order to

see how the subject acts during the trainings, and evaluate the improvements of performance after trainings. The data collected by WB-3 IMU, moreover, provides an important baseline for design specification and performance evaluation of microsurgical instruments. The feedback of quantitative motion information to subjects shows which motion parameter has poor performance and should be improved.

5.2.1 Experimental Evaluation

A) Experimental setup

1) Bipolar forceps

During neurosurgery, one of the most commonly used instruments is the bipolar forceps (Figure 5.4). The main characteristics of the system used in the experiments are summarized in Table 5.1. A connector made by acrylonitrile butadiene styrene (ABS) polymer in rapid prototyping for housing WB-3 IMU is placed at the proximal end of the bipolar forceps. The WB-3 IMU's extremely reduced weight and size allows it to be mounted on the bipolar forceps, and to be used during normal trainings without disturbing subject's performance.

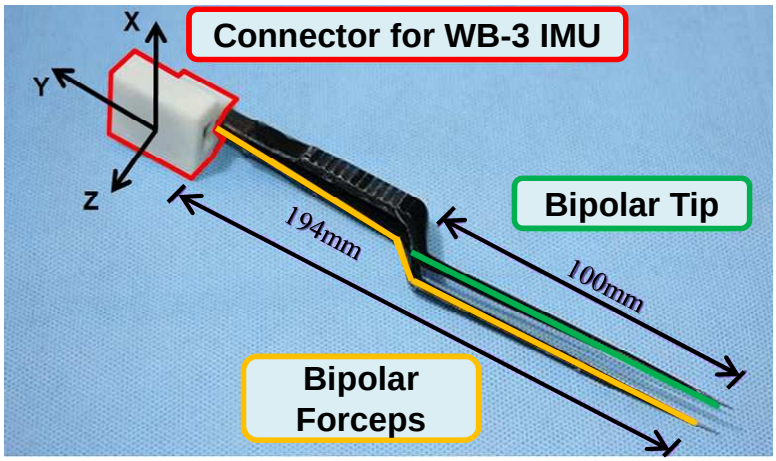

Figure 5.4: Bipolar forceps setup with WB-3 IMU.

Table 5.1: Main characteristics of the bipolar forceps.

Total length	194 mm
Tip length	100 mm
Weight	34.0 g

2) Skill training platform

The skill training platform developed for this experiment is showed in Figure 5.5. The skill training platform was composed by 5 main parts:

- The test bed, made by ABS, simulated the typical surgical space during neurosurgery. This prototype had a size of 60 x 40 x 60 mm which is the most common operation space.
- The support base was an aluminum base of 100 x 100 mm with housing for the test bed made by ABS. This support base's purpose was to hold the whole unit stable.
- The surgical field (size about 50 x 19 mm) simulated the aperture in the human skull. The subject accessed the target area and the goal area from here.
- The target area was a replaceable soft surface (size 25 x 30 mm) on which the targets were placed before the experiments. This area was made by Hitohada skin-like gel RTV-2K#1406 Hardness 0 (EXSEAL Corp., Tokyo, Japan) which was a super-soft urethane resin for modeling similar softness and feeling of human skin. Three different types of target areas, each with 5 surface mounted device (SMD) resistors randomly placed on it (Figure 5.6), were prepared to simulate typical objects to be handled during neurosurgery: BIG: 3.2 x 1.6 x 0.4 mm; MEDIUM: 2.0 x 1.2 x 0.3 mm; SMALL: 1.0 x 0.5 x 0.2 mm.
- The targets picked up from the target area were put into the goal area (size 10 x 30 mm). To facilitate the release of the objects, a putty-like adhesive was placed at the bottom of this goal area.

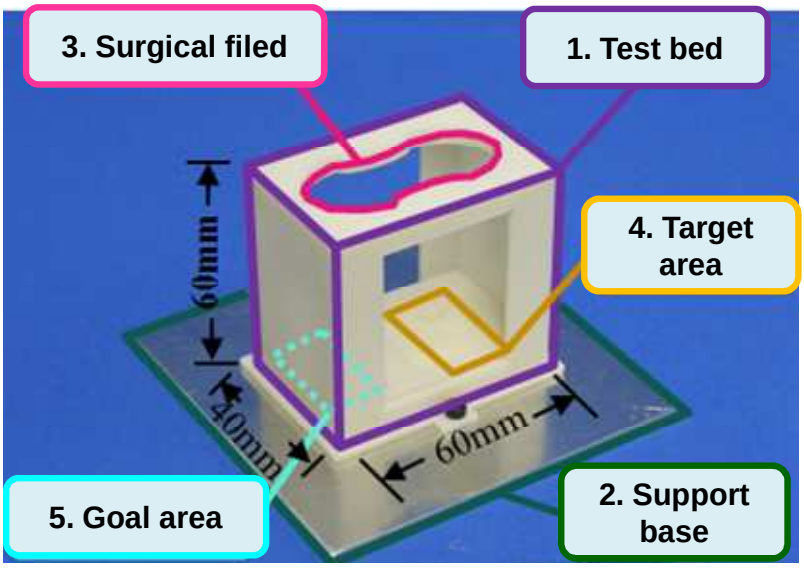

Figure 5.5: Skill training platform developed for neurosurgery.

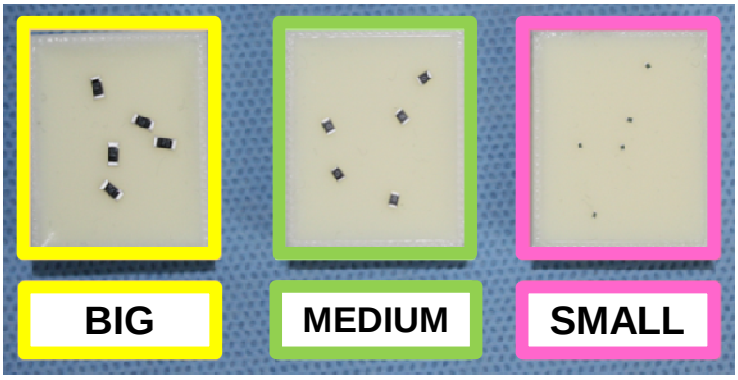

Figure 5.6: Three types of target areas, each with 5 targets randomly disposed on them.

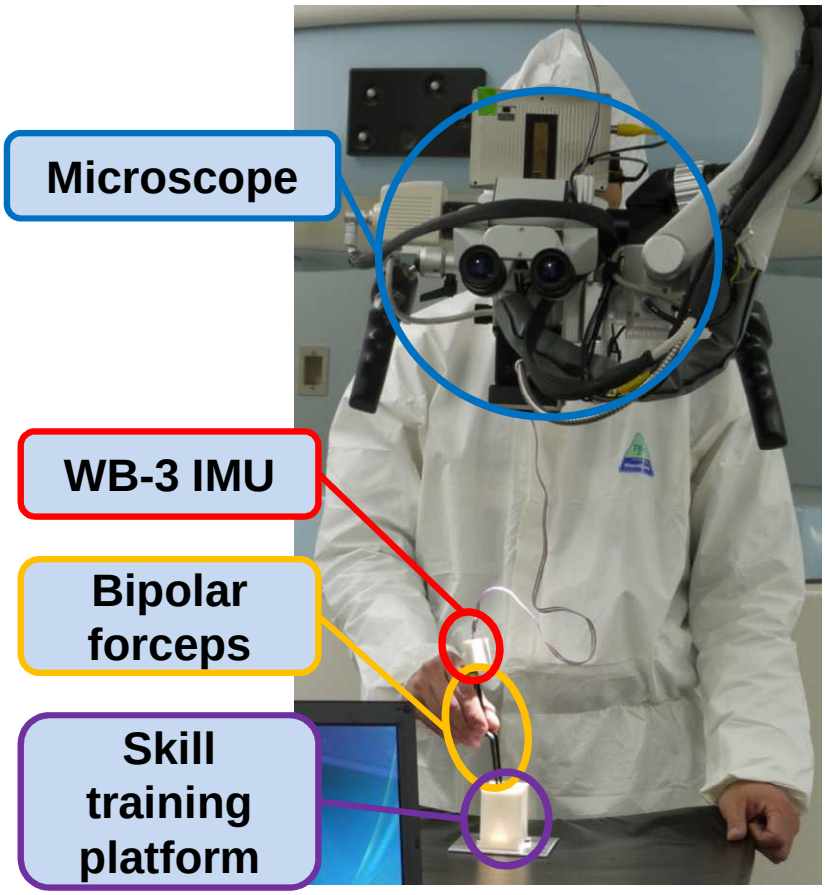

Figure 5.7: Overview of the experimental setup in neurosurgery.

The experimental setup is showed in Figure 5.7. The microscope was a MITAKA MRI (Mitaka Kohki Co., Ltd, Tokyo, Japan). The subject looked trough the microscope to the training platform which was placed on the operation table. All the movement data acquired by WB-3 IMU was saved in a laptop for offline analysis.

B) Experimental protocol

Thirteen non-medical subjects (average age 27.5 years old; age range 22-39; all male; all right hand users) and 1 expert neurosurgeon (age 40) participated in the experiments after providing informed consent. Among the non-medical subjects, only 1 subject (subject #2) had some experience with operating neurosurgical tools, and 1 subject (subject #9) had some training experience with laparoscopic surgery; all the other subjects were totally novices.

The experiments consisted in picking all the objects up from the target area, one by one, and then releasing them in the goal area. The three different types of target areas were replaced by following the order BIG → MEDIUM → SMALL, each repeated 5 times. In total there were 15 trials (3 types x 5 repetitions) executed by each subject.

5.2.2 Data Processing

Acceleration data were sampled at f_a = 160 Hz, gyro data at f_ω = 500 Hz and magnetic data at f_{mag} = 50 Hz. Data were acquired on the laptop for real-time display, and saved for storage and offline analysis.

These raw data are trimmed to remove dead-time at the beginning and at the end of each trial due to the manual start/stop as follows: The beginning of each trial is defined as the first sample while $|a_y| > 9.1$ m/s^2; the end of the trial is defined as the first sample from the end of the data log while $|a_y| > 9.1$ m/s^2, where a_y is the y axis acceleration in corresponding with the long axis of the bipolar forceps as defined in Figure 5.4.

Acceleration components and angular speed components are then filtered and smoothed by using a 10th order bandpass IIR Butterworth filter with cutoff frequencies f_{c1} = 0.05 Hz, f_{c2} = 5 Hz (accelerometer); f_{c1} = 0.05 Hz, f_{c2} = 2 Hz (gyroscope) to remove bias and to remove physiological tremor [59, 127]. In this way only the data due to the voluntary movements of the instrument are analyzed. Furthermore, the filtering reduces the effect of noise in the band outside the human movements (normally <15-20 Hz) improving the SNR (Signal-to-Noise Ratio).

In particular, the following motion features have been found out some significant differences of performance between expert and novices: execution time (*ET*); mean, cumulative distribution function (*CDF*) and power spectral density (*PSD*) of acceleration module $|a|$; mean, *CDF* and peak frequency of angular speed module $|\omega|$.

The fast Fourier transformation (*fft*) for |*a*| is calculated with fft_{size} = 8192 samples obtaining a frequency resolution $f_{res(a)} = f_a / fft_{size}$ = 0.0195 Hz. The *PSD* is estimated in |*a*| with the following formula:

$$PSD = fft \bullet conj(fft) / fft_{size} \tag{5.1}$$

The frequency range chosen for the mean *PSD* evaluation is 0.1 - 3 Hz for |*a*|. The *CDF* of |*a*| and |ω| is calculated for 95% cumulative distribution.

The following figures with (norm.) indicate that the data have been normalized to the average corresponding data of the expert surgeon (subject #14) for an easier visual comparison of the scales. The normalized values are listed in Table 5.2.

Table 5.2: Normalization values of the motion features in neurosuery experiments.

	BIG target	MEDIUM target	SMALL target
ET [s]	11.7	11.2	16.2
Mean |*a*| [m/s^2]	0.55	0.60	0.62
|*a*| $CDF_{95\%}$ [m/s^2]	1.02	1.08	1.25
Mean *PSD* |*a*| [(m/s^2)^2]	0.25	0.27	0.54
Mean |ω| [deg/s]	5.78	5.77	6.14
|ω| $CDF_{95\%}$ [deg/s]	15.98	16.02	16.99
|ω| Peak Freq. [Hz]	1.01	0.87	0.94

5.3 Experimental Results

5.3.1 Execution Time

The expert surgeon performed faster than all the novice subjects in three different targets (Figure 5.8). This indicates that the expert surgeon had better dexterity to manipulate the bipolar forceps and complete the task in such small operation space. The expert also showed high constancy in the execution time of BIG and MEDIUM targets (Table 5.2). Moreover, expert surgeon had much smaller standard deviation in the cases of MEDIUM and SMALL targets after the first 5 trials in BIG target, which means that the expert could adapt himself

well to this training. In the other hand, the novices performed the trainings with higher time variance.

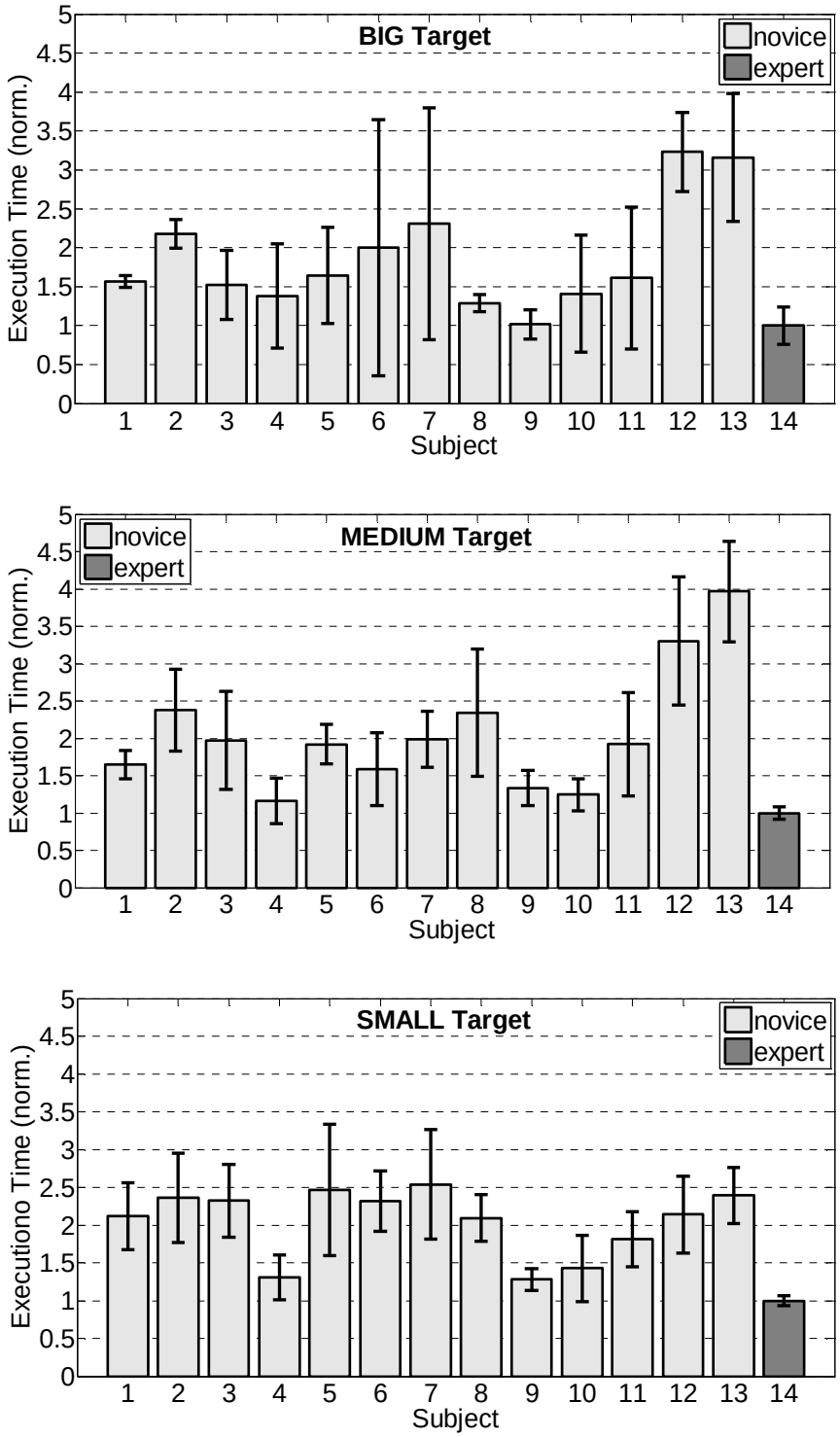

Figure 5.8: Execution time of each subject used in three different training targets.

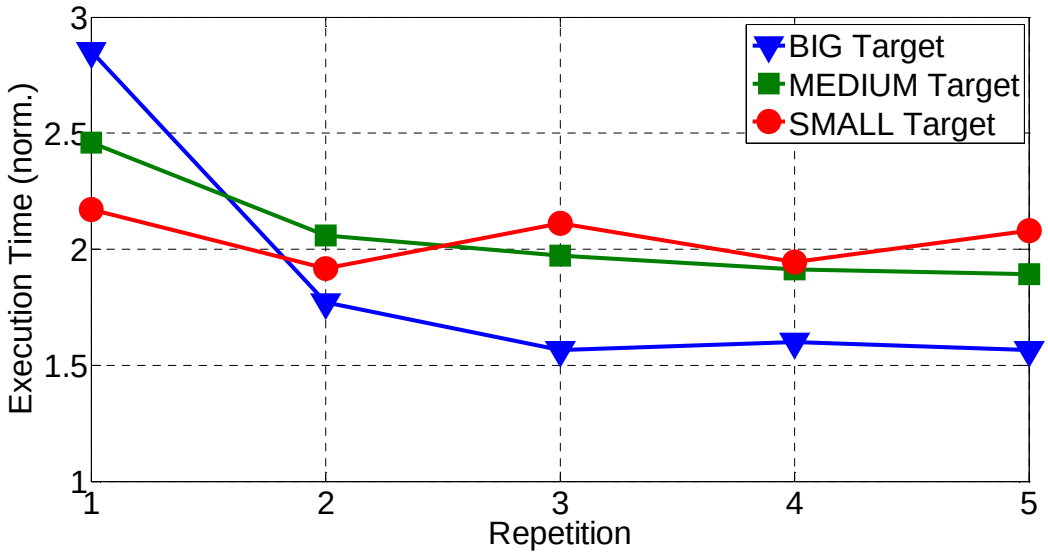

Figure 5.9: Execution time averaged on all novice subjects for each repetition in three different training targets.

Figure 5.9 shows the execution time of all the novice subjects averaged on each repetition. It can be clearly noticed that both the cases of BIG and MEDIUM targets show a fast learning effect for the novices, with the execution time stabilizing after the third repetition. However, this learning effect could not be seen in the case of SMALL target, which might be caused by the difficulty in picking up these objects with smallest sizes. Moreover, the case of BIG target shows higher gradient in reducing the execution time after second repetition, which is compatible with the difficulty of this task containing biggest objects.

5.3.2 Analysis of Acceleration

The mean acceleration values of all the subjects in three different training targets are showed in Figure 5.10. The expert used smaller acceleration than most of other novice subjects in all these trainings. Only subject #2 and subject #11 had similar performance with expert surgeon. Subject #2 (with experience of operating bipolar forceps) had smaller values of this parameter than expert in all the trainings. Subject #9 had almost the same values with expert in all the training targets. However, these two subjects had bigger standard deviations than the expert. The subject #5, #12 and #13 used significant higher mean accelerations than

other subjects in all the training targets, which might indicate that they had poor moving stability. In addition, subject #4 had high standard deviation in the trainings of SMALL target, which indicates that he performed with more variable movements. All the other subjects had intermediate results.

As can be seen in Figure 5.11, the 95% *CDF* of the acceleration |*a*| shows different performance between expert and novices. For the BIG target, the expert surgeon outperformed all the novices with lower cumulated acceleration and standard deviation; only subject #2 and subject #11 had performance close to expert. The data about the MEDIUM target shows similar trends; subject #2 performed the task with smaller *CDF* than expert. Things were different for the SMALL target, when several novices had similar or lower *CDF* than the expert surgeon. These, however, were due to much higher execution time for the novices. In all the trainings of three different targets, both subject #12 and #13 completed the tasks with significant higher *CDF* values than other subjects, which were similar with the results in the parameter of mean acceleration. It can be considered that these two novices also had poor performance in this parameter.

Another parameter which discriminates between the expert surgeon and novices is the *PSD* of the acceleration |*a*| showed in Figure 5.12. The scale of the *PSD* values is logarithmic. The mean *PSD* clearly identifies the experienced expert respectively from all the other subjects. The expert surgeon (subject #14) had significant smaller mean *PSD* values of |*a*| in all the trainings, which indicates that he almost did not use translation movements on this pick & place exercise. Expert performed more rotation movements inside this small operation space in order to reduce the variable linear motion. For the BIG targets, subject #2, #9 and #11 performed in a similar way as the expert regarding this parameter. For the MEDIUM target, only subject #2 had close result to expert. In the case of SMALL target, subject #2, #9 and #10 had smaller values than other novices.

Among all the novices, only subject #2 (with experience of operating bipolar forceps) performed similar results of *PSD* with expert in all the training targets. Subject #9 (with experience of laparoscopic trainings) and subject #11 had similar performance with expert in only the cases of BIG and SMALL targets. In all the trainings, the subject #12 and subject #13 also had significant bigger *PSD* values than other subjects, which were similar to the results in the mean and *CDF* values of acceleration.

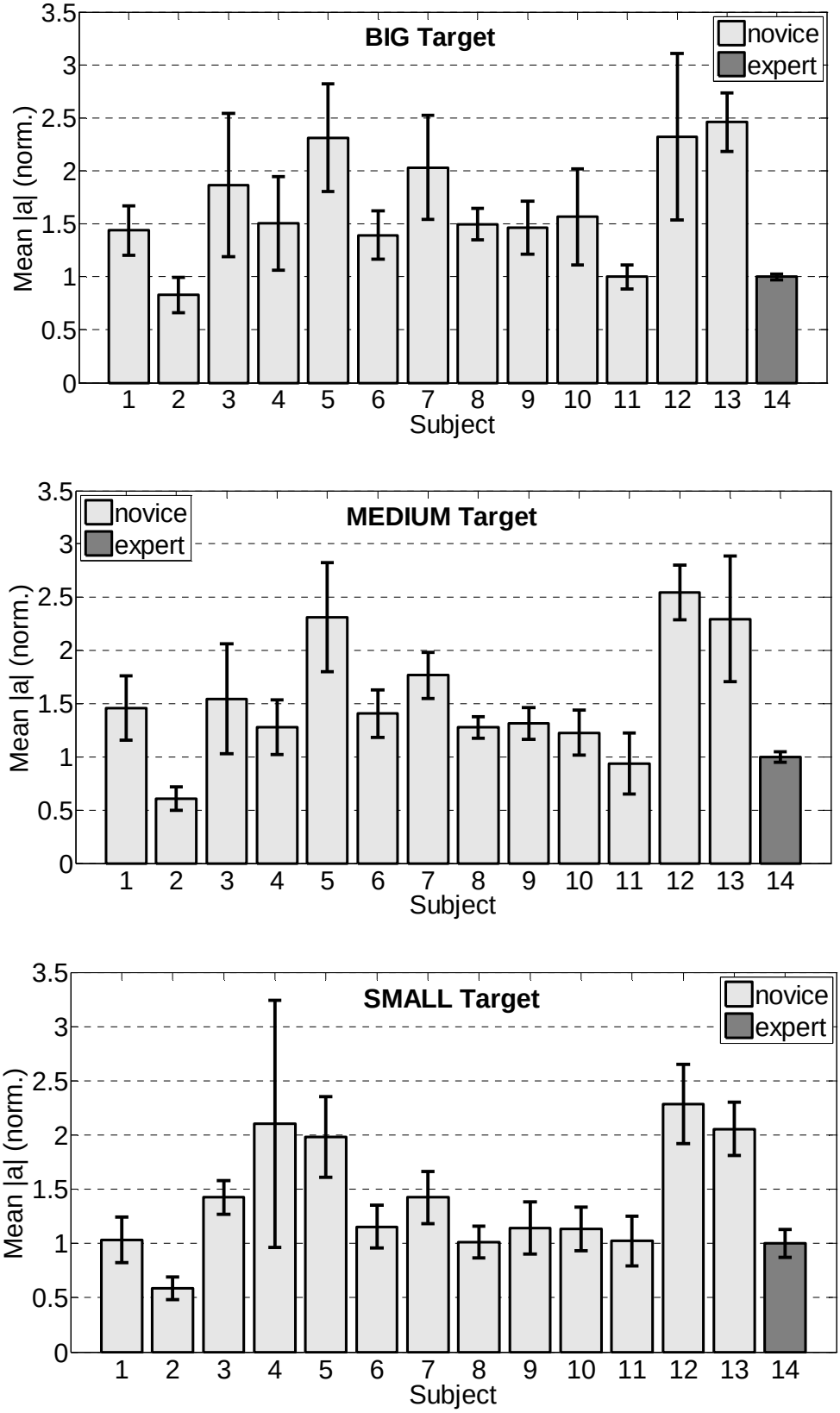

Figure 5.10: Mean |*a*| of each subject in three different training targets.

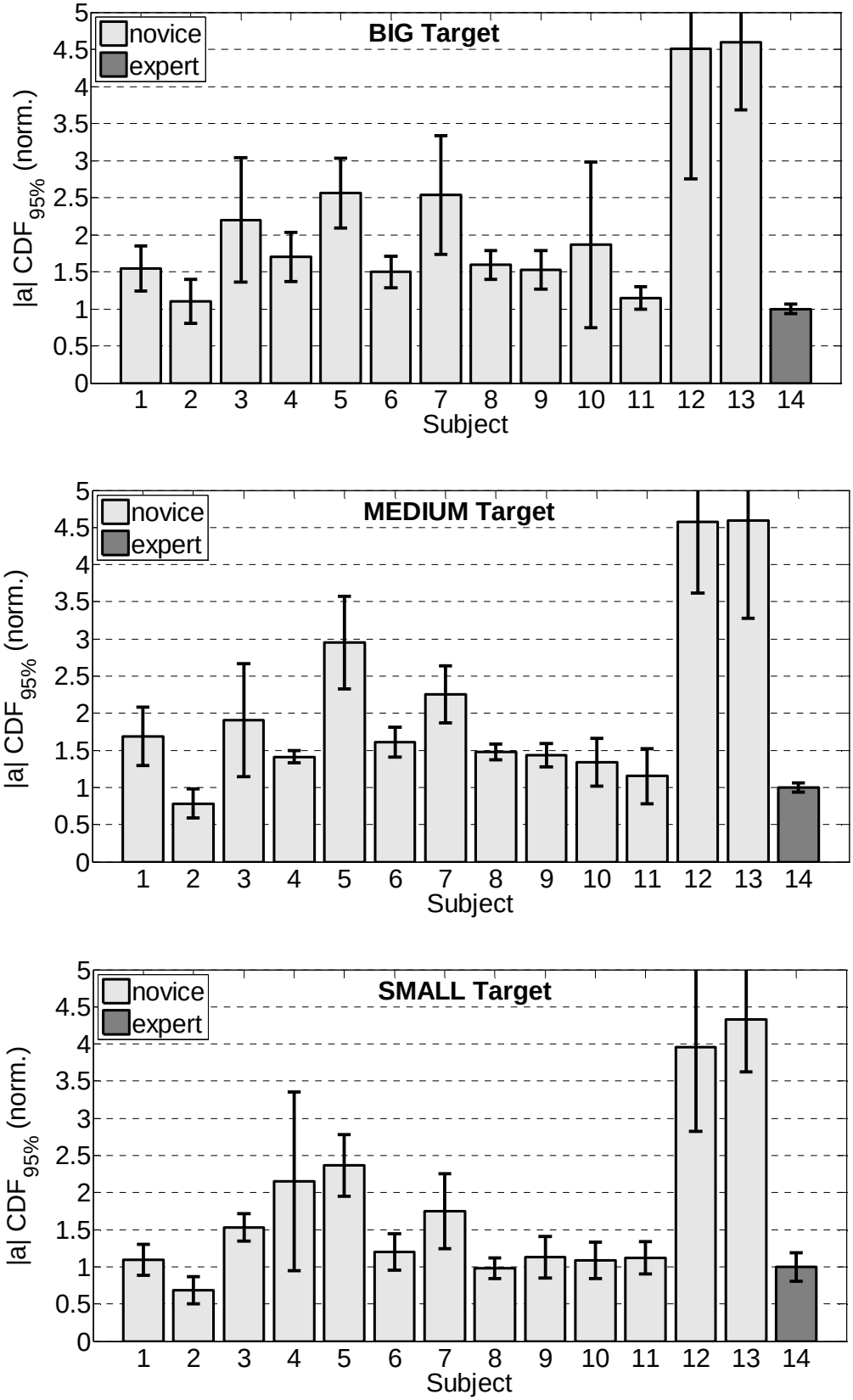

Figure 5.11: 95% *CDF* of |*a*| of each subject in three different training targets.

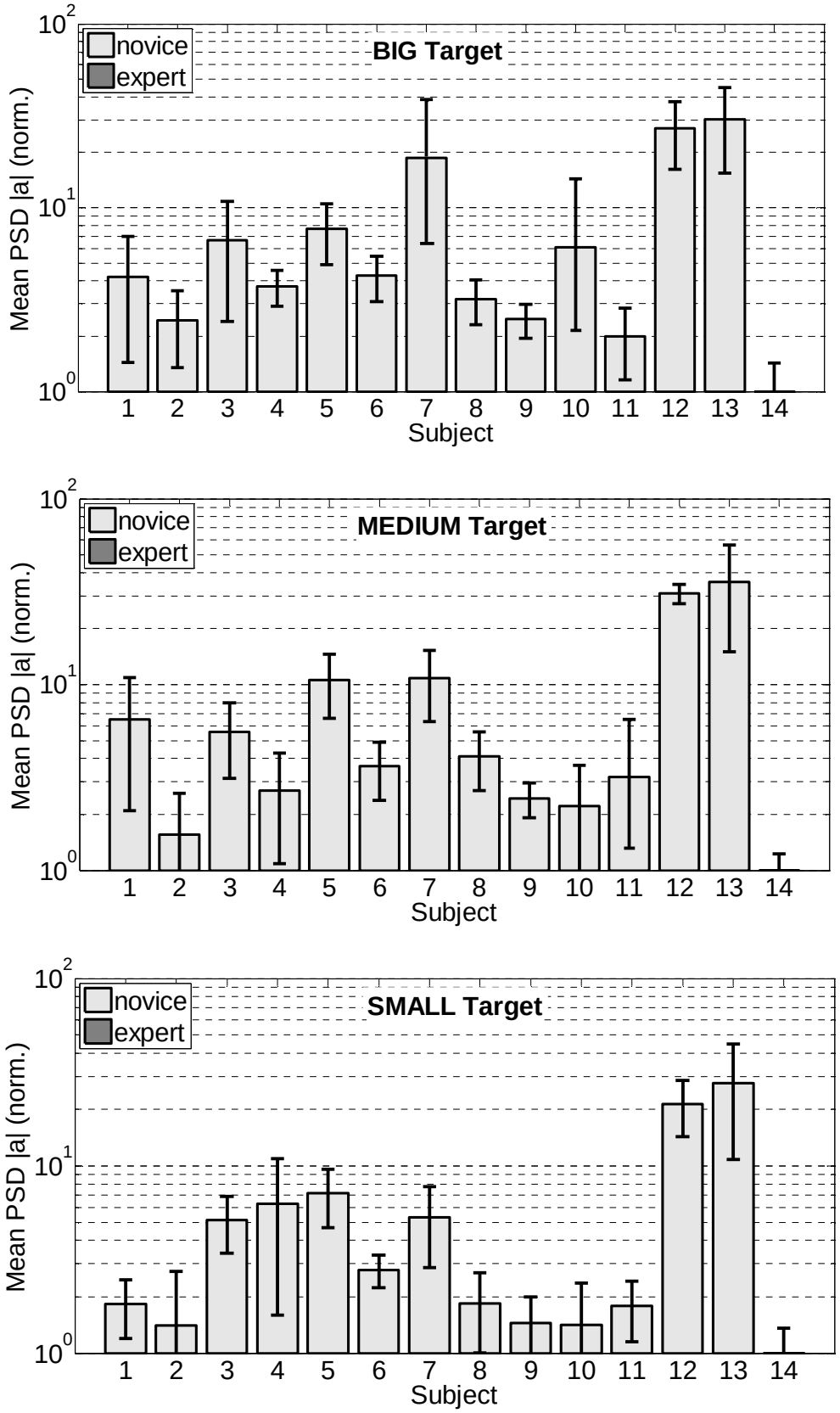

Figure 5.12: Mean *PSD* of |*a*| of each subject in three different training targets.

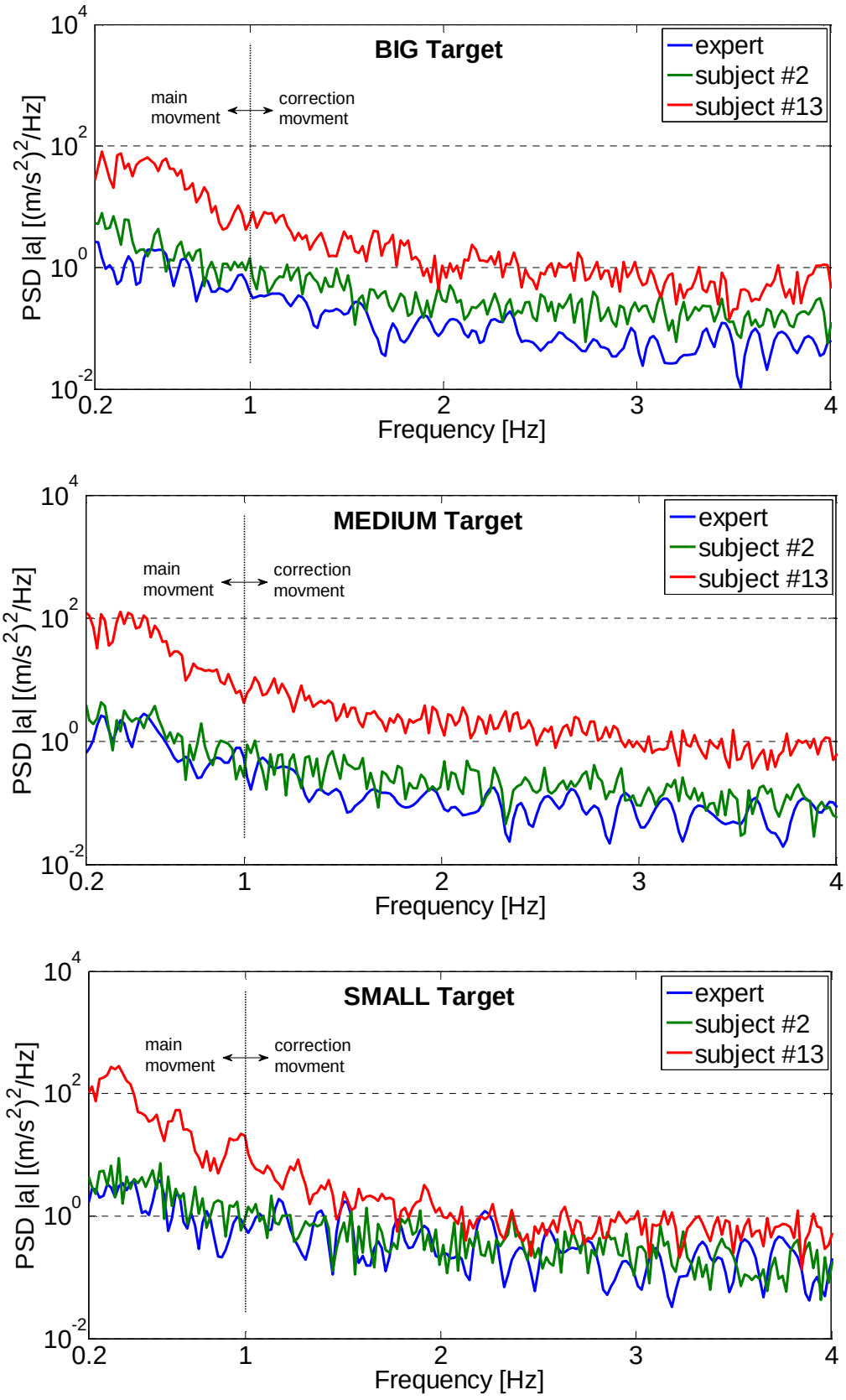

Figure 5.13: *PSD* of |*a*| of subject #2, subject #13 and expert in three different training targets.

Interesting consideration can also be done by analyzing the *PSD* values in low movement frequency range. Figure 5.13 shows the *PSD* values of subject #2, #13 and expert in logarithmic scale. The expert and subject #2 used clearly lower *PSD* of $|a|$ than subject #13 in the frequency range 0.2 - 4 Hz, and they had similar performance with each other. The *PSD* values of these three subjects in the range of 0.2 - 1 Hz were significantly bigger than the values in the range of 1 - 4 Hz, which indicates that the range of 0.2 - 1 Hz covered the main movements and the range of 1 – 4 Hz represented the voluntary movements for the corrections during the trainings.

5.3.3 Analysis of Rate Gyro

As can be seen in Figure 5.14, the expert usually used smaller angular speed than most of the other subjects in the cases of BIG and MEDIUM targets; however, there was no significant difference of performance between expert surgeon and novices in the case of SMALL target. For the BIG and MEDIUM targets, the expert had much smaller standard deviation than novices. Moreover, the expert used almost the same values (5.78 and 5.77 deg/s, showed in Table 5.2) of mean $|\omega|$ in these two targets. For the SMALL target, several novices had similar or lower values than the expert surgeon.

The feature of 95% *CDF* of $|\omega|$ also shows some difference between the expert and the novices (Figure 5.15). The expert surgeon's *CDF* and the corresponding standard deviation were usually lower than the other subjects for the BIG and MEDIUM targets, showing therefore high smoothness and regularity in the movements. The expert had intermediate performance for the SMALL targets, where some subjects reached lower *CDF* values at the expenses of higher *ET*. The subject # 12 and subject #13 showed significant higher values of $|\omega|$ *CDF* than other subjects, which were similar to the results of acceleration data.

Another parameter which discriminates the performance between expert and novices is the peak frequency of $|\omega|$ (Figure 5.16). The expert surgeon used significantly higher angular speed frequency than all the other subjects in three training targets. This frequency of expert was about 1 Hz (showed in Table 5.2) as the main movement frequency during the trainings. In the other hand, the frequencies of novice subjects were normally much smaller in three training targets, where the values were about 0.5 Hz. It indicates that the expert had much higher efficiency and stable movements to complete the training tasks.

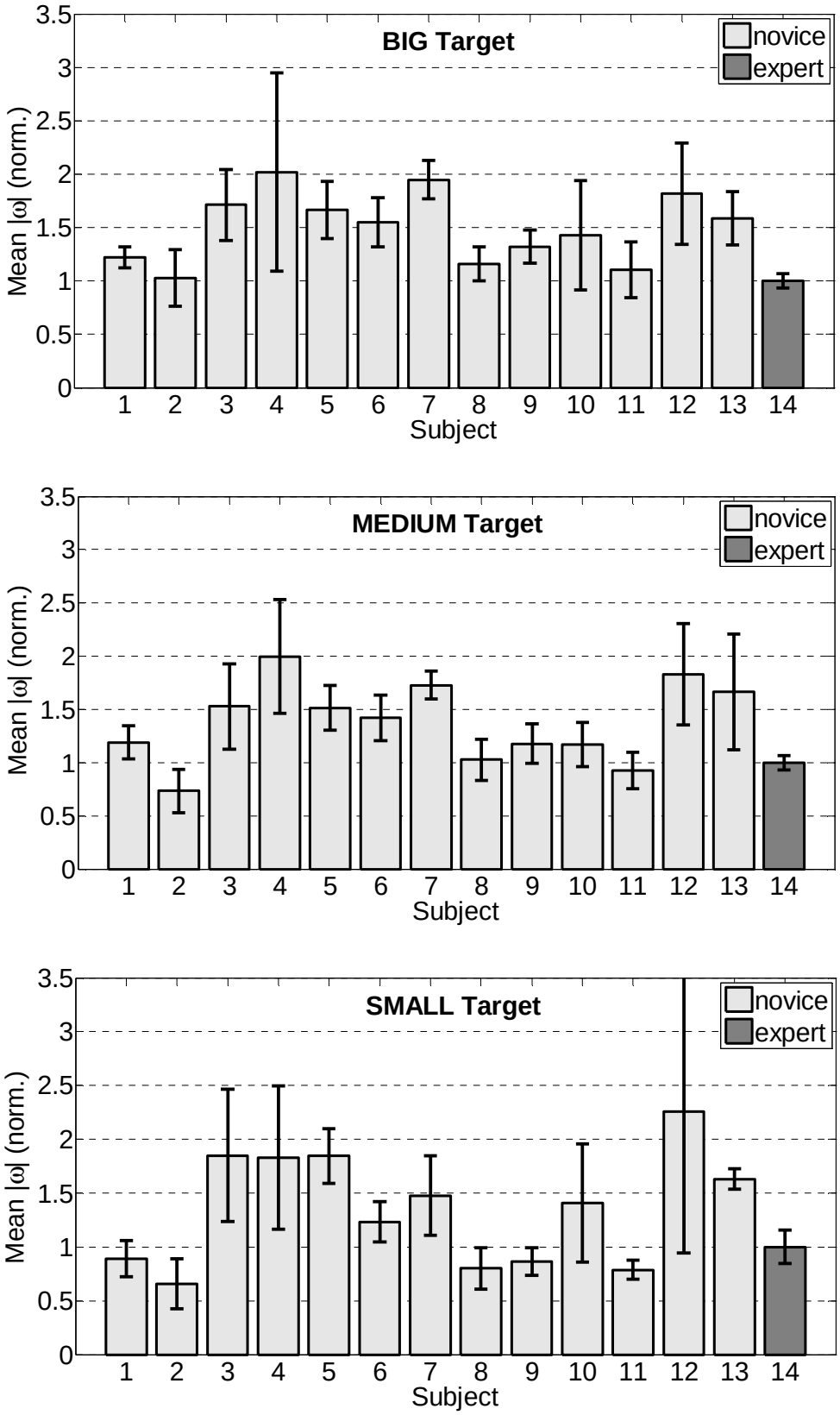

Figure 5.14: Mean $|\omega|$ of each subject in three different training targets.

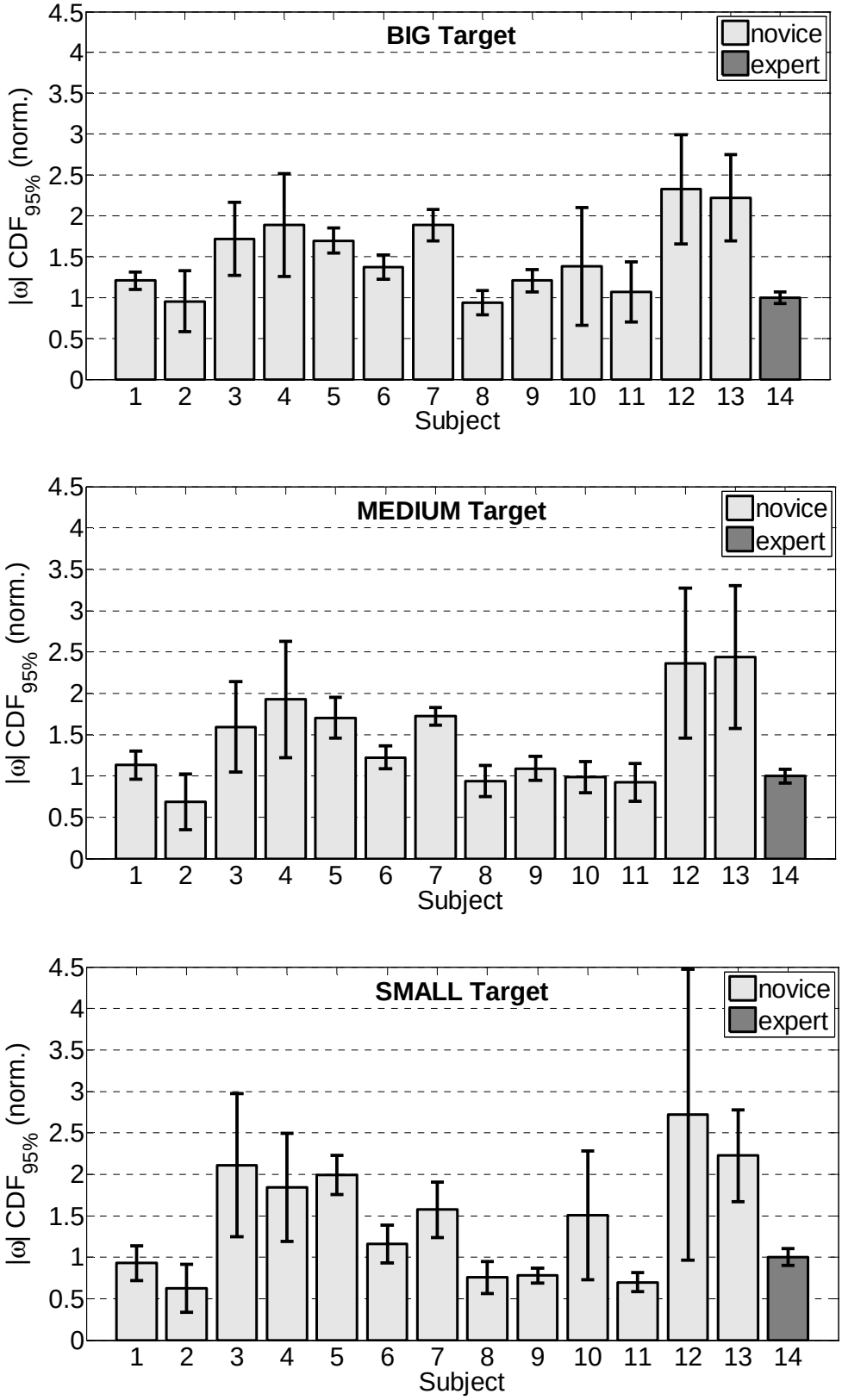

Figure 5.15: 95% *CDF* of $|\omega|$ of each subject in three different training targets.

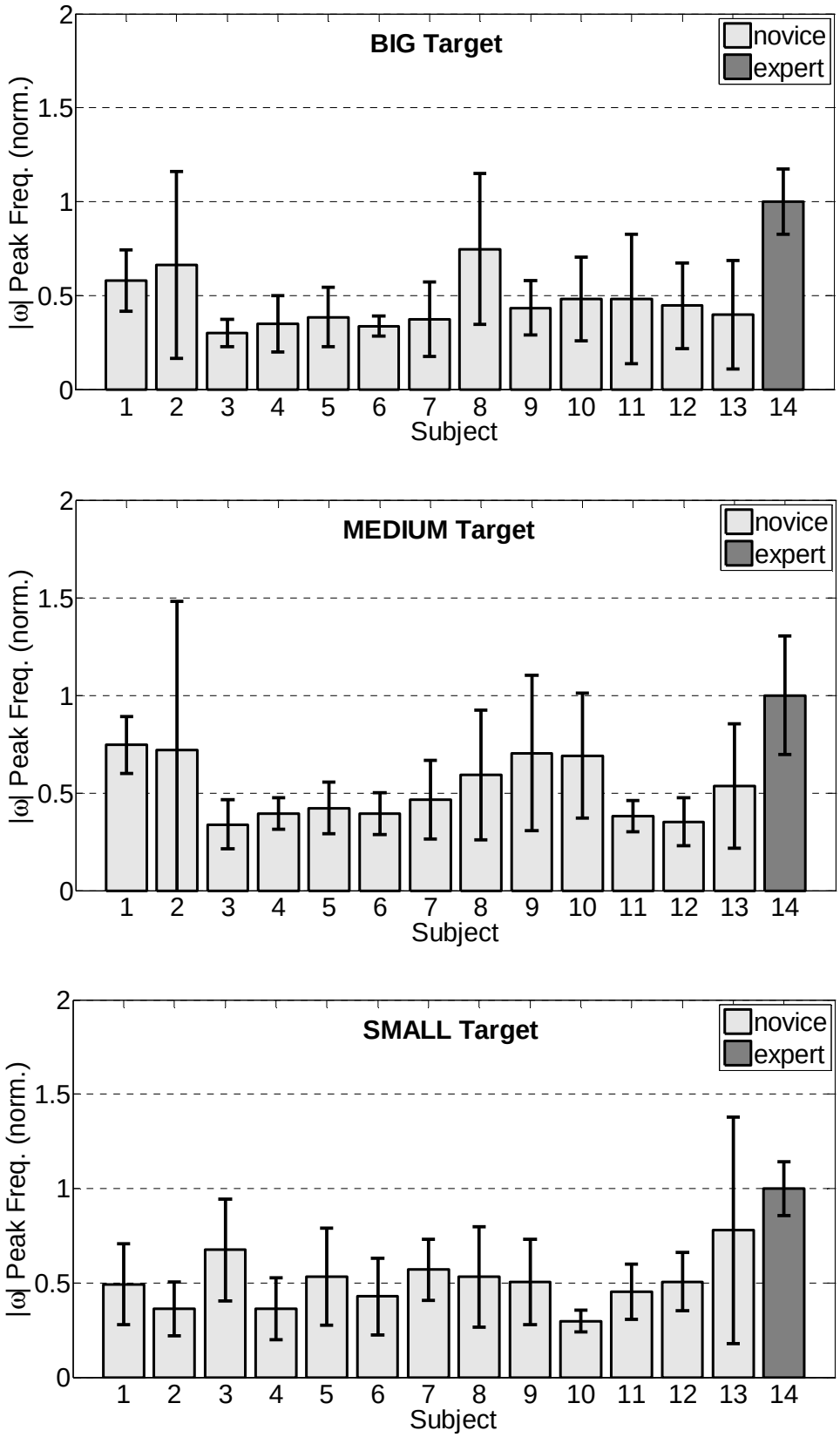

Figure 5.16: Peak frequency of $|\omega|$ of each subject in three different training targets.

5.3.4 Global Performance Evaluation

In order to evaluate the global performance of each subject regarding to the expert surgeon who is as the standardized reference, all the parameters discussed above for the novices are normalized to the corresponding values of expert. In the cases of *ET*, means of |*a*| and |*ω*|, *CDF* of |*a*| and |*ω*|, mean *PSD* of |*a*|, they have been normalized by using the following formulas:

If $Param_{i,j} > Param_{expert}$:

$$Score_{i,j} = Param_{expert} / Param_{i,j} \tag{5.2}$$

If $Param_{i,j} <= Param_{expert}$:

$$Score_{i,j} = 1 \tag{5.3}$$

Where, *i* means the subject number from 1 to 14; and *j* indicates the *ET*, means of |*a*| and |*ω*|, *CDF* of |*a*| and |*ω*|, mean *PSD* of |*a*|, in total 7 parameters.

For the parameter of peak frequency of |*ω*|, it has been normalized by the following formulas:

If $PeakFreq_{i,} > PeakFreq_{expert}$:

$$Score_{i} = 1 \tag{5.4}$$

If $PeakFreq_{i} <= PeakFreq_{expert}$:

$$Score_{i} = PeakFreq_{i} / PeakFreq_{expert} \tag{5.5}$$

Figure 5.17 and Figure 5.18 show the global evaluation of all parameters for all the novices compared with expert in three different training targets. It is clear that there is significant difference of performance between expert and novices.

In Figure 5.17, it shows the global evaluation results of subject #1 to subject #7 compared with expert. Among all the training targets, only subject #2 (with experience of operating

bipolar forceps) had similar performance with expert surgeon. He achieved good scores at the parameters of mean |*a*|, 95% *CDF* of |*a*|, mean |*ω*| and 95% *CDF* of |*ω*|, which were almost the same values as expert surgeon. In the other parameters, such as the mean *PSD* of |*a*| and peak frequency of |*ω*|, subject #2 also performed better than other 6 novice subjects. Subject #2 could be considered a high level performer in this pick & place training task.

Among other novice subjects, subject #1 also had good global results. In particular, he achieved almost same values as expert in the parameters of mean |*a*|, 95% *CDF* of |*a*|, mean |*ω*| and 95% *CDF* of |*ω*| in the case of SMALL target. Moreover, subject #1 had similar performance (similar shapes) among all the parameters between the BIG and MEDIUM training targets, which might indicate that these two targets did not cause significant different difficulty to him. Subject #1 could be considered an intermediate level performer.

From subject #3 to subject #7, they had relatively poor global results among all the parameters in these three training targets, which could be considered the group with low level performance.

In Figure 5.18, it shows the general evaluation results of subject #8 to subject #13 compared with expert. Generally in three training targets, the subject # 8, subject #9 and subject #11 could be considered as high level performers. Especially, subject #11 had almost the same values as expert surgeon in the parameters of mean |*a*|, 95% *CDF* of |*a*|, mean |*ω*| and 95% *CDF* of |*ω*| among all the training targets. Subject # 8 and subject #9 (with experience of laparoscopic trainings) also achieved these same results as expert in the case of SMALL target.

Subject #10 could be considered the intermediate level performer. He had better overall results in the cases of MEDIUM and SMALL targets, which might indicate that he could adapt better to this pick & place training task after the first 5 trails in BIG targets.

Subject #12 and subject #13 had the worst performance among all the novice subjects. As discussed above, these two novices always performed significantly different from other subjects, which resulted in lower global scores. These two subjects could be considered as the low level performers.

It is clear that this global evaluation allows us to understand the overall movement performance of subject’s operative skills. Moreover, it provides the detail information of the critical parameters which have poor performance and should be improved.

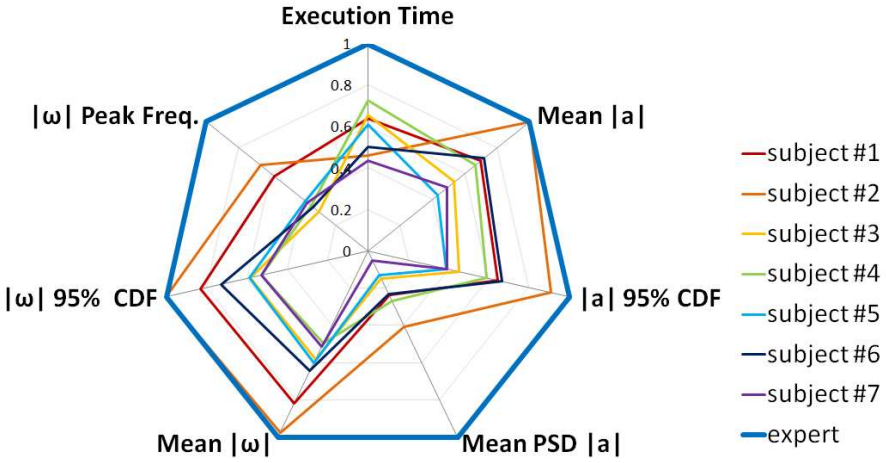

(a) BIG target

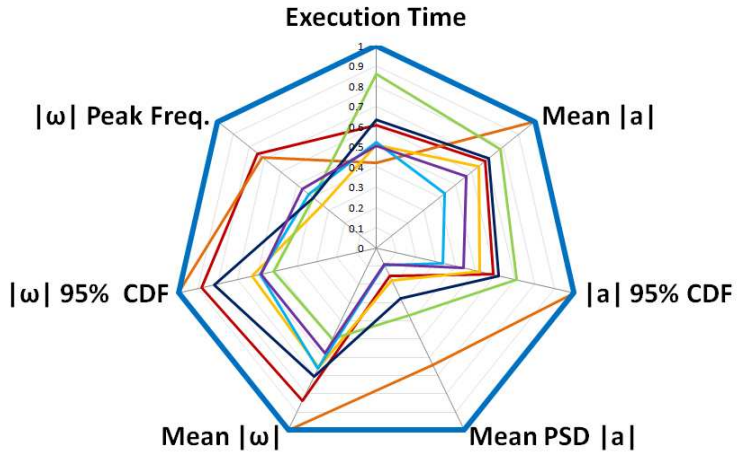

(b) MEDIUM target

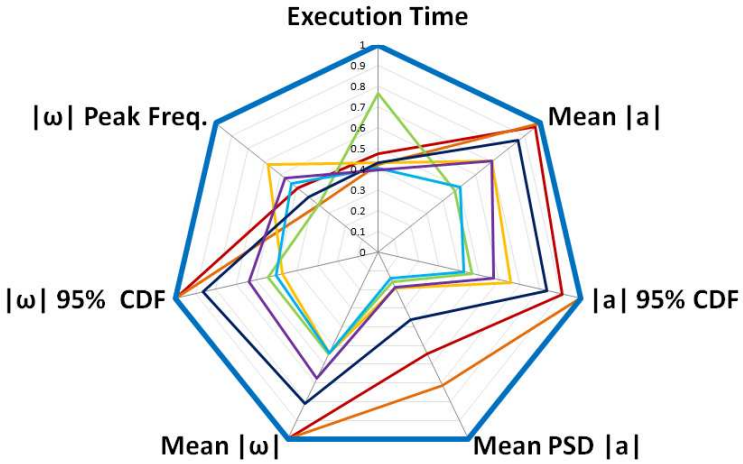

(c) SMALL target

Figure 5.17: Global evaluation of all parameters for subject #1 to #7 with expert.

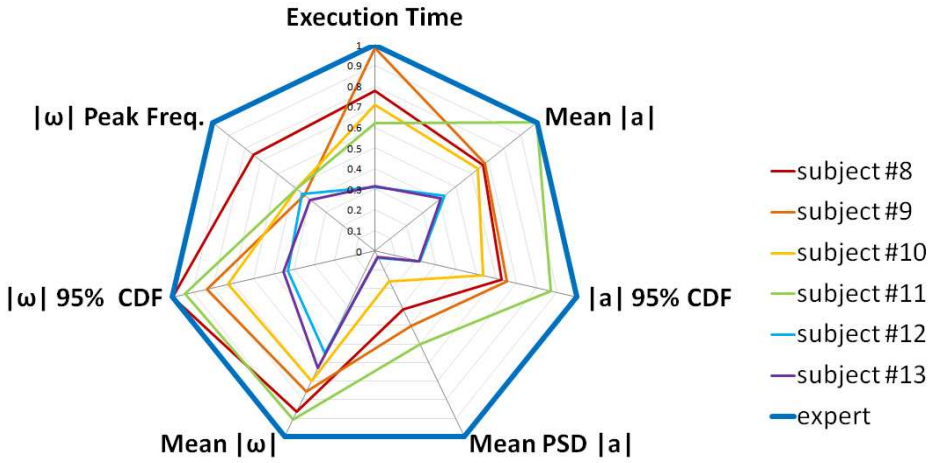

(a) BIG target

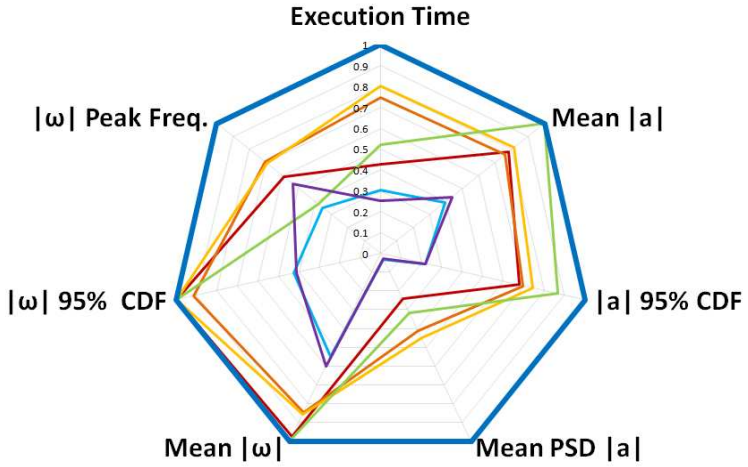

(b) MEDIUM target

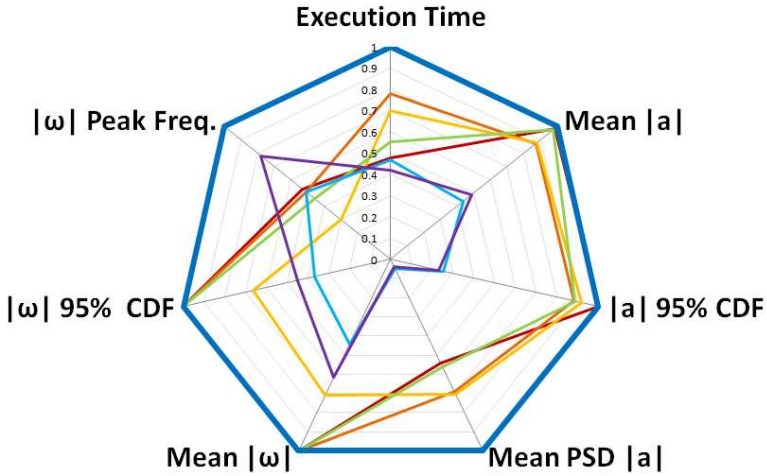

(c) SMALL target

Figure 5.18: Global evaluation of all parameters for subject #8 to #13 with expert.

5.4 Discussion

This chapter discussed the utilization of WB-3 IMU for the neurosurgical operative skill evaluation due to its very low size and weight, and its high performance. The motion information of neurosurgical instrument acquired by WB-3 IMU was evaluated with a group of non-medical novices and one expert neurosurgeon in the pick and place training tasks. The experimental results proved that several parameters extracted from the WB-3 IMU's data, such as the mean $|a|$, 95% *CDF* and mean *PSD* of $|a|$, mean $|\omega|$, 95% *CDF* and peak frequency of $|\omega|$, allowed a clear distinction of performance between the expert surgeon and novices. Moreover, the evaluation results could show which novice performed similarly to the expert, and how, thus validating the proposed methodology in Chapter1. This study is a basis for us to see how the subjects of different expertise act during the training procedures, and to evaluate their improvements of performance after trainings.

The execution time was considered as an evaluated parameter in this experiment. This is not the motion data acquired by WB-3 IMU, but it is a feature regularly considered in the surgical training. It could be a complementary parameter with the motion data for realizing better operative skill evaluation.

In the analysis of acceleration, some novice subjects had close or smaller values of *CDF* values than the expert, which might be due to the bigger execution time of these novices. This parameter could be further evaluated with time requirements for completing the task or more experts' data. The mean *PSD* of acceleration used by the expert was significantly smaller than novices, which might indicate that rotation movements were more important for this training task performed in such small operation space. The expert might normally use very few linear movements in the real operation in order to avoid bigger vibrations of hands.

In the analysis of angular speed, the mean and *CDF* of $|\omega|$ showed some differences between expert and novices. However, these results were not significant as the results of peak frequency of $|\omega|$, which should be further evaluated with more subject data. All the novice subjects used much smaller rotation frequencies (much less than 1 Hz) than expert for the main movements. It indicates that the expert had higher competence for operating bipolar forceps in such small operation space with the use of microscope.

The motion analysis of WB-3 IMU was focused on the physical parameters of acceleration and angular speed. The orientation of the bipolar forceps could be also an

important feature for distinguishing the operative skill levels between expert and novice. This could be enhanced by defining the same initial positions and gestures of experimental setup for all the subjects in order to realize better orientation estimate of instruments. The experimental results were limited to the data of 14 subjects, especially only one expert neurosurgeon. These results could be improved and further evaluated by more novice and expert data and repetitions of different training tasks. With more samples, the global evaluation could be used to develop the skill evaluation function for final scoring.

The experiment data was acquired by a WB-3 IMU, which could be also achieved by using one WB-4 wireless IMU. This could improve the system wearability with wireless data transmission. In order to keep the experiment continuity for all the subjects and avoid the replacement of battery, this experiment was only elaborated by WB-3 system.

5.5 Conclusion of this Chapter

With the diffusion of more and more advanced tools and technologies in the operation room, it is fundamental to establish more efficient training exercises and to define objective metrics to enhance the dexterity of neurosurgeons. The extremely small movements and sizes involved in neurosurgery, however, have prevented until now the development of such methodologies and systems.

This chapter presented the application of the proposed methodology for objective skill evaluation in neurosurgery. The resulting skill evaluation system was used to assess subject's operative skills based on the motion analysis of neurosurgical instruments. The results showed that the significant motion features extracted from WB-3 IMU data allowed us to characterize subject's movements during surgical trainings and distinguish the performance between expert and novices, which satisfies the objective of this study.

The proposed methodology for objective skill evaluation has been evaluated and verified in two surgical applications: laparoscopic surgery and neurosurgery. In other medical scopes, such as clinical practice, skill evaluation is also a critical issue for assisting clinical diagnosing and treatment in modern medical system. Next chapter, therefore, will discuss the application of the skill evacuation system for clinical practice of mastication analysis, which further validates the adaptive characteristics of the proposed methodology.

Chapter 6

Evaluation of Masticatory Performance

6.1 Introduction

6.1.1 Background

The analysis of mastication has long been used as a measure for clinical diagnosis and treatment of prosthodontics, orthodontics and oral surgery; for example the temporomandibular joint and muscle disorders (TMJDs), between 5 and 15% of people in the United States experience pain associated with this disease [128]. Often, the goal of mastication analysis has been to provide an objective basis for diagnosing musculoskeletal disorders of the jaws or to monitor the progress of active treatment methods. The extent to which jaw tracking provides a useful research tool, a diagnostic aid, or a therapeutic monitor clearly depends on what is being measured, how the process is carried out, and why the information is important [14, 129]. Therefore, the use and development of devices for quantitatively measuring and analyzing jaw movements has recently become more common and popular in the clinic [130]. Moreover, these analyses represent a significant step towards the automatization and the robotic assistance of medical treatment.

Conventional optical methods for jaw movement tracking offer a reliable and accurate way to record the jaw movements [131]; however, this approach is poor in wearability and

portability (Figure 6.1). In fact, optical methods use 3D markers, such as light-emitting diodes or passive reflectors, placed on the head and mandible. They compute the exact locations of the markers from the images recorded by the surrounding cameras using triangulation methods; therefore, they can be used only in a structured environment.

Conventional mechanical methods, such as JMA system of Zebris Company [12] and K7/CMS mandibular scanner of Myotronics-Noramed, Inc. (Figure 6.2) [132], usually use special mechanisms put on the head in order to capture jaw movements. The configuration is totally non-invasive. However, these mechanisms are relatively bulky and make the patients feel not natural during the routine tests.

Figure 6.1: Optical method for jaw motion tracking.

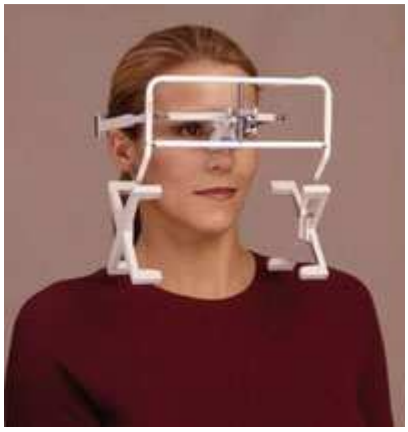

Figure 6.2: K7/CMS mandibular scanner.

Conventional magnetic methods have utilized a permanent magnet and magnetic field sensors, but these methods have the inherent limitation that the system provides only the positions of the point source and then obtain rotations and accelerations by successive derivations which introduce more noise [133].

In most cases, the systems that have been described are relatively bulky, heavy or not handy, complicated to be used. The more wearable and portable jaw tracking system for mastication analysis, which can be used not only in the hospital, but also can be used at home, is strongly needed for assisting the jaw disease treatments and jaw performance rehabilitation during the everyday living [134, 135].

6.1.2 Objective

The aim of this study, therefore, is to develop novel masticatory performance evaluation system to improve the portability and operability of tools for quantitatively measuring jaw movements and analyzing mastication ability.

In particular, this masticatory performance evaluation system should satisfy the following requirements:

- Capability of measuring the movements of jaw joint during regular clinical practice and rehabilitation treatments.
- Extraction of the significant motion features of each subject during different kinds of mastication movements.
- Mastication skill and pattern analysis.
- Feedback of quantitative jaw motion information for assisting clinical diagnosing and treatments.

6.2 Materials and Methods

According to the general methodology introduced in Chapter 1, the block diagram of the corresponding methodology for realizing the masticatory performance evaluation system is showed in Figure 6.3.

The approach is to utilize WB IMU to measure jaw movements for analyzing subject’s chewing habits, and define a set of parameters that allow us to characterize these movements

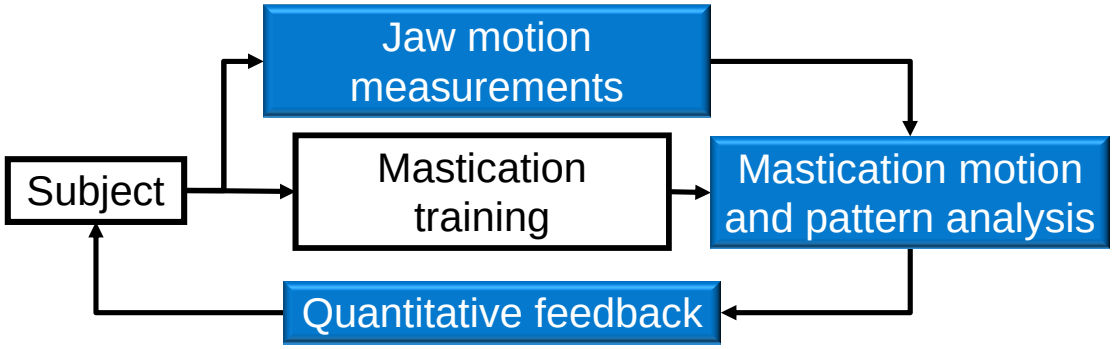

Figure 6.3: Proposed methodology for masticatory performance evaluation.

during various mastication procedures, in order to see how the subject acts during the clinical practice and evaluate the masticatory performance. The feedback of quantitative jaw motion information could help the doctors to realize better diagnosing and rehabilitation treatments of dental diseases.

In particular, two types of experiments were respectively elaborated for the mastication analysis by WB-3 IMU and WB-4 wireless IMU in this study. The first experiment with WB-3 IMU was to chew different kinds of food with different hardness. The second experiment with WB-4 wireless IMU was to chew gum by different sides of molars. The detail description of experiment setup and protocol are discussed in the following sections.

6.2.1 Experimental Evaluation #1: Chewing Food with Different Hardness

A) Experimental setup

The experimental setup is showed in Figure 6.4. One WB-3 IMU was adhered to subject's mandible in order to measure the jaw movements while freely chewing three different foods: marshmallow, biscuit and almond, showed in Figure 6.5, whose weights were 8.0 ± 1.0 g, 7.0 ± 0.1 g and 4.3 ± 0.4 g, respectively. The experimental foods were chosen from the everyday living to represent different hardness of food. The subject was instructed to lean his/her head on the wall during chewing the food in order to minimize the influence of head's movements.

B) Experimental protocol

Thirteen male and two female subjects (age range: 21-36 years) with healthy mastication systems and complete dentition participated in the study after providing informed consent.

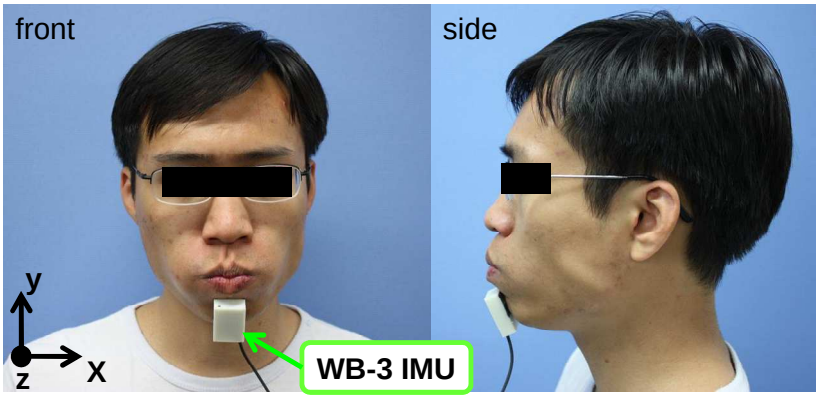

Figure 6.4: Experimental setup with WB-3 IMU for mastication analysis.

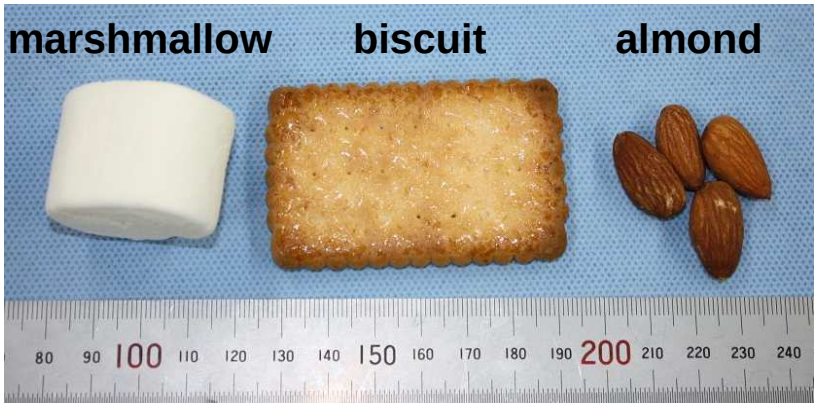

Figure 6.5: Three experimental foods in mastication analysis.

Each subject eats the food by following the order: marshmallow → biscuit → almond. Each food is tested 3 times. Therefore, 9 repetitions are organized for each subject (3 foods × 3 times). At the beginning of each repetition, subjects put the food inside the mouth and keep mouth closed. A repetition is defined to start chewing the food and stop at swallowing down the food. Subjects are instructed to chewing the foods freely as usual as their regular eating habits.

All the data were sampled at frequency f = 100 Hz and saved as comma separated value (CSV) files and then loaded in MATLAB® for further processing and analysis.

C) Data processing

Acceleration components, angular speed components and magnetic components are filtered and smoothed by using a 10th order bandpass IIR Butterworth filter with cutoff

frequencies f_{c1} = 0.05 Hz, f_{c2} = 5 Hz, to remove bias and physiological tremor [59, 127]. In this way only the data due to the voluntary jaw movement is analyzed.

In particular, the following paramters are calculated and analyzed in this study: chewing time (*CT*); chewing frequency (*CF*); mean power spectrum density (*PSD*) of jaw's x-axis angular speed ω_x and acceleration module $|a|$; cumulative distribution function (*CDF*) of jaw's acceleration module $|a|$; and mouth opening angle (*MOA*). These parameters are related to the masticator efficiency and patterns while chewing different foods.

The fast Fourier transformation (*fft*) for acceleration and angular speed is calculated with fft_{size} = 8192 samples and frequency resolution $f_{res} = f / fft_{size}$ = 0.0122 Hz. The *PSD* is estimated in using the formula:

$$PSD = fft \bullet conj(fft) / fft_{size} \tag{6.1}$$

The frequency range chosen for the *PSD* evaluation is 0.1 - 5 Hz to take into account only the voluntary movements. The *CDF* of acceleration $|a|$ is calculated as evaluated for 95%.

The below figures with the (norm.) indicate that each subject's data have been normalized to his average value of biscuit in order to remove the effect of inter-subject anatomical difference. The normalization values are summarized in Table 5.2.

Table 6.1: Normalization values of each subject in mastication analysis with WB-3.

Subject	*CT* [s]	*CF* [Hz]	$PSD_{\omega x}$ $[(deg/s)^2]$	$PSD_{\|a\|}$ $[(m/s^2)^2]$	$CDF_{\|a\|95\%}$ $[m/s^2]$	*MOA* [deg]
1	31.2	1.57	8.0e+03	3.15	1.70	17.1
2	43.9	1.35	1.1e+04	2.67	1.22	18.5
3	32.6	1.66	3.5e+03	7.59	1.89	11.0
4	19.5	1.72	4.2e+03	4.75	1.42	13.2
5	27.0	1.46	3.0e+03	4.62	1.34	8.5
6	21.6	1.89	5.0e+03	4.00	1.30	12.8
7	37.4	1.62	6.7e+03	4.43	1.38	10.8
8	22.7	1.55	3.2e+03	4.68	1.34	11.6
9	24.7	1.72	8.5e+03	5.34	1.48	15.9
10	42.0	1.22	3.5 e+03	1.87	0.92	10.6
11	17.5	1.68	1.1 e+03	3.64	1.21	7.5
12	20.1	1.75	4.1 e+03	3.89	1.29	12.5
13	33.1	1.72	3.7 e+03	5.51	1.47	11.9
14	45.8	1.44	1.1 e+04	4.35	1.40	16.9
15	33.5	1.40	3.8 e+03	3.70	1.23	8.5

Figure 6.6: Experimental setup with two WB-4 IMUs for mastication analysis.

6.2.2 Experimental Evaluation #2: Chewing Gum with Different Molars

A) Experimental setup

The experimental setup is showed in Figure 6.6. One WB-4 IMU was attached to subject's mandible in order to measure the jaw movements, another one attached on the forehead by a belt for head movement compensation during the mastication. Tasks of chewing gum were used in the experience for evaluating the masticatory performance. The gum had the size of 20 x 12 x 6 mm and weight of 1.4 g.

B) Experimental protocol

Nine male subjects (age: 23.1±1.0 years old) with healthy mastication systems and complete dentition participated in the study after providing informed consent. Three types of trials were elaborated: (1) chewing the gum naturally by all the teeth; (2) chewing the gum only used the molars on right side; (3) chewing the gum only used the molars on left side. Each subject executed these three types of trials in the order from type (1) to type (3). Each trial lasted for 60 seconds and tested 5 times. Therefore, 15 repetitions were totally organized for each subject (3 trials x 5 times).

All the data were sampled at frequency f = 100 Hz and saved as CSV files, and then loaded in MATLAB® for post processing and analysis.

C) Data processing

Acceleration components, angular speed components and magnetic components are filtered and smoothed by using a 6th order bandpass IIR Butterworth filter with cut off frequencies f_{c1} = 0.05 Hz, f_{c2} = 7 Hz, to remove bias and physiological tremor[59].

The experiment analysis is focused on the frequency domain. Some significant results are found from the angular speed component of WB-4 IMUs. For the trial #1, the *PSD* of jaw's angular speed $|\omega|$ is analyzed among all the subjects. The *PSD* of $|\omega|$ can indicate the subject's chewing frequency and rotation energy used during the mastication. For the trial #2 together with trial #3, the mean *PSD* of $|\omega|$ is calculated and compared between the cases of only using right side molars and only using left side molars for the mastication. This comparison can show the difference of rotation energy used by the molars on each side of the subject, and indicate which side of molars used more frequently by the subject or have better mastication ability.

The *fft* for angular speed $|\omega|$ is calculated with fft_{size} = 8192 samples and frequency resolution $f_{res} = f / fft_{size}$ = 0.0122 Hz. The mean *PSD* is also estimated by using the Equation (6.1) with the frequency range of 0.1 - 5 Hz.

In order to remove the effect of inter-subject anatomical difference, in the results of trial #1, the figures with (norm.) indicate that each subject's *PSD* data have been normalized to his maximum value. In the results of trial #2 and trial #3, the figures with (norm.) indicate that each subject's mean *PSD* data have been normalized to the mean value of right side molars averaged on the 5 repetitions. The normalization values are summarized in Table 6.2.

Table 6.2: Normalization values of each subject in mastication analysis with WB-4.

Subject	Max $PSD_{\|\omega\|}$ [(deg/s)^2] (trial #1)	Mean $PSD_{\|\omega\|}$ [(deg/s)^2] (trial #2 and #3)
1	11.7e+3	2.6 e+3
2	10.8e+3	1.8 e+3
3	16.6 e+3	3.0 e+3
4	10.6 e+3	2.4 e+3
5	17.3 e+3	3.2 e+3
6	7.7 e+3	1.5 e+3
7	11.3 e+3	1.7 e+3
8	16.2 e+3	4.5 e+3
9	13.4 e+3	2.5 e+3

6.3 Experimental Results

6.3.1 Results of Experiment #1

A) Chewing time

Most subjects proved to be usually using less time in chewing marshmallow than chewing almond, as showed in Figure 6.7 (a). Only subject #9 and subject #10 happened to use more time for chewing marshmallow than almond. They were still using significantly more time for almond than for biscuit, though. As showed in Figure 6.7 (b), the chewing time for soft food averaged on all subjects was significantly ($p<0.01$) lower than the case of the hard food. It was apparent that eating soft food was easier than hard food.

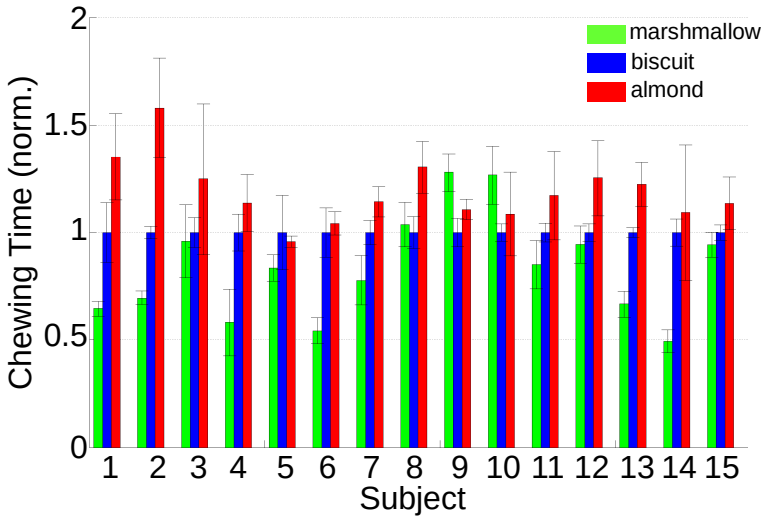

(a) Chewing time of all the subjects for 3 different foods.

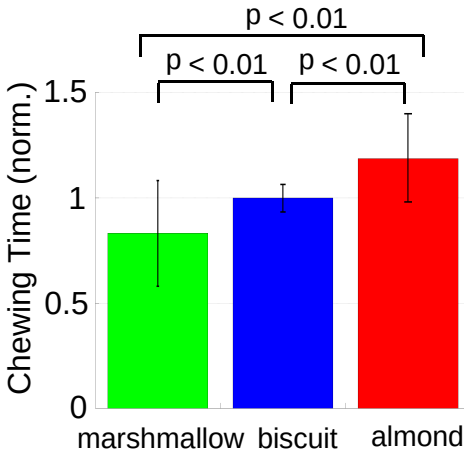

(b) Chewing time averaged on all subjects for each food.

Figure 6.7: Chewing time for 3 types of food with different hardness.

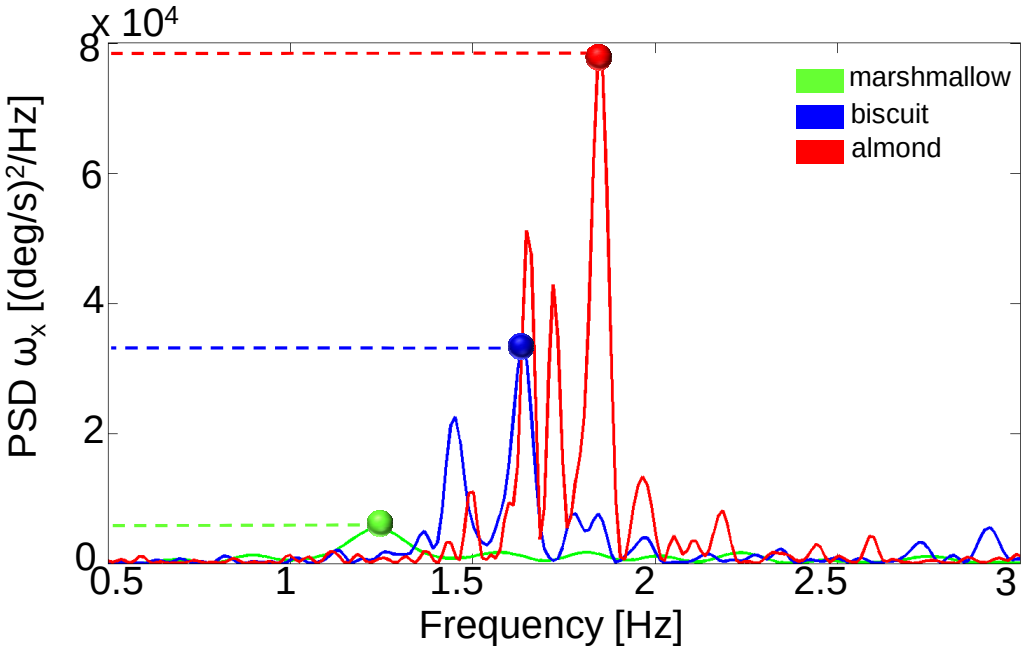

Figure 6.8: *PSD* of the x-axis angular speed ω_x of subject #1.

B) Chewing frequency

The chewing frequency is analyzed from the *PSD* of jaw's angular speed about x-axis (i.e., on the sagittal plane) whose rotation was more salient than y and z-axis's rotation during mastication. In Figure 6.8, only subject #1's *PSD* of jaw's angular speed about x-axis in one repetition is showed, but similar results appear in the cases of other subjects as well. The curves of all the foods have one maximum peak which is related to the highest *PSD* value and the main movement during the mastication procedures. It means that the subject usually had one primary cycle for mastication which took most rotation energy. The frequency of this peak is used as the chewing frequency for each food.

As can be seen in Figure 6.9 (a), most subjects used higher chewing frequency when eating almond which was the hardest food. Only subject #9, subject #10 and subject #11 happened to use higher frequencies for marshmallow, but they still had higher values in the case of almond than the case of biscuit. Subject #2 and subject #3 had almost equivalent values in eating all these three foods, which might indicate that they had quite regular chewing habits. Subject #15 showed high variance while chewing all the foods.

Figure 6.9 (b) clearly shows that subjects used significantly ($p<0.01$) higher frequencies in eating almond than marshmallow and biscuits. This indicates that all the subjects used more

energy in higher frequency for chewing harder food in order to effectively chop and swallow down the food. However, there was no significant difference between the cases of marshmallow and biscuit.

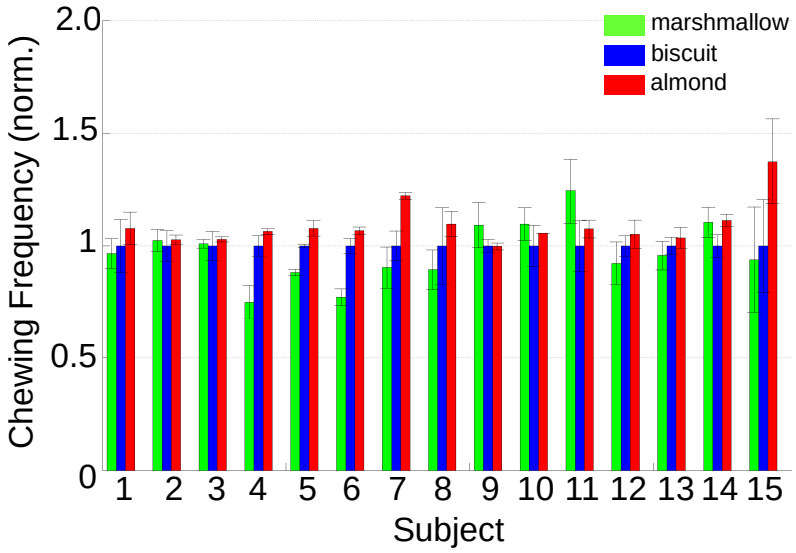

(a) Chewing frequency of all the subjects for 3 different foods.

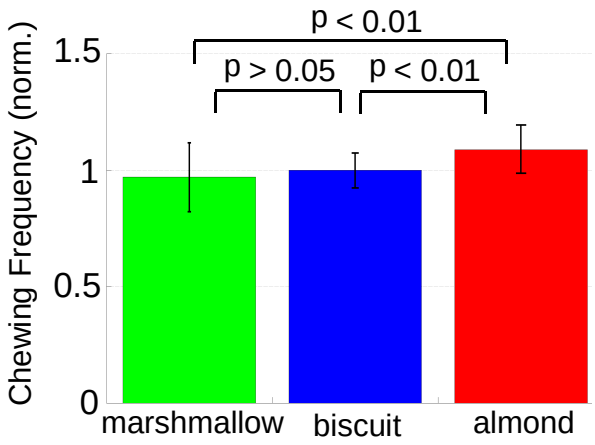

(b) Chewing frequency averaged on all subjects for each food.

Figure 6.9: Chewing frequency for 3 types of food with different hardness.

C) Power spectrum density of angular speed

The mean *PSD* of jaw's angular speed about x-axis (on the sagittal plane) for all subjects is showed in Figure 6.10 (a). It is clear that most subjects used more rotation energy while eating hard food than soft food. Only subject #10 happened to use more energy for marshmallow. Subject #7, #12, #13 and #14 used almost same values in both cases of almond and biscuit. Figure 6.10 (b) shows the mean *PSD* of ω_x averaged on all subjects compared between each food. There was significant difference ($p<0.01$) of this parameter used for these three foods. Most rotation energy was used for chewing the almond, the least used for marshmallow, which is compatible with the fact that more energy is needed for chewing hard food.

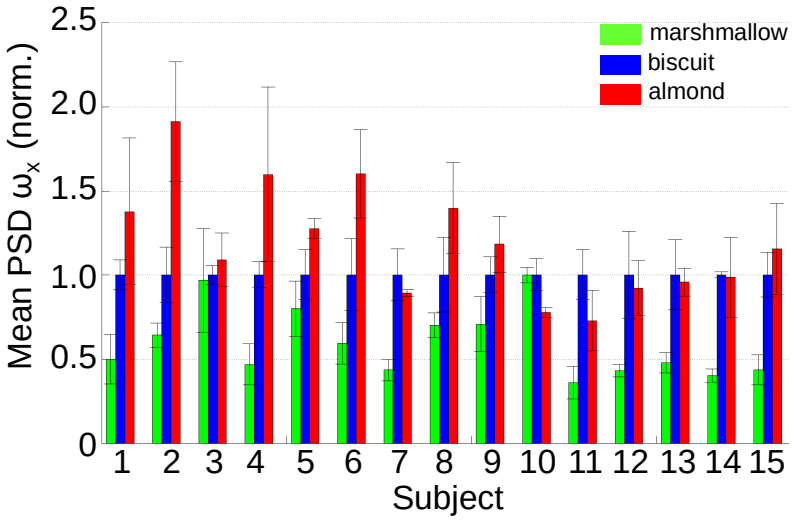

(a) Mean PSD of ω_x of all the subjects for 3 different foods.

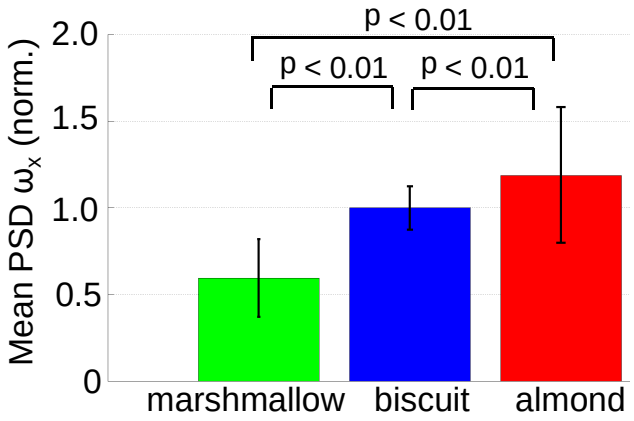

(b) Mean PSD of ω_x averaged on all subjects for each food.

Figure 6.10: Mean *PSD* of ω_x for 3 types of food with different hardness.

D) Power spectrum density of acceleration

The mean *PSD* of jaw's acceleration module |*a*| is showed in Figure 6.11. In Figure 6.11 (a), most subjects used more translation energy for hard food excluding subject #5 who used more translation energy for marshmallow. Subject #1, #2 and #7 used significantly higher mean *PSD* of |*a*| for almond, which was also accompanied with high variance.

Figure 6.11 (b) clearly shows that there was significant difference ($p<0.01$) in mean *PSD* of acceleration while eating these three foods of different hardness. The hardest food (almond) cost most translation energy for mastication.

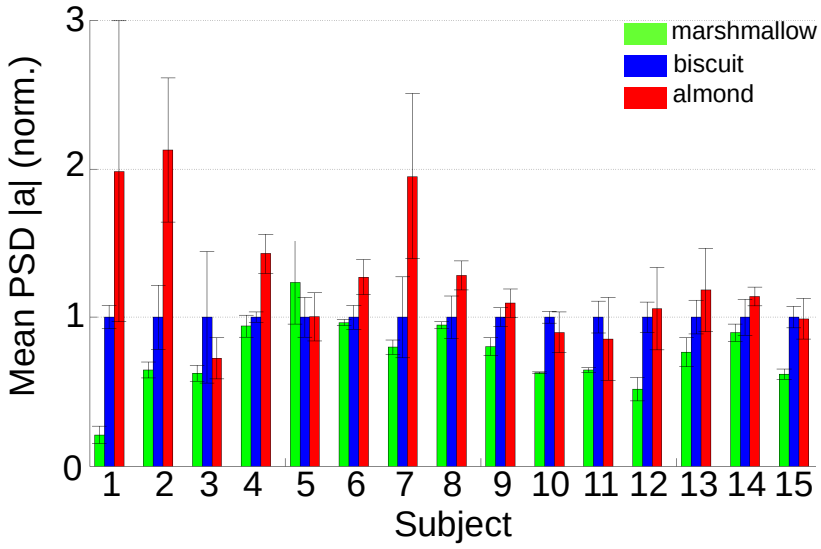

(a) Mean PSD of |*a*| of all the subjects for 3 different foods.

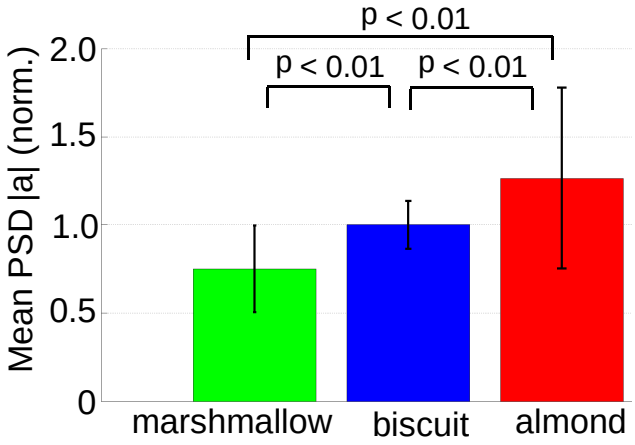

(b) Mean PSD of |*a*| averaged on all subjects for each food.

Figure 6.11: Mean *PSD* of |*a*| for 3 types of food with different hardness.

E) Cumulative distribution function of acceleration

The 95% *CDF* of jaw's acceleration module |*a*| of each subject is showed in Figure 6.12 (a). Most subjects had higher *CDF* values in the cases of almond and biscuit, which might indicate that subjects used bigger forces in chewing hard food. Subject #11 happened to has significantly higher *CDF* values and corresponding variance for marshmallow, which should be further validated about the correction of experiment procedures of this trial.

Figure 6.12 (b) clearly shows that there was significant difference in the parameter of 95% *CDF* of acceleration while eating these three foods with different hardness. All the subjects used higher acceleration in chewing hard food.

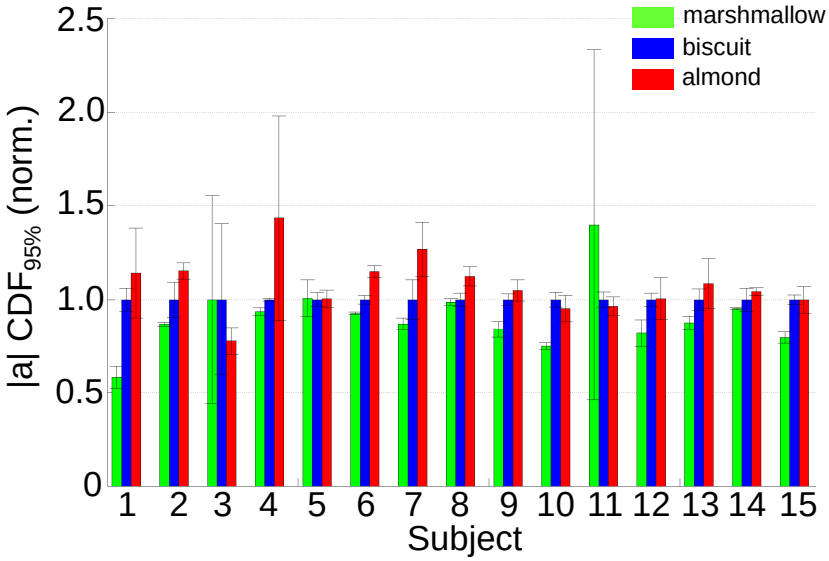

(a) 95% CDF of |*a*| of all the subjects for 3 different foods.

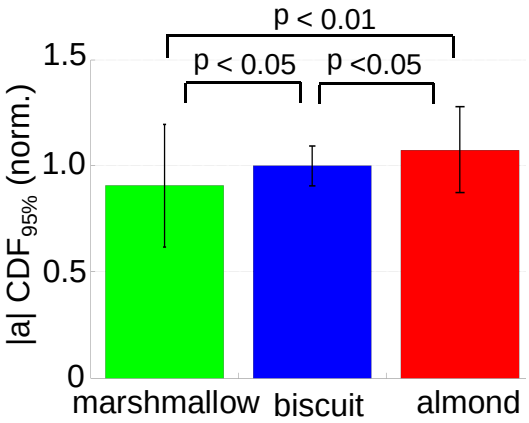

(b) 95% CDF of |*a*| averaged on all subjects for each food.

Figure 6.12: 95% *CDF* of |*a*| for 3 types of food with different hardness.

F) Mouth opening angle

The mean *MOA*s of all the subjects are also evaluated, as showed in Figure 6.13 (a). There was no significant regular pattern of mouth opening angle in chewing these foods among all the subjects.

Figure 6.13 (b) further verifies that there was no significant difference (p>>0.05) of the mouth opening angle range for eating these three foods. This might indicate that mouth opening angle is based on subject's fixed hyoid biomechanics, which leads to a regular eating habit in mouth opening that has less relation to the food with different hardness.

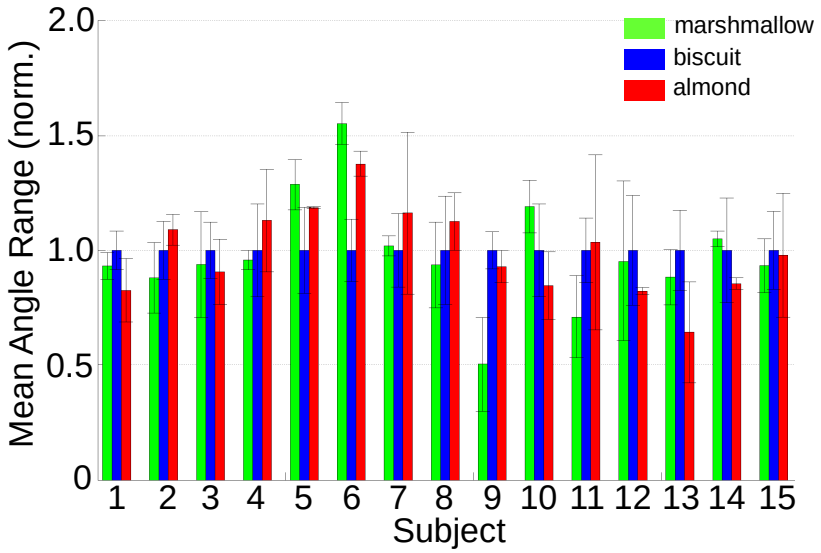

(a) MOA of all the subjects for 3 different foods.

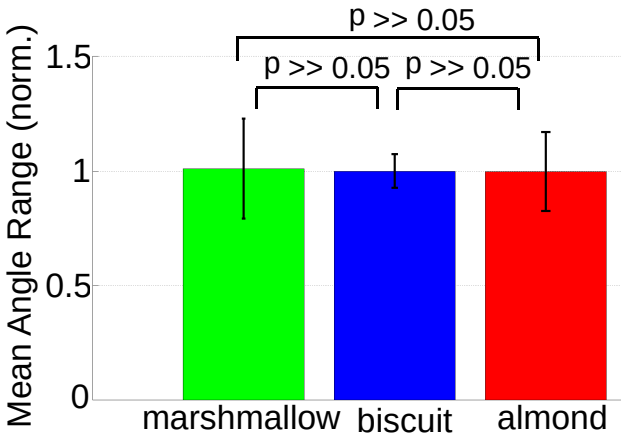

(b) MOA averaged on all subjects for each food.

Figure 6.13: Mouth opening angle used for 3 types of food with different hardness.

6.3.2 Discussion of Experiment #1

This experiment applied WB-3 IMU to subject's mandible for the mastication analysis. The experimental results clearly showed that the subjects used less chewing time, chewing frequency, acceleration *CDF* and energy for eating soft food; higher values were found in the case of hard food. However, there was no significant difference in the parameter of mouth opening angle while eating these three foods.

These results were based on the analysis of acceleration, angular speed and orientation data, which could be improved by adding the jaw movement trajectory analysis. In order to calculate the trajectory by WB-3 IMU, it is needed to model the geometry structure of the mandible. This could be achieved by using the simulation software OpenSim described in Chapter 3 for the kinematics estimate.

During the experiment, the subject was instructed to lean his/her head on the wall during chewing the food in order to minimize the influence of head's movements. This constraint can be easily removed by using two IMUs, one on the mandible for the measurements and one on the head for movement compensation. In addition this setup would also allow the measurements of head movements during free mastication.

Some subjects happened to have higher values at the parameters of *CT*, *CF* and *CDF* for chewing marshmallow, which should be further evaluated with more data and verified whether those trials were executed correctly.

6.3.3 Summary of Experiment #1

The extreme lightweight and its high performance make WB-3 IMU suitable for mastication analysis. The jaw movements during freely chewing three types of food with different shapes and hardness (namely: marshmallows, biscuits and almonds) were evaluated in this study. The following parameters which are related to the masticator efficiency and patterns while chewing different foods were analyzed and evaluated: chewing time; chewing frequency; *PSD* of jaw's x-axis angular speed ω_x and acceleration module $|a|$; 95% *CDF* of acceleration module $|a|$; and mouth opening angle. The analysis of these parameters proved that several parameters extracted from tWB-3 IMU's data allow a clear masticatory efficiency and pattern analysis, which satisfies the objective of the required masticatory performance evaluation system.

6.3.4 Results of Experiment #2

A) Results from first trial

The Figure 6.14, Figure 6.15 and Figure 6.16 show the normalized *PSD* values of jaw's angular speed module $|\omega|$ of all the subjects. Three different mastication patterns are found among all the 9 subjects.

The subject #1, #4, #6 and #8 who had the same mastication pattern were classified into the group #1 (Figure 6.14). They had three peaks of the *PSD* values during freely chewing the gum. The first peak can be considered as the motion and energy used for chewing the gum; the second and third peaks can be considered as the motion for grinding the gum. It is clear that this group used higher rotation energy (bigger *PSD* values in the first peak) for chewing motion. In the cases of another two peaks, subject #6 and subject #8 had similar *PSD* values; however, subject #1 and subject #4 used almost two times values for the second peak than the first peak. It is important to notice that the frequency of the second peak was about two times than the first peak; and the frequency of the third peak was about 3 times than the first peak in this group.

Figure 6.15 shows another mastication pattern found in this study. The subject #2 and #7 were classified into this group, which also contained three peaks of *PSD* values for chewing the gum. However, this group used more rotation energy for the grinding motion (bigger *PSD* values in the second peaks). Subject #2 had almost same values in another two peaks, and the first peak value of subject #7 was twice than the third peak. This group might regularly prefer to use more grinding motion during mastication in everyday living.

The subject #3, #5 and #9 were classified into the third group, which had only one significant peak of the *PSD* values (Figure 6.16). This group primarily used chewing motion during the mastication procedures, and spent most of the rotation energy for chewing, rather than the grinding motion.

It is clear that the mastication patterns could be analyzed and evaluated by using WB-4 IMUs. These three mastication patterns might be related to the subjects' diet habits in everyday living and the different structures of human mandible skeleton.

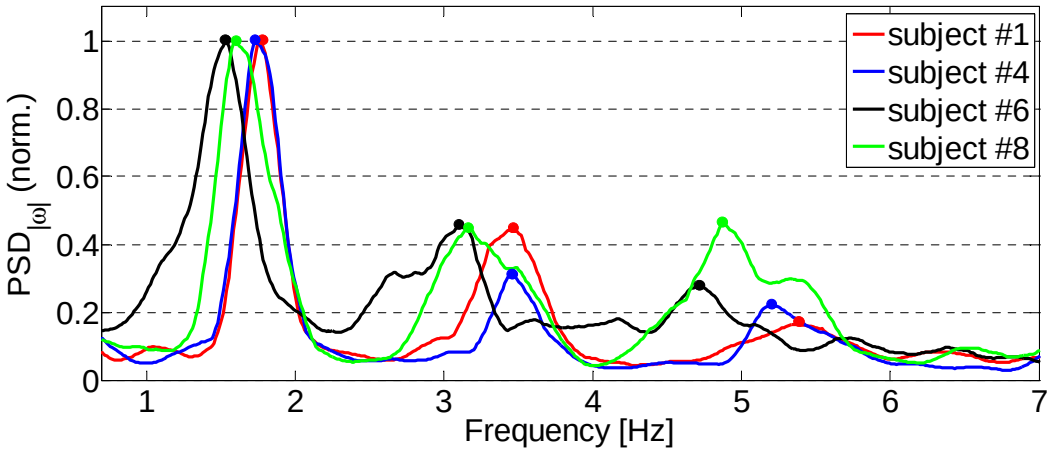

Figure 6.14: Mastication pattern of group #1.

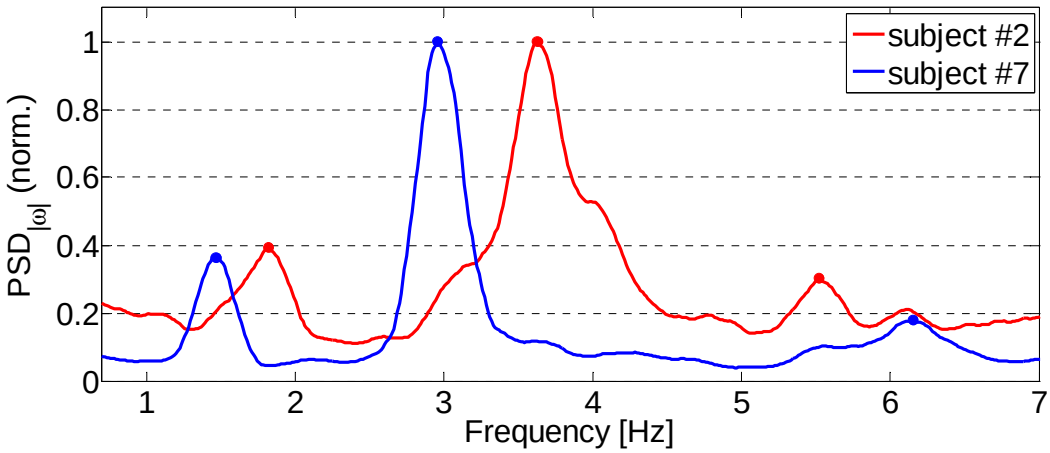

Figure 6.15: Mastication pattern of group #2.

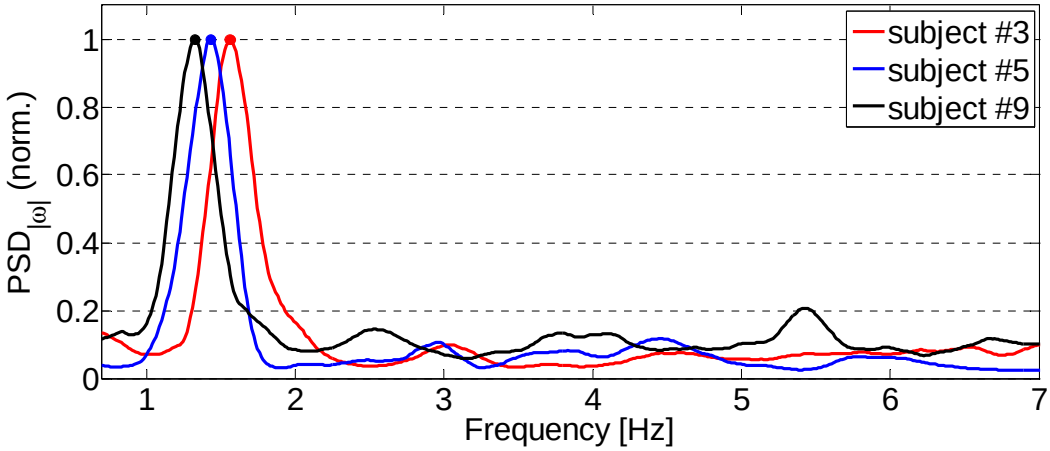

Figure 6.16: Mastication pattern of group #3.

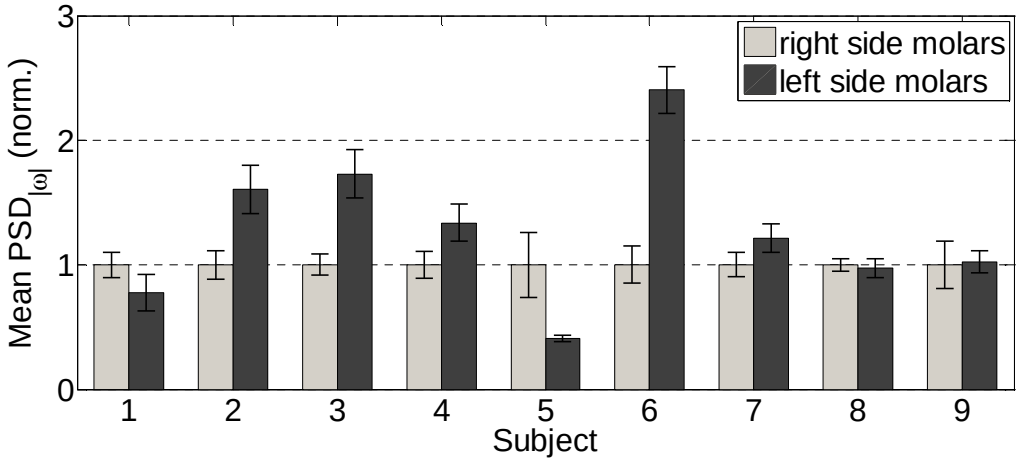

Figure 6.17: Comparison of mean |ω| *PSD* between the right side molars and left side molars.

B) Results from second and third trials

Figure 6.17 shows the results from trial #2 and #3, which are elaborated to evaluate the mastication performance while only using the right side molars and left side molars, respectively. The subject #8 and subject #9 used almost the same *PSD* values on both mastication cases. It might indicate that these two subjects have balanced mastication performances on both sides of the molars, and do not have one-side mastication problem.

The subject #2, #3, #4, #6 and #7 had higher values in the case of using left side molars; however, the subject #1 and #5 had the opposite results. It might indicate that these subjects have unbalanced jaw movement performance and ability while using different side of molars for mastication. Especially, subject #6 had the mean *PSD* value of left side molars almost 2.5 times higher than the right side molars, which might indicate that he has higher mastication ability on the left side molars, and he is more proficient on using it during everyday living.

6.3.5 Discussion of Experiment #2

Three different mastication patterns were found from 9 subjects in this experiment. These results were evaluated by using the *PSD* of the mandible angular speed. These patterns might be related to the diet habits of the subjects in everyday living, which could be further verified by sampling more data from different subjects. The comparison of mean angular speed *PSD* data between right side molars and left side molars could estimate subjects' unbalanced mastication habits for assisting clinical diagnosing and treatment. More insight information

could be supplied by integrating other physiological measurements, such as EMG signal of the muscles around the jaw joint.

6.3.6 Summary of Experiment #2

Two WB-4 IMUs were respectively attached to the mandible and forehead, with minimal physical restriction to subjects. This method was capable of evaluating the mastication performance during chewing gum in three different types of trials: chewing gum naturally; chewing gum only used the right side molars; and chewing gum only used the left side molars. The results proved that the mastication patterns can be evaluated by several parameters extracted from WB-4 IMU, such as such as the *PSD* of jaw's angular speed and its comparison between the right side molar motion and left side molar motion.

6.4 Discussion

With the diffusion of more and more advanced tools and technologies in clinical diagnosis and treatment, it is fundamental to develop more efficient and handy devices or systems for routine tests of clinical practice.

This chapter discussed the use of WB-3 and WB-4 IMU as the tools to track jaw movements for mastication analysis. The extreme lightweight and their extreme high performance make the IMUs suitable for this application. Moreover, the WB IMU directly acquired accelerations and rotations at high frequency, thus providing smooth and virtually noise-free data. Conventional systems, instead, acquire target's position and then obtain rotations and accelerations by successive derivations which introduce more noise.

The WB IMUs were attached to the mandible by using adhesive medical tape, which might be not strong enough to fix the IMUs with the jaw movements. Moreover, the relative movements caused by the skin of mandible during mastication might also affect the motion analysis results. This could be compensated by modeling the mandible skeletal structure with different jaw movements.

6.5 Conclusion of this Chapter

The use of WB-3 or WB-4 IMU for mastication analysis was proved to be a valid and handy method for jaw movement and pattern analysis that may be used clinically as an assistant system for dental diagnosing and treatment.

The experimental results verified that several parameters extracted from the IMU's data allowed a clear masticator efficiency and pattern analysis during chewing foods with different hardness and chewing gum with different sides of molars. In particular, the results clearly showed that the subjects used less chewing time, chewing frequency, acceleration *CDF* and energy to eat soft food; higher values were found in the case of hard food. However, there was no significant difference in mouth opening angle while eating these three foods. In addition, three different chewing patterns were found among the 9 subjects, which may contribute to a further research on human's diet habits.

The proposed methodology for objective skill evaluation was applied to the clinical practice of mastication analysis in this chapter, which further verifies that the resulting skill evaluation system could be adaptive to various medical scopes.

Chapter 7

Conclusions and Future Work

7.1 General Discussion

Since the emphasis on medical safety and the complexity of modern surgical technologies and equipments continuously increase, it is essential to develop innovative and safe training and evaluation methods for surgical operative skills. Training devices, such as box trainers and VR simulators, have already been developed to learn fundamental operative skills outside the operation room. However, the science of objective evaluation of operative performance is still in its infancy. Commonly, the skill evaluation relies heavily on the experience of expert surgeons and, therefore, it is not objective, which may be a variable and biased opinion. Although there is growing amount of researches to assess medical operative competence objectively using motion analysis, they provide only the kinematics information of instruments or trainee' hands for evaluating the performance in a single training device. To date, there is no general methodology capable of integrating human body and instrument motion analyses to achieve objective skill evaluation in various training devices. Moreover, most current skill evaluation methods are limited to the applications in surgery, but can neither be extended to other medical scopes nor clinical practice.

Therefore, this thesis has proposed an innovative and general methodology for realizing a common and objective skill evaluation system, which could be adaptive to various medical scenarios. The resulting skill evaluation system was based on the motion analyses of human and medical instruments, which resulted in the developments of the ultra-miniaturized

inertial-based motion tracking system WB-3 and WB-4. The design and performance of these two systems have been presented and discussed in Chapter 2 and Chapter 3. The resulting skill evaluation system has been implemented and verified in laparoscopic surgery, neurosurgery and clinical practice of mastication analysis, which were presented in Chapter 4, Chapter 5 and Chapter 6, respectively. In the end of each chapter presented before, it has discussed the results and significant issues of the corresponding system design and performance evaluation. Therefore, this chapter is aimed at generally discussing the critical points during the whole procedures of this thesis, which would contribute in conducting the possible directions of future work.

7.1.1 Inertial-based Motion Tracking System for Skill Evaluation

Motion tracking systems are widely used in different application fields, such as for rehabilitation, surgery, game, sport, and so on. These systems can be basically classified into: inertial-based, optical-based, electromagnetic-based, mechanical-based, and acoustic-based technologies, which have been summarized and discussed in Chapter 1. All of these current tracking systems have their own advantages and disadvantages, and have good performance capabilities for some environments and tasks, and fail on others. Figure 7.1 shows a comparison of these systems among some primary features of measurement volume, price, accuracy and adaptive environments.

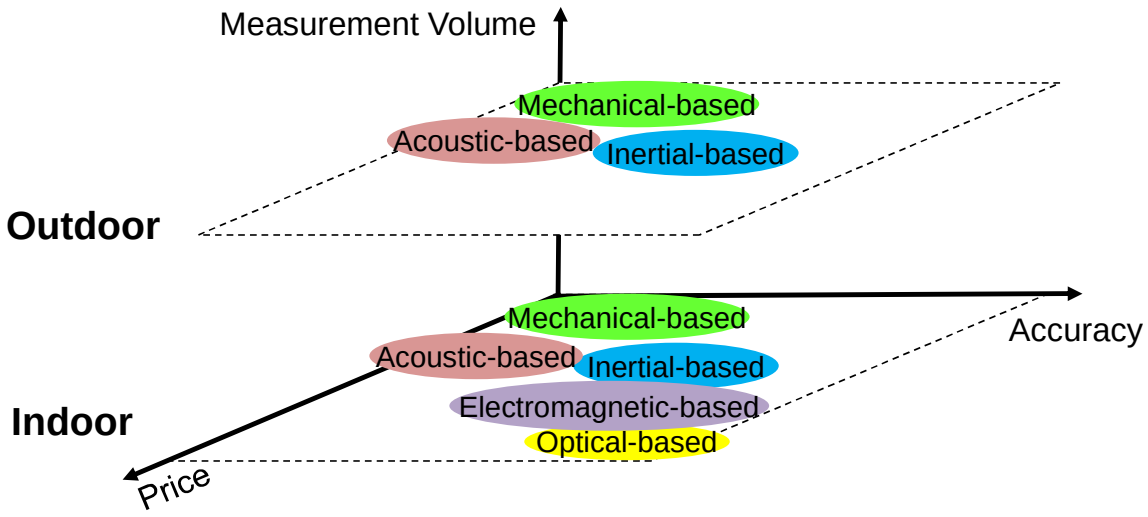

Figure 7.1: Main feature comparison of motion tracking technologies.

The most popular ones are the optical-based, electromagnetic-based and inertial-based technologies. The optical-based system normally has the highest system accuracy but also with higher price. Moreover, it could be only used in a constructed room. Electromagnetic-based system has intermediate price and accuracy performance among these three different technologies. However, it has the problem of limited measurement volume which might be not sufficient enough to measure wide range movements. The inertial-based system has reasonable accuracy, measurement volume (available both indoor and outdoor) and price compared to other technologies. It can be attached on the objects for motion analysis without source signals and used in different environments. All these advantages are the reasons the inertial-based motion tracking system WB-3 and WB-4 have been developed in this thesis for skill evaluation. The performances of WB systems have been evaluated in Chapter 2 and Chapter 3. They can provide orientation accuracy about 2 deg, which is almost the best dynamic performance of the inertial technique can achieve at the current state. Therefore, it allows us to capture adequately the relevant dynamics information of surgical tasks and clinical practice.

It is feasible to use hybrid systems to improve the accuracy performance for analyzing smaller surgical movements, such as inertial-optical-based and inertial-UWB-based motion tracking systems. In the other hand, it might also increase the system expense and complexity of manipulation. Therefore, all these factors should be balanced during the design procedures of the motion tracking systems for operative skill evaluation. This thesis has selected only the inertial-based technology, which has reasonable performance for motion tracking, and also helps us to simply the system configuration.

7.1.2 Common Skill Evaluation System for Different Medical Applications

Measuring the movements both of surgical instruments and trainees is a significant challenge while developing a common operative skill evaluation system based on motion analysis. In some medical scopes, such as surgery and clinical practice, various approaches to this challenge have been studied (Chapter 4, Chapter 5 and Chapter 6). None of them, however, came out as a general methodology adapted to different medical operation procedures. A great number of current evaluation systems only focused on the instrument

motion analysis. The possibility of recording the movements of both the trainees and instruments is still a critical issue for objective skill evaluation in the current state.

The general methodology proposed in this thesis has integrated the motion analyses of instruments and human. The resulting skill evaluation system based on this methodology has been implemented in three different medical applications. The results have showed that subject's motion features acquired from WB systems allow us to evaluate his/her operative expertise levels. Benefitting from the ultra-miniaturized design, WB systems could be easily attached on the objects for motion analysis. They solve the problems of measuring both human and instrument movements for skill evaluation.

Although the proposed general methodology has been evaluated in three medical applications: laparoscopic sugary, neurosurgery and mastication analysis; more validations in different medical scenarios are still needed, such as colonoscopy where the doctors are experiencing difficulty in manipulating the colonoscope and need trainings. Moreover, there were the limitations of subject number in the implemented applications, which should be further improved with more sample data.

7.2 Conclusions

In this thesis, the road towards the realization of common skill evaluation system for multiple medical applications has been presented. After a deep review of the state of the art, a general methodology based on the development of an ultra-miniaturized motion tracking system has been proposed. This methodology can be implemented in various training platforms. In particular, the motion tracking system has been aimed at high wearability and performance by using MEMS-based inertial sensing technologies. The validity of the resulting skill evaluation system has been verified in laparoscopy, neurosurgery and in the clinical practice of mastication analysis. The results were extremely promising, and showed that the skill dexterity and competence could be effectively assessed and classified by using the developed systems.

This thesis is divided into seven chapters, which are discussed and laid out as below.

Chapter 1 has introduced the research background with a detailed analysis of the state of the art of related researches on motion tracking technologies for medical operative skill

evaluation. After that, the goals, methodology, innovation, and significance of this thesis have been discussed.

Chapter 2 has presented the developments of the ultra-miniaturized wearable motion tracking system WB-3 and WB-4. The system specification, design methods and materials, and performance validation of both systems have been discussed in detail. The WB-3 system primarily consists of a set of up to 20 IMUs, each of them composed by 3-axis gyroscope, 3-axis accelerometer and 3-axis magnetometer. Each WB-3 IMU has been directly attached on human and/or objects in order to measure and analyze its movements. The communication between all the WB-3 IMUs and PC is performed using CAN BUS interface at 1 Mb/s. The WB-3 IMU which is very compact and lightweight (size 26 x 20 x 8 mm and weight 2.9 g) has higher wearability than other IMUs currently on the market. It also provides high performance on the aspects of power consumption (150 mW), accuracy (less than 2 deg), and sampling rate (200 Hz), which are comparable with the commercial products. All these advanced features allow WB-3 system suitable for tracking human motions or other objects in a more wearable manner, especially for tracking some small surgical instruments.

WB-4 system has similar performance with WB-3. The main innovative feature is the wireless communication between the WB-4 IMU and PC using Bluetooth technology. The WB-4 IMU contains a mother board for motion sensing, a Bluetooth module for wireless communication and a Li-Polymer battery for power supply. The data transmission distance is up to 10 m with 1 hour continuous working time. The resulting size (37 x 23 x 12 mm) and weight (7.0 g) of WB-4 IMU make it become the most compact and lightweight wireless IMU in the world.

The motion tracking system is the key unit of the proposed skill evaluation system discussed in Chapter 1. It could use either the WB-3 (wired version) or WB-4 (wireless version) for motion analysis and skill assessment, depending on the requirements of different medical applications.

Chapter 3 has introduced the sensor fusion algorithm for WB IMU orientation estimate, and discussed the biomechanical analysis by using the kinematics data of WB-3 system. The quaternion-based EKF has been implemented for the sensor fusion, which solves the singularity problem of Euler-based methods. In particular, an R-Adaptive algorithm integrated in the EKF has been proposed for achieving better dynamic performance of motion tracking. The angular accuracy performance has been evaluated by the comparison between WB-3

IMU with a commercial IMU InertiaCube3 in regard to Vicon reference system. The experimental results have verified that the dynamic performances of WB-3 IMU (less than 2 deg) are better than the commercial product and satisfy the system specification discussed in Chapter 2. The biomechanical analysis by using WB-3 system has been also presented in this chapter, in order to understand more insight information of neuromuscular status caused by different kinds of motion. In particular, joint moments and individual muscle forces of one upper limb have been investigated by using two WB-3 IMUs with a musculoskeletal model in simulation software OpenSim. The experiment of lifting up loads using different joint movements has been conducted. The results have showed that the joint moments of shoulder and elbow, and the main muscle tendon force can be efficiently estimated using the motion data from WB-3 system.

Chapter 4 has described the use of WB-3 system to evaluate the operative skills of laparoscopic surgery based on the methodology proposed in Chapter 1. The skill evaluation model was trained by using the trainees' motion features acquired from WB-3 system and further validated to classify the operative expertise levels of the trainees with different laparoscopic experience. In the conducted experiments of regular laparoscopic training tasks, eight WB-3 IMUs were put on the trainee's upper body. The results have showed that the rotations of surgeon's shoulder were faster than novices, and the main movement frequencies of surgeon's shoulders were also bigger than novice. Moreover, surgeons used more energy for the rotations of wrist and elbow, but not shoulder. Based on these significant parameters, the skill evaluation model has achieved high discrimination performance at 93.8% to classify the trainees into expert group or novice group.

Chapter 5 has presented the application of the proposed skill evaluation system in neurosurgery by using WB-3 system. Benefiting from the small size and low weight, the WB-3 IMU can be easily attached on the small instruments of neurosurgery for tracking the extremely small hand movements of the trainees. The pick and place test has been evaluated with a group of non-medical novices and one professional neurosurgeon. The results have proved that several parameters extracted from the WB-3 IMU's data, such as the *PSD* and *CDF* of both acceleration and angular speed, allow a clear distinction between the expert neurosurgeon and the novices, and understand who performs similarly to the expert, and how.

Chapter 6 has introduced the extended medical application of the proposed skill evaluation system for the clinical practice of mastication analysis. Two experiments for

validating the system performance have been elaborated by using WB-3 IMU and WB-4 IMU, respectively. The WB IMUs were attached on the trainee's mandible in order to measure the jaw movements and analyze the mastication patterns. The results have proved that the mastication performance can be evaluated by several parameters extracted from WB IMUs, such as mouth opening angle, chewing frequency, and PSD of jaw's angular velocity. Moreover, three different mastication patterns have been found for evaluating the unbalanced mastication habit among different trainees.

Finally, this chapter generally discusses and concludes the results of this thesis, and proposes some possible directions for the continuation of this work.

This thesis has proposed and demonstrated a general and innovative methodology for developing a common and objective medical skill evaluation system based on motion analysis. The resulting system has proved that it is possible to construct a motion tracking system capable of accurately determining human body gestures and instrument movements to classify the trainee's operative skill levels. The two versions of motion tracking system WB-3 (wired) and WB-4 (wireless) are capable of providing wide area motion tracking of trainees and surgical instruments during various training tasks. Due to the miniaturized design, they also overcome the limitations of wearability for tracking small objects. The performance validations in surgery and clinical practice have proved that, the proposed methodology is an effective and promising tool for realizing a common skill evaluation system for various medical scenarios.

Therefore, the goals described in Chapter 1 have been achieved by all these outcomes, which are summarized as below:

- A general methodology based on motion analysis for objective operative skill evaluation has been proposed. (Chapter 1, Figure 1.21)
- The inertial-based ultra-miniaturized motion tracking system WB-3 has been developed. Benefiting from the compact size of 26 x 20 x 8 mm and lightweight 2.9 g, the WB-3 IMUs could be easily attached on the objects for motion analysis. (Chapter 2, Figure 2.8)
- Compared with the previous system WB-2, the improvements of sensor performance of WB-3 IMU have been evaluated and verified by the calibration system WBCal-1. (Chapter 2, Figure 2.19 to Figure 2.24)

- The WB-3 IMU has better system performance than commercial products in different features, such as smaller size and weight, less power consumption, faster system sampling rate, and less cost. (Chapter 2, Table 2.4)
- The WB-4 wireless IMU has been developed. It is very compact and lightweight (size 37 x 23 x 12 mm and weight 7 g) – at present the smallest, lightest wireless IMU in the world. (Chapter 2, Figure 2.25)
- The R-Adaptive algorithm embedded with EKF has been proposed for orientation estimate, to overcome the problems related to the correction of the attitude using the data from the accelerometer. (Chapter 3, Figure 3.2)
- The performance of R-Adaptive algorithm with EKF has been evaluated with WB-3 IMU. The experiment was elaborated by using the WB-3 IMU compared with the commercial IMU in regard to the Vicon motion capture system. The results proved that the WB-3 IMU has the average accuracy less than 2 deg, which satisfied the system requirements. (Chapter 3, Table 3.1, Table 3.2)
- Biomechanical analysis of upper limb has been implemented by integrating the data of 2 WB-3 IMUs with a musculoskeletal model in OpenSim software. The results verified that the joint moments and muscle tendon forces of different inter-segmental movements could be effectively estimated by using the kinematic information acquired by WB-3 system. (Chapter 3, Figure 3.21, Figure 3.22)
- The general methodology has been implemented for laparoscopic operative skill evaluation based on WB-3 system to measure and analyze the movements of subject's upper limbs. Some significant motion features between expert surgeons and novices have been extracted, and the expertise classification results achieved 93.75% correct rates. (Chapter 4, Figure 4.4, Table 4.3)
- The general methodology has been implemented for objective skill evaluation in neurosurgery. The results have proved that the significant motion features extracted from WB-3 IMU data allow us to characterize subject's movements during surgical trainings and distinguish the performance between expert and novices. (Chapter 5, Figure 5.17, Figure 5.18)
- The use of WB-3 or WB-4 IMUs for mastication analysis has been proved to be a valid and handy method for jaw movement and pattern analysis. The experimental results

proved that several parameters extracted from the IMU's data allow a clear masticator efficiency and pattern analysis during chewing foods with different hardness and chewing gum with different sides of molars. (Chapter 6, Figure 6.7 to Figure 6.17)

This thesis contributes in providing a general solution of objectively evaluating operative skill performance in various medical scenarios, and then realizing better medical safety to patients. This will result in reducing the financial burden to hospitals for purchasing different kinds of skill evaluation systems, in order to assess doctors' skills in different medical areas. This study also represents a significantly important basis and step towards the realization of skill evaluation in the real operation room and clinical treatment. The wide applicable scopes of this study are not limited to medical fields, but can be also further implemented and contributed in other applications, such as sport performance evaluation, rehabilitation, entertainment, and so on.

7.3 Future Work

In recent years, many generations of IMU have been introduced. The sensor fusion algorithms (EKF) of these modules can be executed in real time by the embedded microcontrollers. With the development of MEMS technologies, the accuracies of inertial sensors keep increasing and noise levels keep going down. For orientation estimate, this implies the EKF can rely more on the gyroscopes, and the weights of accelerometer and magnetometer can be reduced. This will result in better acceleration and magnetic disturbance estimates, and therefore, less interference problems. Moreover, the innovative miniature gyroscopes are coming out with less drift rates by which the dynamic accuracy of IMUs can be improved. Therefore, implementations of novel and high performance inertial sensors help to improve the performance of WB-3 and WB-4 systems.

Besides the developments in sensor technologies, advances can be also expected in power supply (rechargeable batteries with miniaturized size and high capacity) for WB-4 system. With increasing battery capacity and power reduction of electronic components, the WB-4 IMU could provide much longer continuously working hour for wireless communication. In addition, the sensor fusion performance of WB-4 system still needs to be evaluated, and the balance between higher battery power supply and more compact size of the IMU should also be considered.

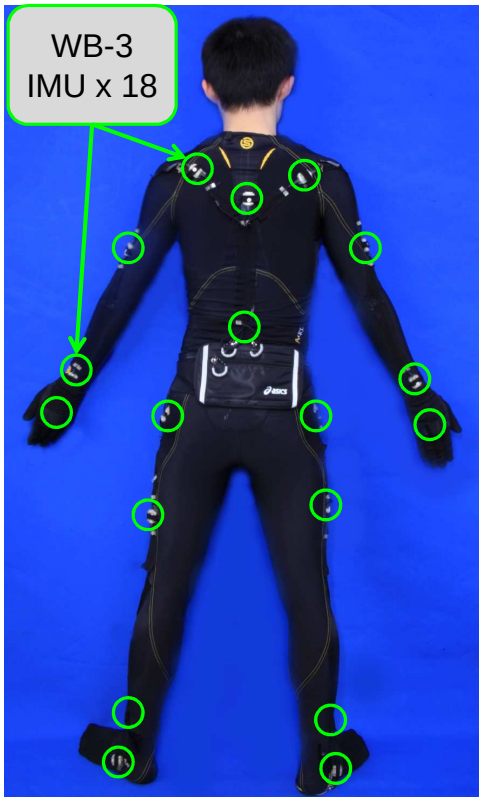

Figure 7.2: Motion capture suit with flexible cables.

To perform human motion analysis with IMUs, human body segment kinematics information has to be derived from the sensor kinematics. For this reason, the sensors should be mounted as stable as possible after which the relative orientation and position between the sensor frame and human segment frame are determined. This shows the importance of developing a motion capture suit which could better fix the IMUs on the human body. Figure 7.2 shows the ideas of full body motion capture suit for WB-3 system with flexible cables. The use of flexible cables could improve the system compactness and wearability.

The musculoskeletal model for biomechanical analysis discussed in Chapter 3 was still just a starting point. More experiments and more complicated models are needed in order to realize more authentic evaluation results of human biomechanics characteristics. Therefore, the sEMG (surface Electromyography) signal measurements would be a good solution for this problem (Figure 7.3). Integrating WB-3 system motion data with sEMG data for muscle tendon force estimate on the human upper limbs, the biomechanical model could provide more close simulation results to the real condition of human musculoskeletal status.

The proposed general skill evaluation methodology in Chapter 1 could be further improved with physiological measurements (Figure 7.4), such as ECG, heartbeat, respiration, and so on. This could provide us more insight information about the subject's mental status by which the skill evaluation would be more objective. In addition, the development of advice generation model helps the subjects improve their skill more efficiently. It would provide a list of advice about how the subjects should perform in the next steps or trainings, according to his/her skill motion performance. The ultimate challenge in this field is not only distinguishing the ranks between expert surgeons and novices, but also providing specific guidance to trainees as they move through their residencies.

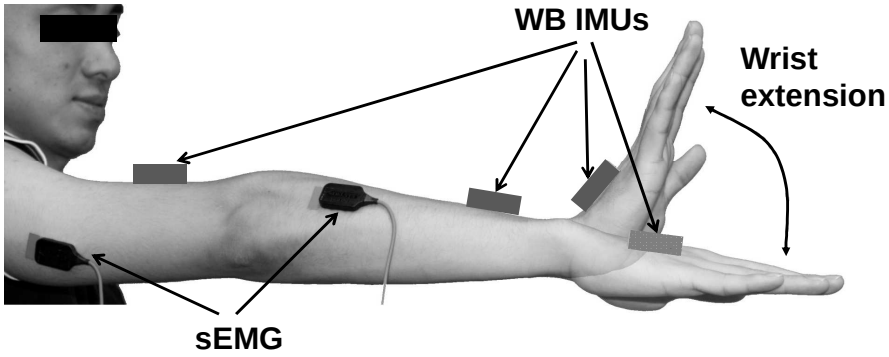

Figure 7.3: Biomechanical analysis integrating WB system and EMG measurements.

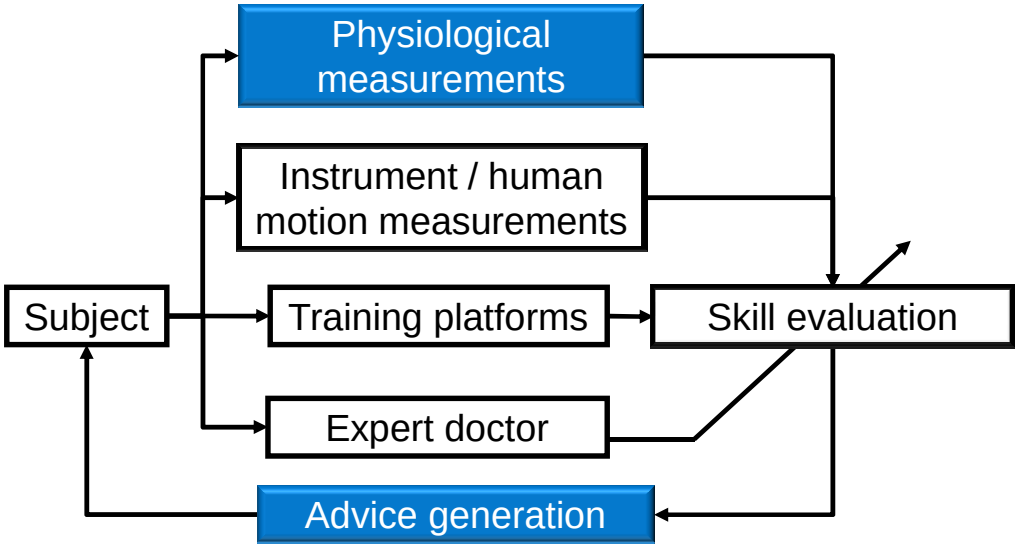

Figure 7.4: General skill evaluation methodology with physiological measurements and advice generation model.

Appendix A

Electronic Design of WB-3 IMU

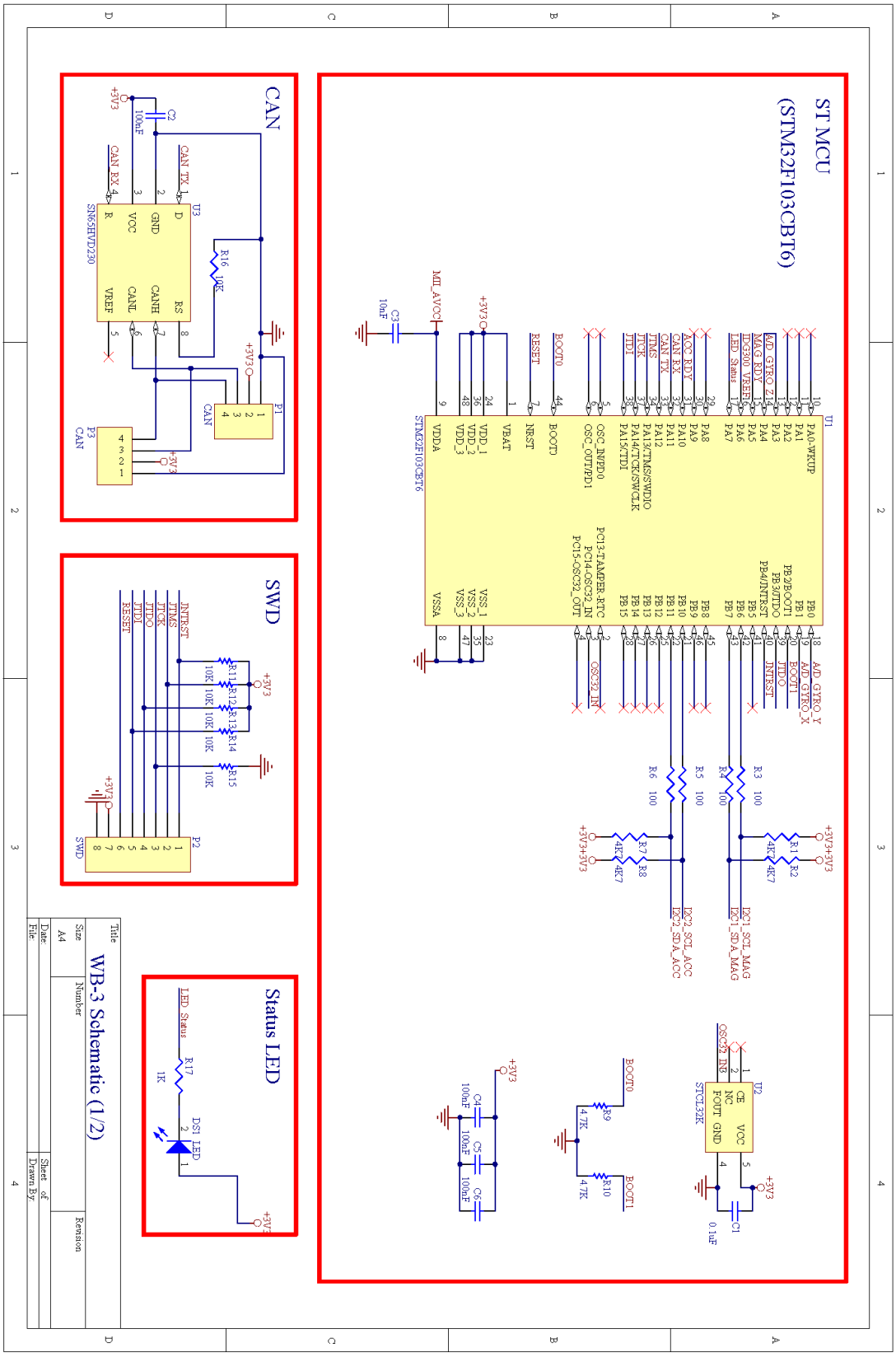

Figure A.1: Circuit schematics of WB-3 IMU (1/2).

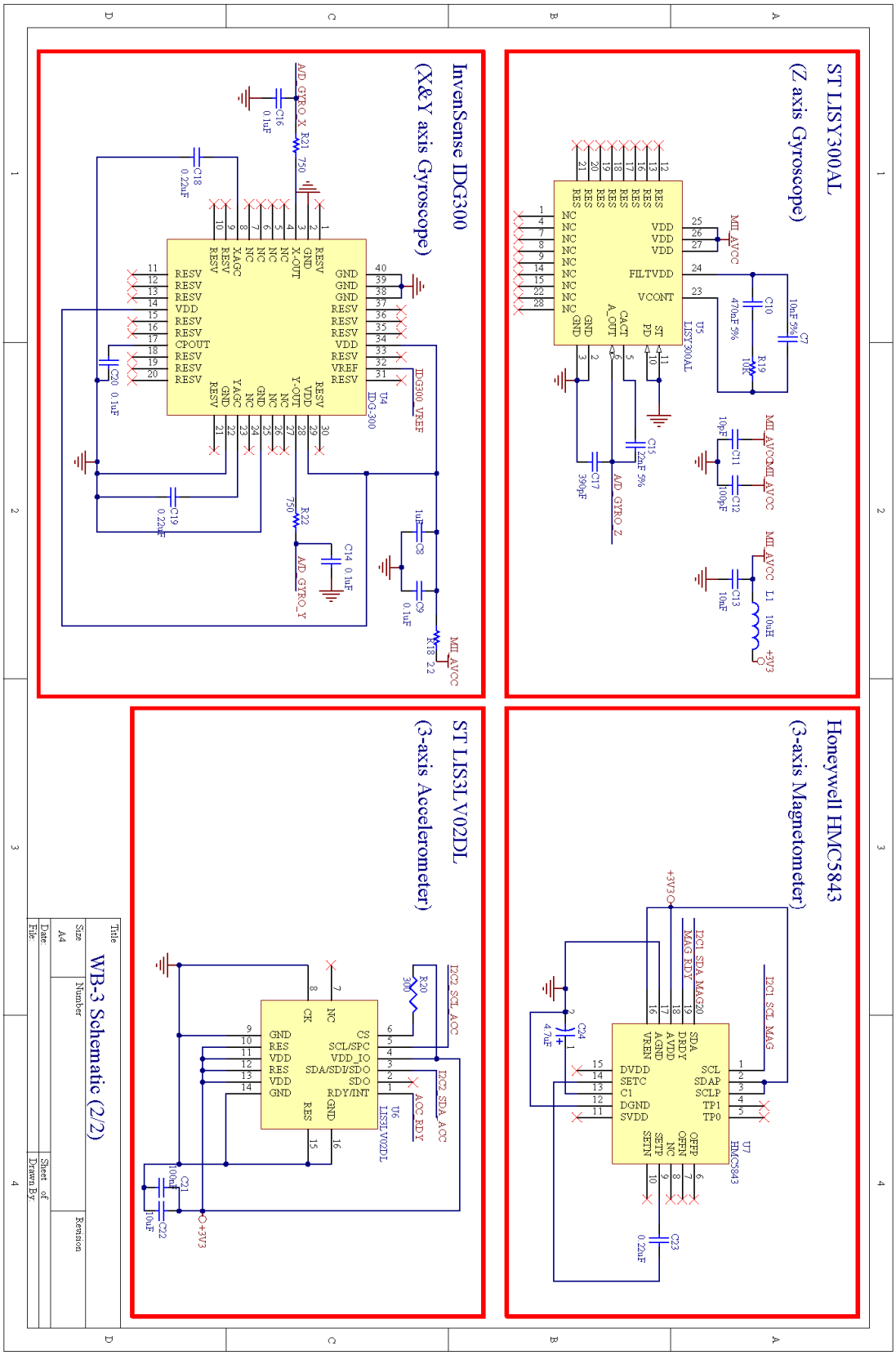

Figure A.2: Circuit schematics of WB-3 IMU (2/2).

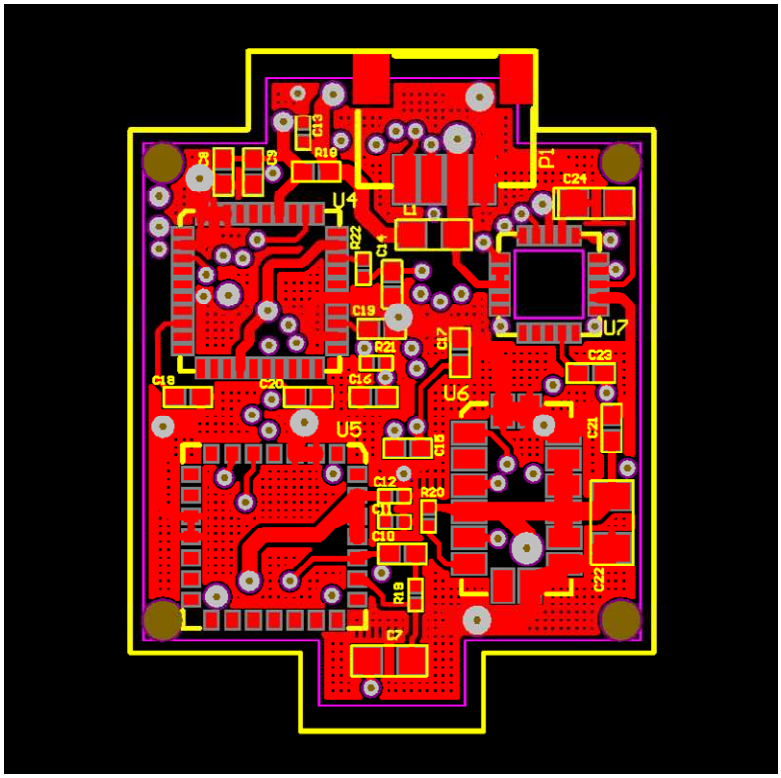

Figure A.3: Top signal layer of WB-3 PCB.

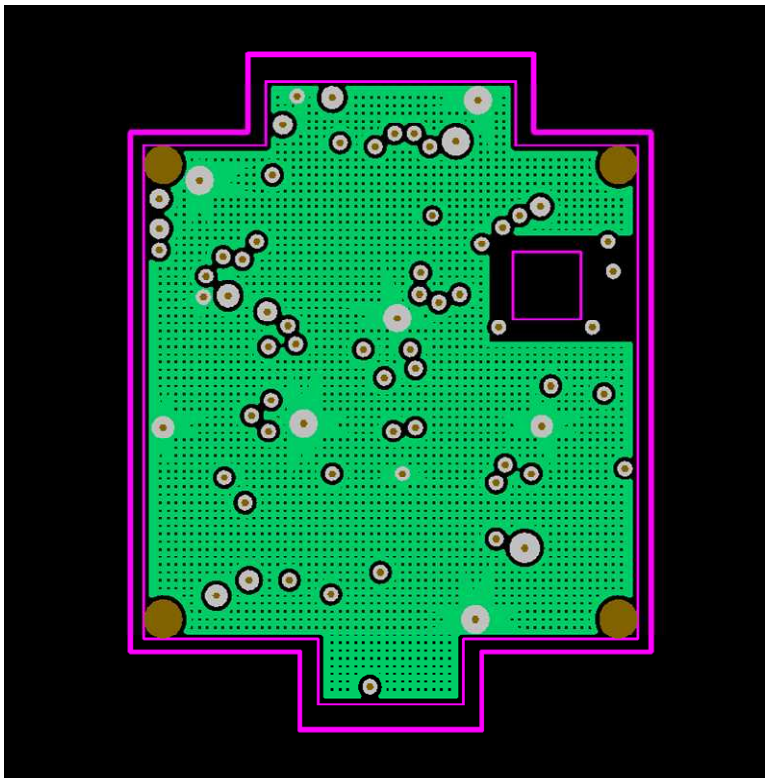

Figure A.4: GND layer of WB-3 PCB..

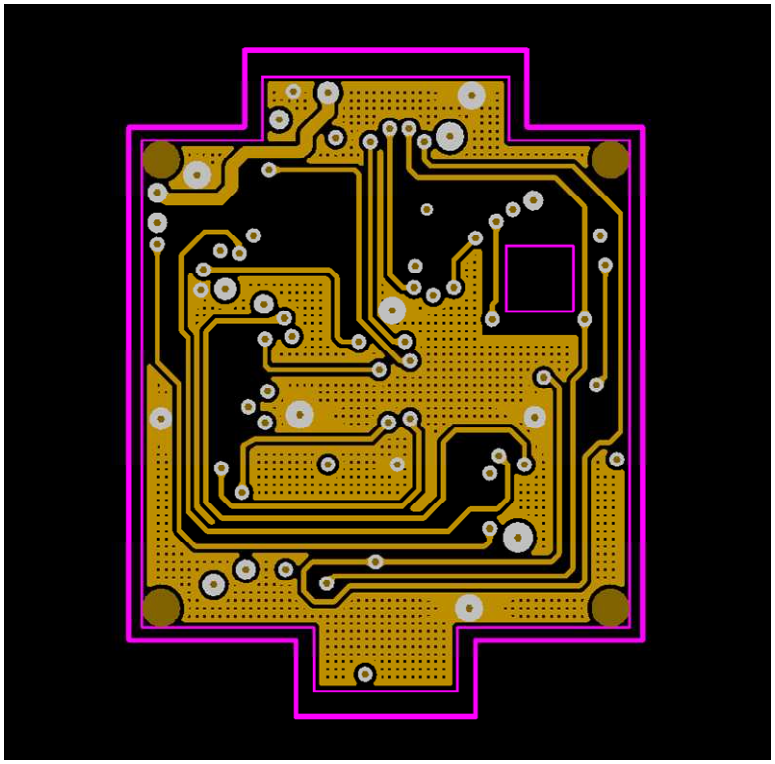

Figure A.5: Mid-signal layer1 of WB-3 PCB.

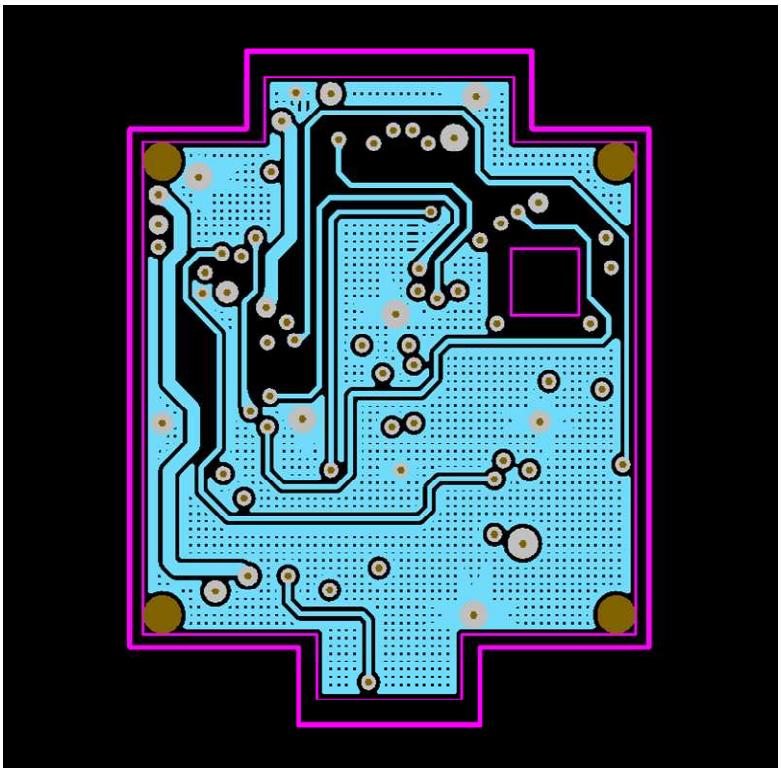

Figure A.6: Mid-signal layer2 of WB-3 PCB.

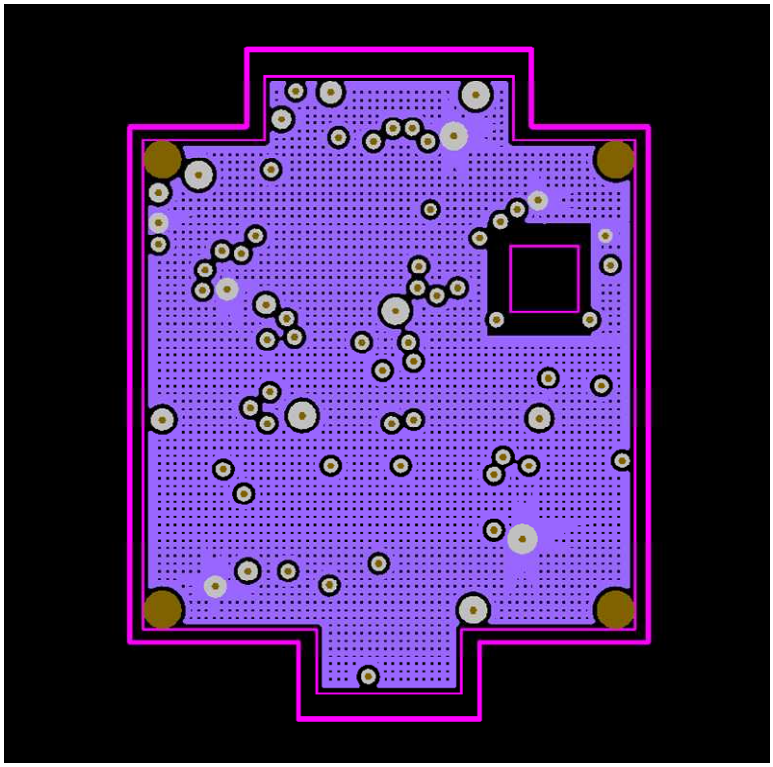

Figure A.7: Power layer of WB-3 PCB.

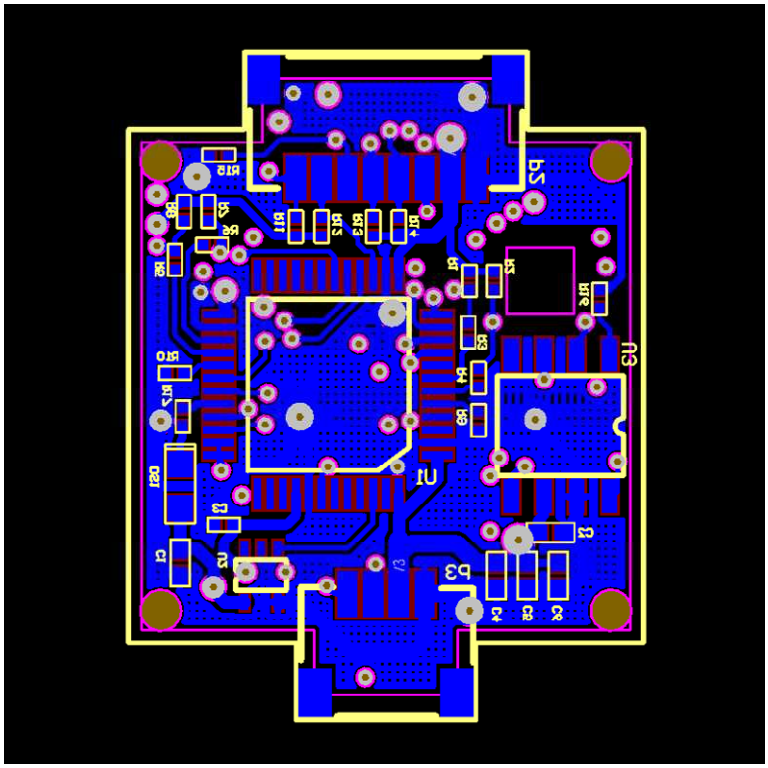

Figure A.8: Bottom signal layer of WB-3 PCB.

Table A.1: Bill of Materials of WB-3 IMU (1/2).

Category	Maker	Part Number	Quantity	Symbol	Value	Footprint
Capacitor	TDK	C1005JB1C104K	1	C1	0.1uF	1005
Capacitor	TDK	C1005JB1C104K	1	C2	100nF	1005
Capacitor	TDK	C0603JB1A103K	1	C3	10nF	0603
Capacitor	TDK	C1005JB1C104K	1	C4	100nF	1005
Capacitor	TDK	C1005JB1C104K	1	C5	100nF	1005
Capacitor	TDK	C1005JB1C104K	1	C6	100nF	1005
Capacitor	TDK	C1608CH1E103J	1	C7	10nF	1608
Capacitor	TDK	C1005X5R0J105K	1	C8	1uF	1005
Capacitor	TDK	C1005JB1C104K	1	C9	0.1uF	1005
Capacitor	TDK	C1005JB0J474K	1	C10	470nF	1005
Capacitor	TDK	C0603CH1E100D	1	C11	10pF	0603
Capacitor	TDK	C0603CH1E101J	1	C12	100pF	0603
Capacitor	TDK	C0603JB1A103K	1	C13	10nF	0603
Capacitor	TDK	C1005JB1C104K	1	C14	0.1uF	1005
Capacitor	TDK	C1005JB1E223K	1	C15	22nF	1005
Capacitor	TDK	C1005JB1C104K	1	C16	0.1uF	1005
Capacitor	TDK	C1005CH1H391J	1	C17	390pF	1005
Capacitor	TDK	C1005JB0J224K	1	C18	0.22uF	1005
Capacitor	TDK	C1005JB0J224K	1	C19	0.22uF	1005
Capacitor	TDK	C1005JB1C104K	1	C20	0.1uF	1005
Capacitor	TDK	C1005JB1C104K	1	C21	100nF	1005
Capacitor	TDK	C2012X5R0J106K	1	C22	10uF	2012
Capacitor	TDK	C1005JB0J224K	1	C23	0.22uF	1005
Capacitor	TDK	C2012JB1A475K	1	C24	4.7uF	2012
LED	スタン	FR1111C	1	DS1	Red,	1608
Inductor	TDK	GLF1608T100M	1	L1	10uH	1608
Connector	JST	SM04B-SRSS-TB(LF)	1	P1	4 pins	
Connector	JST	SM08B-SRSS-TB(LF)	1	P2	8 pins	
Connector	JST	SM04B-SRSS-TB(LF)	1	P3	4 pins	
Resistor	釜屋電	P-RMC1/20-472FRA	1	R1	4K7	0603
Resistor	釜屋電	P-RMC1/20-472FRA	1	R2	4K7	0603
Resistor	釜屋電	P-RMC1/20-101FRA	1	R3	100	0603
Resistor	釜屋電	P-RMC1/20-101FRA	1	R4	100	0603
Resistor	釜屋電	P-RMC1/20-101FRA	1	R5	100	0603
Resistor	釜屋電	P-RMC1/20-101FRA	1	R6	100	0603
Resistor	釜屋電	P-RMC1/20-472FRA	1	R7	4K7	0603
Resistor	釜屋電	P-RMC1/20-472FRA	1	R8	4K7	0603
Resistor	釜屋電	P-RMC1/20-472FRA	1	R9	4.7K	0603
Resistor	釜屋電	P-RMC1/20-472FRA	1	R10	4.7K	0603
Resistor	釜屋電	P-RMC1/20-103FRA	1	R11	10K	0603
Resistor	釜屋電	P-RMC1/20-103FRA	1	R12	10K	0603
Resistor	釜屋電	P-RMC1/20-103FRA	1	R13	10K	0603

Table A.2: Bill of Materials of WB-3 IMU (2/2).

Category	Maker	Part Number	Quantity	Symbol	Value	Footprint
Resistor	釜屋電機	P-RMC1/20-103FRA	1	R14	10K	0603
Resistor	釜屋電機	P-RMC1/20-103FRA	1	R15	10K	0603
Resistor	釜屋電機	P-RMC1/20-103FRA	1	R16	10K	0603
Resistor	釜屋電機	P-RMC1/20-102FRA	1	R17	1K	0603
Resistor	釜屋電機	RMC1/16S-2R0FTH	1	R18	2.2	1005
Resistor	釜屋電機	P-RMC1/20-103FRA	1	R19	10K	0603
Resistor	釜屋電機	P-RMC1/20-301FRA	1	R20	300	0603
Resistor	釜屋電機	P-RMC1/20-751FRA	1	R21	750	0603
Resistor	釜屋電機	P-RMC1/20-751FRA	1	R22	750	0603
MCU	ST	STM32F103CBT6	1	U1		LQFP-
Oscillator	ST	STCL132K	1	U2	3.2KHz	SOT-5
CAN BUS	TI	SN65HVD230D	1	U3		SOIC-8
gyro	InvenSense	IDG-300	1	U4	2-axix	QFN-40
gyro	ST	LISY300AL	1	U5	1-axix	LGA-28
Acc.	ST	LIS3LV02DL	1	U6	3-axix	LGA-16
Mag.	Honeywell	HMC5843	1	U7	3-axix	LCC-20

Appendix B

Electronic Design of WB-4 IMU

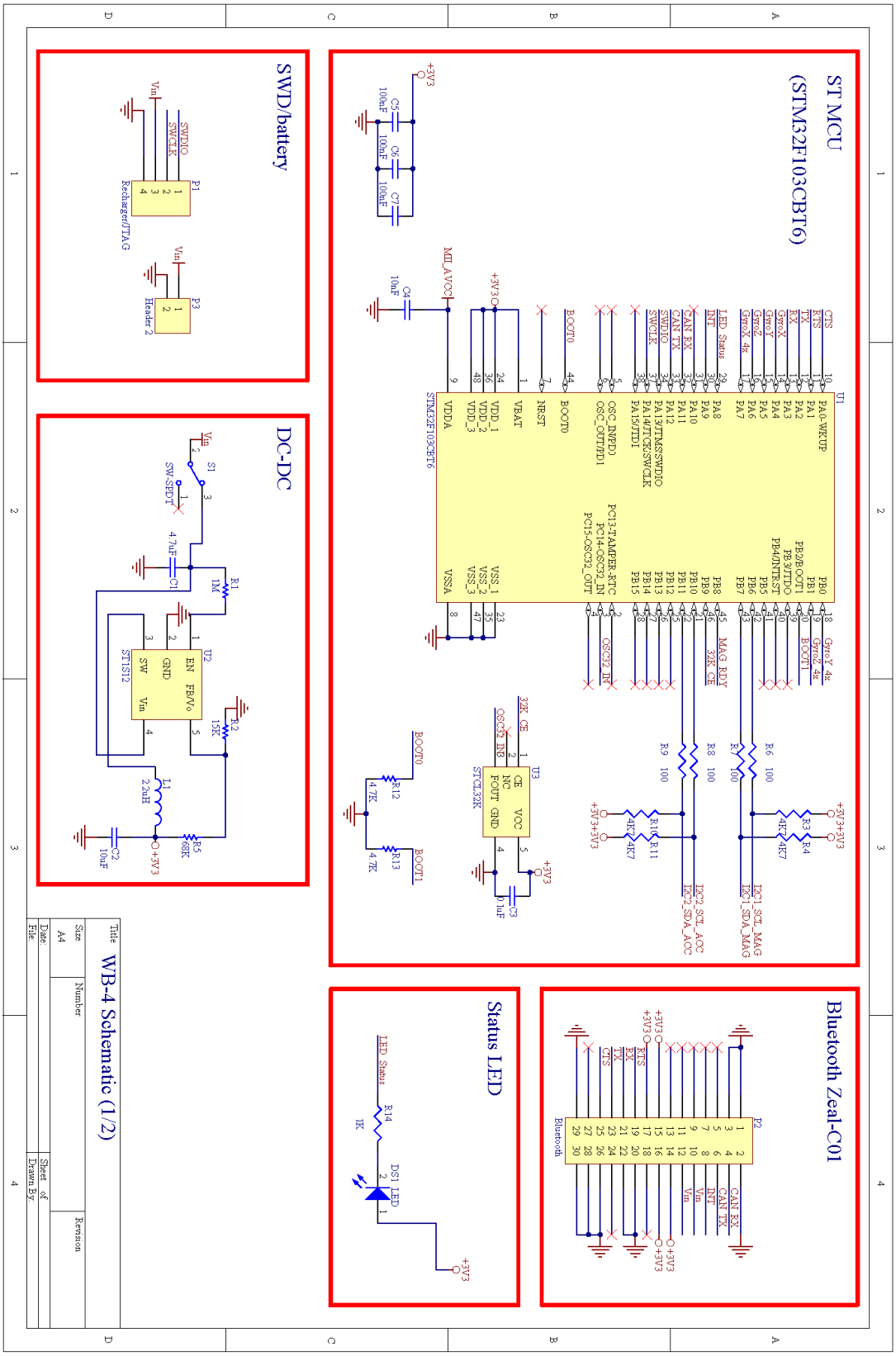

Figure B.1: Circuit schematics of WB-4 mother board (1/2).

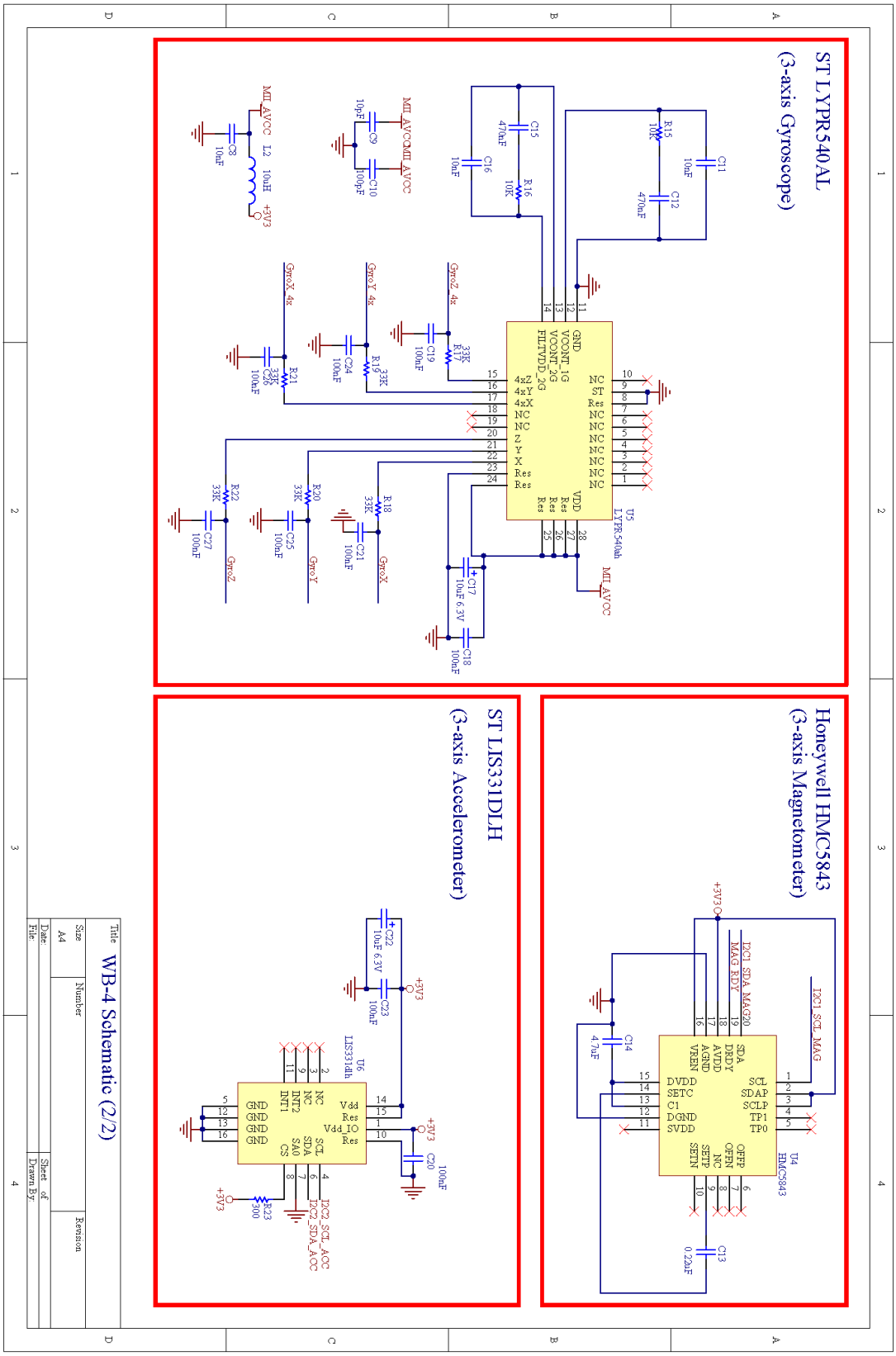

Figure B.2: Circuit schematics of WB-4 mother board (2/2).

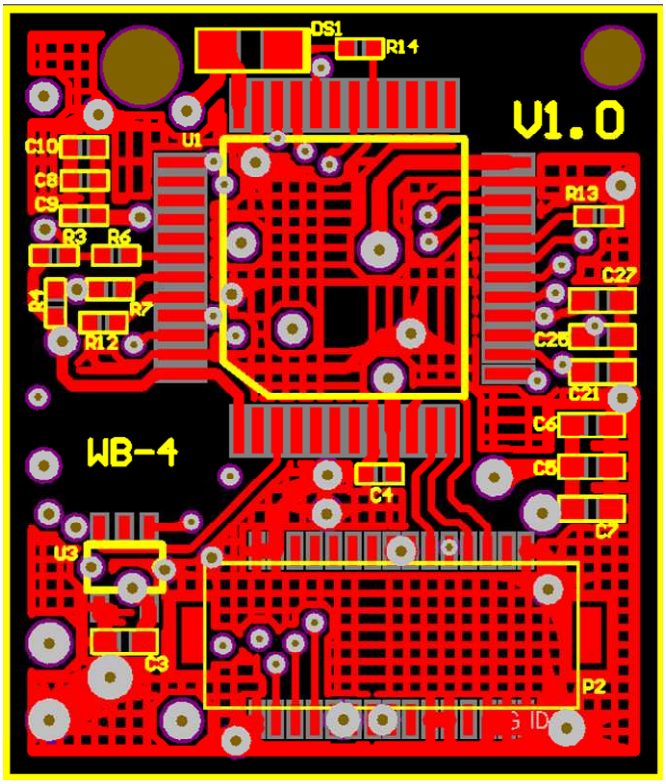

Figure B.3: Top signal layer of WB-4 mother board PCB.

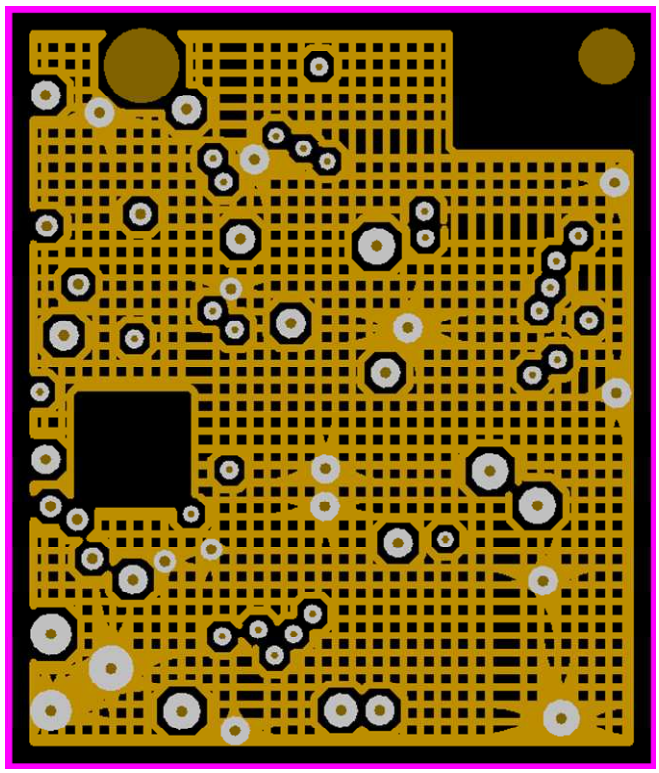

Figure B.4: GND layer of WB-4 mother board PCB.

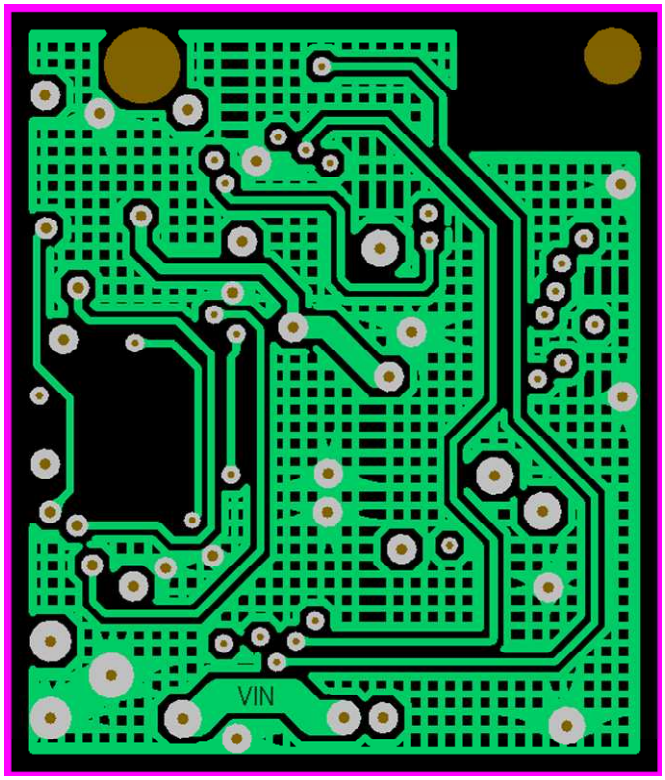

Figure B.5: Mid-signal layer1 of WB-4 mother board PCB.

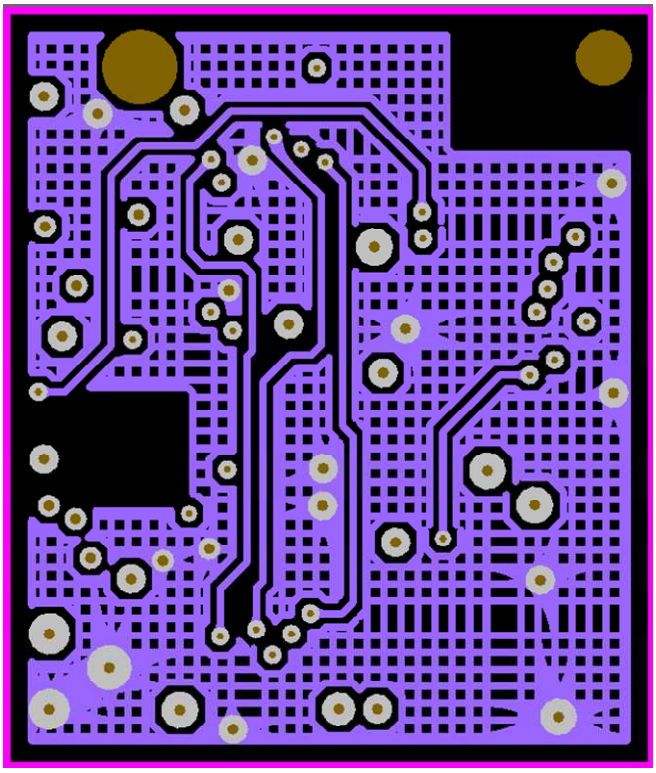

Figure B.6: Mid-signal layer2 of WB-4 mother board PCB.

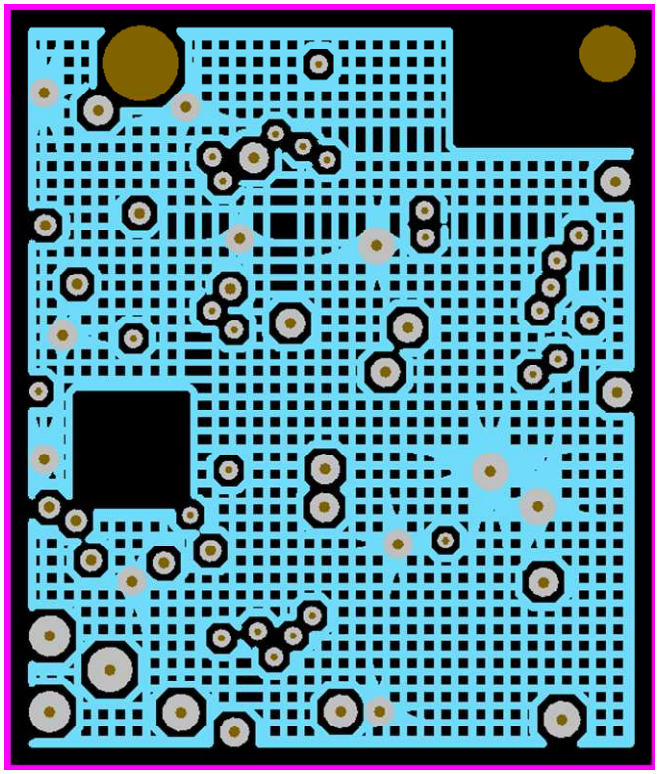

Figure B.7: Power layer of WB-4 mother board PCB.

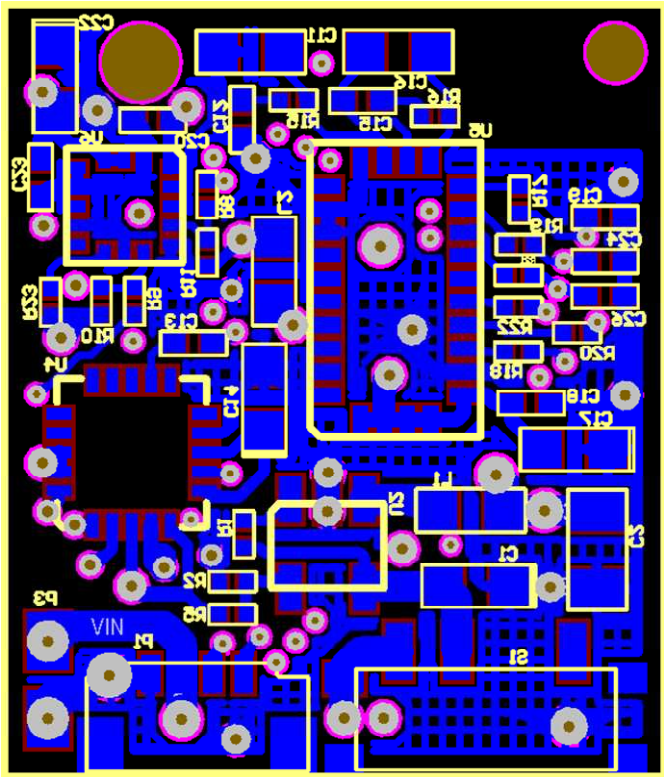

Figure B.8: Bottom signal layer of WB-4 mother board PCB.

Table B.1: Bill of Materials of WB-4 mother board (1/2).

Category	Maker	Part Number	Quantity	Symbol	Value	Footprint
Capacitor	TDK	C2012X5R1A475K	1	C1	4.7uF	2012
Capacitor	TDK	C2012X5R0J106K	1	C2	10uF	2012
Capacitor	TDK	C1005JB1C104K	1	C3	100nF	1005
Capacitor	TDK	C0603JB1A103K	1	C4	10nF	0603
Capacitor	TDK	C1005JB1C104K	1	C5	100nF	1005
Capacitor	TDK	C1005JB1C104K	1	C6	100nF	1005
Capacitor	TDK	C1005JB1C104K	1	C7	100nF	1005
Capacitor	TDK	C0603JB1A103K	1	C8	10nF	0603
Capacitor	TDK	C0603CH1E100D	1	C9	10pF	0603
Capacitor	TDK	C0603CH1E101J	1	C10	100pF	0603
Capacitor	TDK	C1608CH1E103J	1	C11	10nF	1608
Capacitor	TDK	C1005JB0J474K	1	C12	470nF	1005
Capacitor	TDK	C1005JB0J224K	1	C13	220nF	1005
Capacitor	TDK	C2012X5R1A475K	1	C14	4.7uF	2012
Capacitor	TDK	C1005JB0J474K	1	C15	470nF	1005
Capacitor	TDK	C1608CH1E103J	1	C16	10nF	1608
Capacitor	TDK	C2012X5R0J106K	1	C17	10uF	2012
Capacitor	TDK	C1005JB1C104K	1	C18	100nF	1005
Capacitor	TDK	C1005JB1C104K	1	C19	100nF	1005
Capacitor	TDK	C1005JB1C104K	1	C20	100nF	1005
Capacitor	TDK	C1005JB1C104K	1	C21	100nF	1005
Capacitor	TDK	TEESVP1A106M8R	1	C22	10uF	2012
Capacitor	TDK	C1005JB1C104K	1	C23	100nF	1005
Capacitor	TDK	C1005JB1C104K	1	C24	100nF	1005
Capacitor	TDK	C1005JB1C104K	1	C25	100nF	1005
Capacitor	TDK	C1005JB1C104K	1	C26	100nF	1005
Capacitor	TDK	C1005JB1C104K	1	C27	100nF	1005
LED	スタンレ	FR1111C	1	DS1	red	1608
Inductor	TDK	GLF2012T2R2M	1	L1	2.2uH	1608
Inductor	TDK	GLF1608T100M	1	L2	10uH	1608
Connector	RoHS	DF12(3.0)-30DP-	1	P2	30pins	30 pins
Resistor	panasonic	ERJ1GEJ105C		R1	1M	0603
Resistor	panasonic	RGC1/16SC133DTH		R2	15K	0603
Resistor	釜屋電機	P-RMC1/20-472FPA	1	R3	4K7	0603
Resistor	釜屋電機	P-RMC1/20-472FPA	1	R4	4K7	0603
Resistor	panasonic	RGC1/16SC513DTH	1	R5	68K	0603
Resistor	panasonic	ERJ1GEF1000C	1	R6	100	0603
Resistor	panasonic	ERJ1GEF1000C	1	R7	100	0603
Resistor	panasonic	ERJ1GEF1000C	1	R8	100	0603
Resistor	panasonic	ERJ1GEF1000C	1	R9	100	0603
Resistor	釜屋電機	P-RMC1/20-472FPA	1	R10	4K7	0603
Resistor	釜屋電機	P-RMC1/20-472FPA	1	R11	4K7	0603

Table B.2: Bill of Materials of WB-4 mother board (2/2).

Category	Maker	Part Number	Quantity	Symbol	Value	Footprint
Resistor	釜屋電機	P-RMC1/20-472FPA	1	R12	4.7K	0603
Resistor	釜屋電機	P-RMC1/20-472FPA	1	R13	4.7K	0603
Resistor	Panasonic	ERJ1GEJ102C	1	R14	1K	0603
Resistor	Panasonic	ERJ1GEF1002C	1	R15	10K	0603
Resistor	Panasonic	ERJ1GEF1002C	1	R16	10K	0603
Resistor	釜屋電機	P-RMC1/20-333FPA	1	R17	33K	0603
Resistor	釜屋電機	P-RMC1/20-333FPA	1	R18	33K	0603
Resistor	釜屋電機	P-RMC1/20-333FPA	1	R19	33K	0603
Resistor	釜屋電機	P-RMC1/20-333FPA	1	R20	33K	0603
Resistor	釜屋電機	P-RMC1/20-333FPA	1	R21	33K	0603
Resistor	釜屋電機	P-RMC1/20-333FPA	1	R22	33K	0603
Resistor	釜屋電機	P-RMC1/20-301FPA	1	R23	300	0603
Switch	COPAL	CUS-12B	1	S1		
MCU	ST	STM32F103CBT6	1	U1	64pins	LQFP48
DC-DC	ST	ST1S12	1	U2		TSOT-5
Oscillator	ST	STCL132K	1	U3	32.768	SOP-5
Mag.	Honeywel	HMC5843	1	U4	3-axis	LCC-20
Acc.	ST	LIS331DLH	1	U6	3-axis	LGA-16
Gyro	ST	LYPR540ah	1	U5	3-axis	LGA-28
Connector	JST	04SUR-32S	1	P1	4pins	4pins

Reference

[1] P. Kazanzides, G. Fichtinger, G. Hager, A. Okamura, L. Whitcomb, and R. Taylor, "Surgical and Interventional Robotics - Core Concepts, Technology, and Design [Tutorial]," *Robotics & Automation Magazine, IEEE*, vol. 15, no. 2, pp. 122-130, 2008.

[2] G. Fichtinger, P. Kazanzides, A. Okamura, G. Hager, L. Whitcomb, and R. Taylor, "Surgical and interventional robotics: Part II," *Robotics & Automation Magazine, IEEE*, vol. 15, no. 3, pp. 94-102, 2008.

[3] G. Chen, G. Thomann, M. Pham, M. Betemps, and T. Redarce, "Modeling and control of a colonoscopic tip under disturbance of the insertion of colonoscope," *Proceedings of IEEE/RSJ International Conference on Intelligent Robots and Systems*, vol. 4, pp. 3315-3320, 2004.

[4] M. Aschke, C. Wirtz, J. Raczkowsky, H. Worn, and S. Kunze, "Augmented reality in operating microscopes for neurosurgical interventions," *Proceedings of First IEEE/EMBS International Conference on Neural Engineering*, pp. 652-655, 2003.

[5] K. Ohuchida et al., "The effect of CyberDome, a novel 3-dimensional dome-shaped display system, on laparoscopic procedures," *International Journal of Computer Assisted Radiology and Surgery*, vol. 4, no. 2, pp. 125-132, Mar. 2009.

[6] "LRP is a minimally invasive prostate cancer treatment," [Online]. Available: http://www.laprp.com/question_answer.php.

[7] "Asia Cardiovascular Products," [Online]. Available: http://www.acp-asia.com.hk/web/product.php.

[8] F. Zullo et al., "Laparoscopic surgery vs laparotomy for early stage endometrial cancer: long-term data of a randomized controlled trial," *American Journal of Obstetrics and Gynecology*, vol. 200, no. 3, pp. 296.e1-9, Mar. 2009.

[9] ARMA Laboratory, [Online]. Available: http://www.columbia.edu.

[10] E. Eckersberger et al., "Uro-oncological controversies in euro-oncology: highlights from the European association of urology section of oncological urology," *Reviews in Urology*, vol. 12, no. 2, pp. 125-128, 2010.

[11] M. F. Kaminski et al., "Quality indicators for colonoscopy and the risk of interval

cancer," *The New England Journal of Medicine*, vol. 362, no. 19, pp. 1795-1803, May. 2010.

[12] R. Enciso, A. Memon, and J. Mah, "Three-dimensional visualization of the craniofacial patient: volume segmentation, data integration and animation," *Orthodontics & Craniofacial Research*, vol. 6, pp. 66-71, 2003.

[13] "Swiss Dentures Technique," [Online]. Available: http://www.burnsidedental.com.

[14] U. Soboļeva, L. Lauriņa, and A. Slaidiņa, "Jaw tracking devices-historical review of methods development. Part II," *Stomatologija*, vol. 7, no. 3, pp. 72-76, 2005.

[15] S. Cotin, N. Stylopoulos, M. Ottensmeyer, P. Neumann, D. Rattner, and S. Dawson, "Metrics for laparoscopic skills trainers: the weakest link!," *Medical Image Computing and Computer-Assisted Intervention*, pp. 35-43, 2002.

[16] J. Haase and E. Boisen, "Neurosurgical training: more hours needed or a new learning culture?," *Surgical Neurology*, vol. 72, no. 1, pp. 89-95, Jul. 2009.

[17] M. Wentink, L. P. S. Stassen, I. Alwayn, R. J. A. W. Hosman, and H. G. Stassen, "Rasmussen's model of human behavior in laparoscopy training," *Surgical Endoscopy*, vol. 17, no. 8, pp. 1241-1246, Aug. 2003.

[18] K. Moorthy, Y. Munz, A. Dosis, F. Bello, and A. Darzi, "Motion analysis in the training and assessment of minimally invasive surgery," *Minimally Invasive Therapy & Allied Technologies: MITAT: Official Journal of the Society for Minimally Invasive Therapy*, vol. 12, no. 3, pp. 137-142, Jul. 2003.

[19] N. Stylopoulos et al., "Computer-enhanced laparoscopic training system (CELTS): bridging the gap," *Surgical Endoscopy*, vol. 18, no. 5, pp. 782-789, 2004.

[20] R. Rosenthal et al., "The future of patient safety: Surgical trainees accept virtual reality as a new training tool," *Patient Safety in Surgery*, vol. 2, no. 1, pp. 16, 2008.

[21] K. Tanoue et al., "Effectiveness of endoscopic surgery training for medical students using a virtual reality simulator versus a box trainer: a randomized controlled trial," *Surgical Endoscopy*, vol. 22, no. 4, pp. 985-990, Apr. 2008.

[22] D. Risucci, J. A. Cohen, J. E. Garbus, M. Goldstein, and M. G. Cohen, "The effects of practice and instruction on speed and accuracy during resident acquisition of simulated laparoscopic skills," *Curr Surg*, vol. 58, pp. 230-235, 2001.

[23] N. Stylopoulos and K. G. Vosburgh, "Assessing technical skill in surgery and endoscopy: a set of metrics and an algorithm (C-PASS) to assess skills in surgical and endoscopic procedures," *Surg Innov*, vol. 14, pp. 113-21, 2007.

[24] C. E. Reiley, H. C. Lin, D. D. Yuh, and G. D. Hager, "Review of methods for objective surgical skill evaluation," *Surgical Endoscopy*, Jul. 2010.

[25] A. Peracchia, “Surgical education in the third millennium,” *Annals of Surgery*, vol. 234, no. 6, pp. 709-712, Dec. 2001.

[26] M. Tavakol, M. A. Mohagheghi, and R. Dennick, “Assessing the skills of surgical residents using simulation,” *Journal of Surgical Education*, vol. 65, no. 2, pp. 77-83, Apr. 2008.

[27] H. C. Lin, I. Shafran, D. Yuh, and G. D. Hager, “Towards automatic skill evaluation: detection and segmentation of tobot-assisted surgical motions,” *Computer Aided Surgery: Official Journal of the International Society for Computer Aided Surgery*, vol. 11, no. 5, pp. 220-230, Sep. 2006.

[28] K. Itoh et al., “Development of a bioinstrumentation system in the interaction between a human and a robot,” *Proceedings of IEEE/RSJ International Conference on Intelligent Robots and Systems*, pp. 2620-2625, 2006.

[29] J. Perry, J. Rosen, and S. Burns, “Upper-limb powered exoskeleton design,” *IEEE/ASME Transactions on Mechatronics*, vol. 12, no. 4, pp. 408-417, 2007.

[30] Zebris Inc., [Online]. Available: http://www.zebris.de.

[31] VICON Inc., [Online]. Available: http://www.vivometrics.com.

[32] NDI Inc., [Online]. Available: http://www.ndigital.com.

[33] Organic Motion Inc., [Online]. Available: http://www.organicmotion.com.

[34] Polhemus Inc., [Online]. Available: http://www.polhemus.com.

[35] “Aurora Electromagnetic Measurement System,” [Online]. Available: http://www.ndigital.com/medical/aurora.php.

[36] “Ultrasonic Industrial Positioning Systems,” [Online]. Available: http://www.hexamite.com.

[37] M. Zecca et al., “Development of the waseda bioinstrumentation system WB-2 - the new inertial measurement unit -,” *Proceedings of IEEE International Conference on Robotics and Biomimetics*, pp. 139 - 144, 2007.

[38] Xsens Inc., [Online]. Available: http://www.xsens.com.

[39] M. Zecca et al., “Development of an ultra-miniaturized inertial measurement unit for objective skill analysis and assessment in neurosurgery: preliminary results,” *Proceedings of 12th International Conference on Medical Image Computing and Computer Assisted Intervention*, pp. P1-12-W, 2009.

[40] “Kinect,” [Online]. Available: http://www.xbox.com/en-US/kinect.

[41] J. A. Corrales, F. A. Candelas, and F. Torres, “Hybrid tracking of human operators

using IMU/UWB data fusion by a Kalman filter," *Proceedings of the 3rd ACM/IEEE international conference on Human robot interaction*, pp. 193-200, 2008.

[42] G. Ogris, T. Stiefmeier, H. Junker, P. Lukowicz, and G. Troster, "Using ultrasonic hand tracking to augment motion analysis based recognition of manipulative gestures," *Proceedings of the Ninth IEEE International Symposium on Wearable Computers*, pp. 152-159, 2005.

[43] Y. Masuda et al., "An unconstrained monitoring system for home rehabilitation," *Engineering in Medicine and Biology Magazine, IEEE*, vol. 24, pp. 43-47, 2005.

[44] B. Jarochowski, SeungJung Shin, DaeHyun Ryu, and HyungJun Kim, "Ubiquitous rehabilitation center: an implementation of a wireless sensor network based rehabilitation management system," *Proceedings of International Conference on Convergence Information Technology*, pp. 2349-2358, 2007.

[45] H. Lee, Y. Kim, J. Jung, K. Park, D. Kim, and Z. Z. Bien, "A 24-hour health monitoring system in a smart house," *Gerontechnology*, vol. 7, pp. 22-35, 2008.

[46] S. Bhardwaj, D. Lee, S. C. Mukhopadhyay, and W. Chung, "Ubiquitous healthcare data analysis and monitoring using multiple wireless sensors for elderly person," *Sensors & Transducers Journal, Special Issue: Modern Sensing Technologies*, vol. 90, pp. 87-99, 2008.

[47] M. S. Orendurff, J. A. Schoen, G. C. Bernatz, A. D. Segal, and G. K. Klute, "How humans walk: bout duration, steps per bout, and rest duration," *Journal of Rehabilitation Research and Development*, vol. 45, no. 7, pp. 1077-1089, 2008.

[48] Yisheng Chen, J. Lee, R. Parent, and R. Machiraju, "Markerless monocular motion capture using image features and physical constraints," *Proceedings of the Computer Graphics International Conference*, pp. 36-43, 2005.

[49] M. Zecca et al., "Analysis of the Surgeon's Performance during Laparoscopy by Using the Bioinstrumentation System WB-1R– towards the development of a Global Performance Index -," *Proceedings of IEEE/RSJ International Conference on Intelligent Robots and Systems*, vol. 7, pp. 1272-1277, 2007.

[50] D. Vlasic et al., "Practical motion capture in everyday surroundings," *ACM Trans. Graph.*, vol. 26, no. 3, pp. 35, 2007.

[51] G. Venture, K. Yamane, Y. Nakamura, and T. Yamamoto, "Identification of Human Limb Viscoelasticity using Robotics Methods to Support the Diagnosis of Neuromuscular Diseases," *Int. J. Rob. Res.*, vol. 28, no. 10, pp. 1322-1333, 2009.

[52] Y. Nakamura, K. Yamane, Y. Fujita, and I. Suzuki, "Somatosensory computation for man-machine interface from motion-capture data and musculoskeletal human model," *IEEE Transactions on Robotics*, vol. 21, no. 1, pp. 58-66, 2005.

[53] E. R. Bachmann, R. B. McGhee, X. Yun, and M. J. Zyda, "Inertial and Magnetic

Posture Tracking for Inserting Humans Into Networked Virtual Environments," *Acm Symposium on Virtual Reality Software and Technology VRST*, pp. 9-16, 2001.

[54] E. Bachmann, Xiaoping Yun, D. McKinney, R. McGhee, and M. Zyda, "Design and implementation of MARG sensors for 3-DOF orientation measurement of rigid bodies," *Proceedings of IEEE International Conference on Robotics and Automation*, vol. 1, pp. 1171-1178 vol.1, 2003.

[55] J. Lötters et al., "Design, fabrication and characterization of a highly symmetrical capacitive triaxial accelerometer," *Sensors and Actuators A: Physical*, vol. 66, no. 1, pp. 205-212, Apr. 1998.

[56] InterSense Inc., [Online]. Available: http://www.intersense.com.

[57] MicroStrain Inc., [Online]. Available: http://www.microstrain.com.

[58] J. Bers, "A body model server for human motion capture and representation," *Presence (Cambridge, Mass.)*, vol. 5, no. 4, pp. 381-392, 1996.

[59] D.O. Ibanez, F.P. Baquerin, D.Y. Choi, and C.N. Riviere, "Performance Envelope and Physiological Tremor in Microsurgery," in *Bioengineering Conference, 2006. Proceedings of the IEEE 32nd Annual Northeast*, pp. 121-122, 2006.

[60] R. G. Brown and P. Y. C. Hwang, *Introduction to Random Signals and Applied Kalman Filtering, 3rd Edition*, 3rd ed. Wiley, 1996.

[61] Nathaniel I. Durlach and Anne S. Mavor, *Virtual Reality: Scientific and Technological Challenges*, Illustrated edition. National Academies Press, 1994.

[62] Altium Inc., [Online]. Available: http://www.altium.com.

[63] NIST/SEMATECH, "e-Handbook of Statistical Methods," [Online]. Available: http://www.itl.nist.gov/div898/handbook/.

[64] 無線化 Inc., [Online]. Available: http://www.musenka.com.

[65] Kayo Battery Co.,Ltd., [Online]. Available: http://www.kayobattery.com.

[66] R. Zhu and Z. Zhou, "A real-time articulated human motion tracking using tri-axis inertial/magnetic sensors package," *IEEE Transactions on Neural Systems and Rehabilitation Engineering: A Publication of the IEEE Engineering in Medicine and Biology Society*, vol. 12, no. 2, pp. 295-302, Jun. 2004.

[67] R. Antonio Benitez, T. Guillermo De Los Santos, and R. Daniel Vallejo, "Forward Kinematics for Virtual Agents," Engineering Letters, 15:2, EL_15_2_08.

[68] A. Sabatini, "Quaternion-based extended Kalman filter for determining orientation by inertial and magnetic sensing," *IEEE Transactions on Biomedical Engineering*, vol. 53, no. 7, pp. 1346-1356, 2006.

[69] T. Harada, T. Gyota, Y. Kuniyoshi, and T. Sato, “Development of Wireless Networked Tiny Orientation Device for Wearable Motion Capture and Measurement of Walking Around, Walking Up and Down, and Jumping Tasks,” *IEEE/RSJ International Conference on Intelligent Robots and Systems*, 2007.

[70] E. R. Bachmann, “Inertial And Magnetic Tracking Of Limb Segment Orientation For Inserting Humans Into Synthetic Environments,” *PH.D. Dissertation, NAVAL Postgraduate School*, 2000.

[71] M. Zecca et al., “On the development of the Waseda Bioinstrumentation WB-2 - Development of the gyro module,” *Proceedings of Robotics and Mechatronics Conference*, pp. 1A1-O09, 2007.

[72] E. Foxlin, “Inertial head-tracker sensor fusion by a complementary separate-bias Kalman filter,” *Proceedings of the IEEE Virtual Reality Annual International Symposium*, pp. 185-194, 267, 1996.

[73] E. Foxlin, “Pedestrian tracking with shoe-mounted inertial sensors,” *Computer Graphics and Applications*, vol. 25, no. 6, pp. 38-46, 2005.

[74] D. Roetenberg, P. Slycke, and P. Veltink, “Ambulatory Position and Orientation Tracking Fusing Magnetic and Inertial Sensing,” *IEEE Transactions on Biomedical Engineering*, vol. 54, no. 5, pp. 883-890, 2007.

[75] S. You and U. Neumann, “Fusion of vision and gyro tracking for robust augmented reality registration,” *Proceedings of IEEE Conference on Virtual Reality*, pp. 71-78, 2001.

[76] J. Hightower and G. Borriello, “Particle filters for location estimation in ubiquitous computing: A case study,” *Proceedings of International Conference on Ubiquitous Computing*, pp. 88-106, 2004.

[77] X. Yun and E. Bachmann, “Design, Implementation, and Experimental Results of a Quaternion-Based Kalman Filter for Human Body Motion Tracking,” *IEEE Transactions on Robotics*, vol. 22, no. 6, pp. 1216-1227, 2006.

[78] A. Kim and M. Golnaraghi, “A quaternion-based orientation estimation algorithm using an inertial measurement unit,” *Proceedings of Position Location and Navigation Symposium*, pp. 268-272, 2004.

[79] E. Kraft, “A quaternion-based unscented Kalman filter for orientation tracking,” *Proceedings of the Sixth International Conference of Information Fusion*, vol. 1, pp. 47-54, 2003.

[80] D. A. Winter, *Biomechanics and Motor Control of Human Movement*, 4th ed. John Wiley & Sons, Inc., 2009.

[81] T. S. Buchanan and D. A. Shreeve, “An Evaluation of Optimization Techniques for the Prediction of Muscle Activation Patterns During Isometric Tasks,” *Journal of*

Biomechanical Engineering, vol. 118, no. 4, pp. 565-574, Nov. 1996.

[82] M. A. Lemay, P. E. Crago, and M. W. Keith, "Restoration of pronosupination control by FNS in tetraplegia--experimental and biomechanical evaluation of feasibility," *Journal of Biomechanics*, vol. 29, no. 4, pp. 435-442, Apr. 1996.

[83] K. R. S. Holzbaur, W. M. Murray, and S. L. Delp, "A model of the upper extremity for simulating musculoskeletal surgery and analyzing neuromuscular control," *Annals of Biomedical Engineering*, vol. 33, no. 6, pp. 829-840, Jun. 2005.

[84] S. Delp et al., "OpenSim: Open-Source Software to Create and Analyze Dynamic Simulations of Movement," *IEEE Transactions on Biomedical Engineering*, vol. 54, no. 11, pp. 1940-1950, 2007.

[85] R. Kalman, "A New Approach to Linear Filtering and Prediction Problems," *Transactions of the ASME – Journal of Basic Engineering*, no. 82, pp. 35-45, 1960.

[86] G. Welch and G. Bishop, "An Introduction to the Kalman Filter," *Technical Report,* University of North Carolina at Chapel Hill, 1995.

[87] R. Alonso and M. D. Shuster, "Attitude-independent magnetometer-bias determination: A survey," *Journal of the Astronautical Sciences*, vol. 50, no. 4, pp. 453-475, 2002.

[88] D. Gebre-egziabher, G. H. Elkaim, J. D. Powell, and B. W. Parkinson, "A non-linear, two-step estimation algorithm for calibrating solid-state strapdown magnetometers," *8th International ST. Petersburg Conference on Navigation Systems*, pp. 28-30, 2001.

[89] D. Gebre-Egziabher, G. H. Elkaim, J. D. Powell, and B. W. Parkinson, "Calibration of Strapdown Magnetometers in Magnetic Field Domain," *Journal of Aerospace Engineering*, vol. 19, no. 2, pp. 87-102, Apr. 2006.

[90] D. Campolo, M. Fabris, G. Cavallo, D. Accoto, F. Keller, and E. Guglielmelli, "A Novel Procedure for In-field Calibration of Sourceless Inertial/Magnetic Orientation Tracking Wearable Devices," *Proceedings of the First IEEE/RAS-EMBS International Conference on Biomedical Robotics and Biomechatronics*, pp. 471-476, 2006.

[91] J. J. Kavanagh and H. B. Menz, "Accelerometry: a technique for quantifying movement patterns during walking," *Gait & Posture*, vol. 28, no. 1, pp. 1-15, Jul. 2008.

[92] D. Sankoff and J. B. Kruskal, *Time warps, string edits, and macromolecules: The theory and practice of sequence comparison*. Addison-Wesley Publishing Company, Inc., 1983.

[93] E. Bachmann, Xiaoping Yun, and C. Peterson, "An investigation of the effects of magnetic variations on inertial/magnetic orientation sensors," *Proceedings of IEEE International Conference on Robotics and Automation*, vol. 2, pp. 1115-1122, 2004.

[94] H. Xin, J. S. Zelek, and H. Carnahan, "Laparoscopic surgery, perceptual limitations and force: A review," *First Canadian Student Conference on Biomedical Computing*, 2006.

[95] MC MEDICAL Inc., [Online]. Available: http://www.mcmed.co.jp/index.html.

[96] A. Gallagher, Y. Matsuoka, and A. Wei-Tech, “An efficient real-time human posture tracking algorithm using low-cost inertial and magnetic sensors,” *Proceedings of IEEE/RSJ International Conference on Intelligent Robots and Systems*, vol. 3, pp. 2967-2972, 2004.

[97] J. A. Martin et al., “Objective Structured Assessment of Technical Skill (OSATS) for Surgical Residents,” *The British Journal of Surgery*, vol. 84, no. 2, pp. 273-278, Feb. 1997.

[98] R. McCloy and R. Stone, “Science, Medicine, and the Future. Virtual Reality in Surgery,” *BMJ (Clinical Research Ed.)*, vol. 323, no. 7318, pp. 912-915, Oct. 2001.

[99] K. Moorthy, Y. Munz, A. Dosis, F. Bello, A. Chang, and A. Darzi, “Bimodal Assessment of Laparoscopic Suturing Skills: Construct and Concurrent Validity,” *Surgical Endoscopy*, vol. 18, no. 11, pp. 1608-1612, Nov. 2004.

[100] K. Moorthy, Y. Munz, S. K. Sarker, and A. Darzi, “Objective Assessment of Technical Skills in Surgery,” *BMJ (Clinical Research Ed.)*, vol. 327, no. 7422, pp. 1032-1037, Nov. 2003.

[101] M. Chmarra, F. Jansen, C. Grimbergen, and J. Dankelman, “Retracting and seeking movements during laparoscopic goal-oriented movements. Is the shortest path length optimal?,” *Surgical Endoscopy*, vol. 22, no. 4, pp. 943-949, Apr. 2008.

[102] M. K. Chmarra, N. H. Bakker, C. A. Grimbergen, and J. Dankelman, “TrEndo, a device for tracking minimally invasive surgical instruments in training setups,” *Sensors and Actuators A: Physical*, vol. 126, no. 2, pp. 328-334, Feb. 2006.

[103] J. Rosen, J. D. Brown, L. Chang, M. N. Sinanan, and B. Hannaford, “Generalized approach for modeling minimally invasive surgery as a stochastic process using a discrete Markov model,” *IEEE Transactions on Bio-Medical Engineering*, vol. 53, no. 3, pp. 399-413, Mar. 2006.

[104] J. Rosen, B. Hannaford, C. G. Richards, and M. N. Sinanan, “Markov Modeling of Minimally Invasive Surgery Based on Tool/Tissue Interaction and Force/Torque Signatures for Evaluating Surgical Skills,” *IEEE Transactions on Biomechanical Engineering*, vol. 48, pp. 579-591, 2001.

[105] J. Rosen, B. Hannaford, M. Sinanan, and M. Solazzo, “Objective Evaluation Of Laparoscopic Surgical Skills Using Hidden Markov Models Based On Haptic Information And Tool/tissue Interactions,” *American College of Surgeons Annual Meeting, Washington State Chapter*, Lake Chelan, 2000.

[106] J. Rosen, M. Solazzo, B. Hannaford, and M. Sinanan, “Task decomposition of laparoscopic surgery for objective evaluation of surgical residents' learning curve using hidden Markov model,” *Computer Aided Surgery: Official Journal of the International Society for Computer Aided Surgery*, vol. 7, no. 1, pp. 49-61, 2002.

[107] C. E. Reiley and G. D. Hager, “Task versus Subtask Surgical Skill Evaluation of Robotic Minimally Invasive Surgery,” *Proceedings of the 12th International Conference on Medical Image Computing and Computer-Assisted Intervention: Part I*, pp. 435-442, 2009.

[108] Z. Lin, M. Zecca, S. Sessa, T. Kusano, K. Itoh, and A. Takanishi, “Waseda Bioinstrumentation System WB-2R as a Wearable Tool for an Objective Analysis of Surgeon's Performance,” *Proceedings of IEEE/RSJ International Conference on Advanced Intelligent Machatronics*, pp. 705-710, 2009.

[109] KARL STORZ Inc., [Online]. Available: http://www.karlstorz.com.

[110] W. Kolkman, M. van de Put, R. Wolterbeek, J. Trimbos, and F. Jansen, “Laparoscopic skills simulator: construct validity and establishment of performance standards for residency training,” *Gynecological Surgery*, vol. 5, no. 2, pp. 109-114, May. 2008.

[111] “MATLAB and Simulink for Technical Computing,” [Online]. Available: http://www.mathworks.com.

[112] "Principal Component Analysis," [Online]. Available: http://www.fon.hum.uva.nl/praat/manual/Principal_component_analysis.html.

[113] G. J. McLachlan, *Discriminant Analysis and Statistical Pattern Recognition*. Wiley Inerscience, 2004.

[114] G. M. Fried, “FLS Assessment of Competency Using Simulated Laparoscopic Tasks,” *Journal of Gastrointestinal Surgery*, vol. 12, no. 2, pp. 210-212, 2007.

[115] C. Giorgi, H. Eisenberg, G. Costi, E. Gallo, G. Garibotto, and D. S. Casolino, “Robot-assisted microscope for neurosurgery,” *Journal of Image Guided Surgery*, vol. 1, no. 3, pp. 158-163, 1995.

[116] Shah and Darzi, “The impact of inherent and environmental factors on surgical performance in laparoscopy: a review,” *Minim Invasive Ther Allied Technol*, vol. 12, pp. 69-75, 2003.

[117] A. Mauro, J. Raczkowsky, R. Wirtz, and H. Wörn, “Development of a Microscope Embedded Training System for Neurosurgery,” *Proceedings of the 4th international symposium on Biomedical Simulation*, pp. 209-214, 2008.

[118] M. K. Morgan et al., “The neurosurgical training curriculum in Australia and New Zealand is changing. Why?,” *Journal of Clinical Neuroscience: Official Journal of the Neurosurgical Society of Australasia*, vol. 12, no. 2, pp. 115-118, Feb. 2005.

[119] A. Mauro, J. Raczkowsky, M. E. Halatsch, and H. Wörn, “Mixed Reality Neurosurgical Microscope for Training and Intra-operative Purposes,” *Proceedings of the 3rd International Conference on Virtual and Mixed Reality: Held as Part of HCI International 2009*, pp. 542-549, 2009.

[120] A. de Mauro, J. Raczkowsky, M. Halatsch, and H. Worn, “Virtual Reality Training Embedded in Neurosurgical Microscope,” *IEEE Conference* in *Virtual Reality*, pp. 233-234, 2009.

[121] C. G. L. Cao, C. L. Mackenzie, and S. Payandeh, “Task And Motion Analyses In Endoscopic Surgery,” *Proceedings of 5th Annual Symposium on Haptic Interfaces for Virtual Environment and Teleoperator Systems*, pp. 583-590. 1996.

[122] L. Verner, D. Oleynikov, S. Holtmann, H. Haider, and L. Zhukov, “Measurements of the level of surgical expertise using flight path analysis from da VinciTM robotic surgical system,” *Medicine Meets Virtual Reality*, vol. 11, pp. 373-378, 2003.

[123] S. Payandeh, A. Lomax, J. Dill, C. Mackenzie, and C. G. L. Cao, “On Defining Metrics for Assessing Laparoscopic Surgical Skills in a Training Environment,” *Studies in Health Technology and Informatics - Medicine Meets Virtual Reality*, vol. 85, pp. 334-340, 2002.

[124] G. Megali, S. Sinigaglia, O. Tonet, and P. Dario, “Modelling and evaluation of surgical performance using hidden Markov models,” *IEEE Trans Biomed Eng*, vol. 53, pp. 1911-1919, 2006.

[125] P. A. Woerdeman, P. W. Willems, H. J. Noordmans, and J. W. van der Sprenkel, “The analysis of intraoperative neurosurgical instrument movement using a navigation log-file,” *Int J Med Robot*, vol. 2, pp. 139-145, 2006.

[126] S. Sharma, A. G. Haji, D. K. Vijaykumar, and A. K. Shaji, “Irrigation-coupled bipolar cautery unit: A practical, economical, and simple version,” *ndian J Plast Surg*, vol. 41, no. 2, pp. 162-166, 2008.

[127] K. C. Veluvolu, U. X. Tan, W. T. Latt, C. Y. Shee, and W. T. Ang, “Bandlimited Multiple Fourier Linear Combiner for Real-time Tremor Compensation,” *29th Annual International Conference of the IEEE Engineering in Medicine and Biology Society*, pp. 2847-2850, 2007.

[128] National Institutes of Health, “NIDCR Launches Important Study on Temporomandibular Joint and Muscle Disorders,” [Online]. Available: http://www.nidcr.nih.gov/Research/ResearchResults/NewsReleases/ArchivedNewsReleases/NRY2005/PR12052005.

[129] Y. Otake et al., “Real-time mandibular movement analysis system using four-dimensional cranial bone model,” *Syst. Comput. Japan*, vol. 37, no. 8, pp. 1-12, 2006.

[130] M. Naeije and N. Hofman, “Biomechanics of the human temporomandibular joint during chewing,” *Journal of Dental Research*, vol. 82, no. 7, pp. 528-531, Jul. 2003.

[131] E. M. Wilson and J. R. Green, “The development of jaw motion for mastication,” *Early Human Development*, vol. 85, no. 5, pp. 303-311, May. 2009.

[132] Myotronics Inc., [Online]. Available: http://www.myotronics.com.

[133] S. Yabukami et al., “A new tracking system of jaw movement using two magnets,” *IEEE International Magnetics Conference*, pp. FV8, 2002.

[134] S. C. Flavel, M. A. Nordstrom, and T. S. Miles, “A simple and inexpensive system for monitoring jaw movements in ambulatory humans,” *Journal of Biomechanics*, vol. 35, no. 5, pp. 573-577, May. 2002.

[135] Z. Lin, M. Zecca, S. Sessa, H. Ishii, and A. Takanishi, “Developement of an Ultra-Miniaturized Inertial Measurement Unit for Jaw Movement Analysis during Free Chewing,” *Journal of Computer Science*, vol. 6, pp. 896-903, 2010.

Research Achievements

種類別	題名	発表・発行掲載誌名	発表・発行年月	連名者
1. 論文	Waseda Bioinstrumentation System WB-3 as a Wearable Tool for Objective Laparoscopic Skill Evaluation	2011 IEEE International Conference on Robotics and Automation.	2011 年 5 月 (accepted)	**Zhuohua Lin**, Munenori Uemura, Massimiliano Zecca, Salvatore Sessa, Hiroyuki Ishii, Makoto Hashizume, Atsuo Takanishi
	Development of an Ultra-miniaturized Inertial Measurement Unit WB-3 for Human Body Motion Tracking	Proceedings of 2010 IEEE/SICE International Symposium on System Integration, pp. 414-419, 2010.	2010 年 12 月 (published)	**Zhuohua Lin**, Massimiliano Zecca, Salvatore Sessa, Luca Bartolomeo, Hiroyuki Ishii, Kazuko Itoh, Atsuo Takanishi
	Development of the Miniaturized Wireless Inertial Measurement Unit WB-4: Pilot Test for Mastication Analysis	Proceedings of 2010 IEEE/SICE International Symposium on System Integration, pp. 420-425, 2010.	2010 年 12 月 (published)	**Zhuohua Lin**, Massimiliano Zecca, Salvatore Sessa, Luca Bartolomeo, Hiroyuki Ishii, Kazuko Itoh, Atsuo Takanishi
	Objective Evaluation of Laparoscopic Surgical Skills Using Waseda Bioinstrumentation System WB-3	Proceedings of 2010 IEEE International Conference on Robotics and Biomimetics, pp. 247-252, 2010.	2010 年 12 月 (published)	**Zhuohua Lin**, Munenori Uemura, Massimiliano Zecca, Salvatore Sessa, Hiroyuki Ishii, Luca Bartolomeo, Kazuko Itoh, Morimasa Tomikawa, Takeshi Odaira, Kazuo Tanoue, Satoshi Ieiri, Kozo Konishi, Makoto Hashizume, Atsuo Takanishi
	Ultra-miniaturized WB-3 Inertial Measurement Unit: performance evaluation of the attitude estimation	Proceedings of 2010 IEEE International Conference on Robotics and Biomimetics, pp. 998-1003, 2010.	2010 年 12 月 (published)	Salvatore Sessa, Massimiliano Zecca, **Zhuohua Lin**, Luca Bartolomeo, Kazuko Itoh, Hiroyuki Ishii, Yoshikazu Mukaeda, Yuto Suzuki, Atsuo Takanishi

種類別	題名	発表・発行掲載誌名	発表・発行年月	連名者
論文の続き	Development of an Ultra-Miniaturized Inertial Measurement Unit for Jaw Movement Analysis during Free Chewing	Journal of Computer Science, Vol. 6, No. 8, pp. 896-903.	2010 年 8 月 (published)	**Zhuohua Lin**, Massimiliano Zecca, Salvatore Sessa, Hiroyuki Ishii, Atsuo Takanishi
	Ultra-Miniaturized Inertial Measurement Unit WB-3 for Jaw Movement Analysis during Free Chewing	Proceedings of 2010 International Symposium on Robotics and Intelligent Sensors, pp. 213-218, 2010.	2010 年 3 月 (published)	**Zhuohua Lin**, Massimiliano Zecca, Salvatore Sessa, Hiroyuki Ishii, Atsuo Takanishi
	Development of the Ultra-Miniaturized Inertial Measurement Unit WB3 for Objective Skill Analysis and Assessment in Neurosurgery: Preliminary Results	Lecture Notes in Computer Science, Vol. 5761/2009, pp. 443-450.	2009 年 10 月 (published)	Massimiliano Zecca, Salvatore Sessa, **Zhuohua Lin**, Takashi Suzuki, Tomoya Sasaki, Kazuko Itoh, Hiroshi Iseki, Atsuo Takanishi
	Objective Skill Analysis and Assessment of Neurosurgery by using the Waseda Bioinstrumentation System WB-3 -Pilot tests-	Proceedings of 2009 IEEE/RSJ International Conference on Intelligent Robots and Systems, pp. 4086-4091, 2009.	2009 年 10 月 (published)	Salvatore Sessa, Massimiliano Zecca, **Zhuohua Lin**, Tomoya Sasaki, Takashi Suzuki, Kazuko Itoh, Hiroshi Iseki, Atsuo Takanishi
	Objective Skill Analysis and Assessment in Neurosurgery by Using an Ultra-Miniaturized Inertial Measurement Unit WB-3 –Pilot tests-	Proceedings of 31st Annual International Conference of IEEE Engineering in Medicine and Biology Society, pp. 2320-2323.	2009 年 9 月 (published)	**Zhuohua Lin**, Massimiliano Zecca, Salvatore Sessa, Tomoya Sasaki, Takashi Suzuki, Kazuko Itoh, Hiroshi Iseki, Atsuo Takanishi
	Development of an Ultra-Miniaturized Inertial Measurement Unit for Objective Skill Analysis and Assessment in Neurosurgery: preliminary results	Proceedings of 12th International Conference on Medical Image Computing and Computer Assisted Intervention, pp. 443-450, 2009.	2009 年 9 月 (published)	Massimiliano Zecca, Salvatore Sessa, **Zhuohua Lin**, Takashi Suzuki, Tomoya Sasaki, Kazuko Itoh, Hiroshi Iseki, Atsuo Takanishi

種類別	題名	発表・発行掲載誌名	発表・発行年月	連名者
論文の続き	Waseda Bioinstrumentation System WB-2R as a Wearable Tool for an Objective Analysis of Surgeon's Performance	Proceedings of 2009 IEEE/ASME International Conference on Advanced Intelligent Mechatronics, pp.705-710, 2009.	2009 年 7 月 (published)	**Zhuohua Lin**, Massimiliano Zecca, Salvatore Sessa, Toshihiro Kusano, Kazuko Itoh, Atsuo Takanishi
	Waseda Bioinstrumentation System #3 as a tool for objective rehabilitation measurement and assessment - development of the inertial measurement unit-	Proceedings of 2009 IEEE 11th International Conference on Rehabilitation Robotics, pp. 115-120, 2009.	2009 年 6 月 (published)	Salvatore Sessa, Massimiliano Zecca, **Zhuohua Lin**, Tomoya Sasaki, Kazuko Itoh, Atsuo Takanishi
2. 講演	超小型無線センサユニットの開発	第 11 回計測自動制御学会	2010 年 12 月	迎田美和, 鈴木悠人, **林焯華**, ルカ バルトロメオ, 伊藤加寿子, 石井裕之, サルバトーレセッサ, マッシミリアーノ ゼッカ 高西淳夫
	生体計測システム WB-3 を用いた腹腔鏡手術技能の客観的評価	第 19 回 日本コンピュータ外科学会大会	2010 年 11 月	鈴木悠人, 迎田美和, **林焯華**, ルカ バルトロメオ, 伊藤加寿子, 石井裕之, サルバトーレセッサ, マッシミリアーノ ゼッカ 植村宗則, 富川盛雅, 大平猛, 田上和夫, 家入里志, 小西晃造, 橋爪誠, 高西淳夫

種類別	題名	発表・発行掲載誌名	発表・発行年月	連名者
講演の続き	顎運動を定量的に計測可能な小型センサの製作	日本咀嚼学会 第21回学術大会	2010年10月	迎田美和, 鈴木悠人, **林焯華,** サルバトーレセッサ, ルカ バルトロメオ, 石井裕之, マッシミリアーノ ゼッカ 高西淳夫
	超小型姿勢センサユニットWB-3の開発:姿勢センサIntertiaCubeとVICONモーションキャプチャシステムとの比較	第28回日本ロボット学会	2010年9月	鈴木悠人, 迎田美和 **林焯華,** ルカ バルトロメオ, 伊藤加寿子, 石井裕之, サルバトーレセッサ, マッシミリアーノ ゼッカ 高西淳夫
	イナーシャル・メジャーメント・ユニットWB3の開発について	2009日本咀嚼学会第20回記念学術大会	2009年10月	マッシミリアーノ ゼッカ **林焯華,** サルバトーレセッサ, 石井裕之, 高西淳夫
	Objective Skill Analysis and Assessment in Neurosurgery by using the Waseda Bioinstrumentation System WB-3 -Pilot tests-	2009 Robotics and Mechatronics Conference, pp. 1A1-L08(1) - 1A1-L08(4)	2009年5月	**Zhuohua Lin**, Massimiliano Zecca, Salvatore Sessa, Tomoya Sasaki, Takashi Suzuki, Kazuko Itoh, Hiroshi Iseki, Atsuo Takanishi
	The Development of Wearable Human Motion Capture System	5th IEEE Tokyo Young Researchers Workshop, A-10	2008年12月	**Zhuohua Lin**
	Measurement and Evaluation of Surgeon's Skill by Means of the Human Measurement System WB	Shanghai Jiao Tong University-Waseda University Joint Symposium, P2BL0807	2008年12月	**Zhuohua Lin**

種類別	題名	発表・発行掲載誌名	発表・発行年月	連名者
3. その他				
産業財産権	超小型慣性センシングユニット	大学整理番号 1085	2010 年 7 月	高西淳夫, ゼッカマッシミリアーノ サルバトーレセッサ, **林焯华**
賞	T. J. Tarn Best Paper in Robotics Finalist	2010 IEEE International Conference on Robotics and Biomimetics (ROBIO2010)	2010 年 12 月	Salvatore Sessa, Massimiliano Zecca, **Zhuohua Lin**, Luca Bartolomeo, Kazuko Itoh, Hiroyuki Ishii, Yoshikazu Mukaeda, Yuto Suzuki, Atsuo Takanishi
賞	Best Paper Award Finalist	2010 International Symposium on Robotics and Intelligent Sensors(IRIS2010)	2010 年 3 月	**Zhuohua Lin**, Massimiliano Zecca, Salvatore Sessa, Hiroyuki Ishii, Atsuo Takanishi
賞	Best Paper Award	2009 IEEE/ASME International Conference on Advanced Intelligent Mechatronics (AIM2009)	2009 年 7 月	**Zhuohua Lin**, Massimiliano Zecca, Salvatore Sessa, Toshihiro Kusano, Kazuko Itoh, Atsuo Takanishi

Award Certificate

AIM2009

IEEE　ASME

2009 IEEE/ASME International Conference on
Advanced Intelligent Mechatronics
July 14-17, 2009
Singapore

Best Paper Award

This is to certify that the following paper

Waseda Bioinstrumentation System WB-2R As a Wearable Tool for an Objective Analysis of Surgeon's Performance

by

Zhuohua Lin, Massimiliano Zecca, Salvatore Sessa, Toshihiro Kusano, Kazuko Itoh, Atsuo Takanishi

has been awarded the

AIM 2009 Best Paper Award

Professor Han-Pang Huang
Chairman of Award Committee, AIM 2009

Professor I-Ming Chen
Chairman, AIM 2009

Professor Marcelo H Ang Jr
Program Chairman, AIM 2009

Best Paper Award, 1st author.

2009 IEEE/ASME International Conference on Advanced Intelligent Mechatronics.

IRIS2010

Nagoya University　UNIVERSITI TEKNOLOGI MARA

2010 INTERNATIONAL SYMPOSIUM ON ROBOTICS AND INTELLIGENT SENSORS
March 8-11, 2010, Nagoya University, Japan

Best Paper Award Finalist

This is to certify that the following paper

Ultra-Miniaturized Inertial Measurement Unit WB-3 for Jaw Movement Analysis during Free Chewing

by

Zhuohua Lin, Massimiliano Zecca, Salvatore Sessa, Hiroyuki Ishii and Atsuo Takanishi

has been awarded the

IRIS2010 Best Paper Award Finalist

Prof. Masahiro Ohka
General Chair / Finance & Sponsor,IRIS2010

Dr. Hanafiah Yussof
General Chair / Secretariat, IRIS2010

Best Paper Award Finalist, 1st author.

2010 International Symposium on Robotics and Intelligent Sensors.

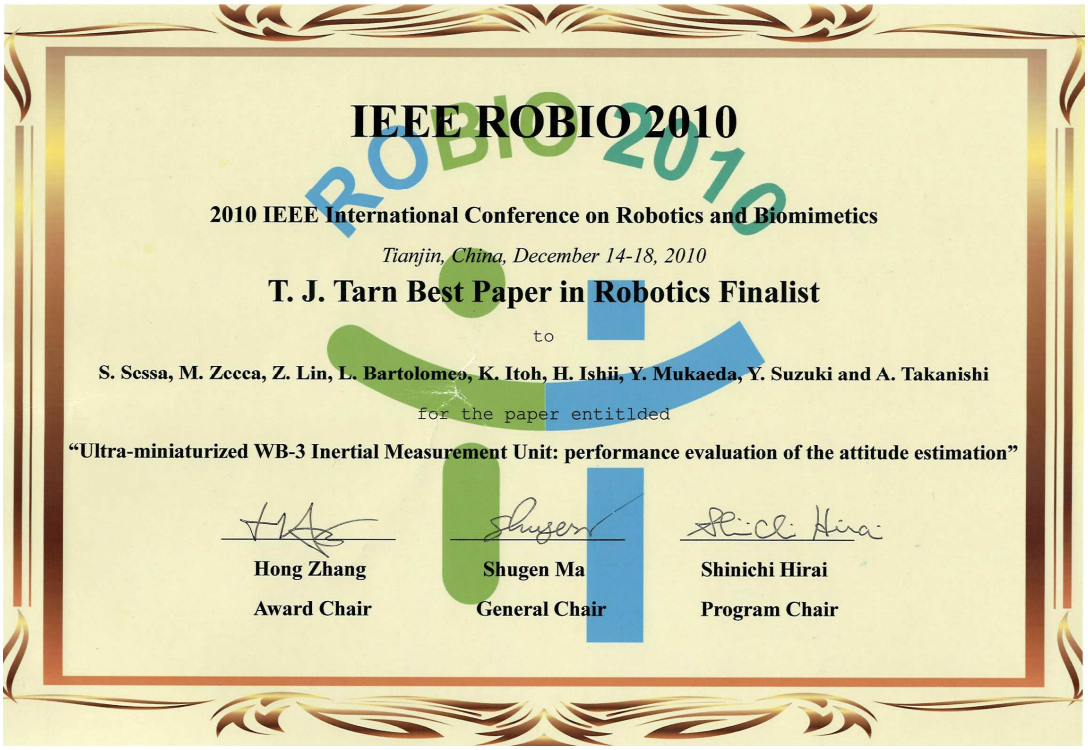

IEEE ROBIO 2010

2010 IEEE International Conference on Robotics and Biomimetics

Tianjin, China, December 14-18, 2010

T. J. Tarn Best Paper in Robotics Finalist

to

S. Scssa, M. Zccca, Z. Lin, L. Bartolomeo, K. Itoh, H. Ishii, Y. Mukaeda, Y. Suzuki and A. Takanishi

for the paper entitlded

"Ultra-miniaturized WB-3 Inertial Measurement Unit: performance evaluation of the attitude estimation"

Hong Zhang	Shugen Ma	Shinichi Hirai
Award Chair	General Chair	Program Chair

T. J. Tarn Best Paper in Robotics Finalist, co-author.

2010 IEEE International Conference on Robotics and Biomimetics.